CORNELL UNIVERSITY
Laboratory of Nuclear Studies
Ithaca, New York

CS-31
R. Yamada
S. Mori
April 27, 1966

MAGNETIC FIELD MEASUREMENT I

Introduction

The Cornell 10 GeV alternating-gradient electron synchrotron, with a diameter of 100m is among the largest synchrotrons existing or under construction. Accordingly, the stability region is very small and high accuracy is required for the pole profile of magnets. Gap heights are one and one-half inches for a wide gap magnet (vertical focusing: positive) and about one inch for a narrow gap magnet (radial focusing: negative). These are the smallest gaps of all synchrotrons. Therefore, the accuracy needed for stamping laminations of the magnets is the most stringent. They were made with an accuracy of ± 0.25 mil. Gradients in the usable region are required to be within a limit of about $\pm 0.5\%$ from the designed values. [1)]

Measurement of magnetic field must be carried out with a compatable accuracy with the above requirement. We have measured the absolute value of $X_0 (= B_0 / \left(\frac{dB}{dx}\right)_0)$ with an accuracy of $\pm 0.15\%$ and the distribution of $X_0(x)$ with a relative accuracy of $\pm 0.1\%$. The measurement was done with high AC excitation of the magnet without and with a DC bias, using search coils and an integrator. The magnetic field at the center was from 2.5 to 5kG (the peak field at an excitation of 15 GeV), which is free from the remanent field and the saturation effect.

The actual profile of pole pieces were determined through computer calculation which assumed a constant magnetic length of 127.5" and a constant gradient length of 126.5", while a

geometrical length of the lamination stack is 126.48" for two types of magnets.[1, 2]

Fringing fields at the ends of the magnets were measured at high AC field using the same technique. Effective magnetic and gradient lengths were also measured along the radial direction. Several hard packs (groups of laminations with a graded profile which are prefabricated for use at the ends of magnets), which were different in shape, were made and measured in order to obtain designed constant magnetic and gradient lengths in the usable regions at high field.

Excitation Curve

The magnet is excited with a DC power supply and the field in the gap was measured with a Rawson rotating coil fluxmeter. The excitation curves of the narrow gap magnet at the center and at one inch outside are shown in Fig. 1. The saturation starts around 16 GeV, but it is due to the thinner back legs, which are 1-1/4" on both sides compared to 4" of the pole piece width. Therefore the gradient of the field is probably not seriously affected by saturation for both types of magnets at least up to 20 GeV. A similar curve was obtained for the wide gap magnet.

Absolute Value of X_o at the Center

The X_o at the center was measured with two small search coils and an integrator.[3] One of the search coils was fixed at some point in the gap as a standard coil and the other moving coil was set at the center at first. A schematic diagram of the system is shown in Fig. 2. The output voltage of the moving coil was compared with that of the standard coil by using voltage dividers. The polarities of the two search coils were opposite so that they were bucking each other. The output of the search coils connected in series was fed into an integrator and then into an oscilloscope,

which was triggered by the signal from a peaking strip placed in the gap. The divider for the standard coil was adjusted such that voltage levels at the two points, where the magnetic field was zero and the maximum, became equal on the scope.

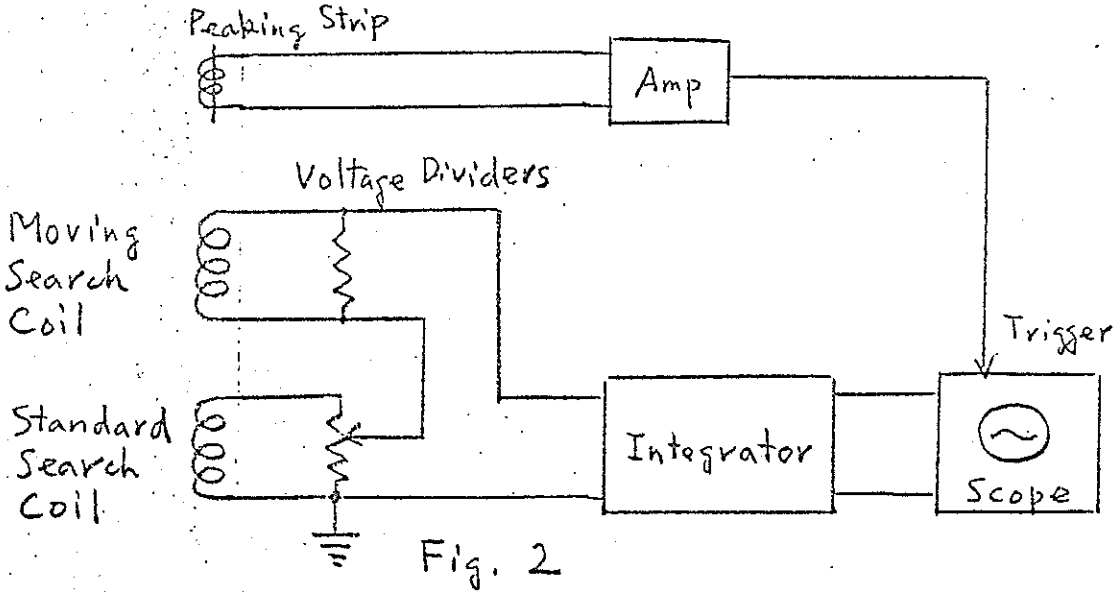

Fig. 2

The output voltage V_o of the two coils connected in series is given by

$$V_o = V_m \frac{Rd}{Rd+Rc} - \alpha V_s \frac{Rd}{Rd+R'_c}, \qquad (1)$$

where V_m and V_s are the output voltages of the moving and standard coils, respectively, α is the setting of the divider for the standard coil, and R_d, R_c and R'_c are the impedances of each divider, the moving coil and standard coil, respectively. The two coils were made identical and $R_c = R'_c = 34\ \Omega$, and $R_d = 10\ k\Omega$. Then the output of the integrator V at $t = t_1$ is given by

$$V = \int_{t_0}^{t_1} V_o\, dt = \frac{Rd}{Rd+Rc} \frac{1}{RC} \int_{t_0}^{t_1} (V_m - \alpha V_s)\, dt, \qquad (2)$$

where R and C are the input resistor and the feedback capacitor of the integrator, respectively. Vm and Vs are expressed as

$$V_m = A_m \frac{dB_m}{dt}, \text{ and } V_s = A_s \frac{dB_s}{dt}, \tag{3}$$

where A_m and A_s are the turn areas of the moving and standard coils, and B_m and B_s are the magnetic fields at the positions where the moving and standard coils are located, respectively. The two coils are almost identical, and $A_s = \beta A_m$, where β is nearly equal to one. Then Eq(2)can be rewritten as

$$V = \frac{Rd}{Rd+Rc} \frac{Am}{RC} \left[Bm - \alpha\beta B_s \right]_{t_0}^{t_1} \tag{4}$$

B_m and B_s at t_o are less than a few gauss and their difference is much smaller than the values at t_1, and we adjust the divider to make $V = 0$ on the scope. Therefore

$$B_m(t_1) = \alpha\beta B_s(t_1), \tag{5}$$

Since $\beta B_s(t_1)$ is constant, α gives the relative field intensity at the moving coil at $t=t_1$.

First the central field was measured as mentioned above and the moving search coil was moved in x direction for a given distance (usually ± 0.5") and the fields at these points were measured also with respect to the standard coil. We took their difference ΔB. Xo(0) is then given by

$$X_o(o) = \frac{B_o(o)}{\left(\frac{\Delta B}{\Delta X}\right)_o}, \tag{6}$$

General Radio 1454-A Decade Voltage Dividers were used, which have a maximum linearity error of ±0.02% and a frequency error of less than 0.1% up to 20kc. They are four digit dividers. We added a 0.1Ω-10 step variable resistor in series with the dividers to read out another digit. Sometimes we used the deflection on the scope for reading out the fifth digit.

The integrator used was Tektronix "O-type" plug-in which was set at the input impedance of 100kΩ and feedback impedance of 0.01μF. Its open gain is 2000 and the effective time constant was 2 sec. which was good enough for the measurement of 60 c/s AC field measurement. There was a small error of about 0.1% in the integration due to the finite gain of the integrator. But this results in a negligible error because only a very small difference signal is integrated. A Tektronix RM 561A - oscilloscope with a 2A63 plug-in unit was used for the display and adjustment of level of the output signal. The sensitivity of the scope was set at ∿2mV/cm.

A peaking strip was used to trigger this scope. The delay of its signal (a fewμs) and the effect of the remanent field 3∿4 gauss) were small compared to the peak field. So, in our present measurement it can be neglected as we were interested only in the field shape due to the pole profile.

The main error of the measurement of $X_0(o)$ came from uncertainty in the positioning of the moving coil at the center of the pole piece gap. This was estimated to be ± 7 mils. Since the field gradient is about 11% / inch, an uncertainty of 0.08% is estimated in the central field value and in $X_0(o)$ due to this effect.

The positioning of the moving coil was done by an indirect method as we could not measure directly the position of the coil far inside the gap. In this indirect method the level of the

magnet was set and the axis of a transit was aligned on the center line of the magnet by using special jigs. A mill table which carried the coil was leveled and aligned parallel to the axis of the magnet by using a micro-dial gauge on the mill table and a long parallel bar extending from one side of the magnet. The search coil, which had a sharp cone as a center pointer, was placed on the center line of the magnet outside the gap with the aid of the transit. Then the search coil was moved about one foot into the gap, where the central field was measured. There might have been a small error due to the inclination and the imperfection of the search coil (< 2 mils).

We measured the radial displacement Δx with a dial gauge and gauge blocks. The possible error in Δx is estimated to be less than 0.5 mil for 1.000" displacement, i.e. 0.05%. Uncertainty in ΔB, which was taken as a difference between two five-digit numbers ($\sim 10^5$), was about 0.02% (corresponding to four-digits) since $\Delta B/B$ was about 0.1. The $X_0(x)$ is not a constant throughout the usable region as will be shown later, but has a linear term of a sextapole. The error in $X_0(0)$ due to the finite values of ΔB and ΔX is negligible for the constant field gradient modified with a linear term. If there had been any big higher terms, the exact value of $X_0(o)$ should be corrected from the curve of X_0 around the center.

The two search coils were made identical with ratios of the diameter to height of 0.72 to give the average central field. The inductance of the coil was about 0.2mH. This is quite small compared to the input impedence of the dividers of 10kΩ. Therefore, its effect was neglected. As two search coils were connected in the opposition any fluctuation in the power supply did make no error.

Thus, the overall uncertainty is estimated to be $\pm$0.15%. Table I gives the measured results together with the designed values for both magnets. There was no detectable difference between the values of excitation corresponding to 7.5 and 15 GeV excitation levels.

Table I: Absolute Values of X_0 at the Geometric Center at High Field

Magnet	Gap Height	Designed Value	Measured Value	Measured Minus Designed	Effect of Punching Error
row Gap	1.022"	9.010"	9.045" $\pm$ 0.014"	+0.035	+0.035"
e Gap	1.501"	9.223"	9.204" $\pm$ 0.014"	-0.019	-0.004"

The errors in the profiles of the punched laminations were measured geometrically. Their effect on $X_0(o)$ were estimated according to Eq. (15) and shown also in Table I. They account for some of the differences between the measured values and the designed ones.

In our case the iron was not saturated so that measurements made without integration gave the same result within the experimental error. Another alternate method was to use two integrators for two search coils and compare them with the dividers. This gave the same results.

Measurement of the Radial Distribution of $X_0(x)$.

We could measure the radial distribution of $X_0(x)$ by the same method as used for the measurement of the absolute X_0 at the center. However, the percentage error was bigger in this case, because the absolute value of ΔX was quite small (0.1" $\sim$ 0.2")

and the error in Δx was the same as in the previous case. The precision of the mechanical positioning device was not sufficient to yeild an accuracy of better than $\pm 0.5\%$ with this method.

Instead of using a single coil as a moving coil we used matched twin coils consisting of a pair of identical coils glued together. Since the distance between the two coils was kept constant, the error in the Δx was negligible. They were connected in series and bucking each other. The radial distribution of $X_o(x)$ was obtained by moving these twin coils along the radial direction, and by comparing their output with that of another fixed standard coil just as in the case of the absolute X_o measurement.

The output of the twin coils V_t is given by

$$V_t = A \frac{d}{dt}(B_1 - B_2) = A \frac{d}{dt}(\Delta B), \qquad (7)$$

where B_1 and B_2 are the magnetic fields at the centers of the first and second coil of the twin coils and A is the turn area of each coil. V_t and ΔB correspond to V_m and B_m in Eq.(3), respectively. Therefore, the distribution of $\Delta B(x)$ can be obtained by adjusting the divider for the standard coil, and that of $X_o(x)$ being calculated.

Although the geometrical shape and the turn number was made the same for each of the twin coils, there was some difference between them. Therefore an additional single turn on one of the coils was adjusted in area, so that the turn areas of the two coils

were matched. The turn areas of the two coils are A at the magnetic field B and A+ΔA at B+ΔB. Then the output voltage of the twin coil is proportional to

$$(A+\Delta A)\cdot(B+\Delta B)-A\cdot B=A\cdot\Delta B+\Delta A\cdot B+\Delta A\cdot\Delta B. \qquad (8)$$

The first term on the right is the term we want and the remaining terms are errors due to the mismatching of the coils. The third term is negligible. The ratio of the error to signal is

$$\left(\frac{\Delta A}{A}\right)\cdot\left(\frac{B}{\Delta B}\right)=36\left(\frac{\Delta A}{A}\right). \qquad \left(\because \frac{B}{\Delta B}=\frac{X_0}{\Delta x}=\frac{9''}{0.25''}=36\right)$$

To make the ratio less than 1%, ΔA/A should be made less than 1/3600. Therefore, careful matching of the twin coil is needed. We made ΔA/A less than 1/10000. Since we did not have a homogeneo AC field, the turn-area was adjusted in a constant gradient AC field, by equalizing the outputs obtained by reversing the twin c

When we take the average of two readings obtained with rever position of the twin coils, the above second term ΔA·B is cancelle out and the ratio of error to signal is ΔA/2A, which is $\sim 5 \times 10^{-5}$

The obtained distributions of $X_0(x)$ for the wide gap and narrow gap magnets are shown in Fig. 3 and Fig. 4. The designed distributionsand the ideal lines are shown also in Figs. 3 and 4 with the limit lines of ±0.5%. The agreement between the designe distributions and the measured ones seem fairly good. The measure distributions were same at 7.5 and 15 Gev.

The twin coilsused had a spacing of 0.25". Therefore this measurement has a spatial resolution due to the spacing of the tw coils, i.e. 0.25". Therefore the usable region of the actual distribution may be wideron both ends by as much as half this spa The widths of the usable regions are estimated 2.35" and 2.75" fo the wide gap and the narrow gap magnets respectively including

Measurement of Gap in Back Leg

The magnet is made of top and bottom halves, which are glue together with Epoxy at the centers of the back legs. This gap height g can be measured magnetically using a Hall probe.

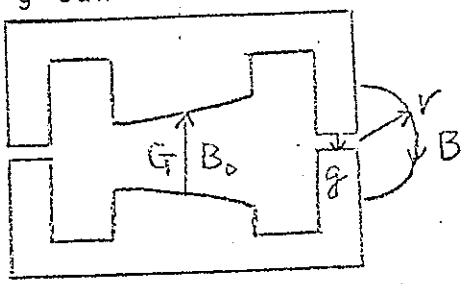

It is given by

$$g = \frac{\pi r B}{k B_o}, \qquad (9)$$

where B_o is the field at the center of the main gap, kB_o the field in the gap of the back leg, k is determined by the ratio of the width of the legs and pole piece and by the leakage flux rat ($k = 1.92$). B is the field at the distance r from the gap of back leg.

Effect of Gap in Back Leg

The calculation of the profile of the pole piece was done assuming a 1 mil gap in the back leg. The measured gap is about 2.0 ± 0.5 mil. And the gap may locally be as large as 3.5 mils. Variation in the back leg gap changes the field distribution, and also moves the isomagnetic line.

When we have an extra gap Δg on both of the back legs, we ha also an extra gap Δg in the central field of the pole piece. Therefore, the change of the field value ΔB_o at the central fiel B_o is,

$$\frac{\Delta B_o}{B_o} = -(1+k)\frac{\Delta g}{G}, \qquad (10)$$

where G is the gap of the magnet. For 1 mil of Δg, the percenta change in B_o is 0.3% and 0.2% for 1" gap and 1.5" gap respective This change in the field value moves the isomagnetic line by an amount Δx given by

$$\Delta x = -(1+k) X_o \frac{\Delta g}{G}. \qquad (11)$$

The amount of shifting due to a 1 mil extra gap is 26 mils and 18 mils for the narrow gap and wide gap magnet respectively.

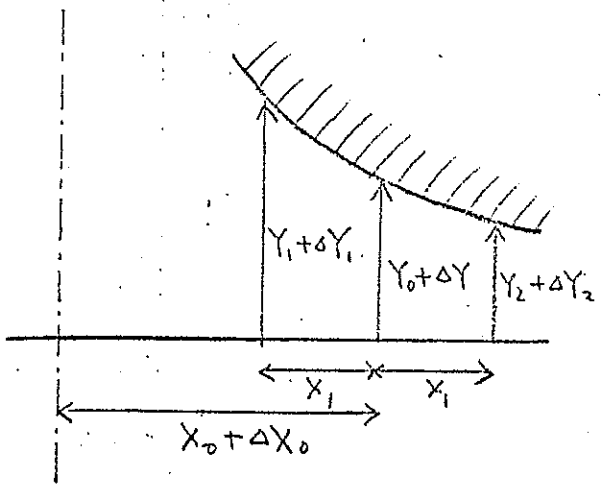

The approximate amount of change ΔX_o in X_o due to an extra gap in the back leg can be derived as follows: Here we treat the case of the constant gradient. The height of the gap from the median plane at the center is Yo, and the gaps at X_1 inches away from the center on both sides are Y_1 and Y_2, Y_1 being taken at the lower field side,

$$X_o = X_1 \frac{Y_1 + Y_2}{Y_1 - Y_2} \tag{12}$$

If we have error ΔY_1 and ΔY_2 then for the small value of x_1 the total change ΔX_o is,

$$\Delta X_o = \frac{X_1}{Y_1 - Y_2}\left\{(\Delta Y_1 + \Delta Y_2) - \frac{X_o}{X_1}(\Delta Y_1 - \Delta Y_2)\right\}, \tag{13}$$

And $Y_1 + Y_2$ is about equal to gap G , then

$$\frac{\Delta X_o}{X_o} \fallingdotseq \frac{1}{G}\left\{(\Delta Y_1 + \Delta Y_2) - \frac{X_o}{X_1}(\Delta Y_1 - \Delta Y_2)\right\}. \tag{14}$$

The term $(\Delta Y_1 + \Delta Y_2)$ gives the effect of an extra gap and the term $(\Delta Y_1 - \Delta Y_2)$ the effect due to the inclination of the pole pieces.

If there is an extra gap δ (mil) at the pole pieces and the pole pieces are inclined by ε (mil/inch) (ε is positive for a bigger gap on the low field side), then

$$\Delta X_o = 8.8(\delta - 18\epsilon)\text{mil, for a narrow gap magnet}$$
$$\Delta X_o = 6.1(\delta - 18\epsilon)\text{mil, for a wide gap magnet} \quad (15)$$

Therefore 1 mil extra gap or 0.05 mil/inch inclination gives of the order of 5∿10 mil change, which is about 0.1% of x_o. These equations can be used for estimation of the accuracy of the lamination profile.

Magnetic and Gradient Lengths

The magnetic length of the magnet at x, $L_B(x)$, is defined by:

$$L_B(x) = \int_{-\infty}^{\infty} B(x,z)\,dz \Big/ B_o(x), \quad (16)$$

where $B_o(x)$ is the magnetic field far inside the magnet at x and z is the coordinate taken in parallel to the magnet axis. Similarly, the gradient length $L_G(x)$ is expressed as

$$L_G(x) = \int_{-\infty}^{\infty} \frac{\partial B(x,z)}{\partial x}\,dz \Big/ \left(\frac{dB(x)}{\partial x}\right)_o, \quad (17)$$

where $\left(\frac{\partial B(x)}{\partial x}\right)_o$ is the field gradient far inside the magnet. $L_B(x)$ and $L_G(x)$ refer to the whole magnet with two hard packs (properly shaped prefabricated end sections), and we define $L'_B(x)$ and $L'_G(x)$ for half the magnet with one hard pack. The geometrical length L_{Go} of both magnets i.e. the length of the stacked lamination, is the same and 126.48". The difference between the $L'_B(x)$ and half the L_{GO} is defined as $\Delta L'_B(x)$ and similarly $\Delta L'_G(x)$ is defined for $L'_G(x)$. Therefore,

$$L_B(x) = 2L_B'(x) = L_{Go} + 2\Delta L'_B(x),$$
$$L_G(x) = 2L'_G(x) = L_{Go} + 2\Delta L'_G(x). \quad (18)$$

The calculation of the operating point and the profiles of the pole pieces was done assuming a constant magnetic length and a constant gradient length for both types of magnets. A half of the

difference between the magnetic and gradient length was assumed half an inch. Therefore, we had to shape the hard packs to satisfy the above requirements. A relation between $L'_B(x)$ and $L'_G(x)$ is given by

$$L'_G(x) - L'_B(x) = \frac{B_o(x)}{\left(\frac{\partial B(x)}{\partial x}\right)_o} \frac{\partial L'_B(x)}{\partial x}$$

$$= X_o \frac{\partial L'_B(x)}{\partial x} \frac{1 + \frac{x}{X_o} + \frac{\epsilon}{2X_o} x^2}{1 + \epsilon x} \qquad (19)$$

$$= X_o \frac{\partial L'_B(x)}{\partial x} \left(1 + \frac{x}{X_o}\right)$$

where X_o is taken as $\left(B_o(0) \Big/ \frac{\partial B_o(0)}{\partial x}\right)_o$, and ϵ corresponds to a sextapole term inside the gap for the correction of momentum shift of the operating point and it is less than 2.5×10^{-2}/inch.[1] At $x = 0$, Eq. (19) gives

$$L'_G(0) - L'_B(0) = X_o \frac{\partial L'_B(0)}{\partial x} \qquad (20)$$

As we should make $L'_G - L'_B = -0.5"$, $\frac{\partial L'_B(0)}{\partial x}$ should be made about ± 55 mil/inch, where + corresponds to the wide gap and - to the narrow gap magnets.

For beam dynamics the magnetic and gradient lengths are important. Therefore, to make the effect of variation of these lengths negligible, the variations of $\Delta L'_B(x)$ and $\Delta L'_G(x)$ should be made less than $\pm 0.5\%$ of a half of the geometrical length; i.e. less than ± 0.3 inch as $\pm 0.5\%$ was taken as the criterion for the limit of X_o[1].

Hard Packs and Fringing Field

In order to obtain the final hard packs which satisfied the above requirements, a number of differently shaped hard packs were

tried with successive improvements for both types of magnets. A 10" long search coil with good parallel surfaces was used (10" x 0.4" glass bobbin with 40 turns) for the measurement of the magnetic and gradient lengths. The output of this search coil was compared with another fixed standard as in the case of the Xo(x) measurement.

We set the moving search coil parallel to the z-axis so that it covered from 3" inside to 7" outside with reference to the lamination end, thus, measuring $\int_{-7''}^{3''} B(x,z)\,dz$. The origin of z-axis is at the lamination end and it is positive to the inside. Then we measured $\int_{-6''}^{4''} B(x,z)\,dz$ by moving the coil one inch into the magnet. As we can see later $z=+3''$ is well inside the uniform magnetic field region and $z=-6''$ is practically outside the magnetic field of the magnet. Therefore, $\Delta L_B'(x)$ in inches was given by

$$\Delta L_B'(x) = \left\{\int_{-7''}^{3''} B(x,z)\,dz \Big/ \int_{3''}^{4''} B(x,z)\,dz\right\} - 3'', \tag{21}$$

where

$$\int_{3''}^{4''} B(x,z)\,dz = \int_{-6''}^{4''} B(x,z)\,dz - \int_{-7''}^{3''} B(x,z)\,dz.$$

For the measurement of $\Delta L_G'(x)$, we moved the search coil radially at 3" and 4". By keeping the radial displacement Δx constant (Δx=0.200"), the gradient length in inches $\Delta L_G'(x)$ was given by

$$\Delta L_G'(x) = \frac{\int_{-7''}^{3''} B\left(x+\frac{\Delta x}{2}, z\right)dz - \int_{-7''}^{3''} B\left(x-\frac{\Delta x}{2}, z\right)dz}{\int_{3''}^{4''} B\left(x+\frac{\Delta x}{2}, z\right)dz - \int_{3''}^{4''} B\left(x-\frac{\Delta x}{2}, z\right)dz} - 3'', \tag{22}$$

Figs. 5 and 6 give the distributions of $L_B'(x)$ and $L_G'(x)$ with final hard packs for both magnets. The designed usable regions at the hard packs, which is narrower on the outer side than that determined from the Xo(x) distribution due to the shifting of the central orbit, are shown in these graphs. It can be seen that our requirements are well satisfied in these regions. These data were taken at 7.5 and 15 Gev excitation. We observed a slight saturation effect at the hard packs in L_B' and L_G', which starts at 10 Gev. L_B' and L_G' shrink in by 13 mils with a wide gap magnet and 50 mils with a narrow gap magnet at 15 Gev Distributions seem unaffected. This effect is due to the side surface of the hard packs which stick out of the surface of the coil. Therefore the narrow gap magnet shows a bigger effect (i.e. about 0.1% in L_B and L_G at 15 Gev). Also in Fig. 6 is shown $L_G'(x)$ of the uncorrected original hard pack.

Table II: Measured L_B and L_G at the center at 7.5 Gev

Magnet	L_{GO}	L_B	L_G	L_B-L_G
Wide Gap	126.48"	127.21" $\pm$ .02"	125.99" $\pm$.04"	1.22"
Narrow Gap	126.48"	127.17" $\pm$ .02"	126.09" $\pm$.04"	1.08"

In Table II is given the values of L_B and L_G at 7.5 Gev with their estimated errors of the measurement for both types of magnets.

Actually there are apparently bigger errors due to manufacturing The errors in L_B and L_G due to this is estimated to be $\pm$40 mils and $\pm$ 110 mils respectively. The thermal expansion of the magnet is of the order of 2 mil/C° for the temperature change of the cooling water.

The final shapes of the hard packs are shown in Fig. 7 and 8. Both sides of the pole pieces are tapered to accept the inside corners of the coils. The inclination of the pole pieces are punched out successively by a die which has two circular shapes of 1" radius connected with a straight line tangentially. The same die is used for both types of hard packs. To keep the same magnetic length and to use the same lamination stacking length in both types of magnets it was necessary to cut back the inclination of the hard packs of the wide gap magnet by about 0.36 inches more than for the narrow gap magnet.

The fringing fields with the final hard packs were measured at 2.5 kG AC excitation by the same technique as used before with two small search coils. The curves are shown in Fig. 9 and 10. The gradients of the fringing fields were obtained by taking the difference between two adjacent points in the radial direction. Figs. 11 and 12 show the gradients for both magnets. They show clearly how the field and gradient distributions are changed to meet our requirements.

References

1. P. N. Bredesen and P. C. Stein, CSDS-24, October 11, 1965
2. D. A. Edwards, CSDS 25 in press.
3. H. Nysater, CEA-29, April 16, 1957

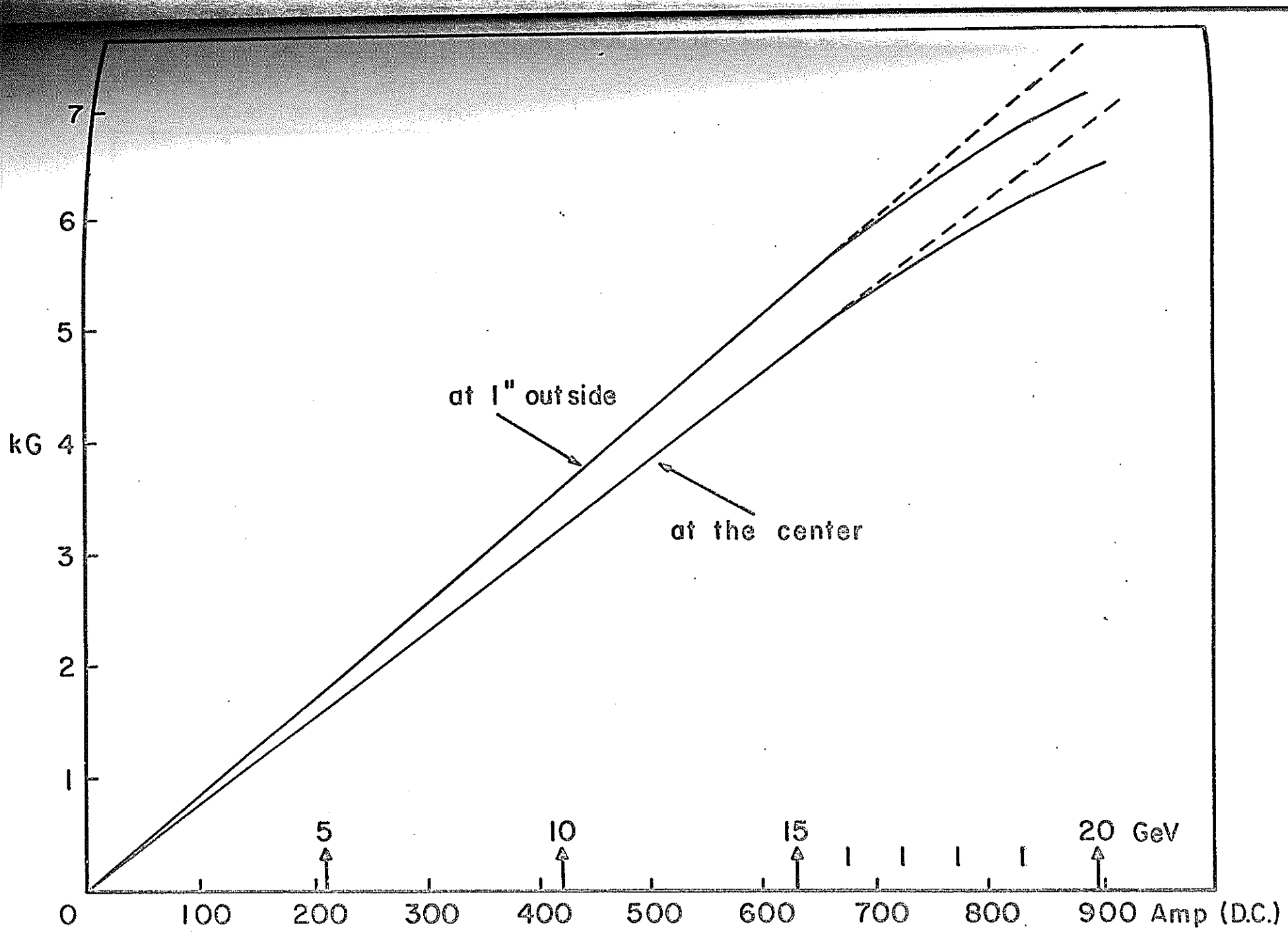

Fig. 1 Excitation Curve of Narrow Gap Magnet

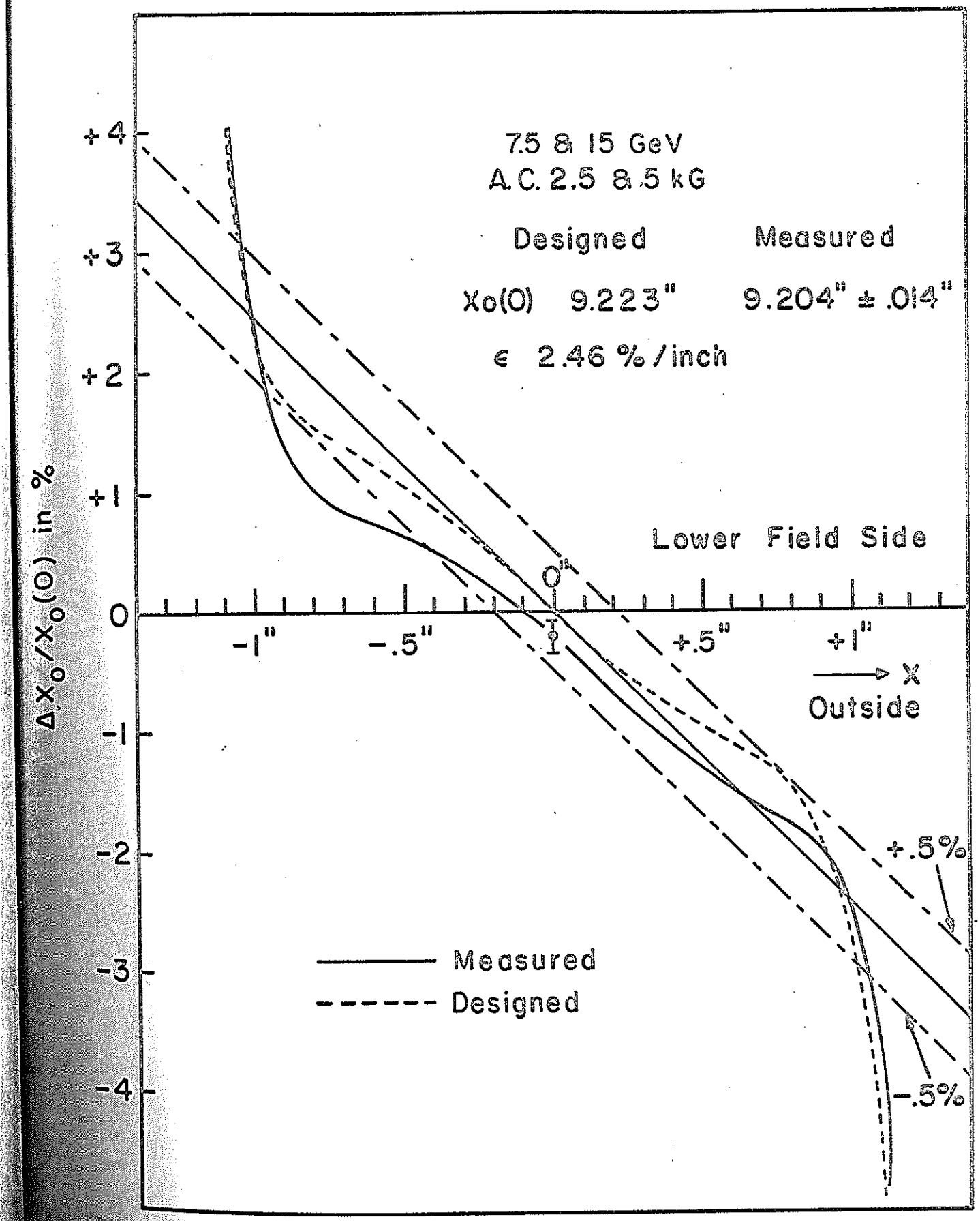

Fig. 3 $X_0(x)$ Distribution of Wide Gap Magnet

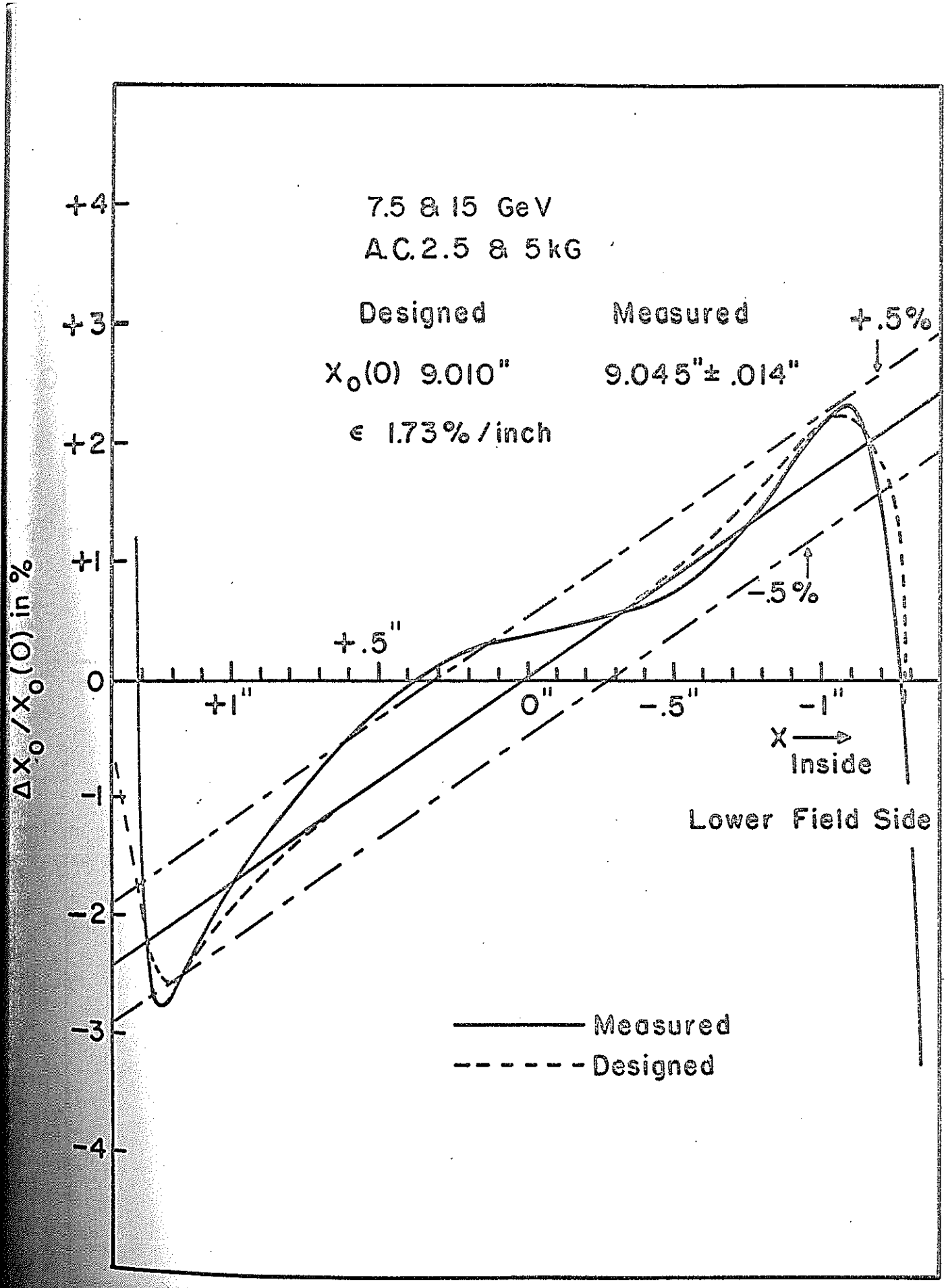

Fig. 4 $X_0(x)$ Distribution of Narrow Gap Magnet

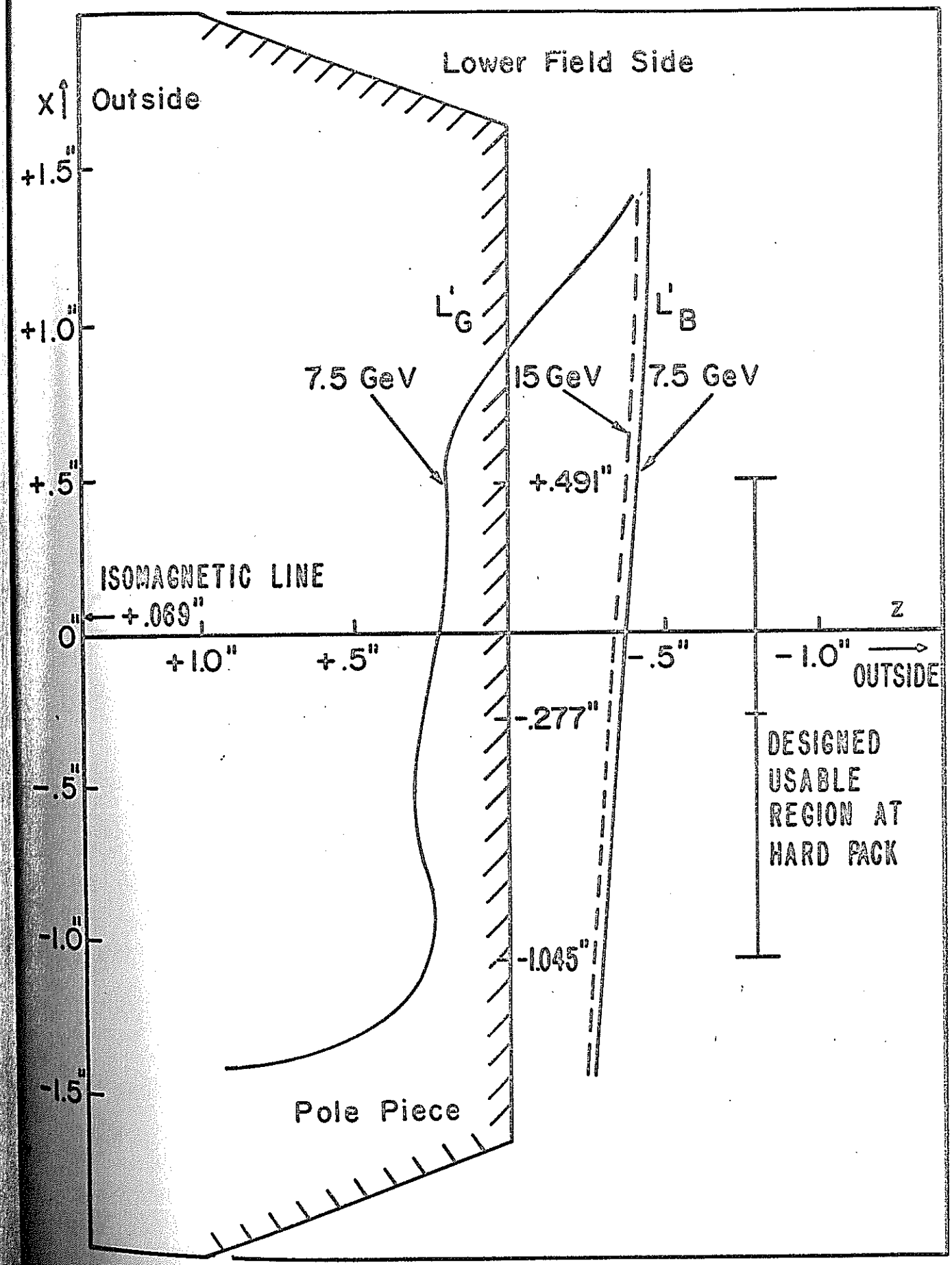

Fig.5 L'_B and L'_G of Wide Gap Magnet

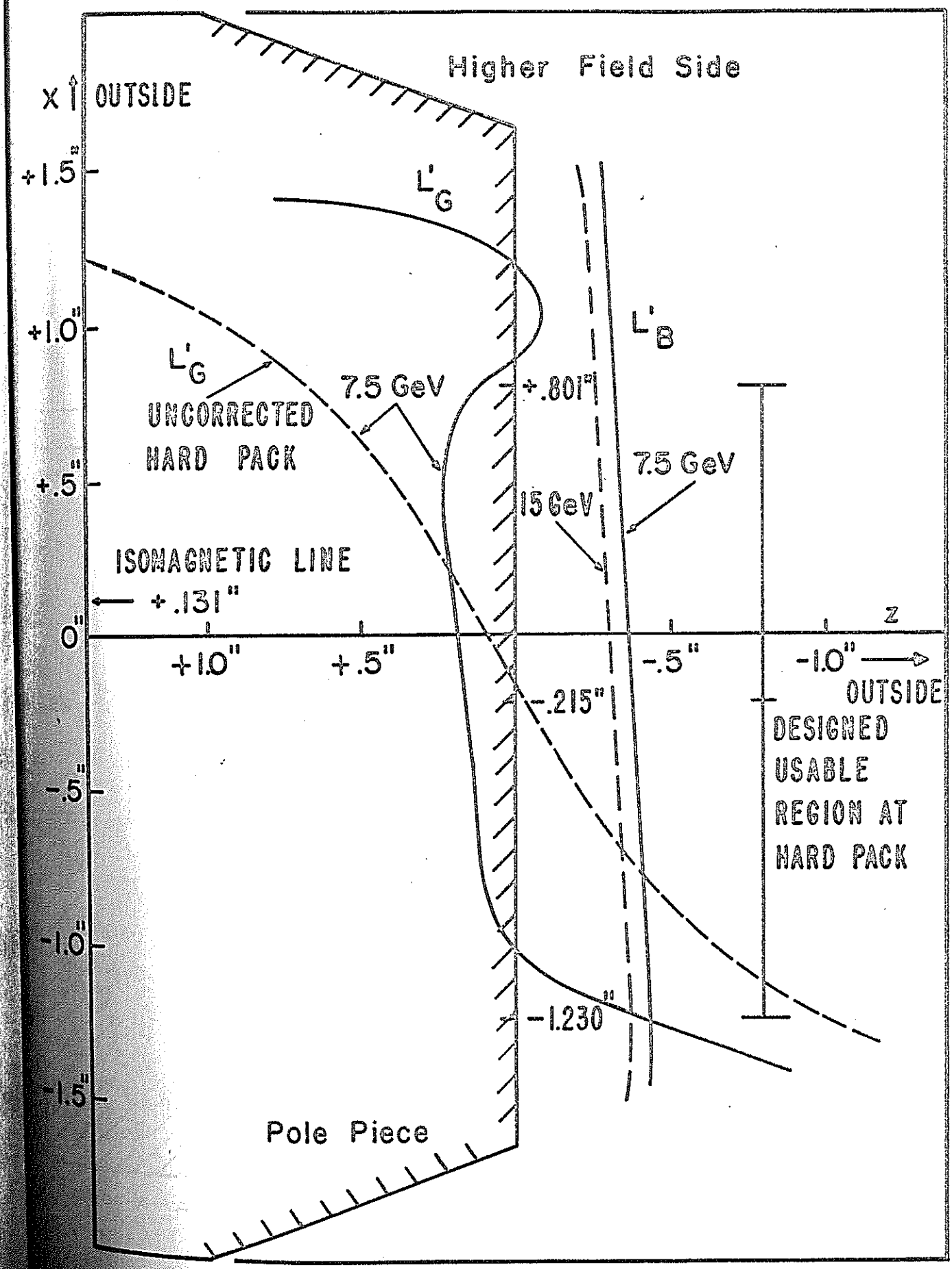

Fig.6 L'_B and L'_G of Narrow Gap Magnet

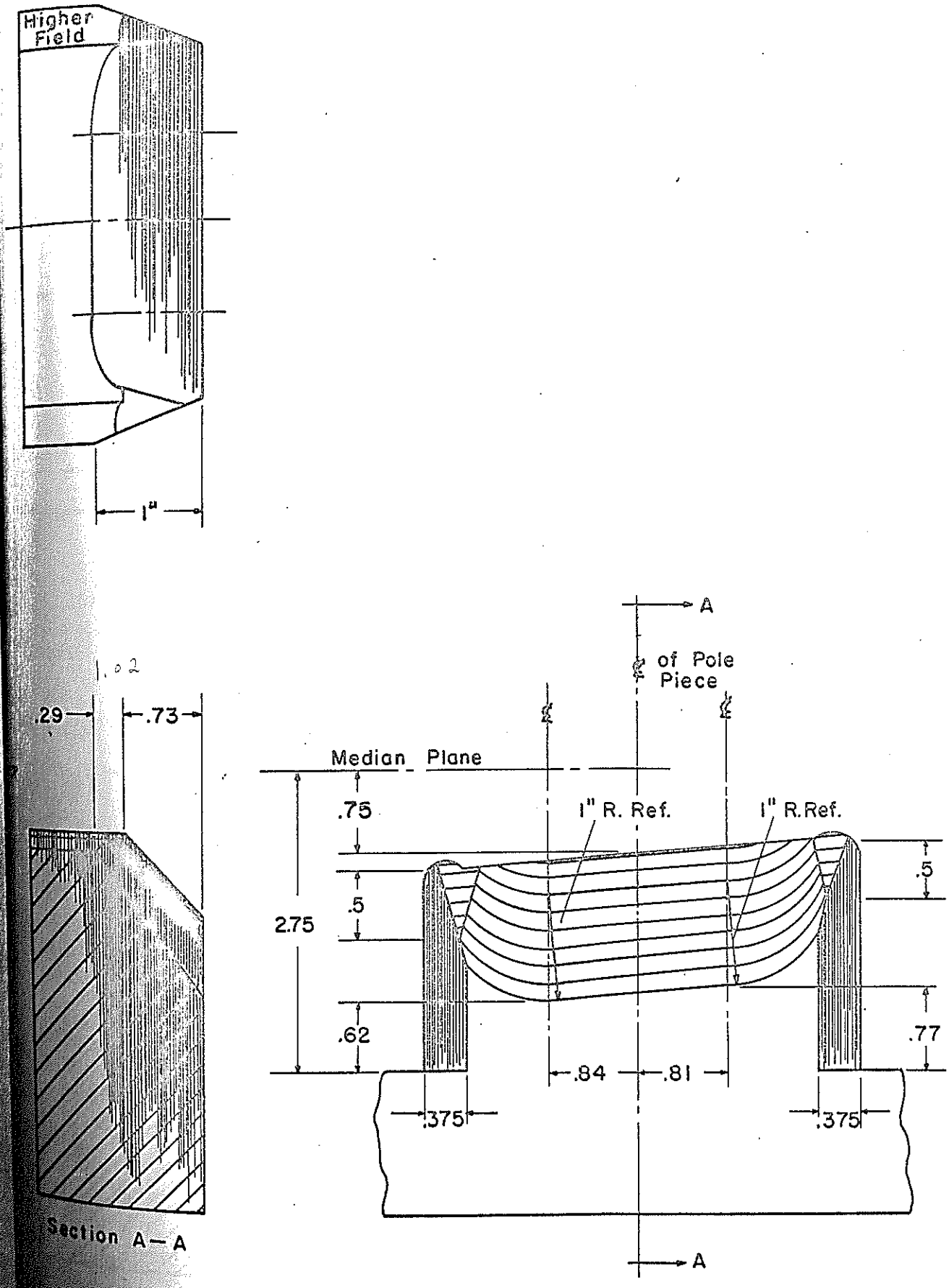

Fig. 7 Hard Pack of Wide Gap Magnet

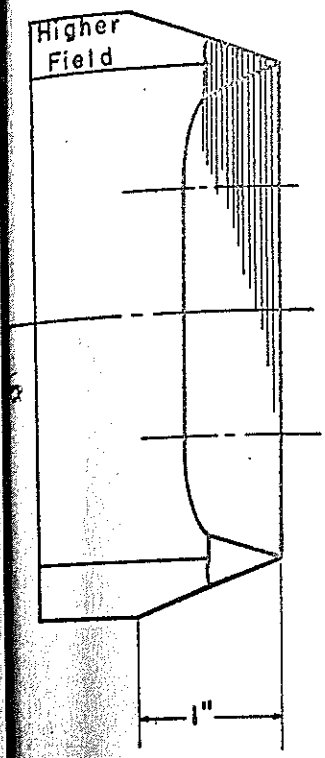

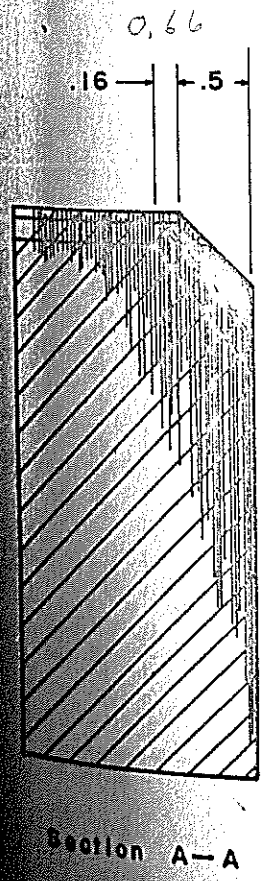

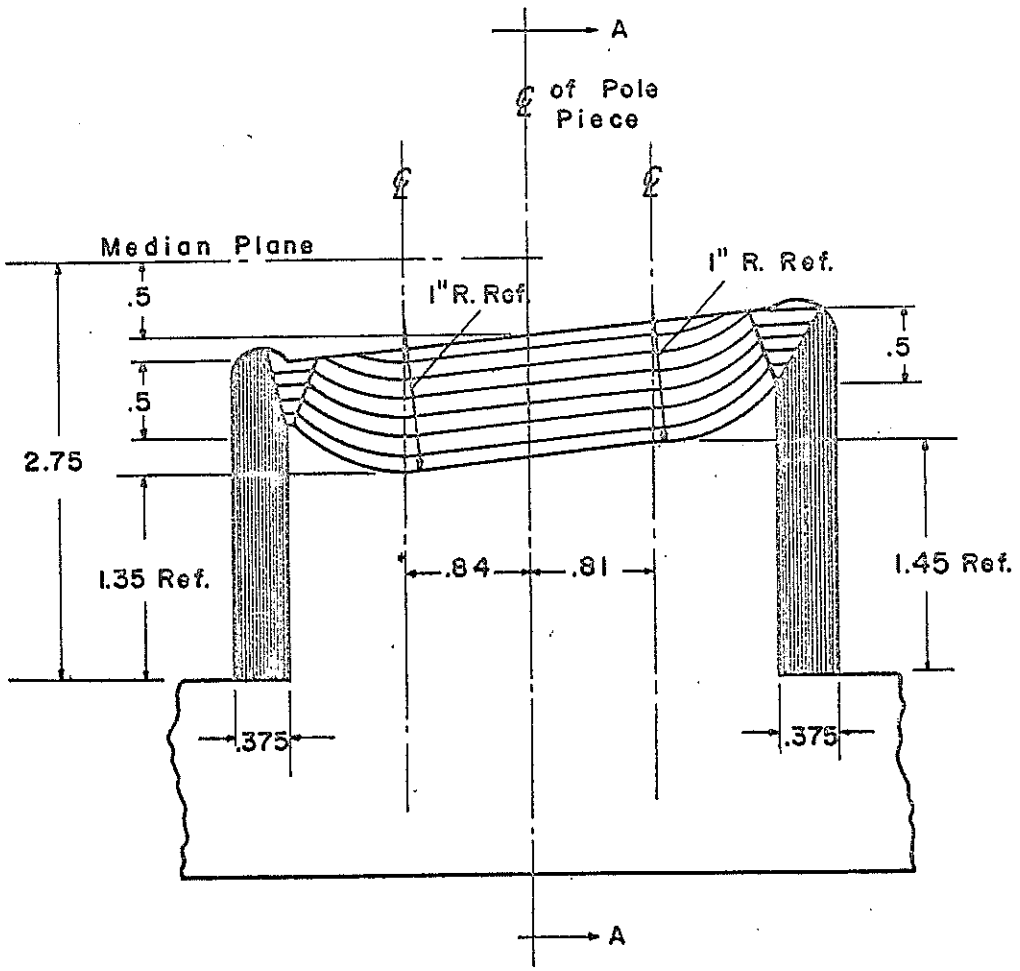

Fig. 8 Hard Pack of Narrow Gap Magnet

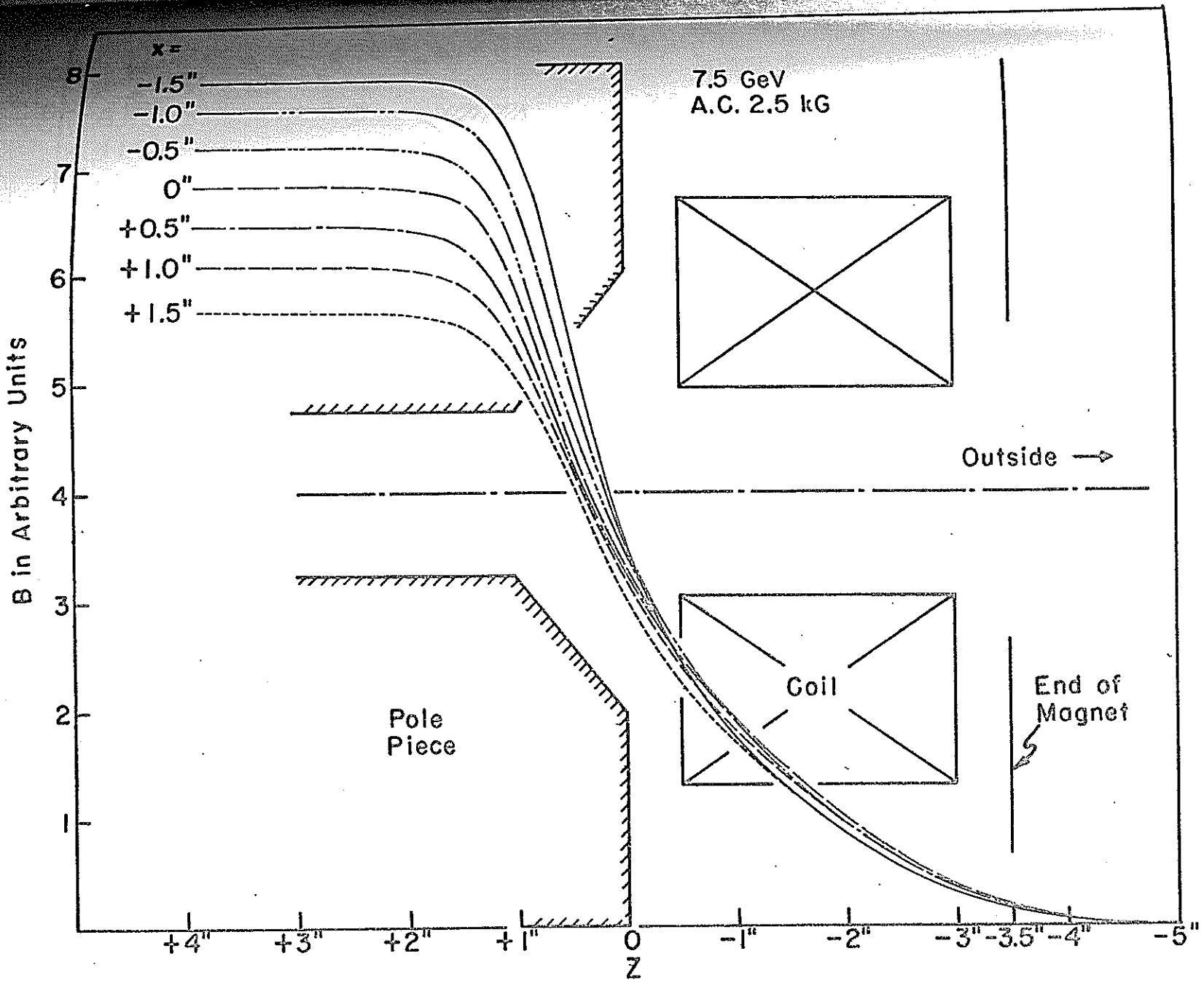

Fig. 9 Fringing Field of Wide Gap Magnet

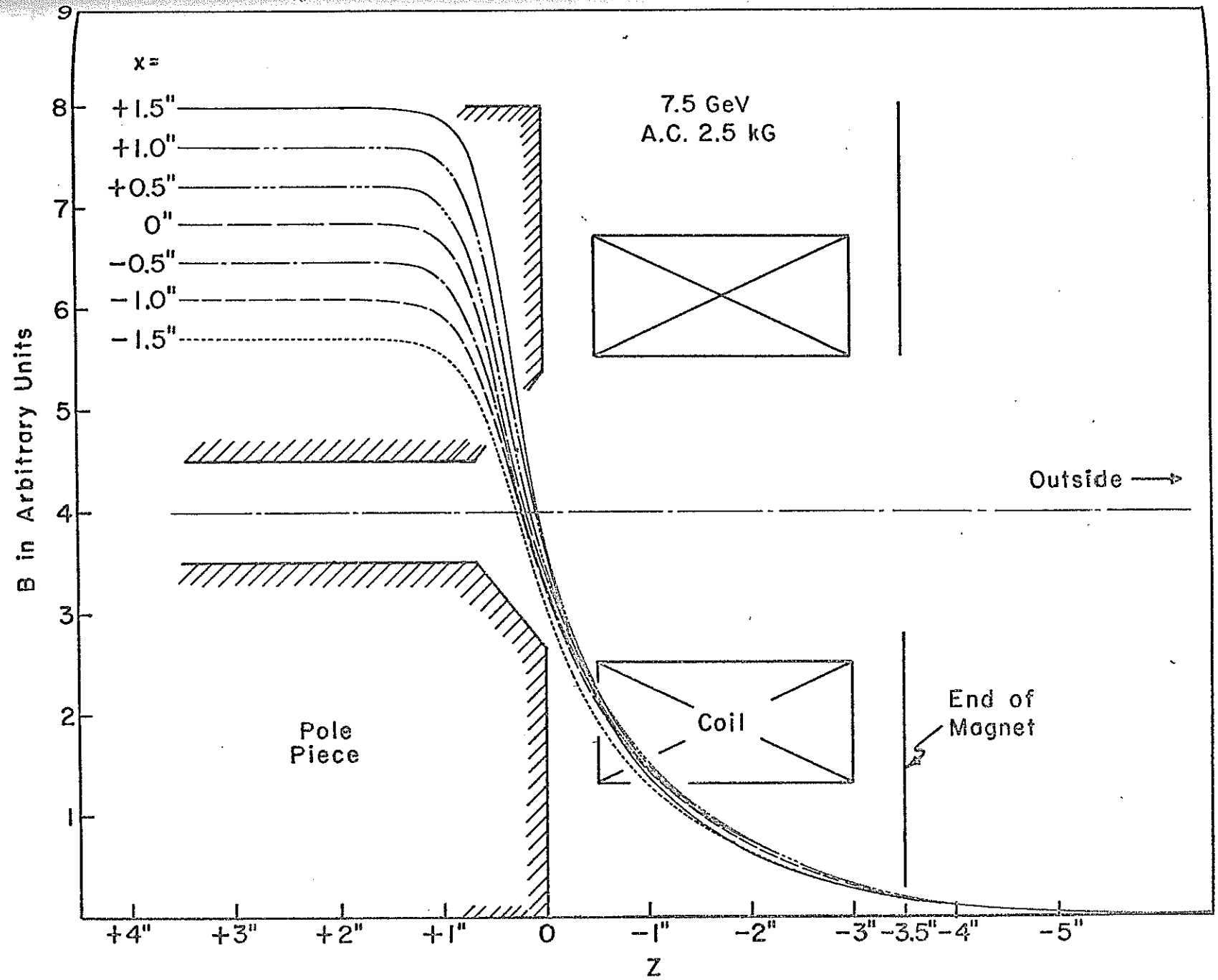

Fig. 10 Fringing Field of Narrow Gap Magnet

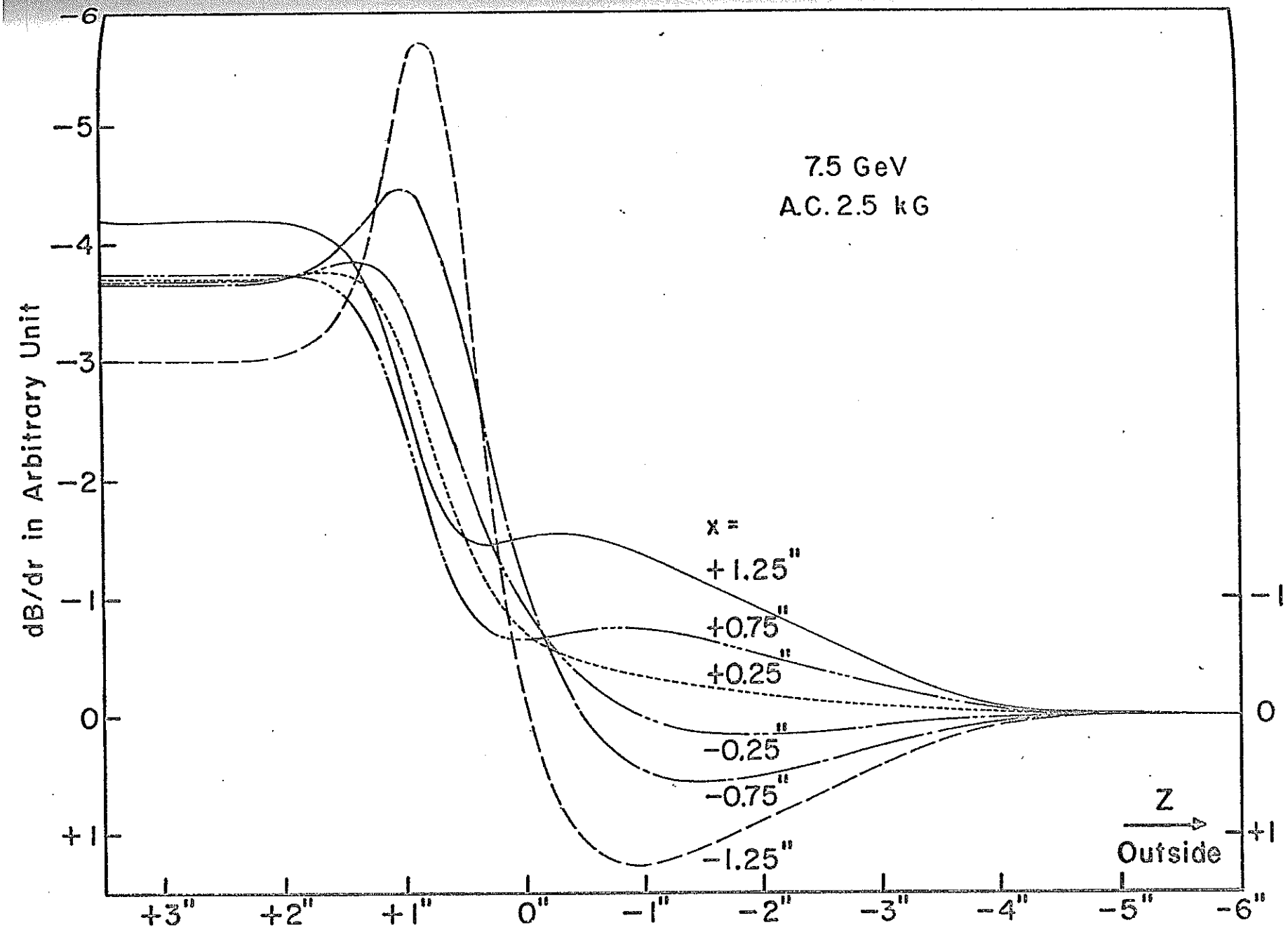

Fig.11 Gradient of Fringing Field of Wide Gap Magnet

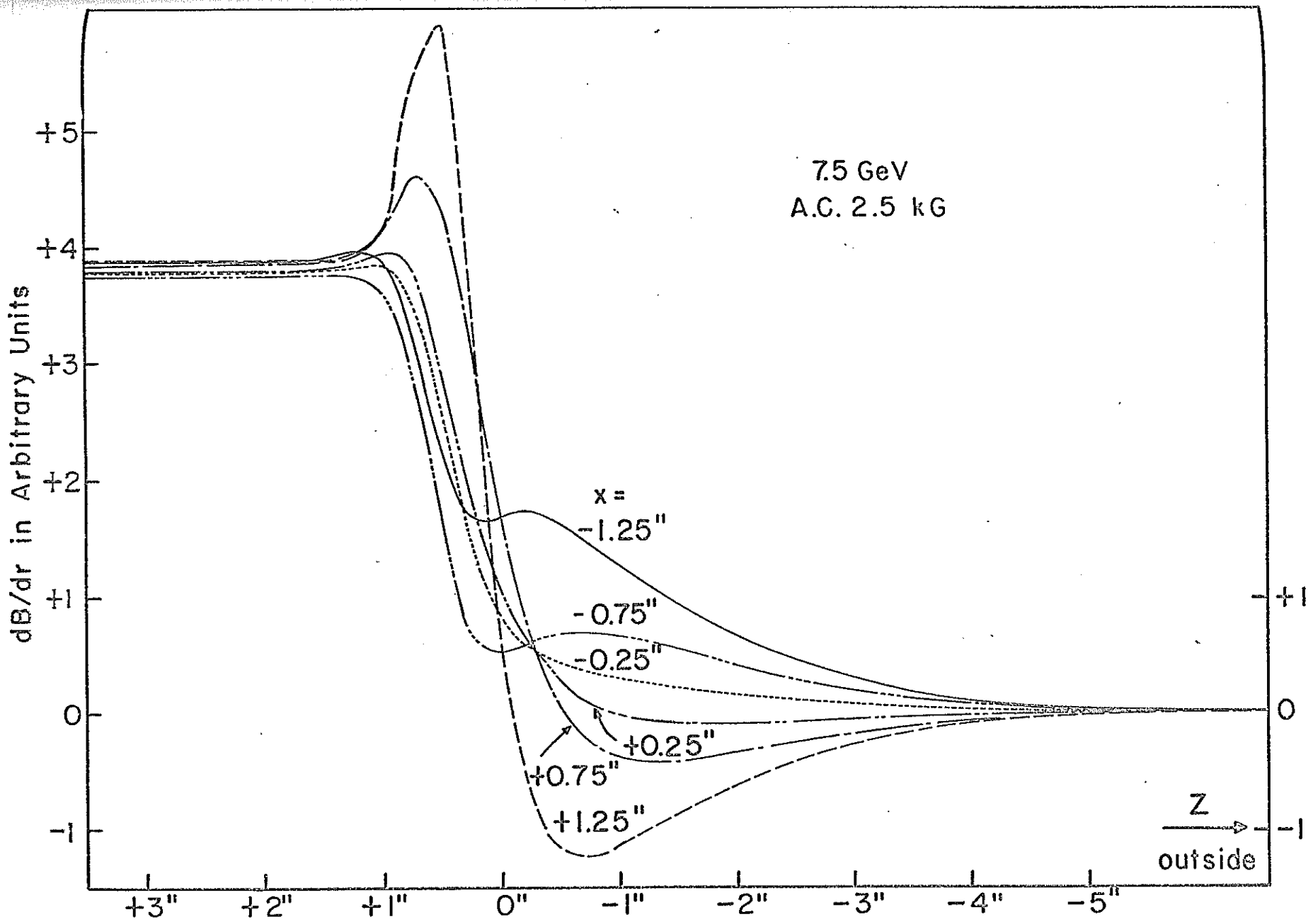

Fig. 12 Gradient of Fringing Field of Narrow Gap Magnet

CS-32
M. Tigner
March 6, 1967

Accelerating System for the Cornell 10 GeV Electron Synchrotron *†

Summary

A system consisting of four lengths of iris loaded waveguide, each driven by an adjacent klystron amplifier, is described. These waveguides which serve as the accelerating elements for a 10 GeV electron synchrotron are operated in the $2\pi/3$ traveling wave mode at 714 MHz. The amplifiers have a common power supply and are driven from a common source which can be synchronized with the injector, a 150 MeV linac.

General Design Considerations

In order to capitalize on the economy and simplicity of low field magnets and to minimize the amount of synchrotron radiation to be endured, the largest possible diameter of the synchrotron, consistent with reasonable real estate requirements, was chosen. The resultant circumference of the ring is about one half mile, giving a radius of curvature for the orbit of 328 ft. This dimension combined with the desired peak beam energy, the choice of 60 Hz sinusoidal magnet excitation and 150 MeV injection energy dictates the energy gain per revolution that is required of the accelerating system. This requirement is shown for three peak energies in Fig. 1.

To meet this demand there are obvious advantages in using a scaled up version of the type of system first used at CEA[1] and later, with variations, at DESY[2] and NINA[3]. These systems are of proven practicality, they give uniform acceleration over the orbit and presumably there are manufacturers poised and ready to reproduce what has been done before without substantial costs for new development and tooling. It turns out, however, that such a system for our application would be rather more complex and costly than necessary. We can effect substantial savings by being able to lump together all the accelerating apparatus at a few places around the ring. The long field free regions necessary to do this are made possible by the use of that great boon to the synchrotron industry, the Collins insertion[4], as modified and extended by D. A. Edwards[5]. This lumping together of many individual accelerating units eliminates at a stroke most of the termination, coupling and monitoring hardware which accompanies the distributed systems and which is, as every rf buff knows, sinfully expensive. The practical length of field free regions, the shunt impedance of reasonable structures, the power levels of available tubes and the required uniformity of acceleration led us to opt for four accelerating stations placed around the ring as shown in Fig. 2. The accelerating units themselves, which we call "synacs"[6], are about 15 ft. in overall length, the usable field free region being about 18 ft. in length. The extra space is used for pumping, correction coils, monitors, etc.

As shown in the layout the power amplifiers are placed adjacent the synacs thus avoiding long, costly and not lossless feed lines. Operating experience with present and past synchrotrons at Cornell has not indicated that any significant advantage is gained by being able to service the amplifiers while the synchrotron is running. As chosen, the system automatically has the advantage that the units can be run individually or in any combination giving a high degree of flexibility. It is interesting to note that with

only one unit operating a peak beam energy of 5 GeV is possible.

The Accelerating Structures

Choice of Operating Frequency

Considerations of shunt impedance, beam dynamics, physical size of practical structures, available power sources and problems of fabrication indicate that any sub-harmonic of the linac frequency, 2856 MHz, in the range 450 to 1000 MHz would be satisfactory. Among these the fourth sub-harmonic, 714 MHz[7], was picked as the best compromise. It should be emphasized that any frequency in the range mentioned would probably be satisfactory.

Choice of Structure Type

Straight forward calculation shows that the simplest type of iris loaded waveguide operating in the traveling wave mode will produce the gradients necessary at powers well within reach of readily available tubes. The machining tolerances are also reasonable even at the low group velocity required and several manufacturers are experienced in fabricating this type of structure.

The parameters of the synchrotron require a three inch beam aperture. If the aperture is kept circular, for symmetry of the fields and ease of fabrication, a reasonable iris thickness gives much too high a group velocity.[8 9] Consideration of the alternatives led us to select magnetic coupling between cells as the simplest method of controling the group velocity.

Experience with iris loaded waveguide acceleration in the Cornell 2 GeV synchrotron indicated that synchrotron radiation in the orbit plane is a powerful agent for inducing heavy discharges in the cavities adjacent the iris lips struck by that radiation. In order to obviate this problem a radial slot is cut in each iris extending from the beam hole in the center to a magnetic coupling hole at the periphery. The radiation then strikes in a

region of low electric field. No measurable phase or amplitude assymetry is introduced in the field pattern by the peripheral hole and slot combination.

$2\pi/3$ operation was chosen for its slight improvement in shunt impedance, its lower weight per unit length and its decreased tendency to multipactoring as compared to a $\pi/2$ structure. Because of the relatively low fields necessary it was decided to use a constant impedance structure to cut down the necessary modeling and simplify fabrication.

Table I lists the measured electrical properties of the synacs each of which is composed of 32 unit cells or cavities. Figure 3 shows a unit cell of the final structure with its dimensions. Using the parameters of the synac in the standard way the power required to excite each synac for 10 GeV peak beam energy can be easily computed. The result is shown in Fig. 1. The beam current used was 7 mA which corresponds to a beam of 10^{11} electrons. The back voltage induced by such a beam is about one MeV around the ring.

In our synac structure the $v_p = c$ line intersects the Brillouin diagram for the TM_{11} hybrid mode just beyond the π point. It is not known however whether this feature is necessary or even helpful in synchrotron operation. No problem caused by the excitation of such a mode has been encountered in the Cornell 2 GeV machine.

Fabrication

OFHC copper forgings form the basic units of the structure. After finish machining the forgings are stacked vertically in sub-assemblies of nine cells each. The stacks which are about 50 inches long and weigh about 600 lb. are then brazed in a dry hydrogen atmosphere. Each sub-assembly is terminated by a stainless steel bolt flange. These sub-assemblies are bolted together end to end, three to a synac. At each end a coupler consisting of two and one half unit cells is fastened in the same manner to

complete the synac.[10]. The vacuum seal at the bolted iris coupling to a short length of WR 975 rectangular waveguide is used. The vacuum seal is made by an o-ring gasketed fused quartz slab window. A waveguide to coax adaptor is bolted over the window, power being fed in on 4 1/2 inch rigid coaxial line. The output is terminated in a 3 1/2 inch coaxial water load. Fig. 4 is a photograph of a completed synac.

Cooling and Temperature Control

Cooling is accomplished by circulating 400 gpm of water through an external water jacket. The temperature of the water is regulated to $\pm$1/2° C by a primary-secondary loop circuit utilizing standard commercial servo control elements.

Vacuum

At present the pumping is done by low backstreaming oil pumps at each end. The capacity of each pump is 300 l/s, achieving a pressure of 3×10^{-7} Torr at the center of the synac.

Tuning

Tuning is done in the spirit of the early work at Stanford[11,12,13] and their techniques are used where possible. Individual cells are tuned by the double plunger and antenna method [14, 15] corrections being effected by deforming the walls of the cell. A correction $\pm$200 kHz can be readily accomplished.

Power Tests

At low power levels multipactoring is encountered when the synac is energized for the first time. After a period of 24 hours or so this multipactoring subsides. Above a power level of about 10 kw peak power sparks seldom occur and last for only a few minutes during conditioning. Full peak power has been applied but long periods of operation at full average power remain to be carried out.

The Transmitter

Selection of the Main Amplifier Tube

A klystron is the natural choice for the main amplifier because of its high gain, proven longevity in the UHF region and relative simplicity. An electron synchrotron with high injection energy is rather insensitive to phase and amplitude fluctuations in the accelerating voltage so very precise control of these parameters need not be considered.

Accordingly the 4KMV 150 LH-1 tube was selected. This tube, fitted with a modulating anode, is commercially rated at 50 kW CW output power. A slight improvement in the gun insulation, however, makes it possible to pulse the tube to 190 kW peak power provided that the average power rating is not exceeded. 190 kW is achieved at about 40 kV beam voltage. In this UHF TV tube then, we have a power source which exceeds our theoretical requirements by a factor of two in both peak and average power.

Modulation

At injection time when most flexibility in the amplitude program is necessary the rf drive is modulated. The power level is so low at that time that high amplifier efficiency is unimportant. Later in the cycle when minimization of power is our goal the mod. anode is used to modulate the current in the tube. The proper waveform is obtained by applying to the mod anode a biased and slightly distorted sinusoid produced by a variac driven transformer and diode distortion network. The tube is shut off at the end of the cycle by a standard tail clipper circuit.

Power Supply, Driver and Protective Circuitry

For simplicity and to assure that beam voltage induced phase variations in the klystron outputs track each other a common power supply is used for the four amplifiers. An auxiliary power supply capable of operating one amplifier at a time is also provided for

testing purposes and to serve as a back-up in case of main supply failure. The power supply is furnished with an ignitron crowbar across its 140 μF capacitor bank to prevent destruction of the amplifiers in case of a fault therein. This crowbar, triggered from a fast body current signal, limits the energy dissipated in any arc to ground to about ten joules as measured by the "tin-foil" test. Protection of the klystron output windows is accomplished by reflected power and optical arc detectors. A signal from either detector switches off rf drive to the klystron in about 5 μs.

The pulsed driver, three tetrodes in series, provides a minimum of 30 db amplification for the one watt CW master oscillator signal. The driver output is split four ways and fed to the klystrons through phase shifters and lengths of 7/8 in. low loss coaxial cable.

Performance

Acceptance tests at the manufacturer's plant[16] indicate that design expectations are well met. Fig. 5 shows a plot of the measured output power from one of the klystrons superimposed on a theoretical curve of the required minimum power for a peak beam energy of 10.4 GeV. Over an eight hour period no significant changes in this output power were observed.

The phase differences between the outputs of the four amplifiers were also measured as a function of time during the cycle. With relative phases set properly at the peak of the cycle the maximum phase difference between the amplifiers occurred during the steeply rising portion of the power waveform and were never more than 4°. The relative phases of any two amplifiers were stable to within $\pm$ 1° during a two hour period.

Table II lists the salient features of the transmitter.

Synchronization and Sub-harmonic Modulation

To achieve the highest capture efficiency possible the linac must be phase locked to the synchrotron accelerator and the linac

beam modulated at the synac frequency. Fig. 6 shows the rf drive chain being built to accomplish the phase lock and to drive the sub-harmonic beam modulator. The diagram is self explanatory with the exception of the provision for frequency modulation. This is added to compensate for the usual drifts in the injection frequency requirement and to enable us to drive the synac off optimum frequency to combat possible beam induced voltage effects at injection time.

Various methods of sub-harmonic modulation of the beam are being investigated. The three methods receiving most attention are: 1) Prebunching of the beam by a small gap cavity driven at the synac frequency followed by bunching at the fundamental; 2) Chopping of the beam by sweeping it across a slit at 714 MHz followed by pre-bunching at the linac frequency; 3) Direct modulation of the electron gun. Method (2) will probably be the first one installed for reasons of expediency.

Acknowledgments

It is a great pleasure to acknowledge the vital contributions of several experts to the design of the synac. Dr. G. A. Loew and O. Altenmueller of SLAC gave a great deal of indispensable help and went so far as to make S-band models to check various properties of the structure. W. J. Gallagher of the Applied Radiation Corporation also gave much valuable help in the design and modeling especially as regards the magnetic coupling. Of course any blunders are in spite of, rather than because of, the good offices mentioned.

References

* Work performed under contract to the United States National Science Foundation.

1. CEA-81, Cambridge Electron Accelerator, Cambridge, Mass.
2. G. Schaffer, IEEE NS-12, 3 p 208, 1965
3. DNPL-1, Daresbury Nuclear Physics Lab., Daresbury, England
4. T. Collins, CEA-85, Cambridge Electron Accelerator, Cambridge, Mass.
5. D. A. Edwards, CSDS-25, Lab of Nuclear Studies, Cornell University, Ithaca, N. Y.
6. This name, coined by R. R. Wilson, is an acronym for synchrotron accelerator.
7. The actual frequency, adjusted for the exact design orbit circumference is 713.939 MHz.
8. M. Chodorow et al, Rev. Sci. Inst. 26, 2 p. 134ff., 1965
9. A. Eldredge et al, SLAC-7 Stanford Linear Accelerator, 1962
10. Waveguide and coupler sections have been made by both Litton Industries Linear Beam Division and Applied Radiation Corp. as well as at Cornell.
11. Ibid. 8
12. Ibid. 9
13. W. J. Gallagher, M-205, W. W. Hansen Laboratories of Physics, Stanford University, 1960
14. P. B. Wilson, private communication
15. T. Nishikawa, 1964 Linac Conference, Midwestern Universities Research Association
16. The transmitter was supplied by Continental Electronics Mfg. Co. J. E. Doherty was the project engineer.

† Presented to National Accelerator Conference, March, 1967.

Table I

Synac Parameters

$\left(\frac{r}{Q}\right)_{\frac{2\pi}{3}} \simeq 12.2 \ \Omega/cm$

$Q \simeq 23.8 \times 10^{3}$, less 10% in the junction cavities

$\alpha \simeq .16$ neper/meter

$L \simeq 4.48$ meter

$V_g/c \simeq 2.1 \times 10^{-3}$

Table II

Transmitter Parameters

Total average RF power output	200 kw
Total peak RF power output	760 kw
Number of final amplifiers	4

Tube type – 4KMV150LHI

Minimum power gain	40 db
Maximum beam voltage	40 kv
Nominal efficiency	35%
Control – modulating anode	

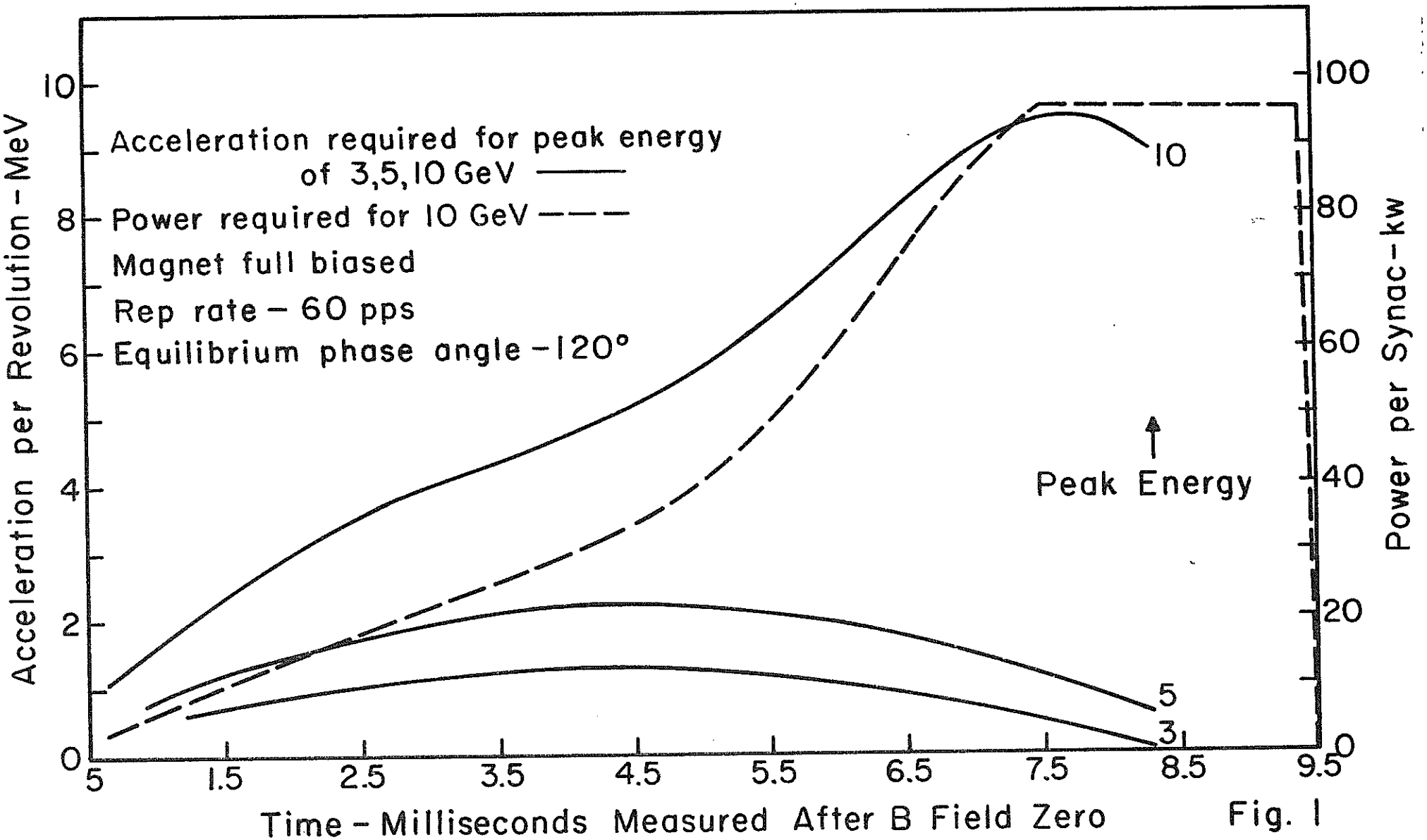
Acceleration required for peak energy of 3,5,10 GeV
Power required for 10 GeV
Magnet full biased
Rep rate – 60 pps
Equilibrium phase angle – 120°
Peak Energy
10
5
3
Acceleration per Revolution – MeV
Power per Synac – kw
Time – Milliseconds Measured After B Field Zero
0
2
4
6
8
10
0
20
40
60
80
100
5
1.5
2.5
3.5
4.5
5.5
6.5
7.5
8.5
9.5

Fig. 1

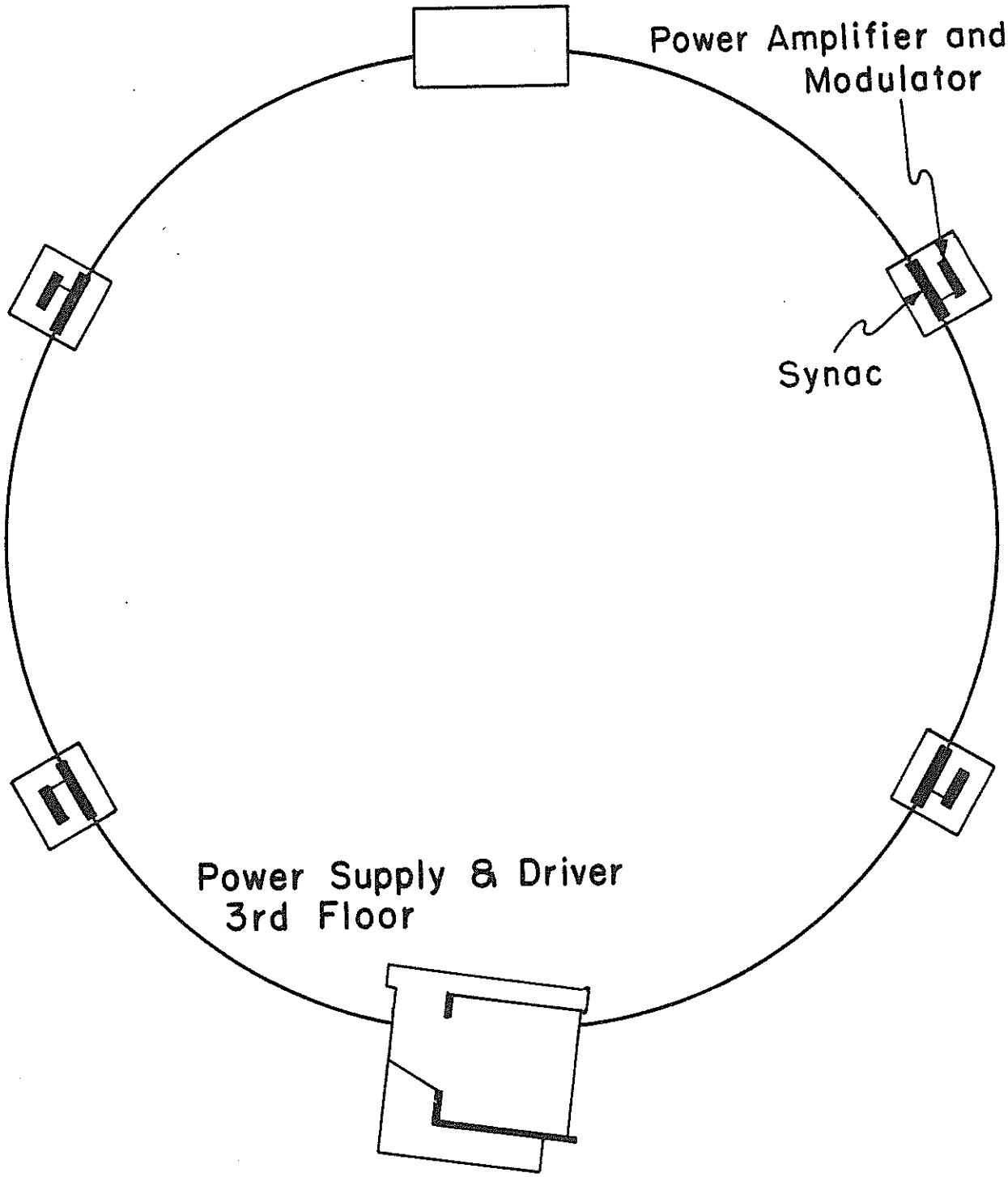

Component Layout

Fig. 2

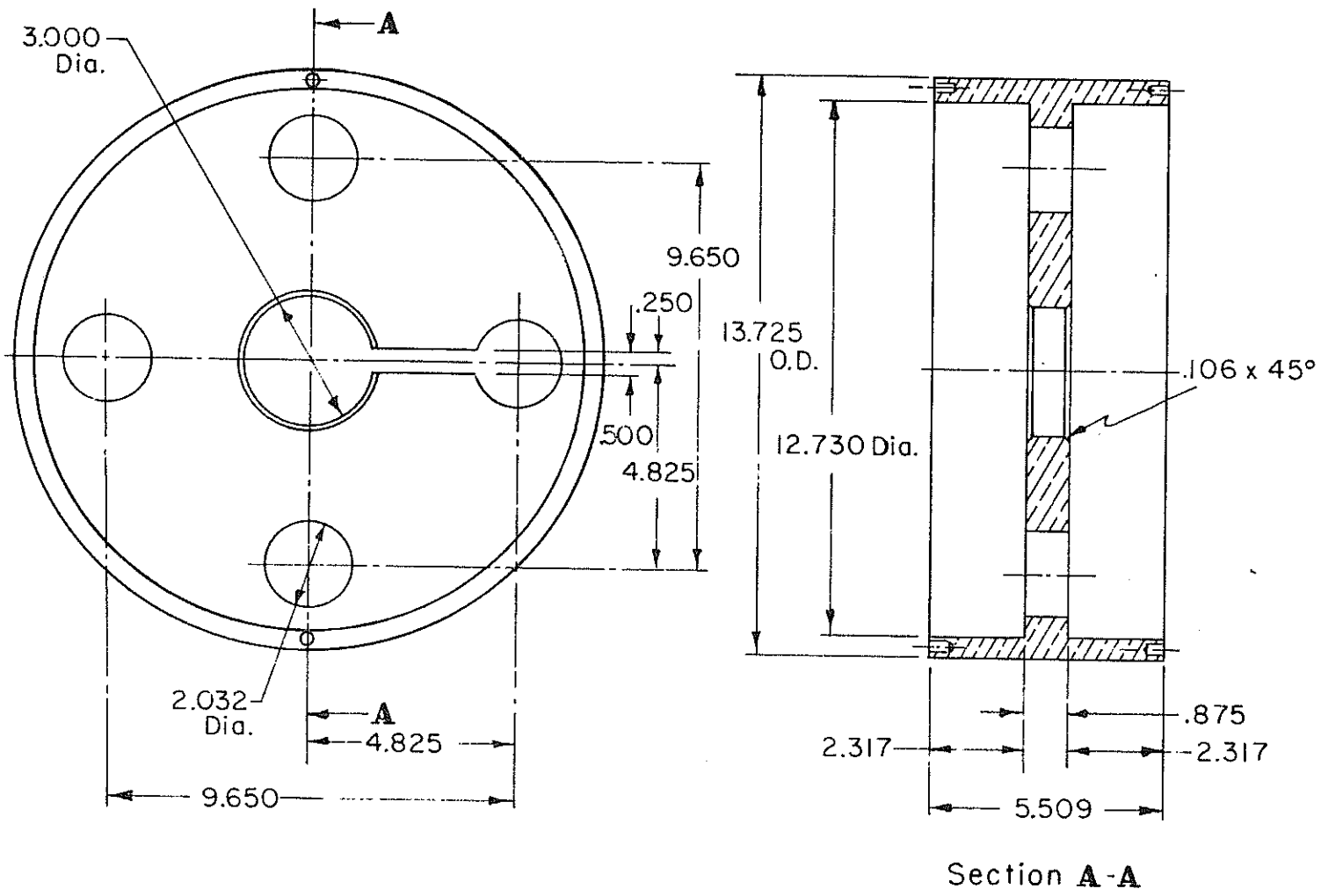

Fig. 3 Synac Unit Cell

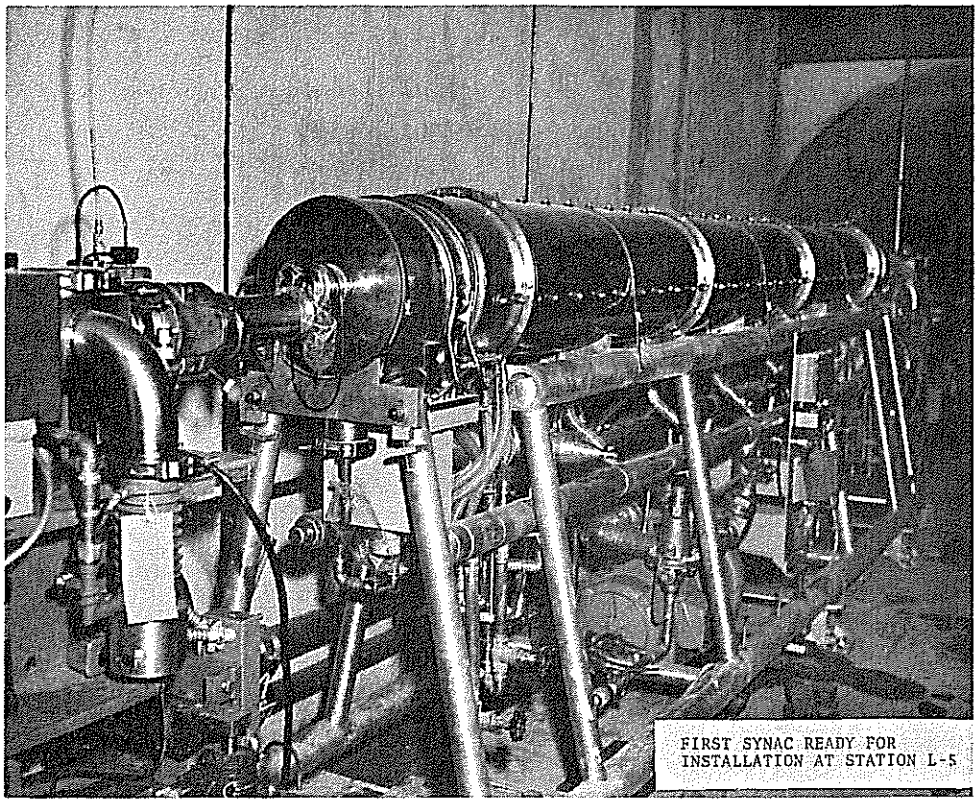

FIRST SYNAC READY FOR INSTALLATION AT STATION L-5

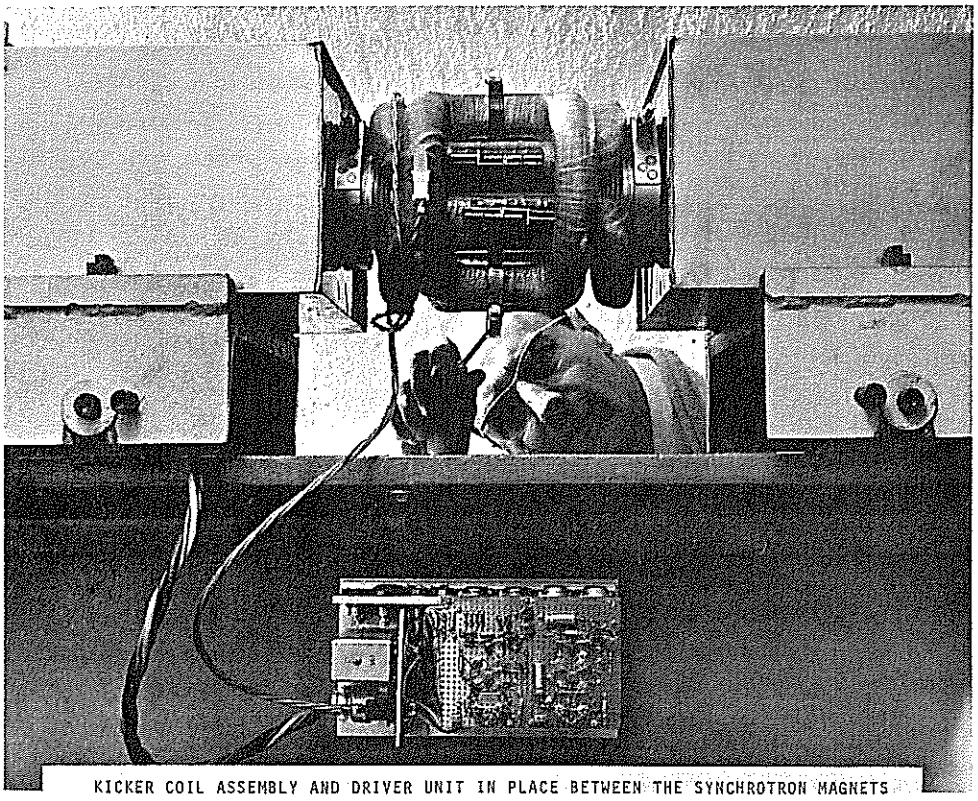

KICKER COIL ASSEMBLY AND DRIVER UNIT IN PLACE BETWEEN THE SYNCHROTRON MAGNETS

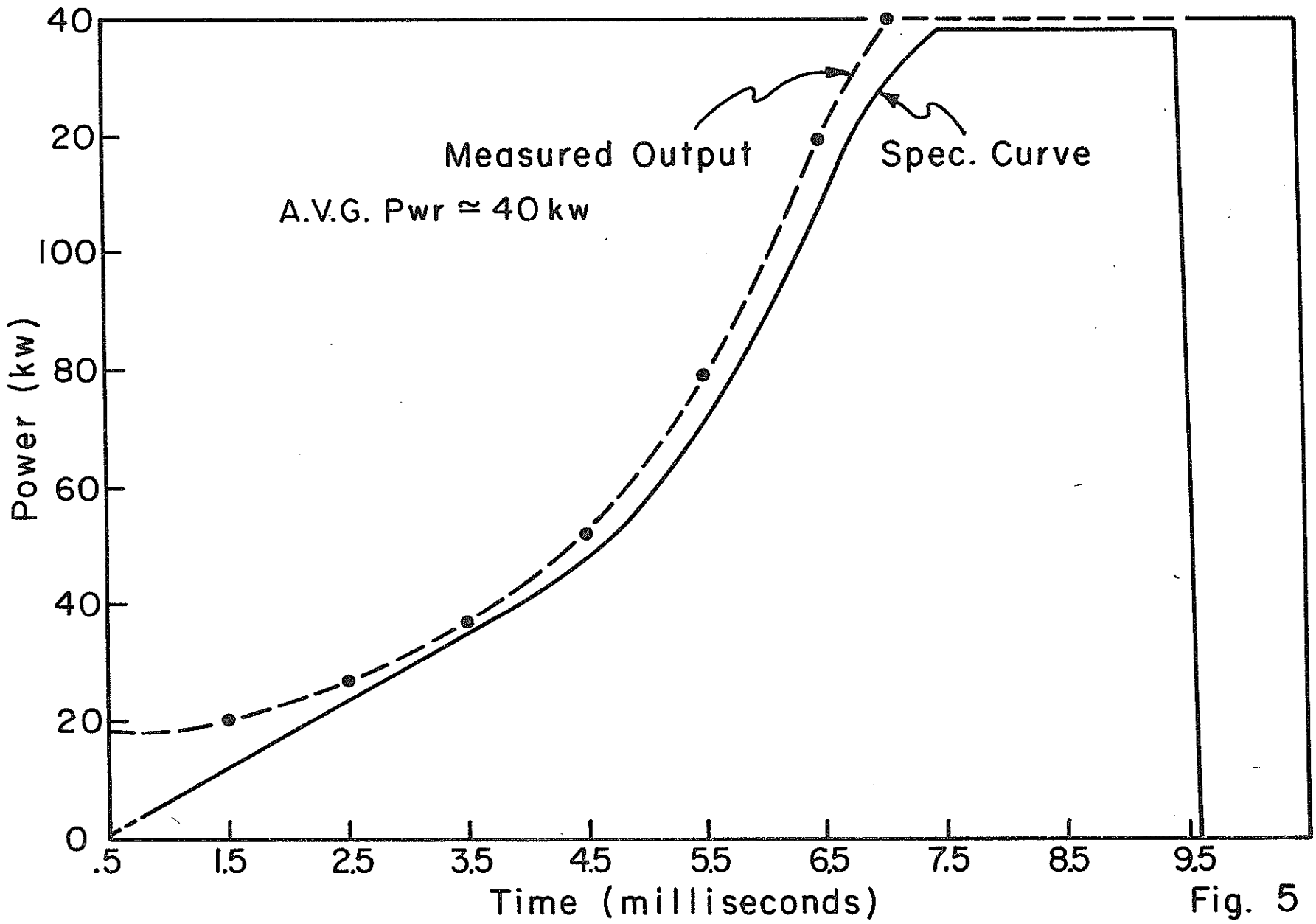
40
20
100
80
60
40
20
0
Power (kw)
Measured Output
Spec. Curve
A.V.G. Pwr ≃ 40 kw
.5
1.5
2.5
3.5
4.5
5.5
6.5
7.5
8.5
9.5
Time (milliseconds)

Fig. 5

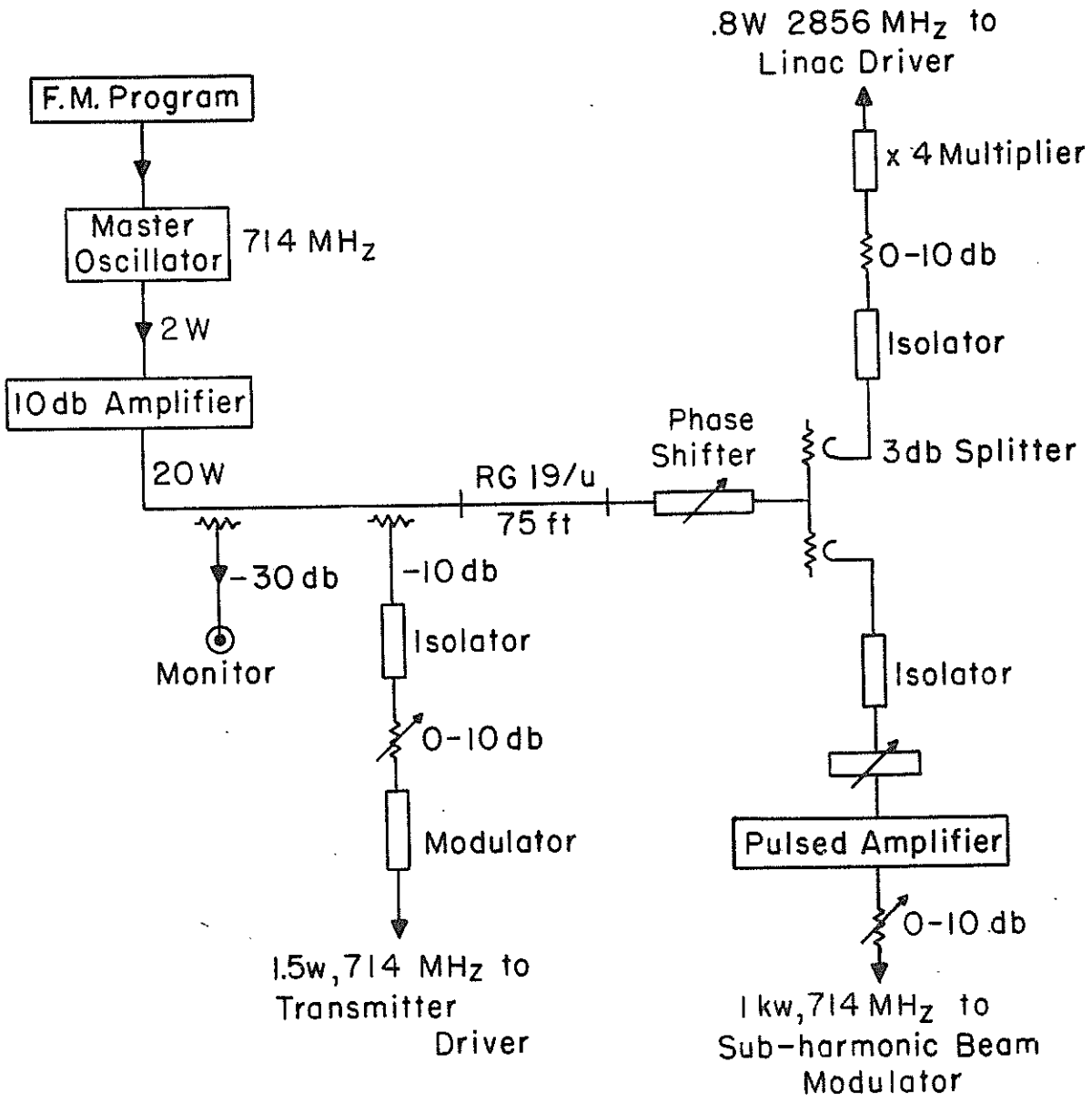

Fig.6 Injector-Synchrotron RF Synchronization Chain

Laboratory of Nuclear Studies
Cornell University
Ithaca, New York

THE 10 TO 20 GEV CORNELL ELECTRON SYNCHROTRON

Table of Contents

Laboratory of Nuclear Studies
Cornell University
Ithaca, New York

CS-33
R. R. Wilson
May 1, 1967

THE 10 TO 20 GEV CORNELL ELECTRON SYNCHROTRON

1. Introduction

The National Science Foundation awarded a contract to Cornell University on April 4, 1965 for the construction of a 10 Gev electron synchrotron. The synchrotron itself has now been built and preliminary tests have been made at low energy. Injection studies were initiated on March 1, and the first synchrotron acceleration was observed March 19. At present, May 1, an energy of over 1 Gev has been reached without trouble. We are limited at present because the Experimental Hall is not finished so that the magnet is powered by a flimsy temporary source. The building will be finished late this summer and as our permanent source of power becomes available we should be able to raise the energy toward its design value of 10 Gev. It is significant though that one Gev can be achieved easily - essentially without the use of any of the corrections or adjustments built into the machine. Our only difficulty so far has been with residual magnetism which was not automatically removed by the low-excitation a.c. field.

The present report is largely a revision and up-dating of CS DC-26 which was written two years ago when the construction of the synchrotron was authorized.

2. Tunnel and Buildings

The tunnel for the synchrotron magnet is located about 40 ft. under the Upper Alumni Athletic Playing Field at Cornell University, and is roughly 800 ft. in diameter. The bore of the tunnel is 10 ft. and the concrete floor is 7.5 ft. from the top of the bore - the walls consisting of gunite concrete that are about 5" thick. For the purpose of attaching things to the walls, there are vertical steel channels (Unistruts) embedded in the concrete at intervals of six feet. The plan of the tunnel is shown in Fig. 1a, and a typical view within the tunnel is shown in Fig. 1b.

The building is located in Cascadilla Gorge and consists largely of an Experimental Hall which is 100' by 100' but which can be extended if necessary. The Experimental Hall is connected to the tunnel by means of the flares shown in Fig. 1a. The west flare is about 100' long and is shaped to allow beams to traverse the Experimental Hall at almost every point. The ancillary equipment for the synchrotron and the experiments are contained in the three story building that is wrapped around the experimental hall but which is shielded from it by a six foot thick wall.[2]

3. Magnet Design and Construction

The arrangement of the magnets is indicated in plan by Fig. 1a and a cross section of one of the magnets is shown by Fig. 2. The orbit radius is very close to 100 meters and there are six straight insertions, two of which are 40' long and four of which are 20' long. Around the ring, there are 192 magnets each of which is about 11 1/2 ft. long - the separation between the iron of the magnets being 18.5 inches (for exact parameters see Sec. 21). The gap of the magnet follows the undulating size of the beam characteristic of strong focusing so that 96 of the magnets are vertically focusing (VF) having 1.5" gaps while the other 96 of the magnets are horizontally focusing (HF) having 1" gaps. Correspondingly, the coils in the VF magnets have 24 turns and in the HF magnets the coils have 16 turns. Fig. 2 illustrates a VF magnet in cross section. The

---

[1] The tunnel was designed by Jacobs Associates under sub-contract to Wm. M. Brobeck & Associates, and has been dug by Traylor Bros. It was started July 15, 1965 and was finished in July 1966.

[2] The building, designed by Ian MacKinlay for Wm. M. Brobeck & Associates is being constructed by Irwin & Leighton, Inc. The excavation was started March 15, 1966. We expect to occupy parts of the building as they are finished, but do not expect the completion of construction before the Fall of 1967. Thus part of the linac was installed in a temporary position in October in the adit of the tunnel and initial injection studies were begun. On December 1, the "Linac Stack" became available so the whole linac was installed in its final position. A temporary structure in the form of a wooden tunnel was then built through the Experimental Hall so that we could finish the magnet and start injection studies before completion of the building.

outside dimensions of the iron are 11 1/2" X 8" for both kinds of magnets. There is no conventional donut but rather a 1/32" thick stainless steel skin covers the outside of the magnet and serves as the vacuum wall.

Each magnet unit is firmly clamped to a base or strong-back made of steel "ship channel" that is about 11' long by 13" wide and 3" deep. Two of these bases with magnets are then supported on a 12" wide I-beam placed at those points which give minimal deflections of the channel due to the load - the average deflection being of the order of several mils. Other screws on the bases adjust and lock the radial and azimuthal positions of the magnets with respect to the I-beams. Although the I-beam deflects about 100 mils under its total load, the magnet units can each be adjusted so as to be level under this loaded condition; hence the vertical position of the magnet should not deviate from level by more than several mils at all positions along the I-beam. Each magnet and channel base weighs about 1.5 tons and the total weight of a completed I-beam together with its ancillary equipment such as chokes and condensers is about 5.5 tons.

After the magnet units are adjusted with respect to the I-beams, the I-beams themselves can be moved as a unit by the kinematically designed device shown in Fig. 3a. The jacks are motor-driven so that the position of the I-beams can be adjusted from the control room. One end of each I-beam rests on a ball joint fastened to its neighboring I-beam and can only follow the motion of the end of that I-beam: effectively, the I-beams are all hinged together. Electric transducers are attached to the I-beams so as to signal the relative radial and vertical positions of the magnets. These signals must be calibrated against a separate survey, but relative readings which can be made to about one mil can be used for automatic or manual positioning of the machine so as to give minimal beam displacements as determined by beam-position-sensing devices.

The magnet units are fabricated by first being assembled in halves by stacking punched iron laminations (14 mil thick Carlite coated Armco A-6 stamped by Hydro-Cam Engineering Company) on a stacking jig which has been machined to be level and straight. One of the prefabricated coils is then placed in position in the coil window, and, with appropriate dams at the ends, epoxy (Hysol R9-2039 with H2-3561 hardener) is poured so that it completely covers the coil. The coils are constructed of stranded cable which is made by twisting ten 1/8" O.D. Formex-insulated wires about a 5/16" O.D. copper tube through which cooling water can be passed. Half of the coils have been wound and epoxy-potted by Pacific Electric Motor Company and the other half were made by Everson Electric Company. A 1/8"-thick layer of lead, consisting of strips about 3/8" wide, is placed so as to cover the coil and thus shield it from scattered synchrotron radiation or from the degraded products of high energy electrons.

After two such magnet halves have been fabricated, they are then keyed and bonded together to make a whole magnet. This unit is slipped inside a 1/32" thick stainless steel box, and the cover and the end pieces are then welded in place so as to make the unit vacuum-tight. The coil leads come through the sides of the box through ceramic insulators. Vacuum flanges with 3 1/2" Conoseal joints are welded to the end pieces. Finally, the unit is completed by being firmly clamped to the ship-channel base as can be seen in Fig. 3b. These unit magnets have been assembled in our shop at the rate of about one per day.

The HF or narrow-gap magnets, in which there is more space because the coils are thinner, have correction coils made of two turns 1/4" O.D. copper tubing. These coils can be used for beam bumping or for correcting the magnetic field. The I-beam units were finished as completely as possible in our shop, i.e. assembled together with their condensers, chokes, and all the necessary bus bars and wiring: then

these were moved over and installed in the tunnel.

4. a. Modified Magnets for Beam Extraction or Injection

Some of the magnets described in Section 3 have been modified as shown in Fig. 4 in order to provide an extension of the yoke to allow for extraction or injection of the beam. As can be seen, the ordinary magnet stampings have had a short length cut off either the outer or the inner return yoke. The magnet is then assembled in the usual manner except that when the two halves are brought together, an additional especially shaped stamping (Fig. 4) is placed between the shortened yokes. The stainless steel sheath must be modified to cover this extension and a 1.5" Conoseal coupling flange is welded to the stainless steel cover in order to attach a window or beam pipe.

In addition to the injection magnet which has the extension of the yoke on the inside, six magnets have been modified with an extension on the outside to allow for the extraction of photon beams. Five of these have been placed on the ring so as to give five beams in the Synchrotron Hall, and one has been placed just upstream from L-3 to give a photon beam in that area. We expect eventually to bring out an external electron beam through one of the modified magnets placed roughly in the vicinity of the 185th magnet so that the beam will traverse the center of the experimental hall.

4. b. The Quadrupoles

In each of the 40' long straight sections are located two quadrupole magnets, one focusing and one defocusing which are important parts of the magnet lattice. (See Section 5) The exciting coils of the quadrupoles, which consist of 32 turns of water-cooled 3/8" square copper tubing, are connected in series with the magnet. The dimensions are given in Section 20: they are roughly about 2' long with a 2' gap

between them, and the gradient is about 5KG per inch at 15 GeV excitation. Fig. 5 a,b shows the construction[3] which is similar to that of the synchrotron magnets in that the laminations and coil are potted inside a stainless steel sheath so that no donut is necessary. The return yokes are only at the top and bottom of the magnets which leave the sides relatively free for extraction of particles or for other experimental uses.

5. The Lattice

The lattice consists of 96 lenses, two magnets per lens, distributed in the roughly circular fashion indicated in Fig. 1a. The magnets are supported by 96 I-beams, i.e., 2 magnets per I-beam, and such that each end of an I-beam splits a lens. This arrangement permits changes to be made in the gradient parameter x_0 of a lens by simply moving the corresponding I-beam support in a radial direction. A half-lens appears at each end of the long straight sections in order to avoid having to make special I-beam bases at these positions. We have also chosen to reverse the sign of the gradient on opposite sides of the long straight sections. This makes the magnet anti-symmetric about the roughly North-South diameter and symmetric about the East-West diameter.

The gradient parameter, x_0, has been chosen to be 9.143" for a positive lens, and 9.121" for a negative lens at the isomagnetic line of the pole pieces, which implies 10-3/4 betatron oscillations per turn. This operating point is shown in the usual "necktie" pattern in Fig. 6. Avoiding possible "1/3" resonances at the positions of the dotted lines, as well as the more classical integer and half-integer resonances, demands that the deviation in x_0 be no more than $\pm 0.5\%$ from the specified values. With constant gradient pole pieces, the variation of the betatron frequency with radius due to a corresponding change in the

---

[3] D. A. Edwards, CS-35

momentum of the electrons is about 3.5% inch. If the full radial aperture of the magnet is to be utilized, then a linear change in x_o with radius amounting to about 2%/inch is required. The pole face profiles have been designed to keep the betatron frequency constant with radius, with a maximum deviation of $\pm$0.5% in x_o from the required value.[4] The resulting shape of field as given by calculation and measurement is shown in Fig. 7a,b It can be seen that the horizontal aperture is about 2.5 inches in the HF magnets and narrows to about 2 inches in the VF magnets.

Straight sections have been accommodated by first calculating orbits as though the positive and negative lenses were distributed in a uniform lattice all around the ring and then by inserting the straight sections in a manner that does not perturb the orbits elsewhere. This has been done by inserting quadrupoles or by making other local changes. Off-momentum orbits are affected, however by the insertion of the straight sections.

In the case of the 20 ft. straight sections, it was found by Edwards[5] that the effects of making these insertions could be nullified by changing the value of x_o in the two adjacent magnets to a value of 4.7" for 9 feet of the magnet. In the case of the 40 ft. straight sections, a quadrupole pair is placed near the center of the insertion; typically, each quadrupole has a length of about 25" and, at 10 BeV, a gradient of about 5000 gauss per inch at 10 GeV. The amplitude function β_z is shown in Fig. 8a. Figure 8b shows the displaced equilibrium orbit. The circumferential momentum compaction factor is 0.010, while the momentum compaction of the maximum radial excursion is .024.

---

[4] P. N. Bredesen and P. C. Stein, CSDS-24, October 11, 1965

[5] D. A. Edwards, CSDS-25, October 1, 1965

The isomagnetic line of a magnet is not the centerline of the pole piece but has been displaced toward larger radii in order to provide for maximum magnetic aperture. The outward shift is different for the two types of magnets, being 0.069" for VF lenses and 0.131" for HF lenses. In order to center the isomagnetic line on the principal orbit, the magnets have been moved radially inward by these same amounts.

Because the orbit is circular, and the magnets are straight, there is a deviation of the principal orbit from the isomagnetic line that amounts to 0.17" outward at the center of the magnet and to 0.35" inward at the ends of the magnet. At the outside edges of the vacuum flanges, which are 3.5" away from the magnet ends, the displacement from the extension of the isomagnetic lines amounts to 0.38. The flanges had been arbitrarily placed 1/4" inward from the centerline of the magnet, hence the principal orbit will pass almost exactly through the center of a flange of a VF magnet but will pass 0.06" inside the center of a flange of an HF magnet.

6. Magnet Excitation

The magnets have been designed to be excited to a peak magnetic field of 5KG which corresponds to an electron energy of 15 GeV. At this excitation the saturation is less than one percent and even at 6.6KG (20 GeV) the saturation is only 7.5%. The frequency is nominally to be 60 cycles per second, and the magnet is biased using the series-resonant circuit shown in Fig. 9. The actual values of the inductances, capacitances, resistances, etc. are given in the list of parameters of Section 21. The condensers and chokes are fastened directly to the I-beam bases under the corresponding magnet units.

At 10 GeV excitation the average loss per magnet unit will be 2KW making the total power to the magnet 400KW. In fact, a total of 800KW must be provided because of an additional loss of 77KW in the condensers, 240KW in the chokes, 50KW in the bus bars and 37KW in the exciting machinery. The water-cooled bus bars are located in the back

groove of the I-beam bases as shown in Fig. 3. The peak voltage that appears above ground is less than 1,000 volts, even at 15 GeV excitation. The overall Q of the magnet system is about 60.

The AC supply will be located in the third floor hallway above the linac tunnel and will consist of a 500KW DC supply, the output of which is made into a square wave by four SCRs. This square wave is then applied to the magnet through a resonant filter which passes primarily only the 60 cycle component.

The DC supply for the magnets is split into six parts, each giving about 200 volts placed around the magnet ring in order to keep down the DC voltage. Each separate supply will be located at or near one of the straight sections. Five of the DC rectifier units, driven by a variable transformer and each rated at 145KW (enough for 15 GeV), are unregulated. The sixth supply is regulated so as to keep the DC current at the required level.

The magnets, chokes and condensers are all to be cooled by water which will be supplied at 65°F and come out at 80°F when the excitation is 10 GeV. This implies a total flow of 350 gal/min.

7. Flat-topping

Provision is being made for flat-topping the magnet current in order to provide a long pulse of high energy electrons of uniform energy. This can be done by means of conventional silicon-controlled rectifiers connected in the circuit of Fig. 10. Using one set of our magnets and chokes as a prototype, Wm. M. Brobeck & Associates have produced a flat-top current pulse of 7msec corresponding to a duty cycle of 40%. By running at 30 cycles per second the duty cycle could be extended to about 75%. We do not expect to install the flat-top circuit until after the synchrotron is running, but we are providing space and terminals for this later installation. Brobeck & Associates estimate that the cost of the flat-topping equipment will be about $200,000.

8. Magnetic Measurements

The shape of the pole tips was determined entirely by computation,[6] however, after a few hundred laminations were punched, the magnetic field was measured and found to correspond almost exactly to the calculated values, as shown in Fig. 7.[7] The experimental values of the field gradient index x_o were 9.204 $\pm$0.014 inches for the VF magnet and 9.045 $\pm$0.014 inches for the HF magnet at the geometrical center of the pole pieces.

The position corresponding to the isomagnetic line is determined by measuring the effective length L_B which is defined as $\int B ds$. The measurement is made by the use of a flux coil consisting of two accurately spaced parallel wires that pass completely through the magnetic field from one end to the other - comparison being made against one of the magnets that has been used as a standard. Thus, even if errors creep into the manufacture of the magnets, for example, by a variance in the gap between the halves, the magnets can be placed so as to minimize those errors. The rms variance from the calculated position has been less than 10 mils and the worst magnet is off by 60 mils. The average effective length is 127.21" for VF magnets and 127.17" for HF magnets.

The integral gradient length $\int \left(\frac{\partial B}{\partial X} ds \Big/ \frac{\partial B}{\partial X}\right)_0$ is 126.0 inches for VF magnets and is 126.1 inches for HF magnets, accurate to about 40 mils. That the ends of the magnets have the peculiar cupped shape that is shown in Fig. 11 is due to the requirements that L_B and L_G vary in the proper manner across the pole piece.

The residual field is about 2.6 gauss for VF magnets and 4.3 gauss for HF magnets after excitation to 3.3KG. The shape of the residual field is close to that of the field which obtains at high excitation,

---

[6] P. N. Bredesen and P. C. Stein, CSDS-24, October 11, 1965

[7] R. Yamada and S. Mori, CS-31, April 27, 1966.

the values of x_0 for the residual field being about 25% stronger than the usual value. Hence, at the injection field of 53 gauss, we can expect the gradient to be in error by about one percent. This implies that it will be necessary to correct the gradient at injection. We plan to do this by placing weak quadrupoles lenses in the straight sections.

9. Magnet Survey

Although in principle it should be possible to line up the machine from the beginning using only the beam, i.e., by leading the beam from one magnet to the next and then by adjusting magnet positions and correction currents so as to keep the beam within the aperture. In fact, we expect to put the magnets in place accurately enough using standard survey techniques so that the machine will work upon injection except for minor adjustments. We did exactly this with our 2 GeV Synchrotron and it should be possible to do the same thing with this machine.

The betatron oscillation wavelength in the 10 BeV machine is nearly 200 feet and displacements of the magnets that occur over distances comparable to this wavelength are the most important in causing large oscillations. In the tunnel, a single line of sight is some 150 feet long which, fortunately, is comparable to the betatron wavelength. A 10 mil r.m.s. displacement of the center of each magnet from the ideal orbit will produce a 2% chance that the actual orbit will be displaced more than 1 cm. from the ideal orbit. Similarly, an r.m.s. error of one milliradian in the radial level or twist of the magnets will produce the same chance of a displacement of one cm. It is worth mentioning here that an r.m.s. variation in H_0 of 10^{-3} from magnet to magnet will also produce this same effect. A radial displacement of just one of the I-beam support points by 10 mils will produce a maximum displacement of $\sim$20 mils in the orbit.

The basic grid for the survey around the ring will consist of 36 monuments most of which are to be mounted at regular intervals on the walls of the tunnel and some of which will be in the Synchrotron Hall. We have a first-order theodolite with which to measure angles and, together with measurements of lengths using steel and invar tapes, it should be feasible to locate points on the monuments to an accuracy of about ten mils. We call this the tunnel survey. More or less independently of this, the magnets are put in place by stretching wires between the index points that are mounted on them and then by measuring off-sets. The horizontal position of the machine is established to about 10 mils using a standard surveyors level. We call the latter survey the magnet survey. A comparison between the two indicates that an accuracy of placement of better than $\pm$10 mils has in fact been achieved.

The magnet survey has been used to calibrate the electric transducers that are attached to the I-beams. It is expected that, after the first survey, the position of beam itself with respect to the magnet aperture will be used to determine further fine adjustments of the magnet positions and currents in the correction coils.

10. Vacuum System

At 10 GeV excitation and 150 MeV injection energy, electrons are lost from the orbit at injection time largely due to single scattering and the loss amounts to about 25% for a pressure of one micron Hg. There is an additional loss of electrons, constant throughout the cycle, due to hard bremsstrahlung collisions with the air. This amounts to several percent for a pressure of one micron. Accordingly, the average pressure around the machine must be better than one micron to avoid a beam loss of 30%. Conservativism suggests that the average pressure be held less than 10^{-4}mm Hg. The straight sections, where the RF accelerators will be located, are special and may require a vacuum of about 10^{-6}mm Hg in order to avoid discharges.

A 3" diffusion pump (NRC - HS2) is provided at every other short straight section, i.e. at the end of each I-beam, hence 102 pumps. The construction is such that pumps can be placed at any short straight section if the need should arise. In an experiment where the pumps were placed only at every fourth magnet, the pressure at the worst place was about four times the pressure indicated at the pumps. Figure 12 shows a typical pump and vacuum box. A 2" fore-vacuum line runs inside the I-beams just under the top flange. In fact, the pressure in the system comes down to below 5×10^{-6} mm Hg but goes up to about 10^{-5} mm Hg when the magnet is excited to the 15 GeV level.

The synchrotron is divided into 18 vacuum zones, one for each straight section and two for each 60° sector of the magnet ring. The zones are separated by pneumatically operated gate valves. At each long straight section there is a vacuum station consisting of a roughing pump (Stokes Model 148-HO) and three fore-pumps (Cenco Hypervac 45) for the three nearest zones. The only valves other than the isolation valves already referred to will be the manually-operated units on the roughing manifold.

The pressure is measured by PIG gauges (Consolidated No. GPH-001) located at each diffusion pump where the pressure reading is roughly 1/2 the average pressure in the magnet. The output current of each gauge is to be shown on a local meter and will be fed into the multiplex system so as to be available for display at the control room.

All flanges on the high vacuum system, except the standard flanges on the isolation valves, are Conoseal medium weight joints. They can be used with polyethelene gaskets or, in locations where the radiation level is high, with copper gaskets.

11. Injection

A Varian S-band 200 MeV Linac was chosen as the source of electrons to be injected into the synchrotron. The linac consists of three units, each fed by a separate klystron, and should give 200 MeV for small loads and 150 MeV when fully loaded, i.e. 2×10^{12} electrons per pulse of which 10^{12} are to be within 1/2% of the average energy. Thus, the initial tuneup can be made at 200 MeV with a very short pulse, while subsequent high intensity operation might occur at 150 MeV. The source can be modulated so as to inject electrons into every fourth cycle of the Linac RF. The Linac is located in a tunnel that is directly adjacent to the Synchrotron Hall so that the electrons enter the synchrotron at magnet No. 10.

The beam from the Linac is bent through about 25° by an achromatic system[8] consisting of two uniform wedge magnets W_1 and W_2 and a quadrupole Q as shown in Fig. 13a,b Magnet No. 10 has been modified to have an elongated return yoke to allow the electrons to enter. At the following straight section (s 11) the electrons are deflected again by a septum magnet S placed as close as possible to the circulating beam orbit. Then in one of the following straight sections, the injected beam intersects the central synchrotron orbit and is deflected by about 1° to make it tangent using the pulsed coil P. The long time for one traversal of the magnet, 2.5μ sec, relaxes the problem of producing the injection pulse in coil P.

It will also be possible to inject positrons from the Linac. The positrons are made by inserting a rotating tungsten converter in the electron beam from the first part of the Linac, for example, at the 50 MeV point. Then the phase in the remaining part of the Linac is

---

[8] K. Berkelman, CSDS-20, October 16, 1964

reversed so that the positrons made in the converter are accelerated and then injected into the synchrotron. We can expect in this way to obtain a high energy beam of roughly 10^7 positrons per second.

This intensity can be improved considerably by making a better match in phase space of the positrons from the converter to the characteristics of the Linac. This is done by using a magnetic lens system. For example, by adding a quadrupole lens system just before the radiator so as to make a smaller spot, a four-fold increase in the intensity should be produced. Then by following the radiator by a strong local solenoid lens and then subsequently by longer but weaker solenoidal lenses a further enhancement can be made so that roughly 10^{10} positrons per second might be accelerated by the synchrotron. It should even be possible to exceed this intensity by going to a more elaborate system.

12. RF System

The RF system consists of linac-like traveling wave accelerators which we call synacs that are placed in the four 20 ft. long straight sections.[9] A prototype synac was first developed and used successfully to accelerate electrons in our 2 Gev synchrotron.

The voltage in MeV required per turn (for fully biased 10 GeV operation) is given by

$$V = 4.4 \sin \omega t + 8.8 \sin^8 \frac{\omega t}{2}$$

which has a maximum of 9.4 MeV at about 7.5 m sec. Thus each of the four synacs must supply about 2.5 MeV per turn at the peak of the cycle.

---

[9] M. Tigner, CSDS-21, December 16, 1964

The synac units consist of a 714 MH_z disc loaded wave guide having a disc spacing of 1/3, i.e. 5.5 inches, and a diameter of about 13 inches, see Fig.14a. The frequency has been chosen to be the fourth subharmonic of the frequency of the injection linac (2855.96 MH_z) so that synchronization of the two systems will be possible. Each synac is made up of five subunits consisting of three pieces of wave guide about 4 ft. in length and two couplers that are bolted together to make an assembled unit about 16 ft. long as shown in Fig.14b. Some of the wave guide units have been fabricated for us by Litton Industries, others by Arco.

Each of the four synacs has an independent Klystron RF power supply; however, the high voltage and drive are common for reasons of economy and phase stability. The total peak power at 10 GeV, will be 425 kW and the average power will be 120kW. The average power going into the beam will be 24kW for a current of 7 ma (10^{11} electrons/pulse). Of this, 10 kW will go into the beam itself and 14 kW will be radiated by the electrons. For comparison, the total resistive loss in the copper will be about 96 kW. By reducing the beam so that the loss due to it is negligible compared to resistive losses, i.e., to about 10^{10} electrons per pulse, and by applying all the power that is available to the Klystrons (~700kW), we should be able to reach an energy of about 11.5 GeV.

The Klystron high voltage is supplied by an "inductrol" regulated transformer- a silicon-diode-rectifier combination with a capacitor bank of 140 mF. This power supply is capable of delivering an average power of 600 kW at an output voltage of 38 kV. An auxiliary supply is also provided to allow flexibility of operation and to serve as a stand-by for the main power supply. The auxiliary supply is capable of delivering 125 kW, enough to run one Klystron station at 43 kW average RF Power. Thus even under standby conditions, more than enough power is available to accelerate the full beam to 5 GeV.

The power amplifier Klystron for each synac is an Eimac 4 KMV 150 LH-1 which is located in the enlargement of the tunnel occurring at each of the 20 ft. straight sections. The Klystron is 66 inches high by 28 inches square. The power amplifiers and the D.C. supplies and modulators have been fabricated for us by Continental Electronics Company.

The electron source of the Linac is modulated so that only the properly phased pulse out of the four pulses available per synchrotron RF cycle will be filled with electrons. This will keep down beam loading in the linac and synchrotron, both of which must be synchronized, and should also reduce radiation damage in the magnet due to the electrons that otherwise would not be accepted at injection time.

13. Controls

Our basic conception of the synchrotron was that it be so simple and so inert that a small university group could build and then operate it. Our goal has been to simplify the controls to the point that one relatively untrained operator should be able to control and adjust essentially everything from the control room. We also wanted to minimize the cost and labor of installing the large number of wires and controls that are usually associated with a large synchrotron. To this end, a time-sharing multiplex system has been worked out by Littauer.

Generally speaking, there are between 50 and 100 values of any particular variable, such as beam positions, vacuum readings, magnet corrections, etc., and groups of these values corresponding to a particular variable can be presented as a histogram on an oscilloscope. It is also possible to present these data as typewritten lists and to

---

[10] R. Littauer, Multiplex Control and Monitoring of a Large Accelerator, (Particle Accelerator Conference, Washington, D. C., March 1965).

store them on punch cards or tape. The data can then be fed back into the system in order to reproduce previous conditions.

We hope to be able eventually to feed the data from the beam position indicators directly to a computer which will automatically calculate and set magnet positions and correction currents so as to optimize the beam of accelerated electrons. Although this may be overly ambitious, nevertheless, where possible controls and monitors have been designed so as to be consistent with this intriguing possibility.

14. Monitoring the Beam Intensity and Position.

Beam sensors are placed around the ring, each separated by about four magnets so that there are about 4 1/2 detectors per betatron oscillation. The detectors consist basically of a frame of ferrite through which the beam passes, see Fig. 15. Around each of the four pieces of ferrite that make the frame are wound a few turns of wire. The size of the signal induced in a particular coil depends on the position of the beam as well as the intensity. By taking an appropriate difference of the signals, the horizontal or vertical position can be determined. By adding signals, a total signal is given that is proportional to the intensity but not dependent on the position. The intensity and position signals are conveyed to the control room in digital form via the multiplex system.

15. Adjustments and Corrections.

Irregularities in the magnetic field fall into two general classifications: those which occur at the low field which exists at injection, and those which occur at high fields. The low field effects are due to residual magnetism, the earth's field, and eddy currents. These effects can be corrected by vertical and horizontal steering coils that are distributed around the ring at roughly the same intervals as are the detectors, namely, every four magnets. See Fig.16.

If one coil is actuated then a rather complicated betatron oscillation is excited. However, by actuating currents in three successive coils in a particular manner then the orbit is disturbed only in the immediate vicinity of these coils. Such a "beam bump" is made by programming the currents in three successive coils in the ratio of 2:-1:2 respectively. This allows for a simple adjustment of the correction currents inasmuch as one can dial a particular position detector on the multiplex system, then by exciting a beam bump at that location one can center the beam in the aperture. In this way one can center the beam in the aperture all around the ring. However, the number of betatron oscillations, easily determinable by the position detectors, or by exciting betatron oscillations by applying an oscillating field of the corresponding frequency to some deflection plates, may be wrong. A few quadrupole coils are distributed in each sector and can be excited so as to make the number of betatron oscillations per turn either the design (10 3/4) or the optimal value.

At high fields the magnetic field can be corrected by exciting currents in the correction coils that have been included in the narrow-gapped magnets. By programming these currents in successive magnets, a radial beam bump similar to that produced by the low-field correction coils can be produced. Vertical motions can be produced by making a vertical motion of the magnets by the use of the motor-driven levelling jacks. Thus either a simple vertical motion or a twist can be given to the magnets. By programming the motion of successive magnets, a localized vertical bump can be produced. In the same manner, horizontal corrections to the magnetic field or to the gradient can be made by making appropriate horizontal motions of the magnets by means of the horizontal jacks. All of these motions are produced at the central control room where one can dial a particular station corresponding to the position of a particular end of an I-beam, and then command changes in the vertical or horizontal positions by actuating the jack-motors - the actual positions being indicated by the transducer signals.

16. Radiation Damage

One of the first of our production magnets was exposed to various conditions of an intense beam of electrons from the first section of our injection Linac. The Linac could give about 300 ma of 20 - 30 MeV electrons in a 2 or 3 μsec pulse. In one series of runs, the beam was directed along the centerline of the magnet and then diffusing foils of increasing thicknesses were successively placed in the beam at the point of entry into the magnet so as to give a general radiation to the iron and the coil. With as much as 900 watts in the beam, i.e. about 300 ma in a 2 usec pulse at 60 pulses per sec, and with diffusers ranging from 16 to 130 units in thickness, a half dozen different runs of about six hours each showed no effects of radiation except for the failure of a rubber gasket at the downstream end of the magnet.

In a different series of runs a current was excited in the magnet so as to cause the beam to be deflected into the magnet yoke about half way down the magnet. In one set of runs, the beam intensity was increased gradually until it reached an average power of 360 watts, i.e., 300 ma for 2 usec at 30 cps. The total running time at this power was equivalent to about 24 hours. Throughout all the run, a transformer supplied 800 volts r.m.s. to one side of the coil: no breakdown was observed. Typically, the pressure in the magnet was observed to increase by a factor of two during the runs - depending on the current. Upon opening the magnet after the test, it was noticed that the epoxy in the area where the beam had struck was discolored and that in the same area the lead strips on the coil had melted due to absorption of scattered electrons. This caused a mess on the lower coil but did not cause a failure of the coil.

It appears that the magnets are quite radiation resistant - but that the very large currents can cause rather serious thermal effects. The expected injection currents should be one or two orders of magnitude smaller than those used in the tests. In order to protect

the machine against an accidental exposure of an unduly large Linac current, the pressure in the machine will be monitored by a circuit which will turn off the Linac if a pressure increase occurs anywhere in the magnet.

The high energy electron and gamma ray beam can also be dangerous. Thus a beam of 10^{13} electrons per second at 10 GeV corresponds to an energy of 16 kW. This can cause severe thermal damage if it is absorbed inside the machine without care. We expect to insert thick metal "scrapers" at the end of each magnet in a position near the beam such that most of the radiation will be absorbed by them.

The spectrum of synchrotron radiation is characterized by being flat in radiated energy per unit photon energy up to a critical energy after which it falls off rapidly. For 10 GeV, this critical energy is 22 Kev and it varies with the cube of the electron energy. For our 2 GeV machine the critical energy is 3 Kev for comparison. The power that is radiated per unit photon energy in the flat part of the spectrum varies as E/R, hence for the 10 GeV machine the power radiated in low energy photons per electron is less than that for the 2 GeV Synchrotron by a factor of three. For some effects, such as the production of photo-electrons in the resonators, this is a consolation.

17. Ultimate Energy and Intensity

It appears now that it will be feasible ultimately to reach an energy of 20 GeV in the synchrotron. The magnet and the power supplies have been constructed to reach 15 GeV but it turns out,[11] by adding condensers and chokes, that the magnet can be excited to a field of 6.6KG corresponding to 20 GeV. About four times as much power must then be supplied - and dissipated - but the 3MW that will be necessary

---

[11] R.R.Wilson, CS-33, August 25, 1966

seems not to be excessive.

The radial size of the beam grows with energy because of anti-damping of the betatron oscillations due to synchrotron radiation. Thus the beam will be 1 cm wide at 10 GeV, 5 cm at 15 GeV, and larger than the aperture at 20 GeV. However, a special damping magnet has been developed by Robinson[12] at C.E.A. that will prevent this kind of growth of the beam, and it should be easy to adapt his design to our magnet.

At 10 GeV roughly 10 MeV per turn must be supplied to compensate for the energy radiated per turn. Since this varies as E^4, we must supply about 50 MeV/turn in order to reach 15 GeV, and 160 MeV/turn to reach 20 GeV. It turns out that powerful klystrons are available that are capable of producing a peak power of 7MW and an average power of 200KW. By using two of these tubes at the straight section L-3 where there is room enough to install two additional synac units, it should be possible to reach 15 GeV at 10 cycles per second. To reach 20 GeV, it would be necessary to install two more synacs in the long straight section in the Synchrotron Hall and to replace the klystrons in the four other straight sections. We have already identified some surplus power supplies that would be adequate and our rough estimate of the rest of the components necessary to reach 20 GeV is 2M$.

An alternative possibility for supplying the RF power is the superconducting Linac. A short section of this kind of Linac has already been successfully produced at Stanford[13] and we are watching their progress with great interest.

The intensity of the electron beam in the synchrotron depends in part on what the Linac can supply and then upon what kind of intensity limitations will occur during the process of acceleration. The Linac is hardly a limitation. Although the first section has already

---

[12] K. W. Robinson, CEAL-TM-155, December 10, 1965

[13] Perry Wilson Accelerator Conference, Washington, D.C. 1965

produced a current of 300 ma, we do not expect eventually to have more than 100 ma in the 1% energy acceptance of the magnet. If we can have the source modulated so that all this current comes in every fourth pulse, then it should all come at the proper phase to be accepted for acceleration by the synchrotron. In that case, close to 10^{14} electrons per second might be accelerated, but then we would be in terrible trouble with thermal and radiative effects.

The amount of RF power that we have provided will initially limit us to some 10^{13} electrons per second. The phenomenon of beam flutter can be expected to manifest itself at roughly this intensity, but this kind of beam blow-up can be controlled by inserting octupole lenses around the magnet. Thus it appears that the practical limitation of our intensity will be our ability to live with the problem of counting rates, of induced radioactivity, and of thermal and radiation damage - but we can expect to obtain and to handle roughly 10^{13} electrons per second.

It has been previously noted that positrons can also be produced by the Linac and that eventually we can expect a beam of about 10^{10} positrons per second, or better, from the Synchrotron.

18. Conversion to a 20 BeV Colliding Beam Facility.

Once a synchrotron works to give an intense beam, the question arises as to whether it can be used as a colliding beam facility for in that case exceedingly high energy phenomena can be studied. A large ring diameter is advantageous in that the radiation by the electrons is decreased but the large radius is disadvantageous because the frequency of revolution is less and hence the number of collisions also becomes less - the two effects apparently just cancel each other.

To use our synchrotron as a colliding beam facility, it will be necessary to inject electrons in the normal direction and positrons in the opposite direction. The magnetic field would be cycled between the injection energy and a sufficiently high energy to cause

the beam oscillation to damp out so that electrons or positrons could be injected on successive cycles until the magnet has been filled. Then the magnetic field would be held at a constant value while the electrons and positrons could circulate through an interaction region in opposite directions. The filling time might take from one to ten seconds and the interaction time might take about 100 seconds after which the beam could be replenished in a cyclical manner. Alternatively, the synchrotron might be run in a flat-top mode at about 20 cycles per second so as to give roughly a 90% duty cycle and such that the beam could be constantly replenished.

There is not much point in allowing the electron beam to circulate freely for much longer times than indicated above inasmuch as an electron will radiate an amount of energy equal to its kinetic energy in a short time, i.e. in $2.5/E^3$ Bev seconds which is about 20 ms for 5 Bev electrons and is about 2 ms for 10 Bev electrons. This is important for the use of our synchrotron because it implies that the vacuum that is presently obtainable in our magnet is probably good enough. In fact, the vacuum could be improved to be 10^{-6} torr simply by doubling the number of diffusion pumps, and it might be improved by another order of magnitude by the use of cold spots. The loss of electrons from the beam by the gas is due to bremsstrahling collisions which cause energy changes greater than can be accepted by the synchrotron. The acceptance energy is about one percent of the electron energy, and this implies that the lifetime of the beam in seconds would be about $10^{-4}/p$, torr i.e. it would be about 100 sec at a pressure of 10^{-6} torr.

Of course, in the vicinity of the interaction region, where the experiments would be made, it would be necessary to have a very good vacuum, of the order 10^{-9} torr, to reduce experimental background effects due to interaction with the gas. It should be quite possible to produce such vacua at the experimental region by the use of differential pumping.

The changes in the synchrotron need not be major. The Linac would have to be augmented so as to give positrons as well as electrons. One possibility would be to use the present Linac and injection system without change for injecting electrons into the magnet. The Linac beam could then be occasionally diverted so as to strike a conversion target in order to make positrons and then these could be bent through about 180° and accelerated in another Linac placed along the back wall of the beam room. The high energy positrons might then be injected into the ring somewhere in the East flare. About one million dollars worth of Linac would be required at present prices.

In order to overcome the anti-dampening that exists because of our particular choice of magnet lattice, a Robinson-type dampening magnet or magnets could be added. It would also be wise to place special magnets near or in one of the 40' straight sections in order to improve the luminosity in the interaction region.

19. Construction Schedule and Costs.

At the present writing, May 1, 1967, the magnet has been fabricated and has been installed in the tunnel. Although the construction of the building has been delayed so that it will not be finished until the Fall of 1967, we are already occupying the part of the building in which the Linac is to be housed, and we have built a temporary tunnel-like structure through the Experimental Hall which is still under construction. This structure isolates us from the construction workers and has allowed us to finish the synchrotron and to test it at low energy using a temporary power source. As soon as the building services and power supplies become available, which may be some time this summer, we hope to reach 10 GeV. If we do not run into serious problems, we can expect to initiate an experimental program this year.

Nearly all of the components of the synchrotron have been purchased or firm construction contracts have been awarded. The costs

have been close to our initial estimates, except for the building whose dimensions are somewhat larger than had been originally planned. The tunnel cost 1.2M$; the building, 4.2M$; the Linac, 1.0M$; the magnet and power supplies, 1.5M$; the Vacuum System, 0.3M$; the RF System, 0.9M$; Labor and Overhead, 1.5M$; and miscellaneous other costs, 0.9M$: This brings the total cost to about 11.5M$ which appears to be comfortably less than the 12M$ that has been made available to us by the National Science Foundation. Included in these items are expanded experimental areas and some components that will allow us eventually to reach much higher energy.

20. The Synchrotroneers.

It is a complex task to try to identify the people who are constructing the synchrotron because some are deeply involved while others are only peripherally concerned. For those on the academic staff it is an activity that must compete with their other University duties such as teaching, research, or committee work. Our system is a loose one in which about a half dozen key people do what is necessary to be done by recognizing problems, acting on them themselves, and then by keeping others informed by conversations in the halls of the Laboratory. Once a week, about a dozen people meet to discuss plans and progress, Fig.17.

The Deputy Director, Prof. Boyce McDaniel and the Associate Director for Operations Mr. Robert Matyas have been crucial in their contributions to the work. They have both carried major responsibilities at every level: Prof. McDaniel tending toward scientific and technical problems while Mr. Matyas was more concerned with problems of management and construction. Prof. McDaniel became completely responsible for the completion of the synchrotron in the Spring of 1967 when the author became Director of the 200 GeV synchrotron. Much of the most critical work has had to do with the design and construction of the tunnel and the buildings: Prof. John DeWire has been responsible for this tremendously complicated operation which has interacted with the basic synchrotron design at every stage. That the timing of building construction has been synchronized with the progress of the accelerator has also been due to his efforts. Prof. Raphael Littauer has been in charge of those elements of the synchrotron that are mainly electrical, such as the

power supplies, the magnet coils, the chokes and condensers, as well as the multiplex system for controlling and monitoring the synchrotron. Without his brilliant and sophisticated solutions of these problems, the Synchrotron would be a different and a much more awkward instrument. Mr. C. Kellers has assisted him with the design and construction of the magnet power supplies. Prof. D. Edwards has made the calculations of orbit theory that led to the final choice of the parameters of the synchrotron. His contribution has been diversified, though, and in addition to an early administrative interaction, he has also designed and supervised the constructing of the quadrupole lenses. Prof. DeWire has been in charge of the vacuum system, the original design of which was due to Littauer. The survey has been the responsibility of Prof. W. Woodward who mastered the cabalistic rites of another profession; and the magnets have been positioned by Prof. R. Talman assisted by Dr. D. Rust. The profile of the pole tips of the magnet was computed by Prof. P. Stein. Dr. R. Yamada made exhaustive measurements on the magnetic field that was actually obtained. The radio frequency system that has evolved has been completely due to Dr. M. Tigner. Prof. A. Silverman was involved in the early planning of the machine and is now concerned with considerations of the experiments to be made with the machine. Prof. K. Berkelman has designed the injection system. The Linac has been the responsibility of Mr. E. von Borstel. Dr. Helen Edwards took charge of the injection studies; she also devised and installed the beam-position detectors that were used by her in bringing the synchrotron into operation.

We have been exceptionally lucky in the excellence of our technical staff. Mr. K. Loveless, the shop foreman has been ingenious not only in helping with the mechanical design but also in devising methods used in the construction. Mr. J. Fuller of the shop was deeply involved at a creative level in the development of the magnets. He constructed a series of proto-types and then led the group of about six men who constructed the 200 or so magnet units at the very fast rate of one-a-day. Mr. R. Bower has been in charge of the assembly of the I-beams and then of connecting them together in the tunnel. He has been responsible for the design and installation of a tremendous amount

of the equipment that makes a synchrotron function. In the installation, he has been aided by Mr. C. Chaffey who has been in charge of the crew doing the work. Mr. J. Sanford has supervised the wiring installations and Mr. D. Miller has been in charge of drafting. Mr. H. Doney has expedited the vast amount of material ordered from industry. Angela Gonzales, the "emminence gris" of the Laboratory, has been much concerned with our esthetic environment not only in her choice of dramatic colors but by being intolerant of those impure lines and unbalanced volumes that tend to creep into the design of the synchrotron.

There are many people who contribute in a vital way to the synchrotron construction even though they are not members of the Laboratory of Nuclear Studies. Dr. Jerome Fregeau of the National Science Foundation is typical. By understanding every facet of the synchrotron construction, sometimes better than we do, he has been able to keep the lines of fiscal authorization open, contributing to the speed of the work, and his over-all view of the project has been constructively useful to us. Mr. John Burton, Vice President for Business at Cornell, is responsible for the construction of the tunnel and the buildings: his decisions on such matters have often been of crucial importance to us. Representing the University on the site is Mr. Frank DelleCave whose knowledge of the minute details of the building construction and his sympathetic but aggressive coordination of our interests with regard to the contractor have kept the work going apace. Mr. Norris Raneer, who was in charge of tunneling for Traylor Bros., did a magnificant job for us; and Mr. A. Wissing of Irwin & Leighton is getting us into the right parts of the building at the right times in spite of great difficulties. We are lucky, too, that Mr. Ian MacKinlay, our architect realized that "form follows function" - especially when a synchrotron is being built - but he has also insisted that the forms be nice too. All of these men have been mentioned here because they have had the kind of transcendental involvement that people get in contributing to a scientific project.

21. Parameters of 10 GeV Synchrotron

General

Nominal electron energy	10 GeV
Nominal electron intensity	10^{13} electrons per second
Possible electron energy	20 GeV
Nominal repetition rate	60 cycles per second
Nominal positron intensity	10^{10} positrons per second
Major diameter of tunnel	811.5 ft.
Orbit circumference	757 meters (2500 ft.) .47m
Orbit period	2.53 usec.
Height of beam	54 inches
Height of tunnel	7-3/4 ft.
Width of tunnel	10 ft.
Straight sections	2 of 40' length 4 of 20' length 186 of 17" lengths

Magnets

Length of magnet unit (overall)	134.98"
Effective length of magnet L_B	323 cm.
Number of magnet units	192
Chord length of I-beam supports	24.160'
Length of small straight sections	43 cm.
Length of "20 ft." straight section	628 cm.
Length of "40 ft." straight section	1238 cm.
Clear length between magnet units	10"
Magnetic field at 10 GeV	3.3 Kg
Injection field at 200 MeV	66 gauss
Magnetic field for 1.5% saturation	5 Kg.
Residual field after 3.3 Kg excitation	∿2 gauss
Gradient length of pole profile, x_o^-	9.045 ± 0.014
Gradient length of pole profile, x_o^+	9.204 ± 0.014
Gradient length near 20' straight section, x_1^-	4.731
Gradient length near 20' straight section, x_1^+	4.738

33

Magnets (Continued)	
Gap height, positive (vertical focusing) lenses	1.501"
Gap height, negative lenses	1.022"
Weight of iron per magnet unit:	
wide gap	1890 lb.
narrow gap	1954 lb.
Weight of copper per magnet unit:	
wide gap	315 lb.
narrow gap	210 lb.
Magnet Excitation	
Current at 10 GeV	424 A peak
Inductance of magnet unit (series):	
wide gap	8.7 mH
narrow gap	5.8 mH
Capacitance per magnet unit at 60 cycles	1.94 mF →
Resistance of magnet unit:	
wide gap	31 mΩ → N=24
narrow gap	21 mΩ N=16
Inductance of choke coil	7.25 mH
Resistance of choke coil	15 mΩ
A.C. voltage (1.5" magnet) at 10 GeV	500 V rms
Total energy dissipation at 10 GeV	770 kW
D.C. i^2R losses at full bias	360 kW
A.C. i^2R losses	180 kW
Core and eddy losses	115 kW
Capacitor loss	80 kW
Busbar losses	35 kW
Magnet Lattice	
Basic period	FFDD
Number of basic periods	46
Length of basic period	580"
Phase shift per basic period	75.4°

Number of betatron oscillations per turn	10-3/4
Maximum orbit excursion for 1% energy variation	1.12" (.63)
Minimum orbit excursion for 1% energy variation	0.10" (.37)
Bending magnet length ℓ_B	127.2"
Effective gradient length ℓ_G	126.0"
Maximum radial compaction factor	0.024
Circumferential compaction factor	0.010
β_{max}	72'
Maximum orbit excursion for 1 mr angle variation between similar magnets	0.86"
Maximum orbit excursion for 1 mr angle variation between lenses	0.66"

Injection

Energy of linac: loaded to 10^{12} p.p.	150 MeV
unloaded	200 MeV
Linac frequency	2855.76 Mc
Duration of linac pulse	2.5 μsec
Momentum width, 50% of beam	$\leq$ 1%
Intensity within $\Delta p/p$ = 1%	$\geq 1.5 \times 10^{12}$ electrons /pulse
Beam divergence	2×10^{-4} radians
Number of linac sections	6

RF System

Frequency	713.94 Mc
Harmonic order	1800
Number of 16' linac sections for 10 GeV	4
Peak voltage required at 10 GeV	10.5 MeV/turn
Average RF power demand at 10 Gev	120 kW
Peak RF power demand at 10 GeV	425 kW
Average power rating of each klystron	50 kW

Vacuum System

Base pressure required for 25% loss	10^{-3} torr
Actual pressure in magnets	5×10^{-6} torr
Pressure at linac sections	10^{-6} torr
Number of diffusion pumps	96

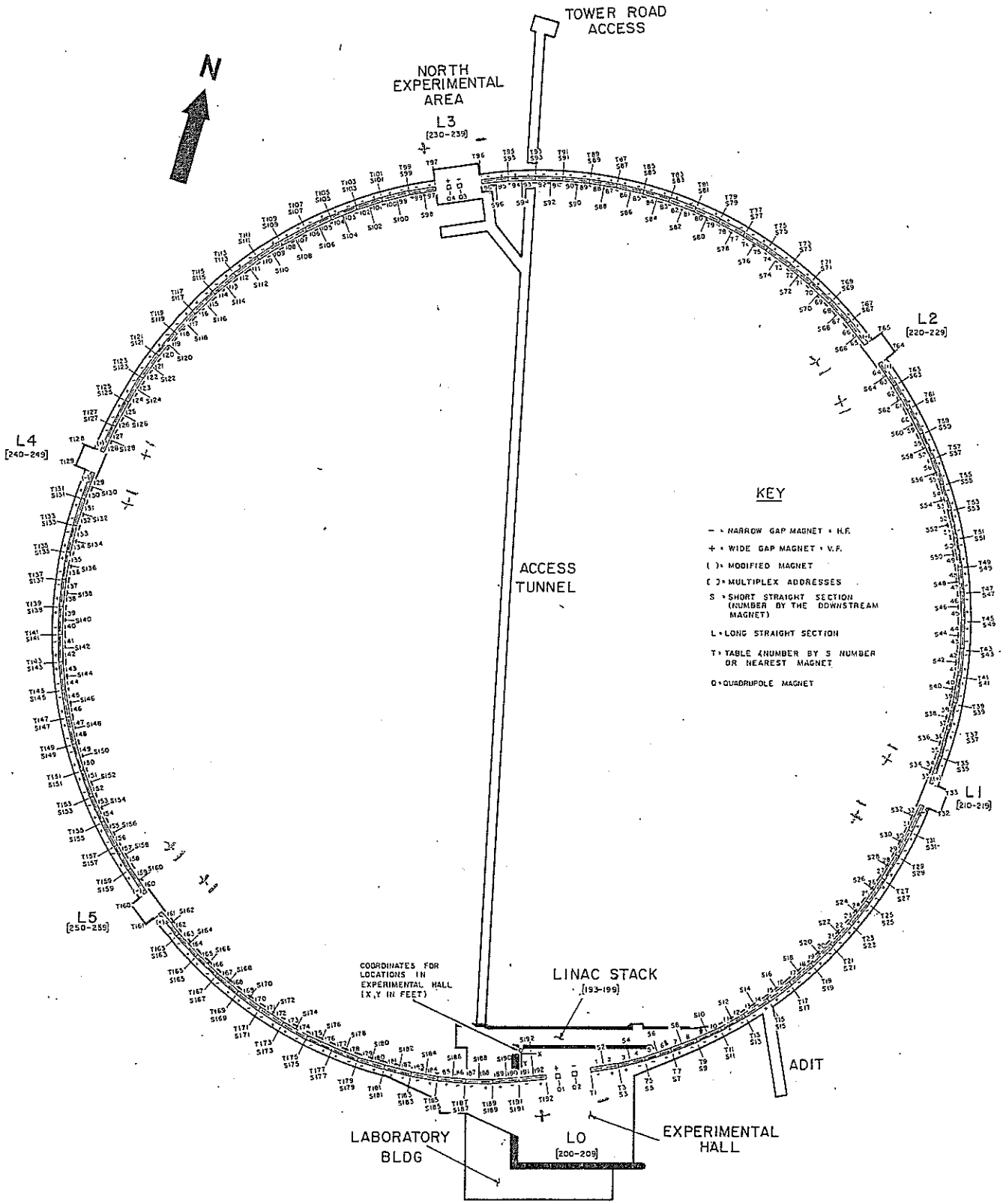
TOWER ROAD ACCESS
N
NORTH EXPERIMENTAL AREA
L3 [230-239]
L2 [220-229]
L4 [240-249]
L1 [210-219]
L5 [250-259]
L0 [200-209]
ACCESS TUNNEL
KEY
- = NARROW GAP MAGNET = H.F.
+ = WIDE GAP MAGNET = V.F.
( ) = MODIFIED MAGNET
[ ] = MULTIPLEX ADDRESSES
S = SHORT STRAIGHT SECTION (NUMBER BY THE DOWNSTREAM MAGNET)
L = LONG STRAIGHT SECTION
T = TABLE (NUMBER BY S NUMBER OR NEAREST MAGNET
Q = QUADRUPOLE MAGNET
COORDINATES FOR LOCATIONS IN EXPERIMENTAL HALL (X,Y IN FEET)
LINAC STACK [193-199]
ADIT
LABORATORY BLDG
EXPERIMENTAL HALL

Fig. 1a

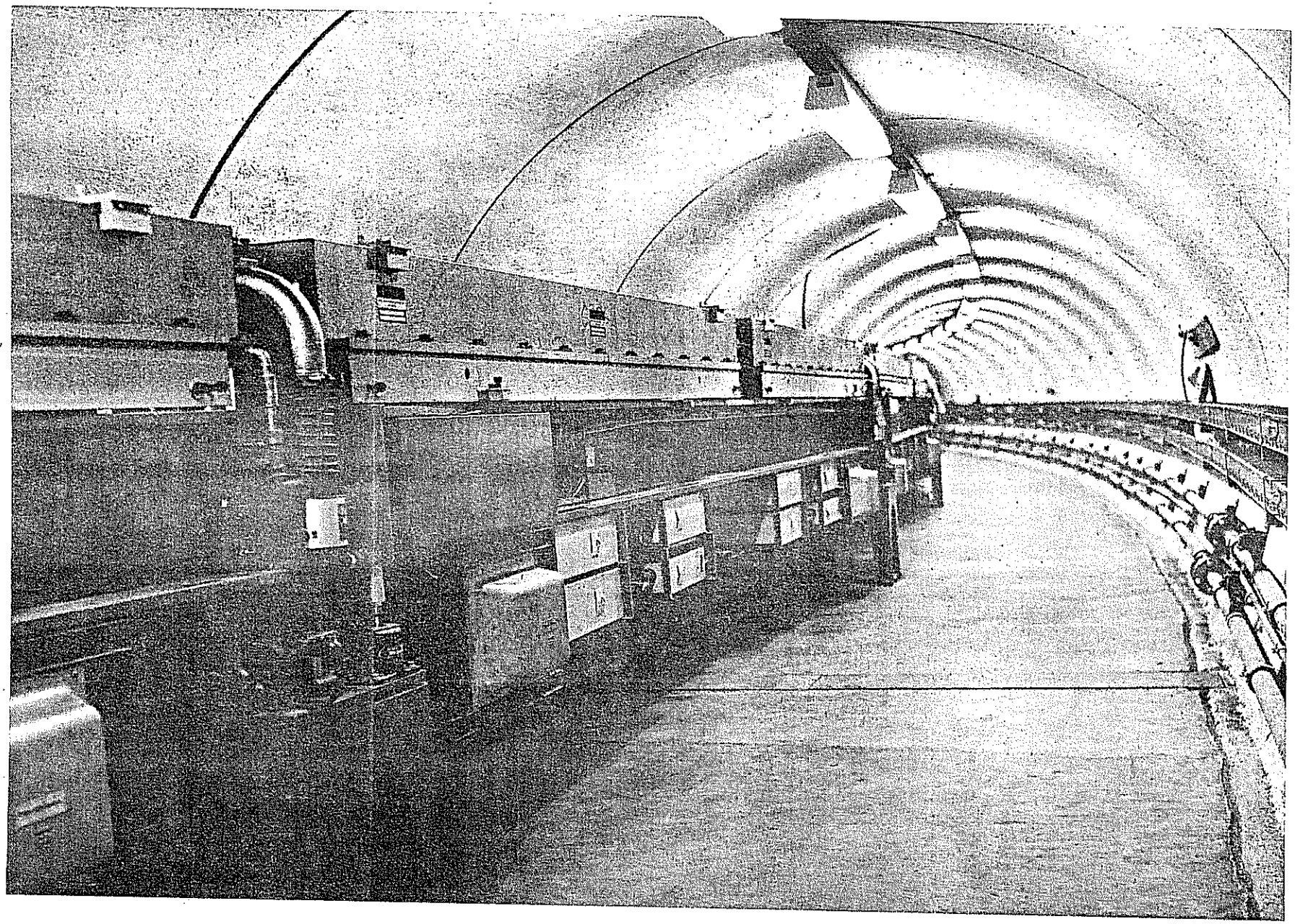

View of installed magnet modules in east half of 10 GeV synchrotron tunnel.

Fig. 1b

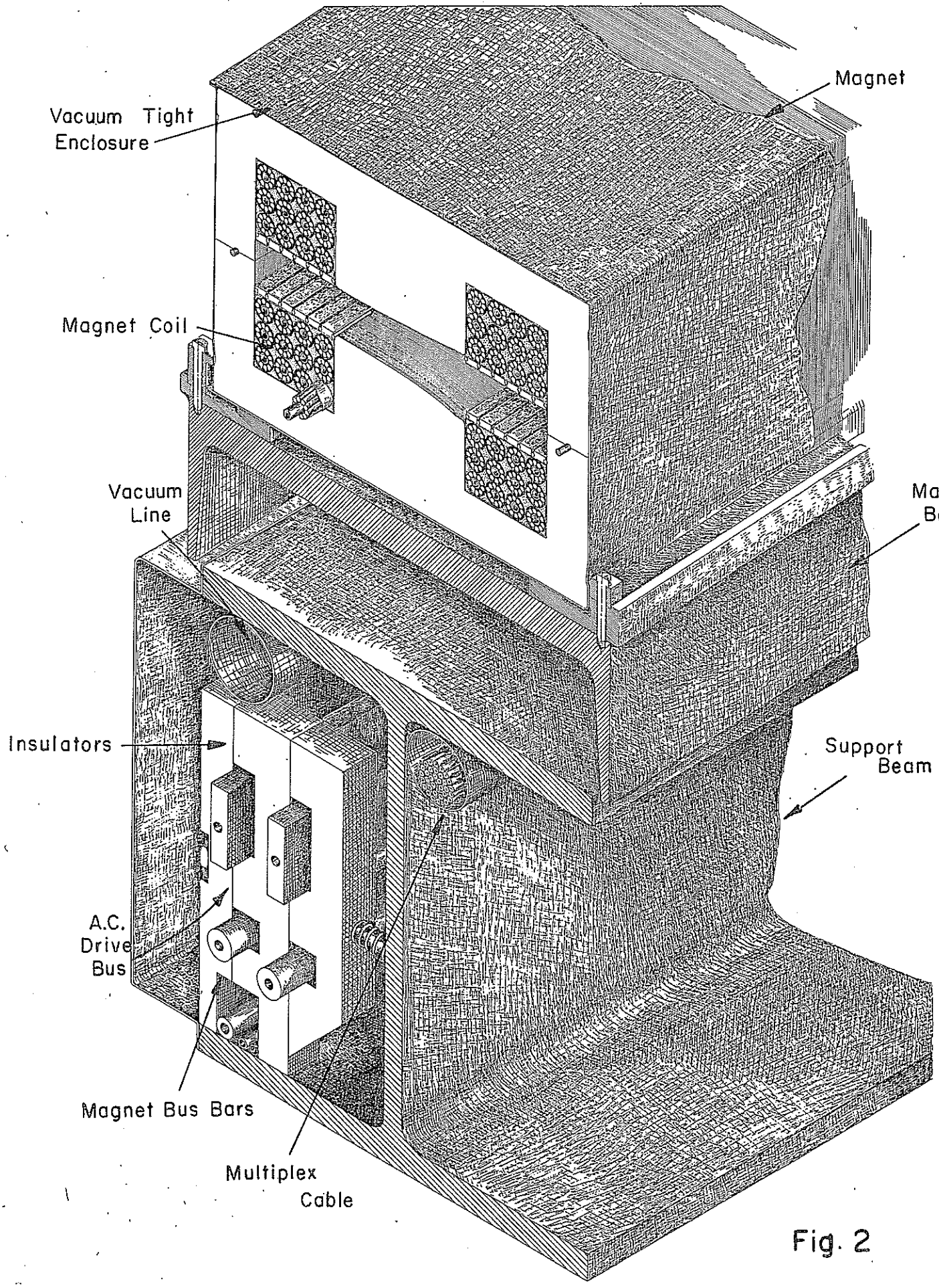

Fig. 2

Cross-Section of a Synchrotron Magnet Unit

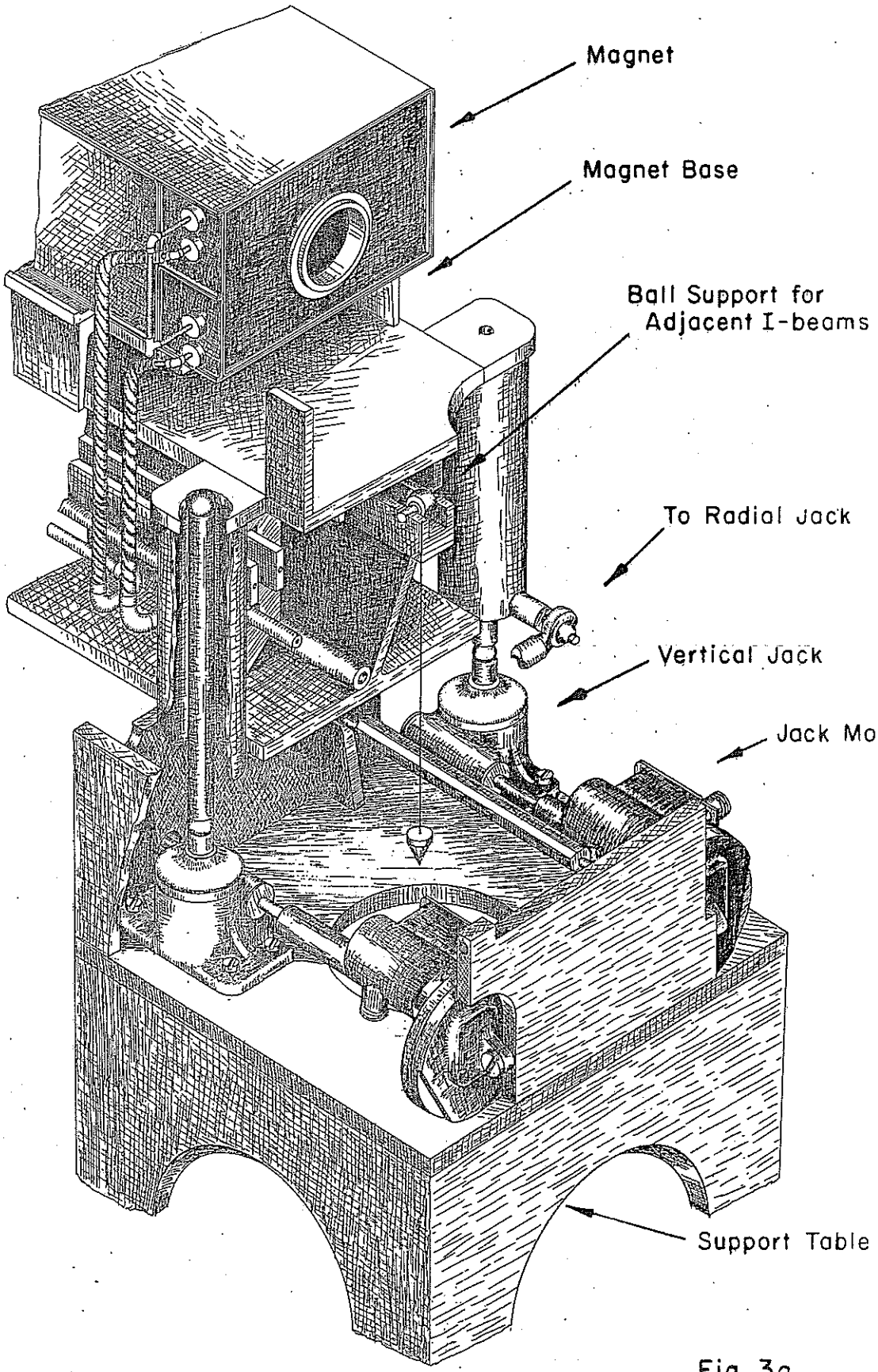
Magnet
Magnet Base
Ball Support for
Adjacent I-beams
To Radial Jack
Vertical Jack
Jack Motor
Support Table

Fig. 3a

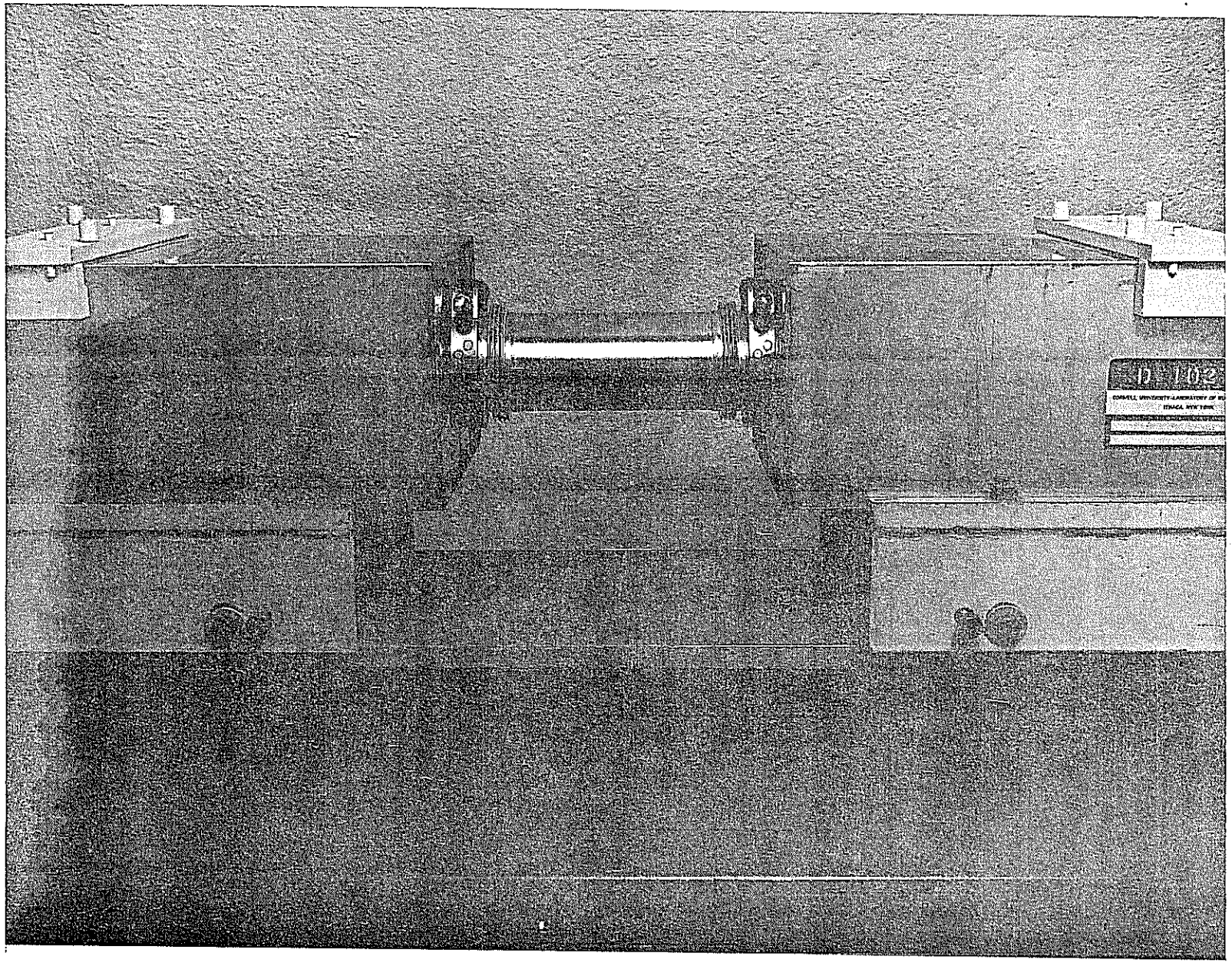

Fig. 3b

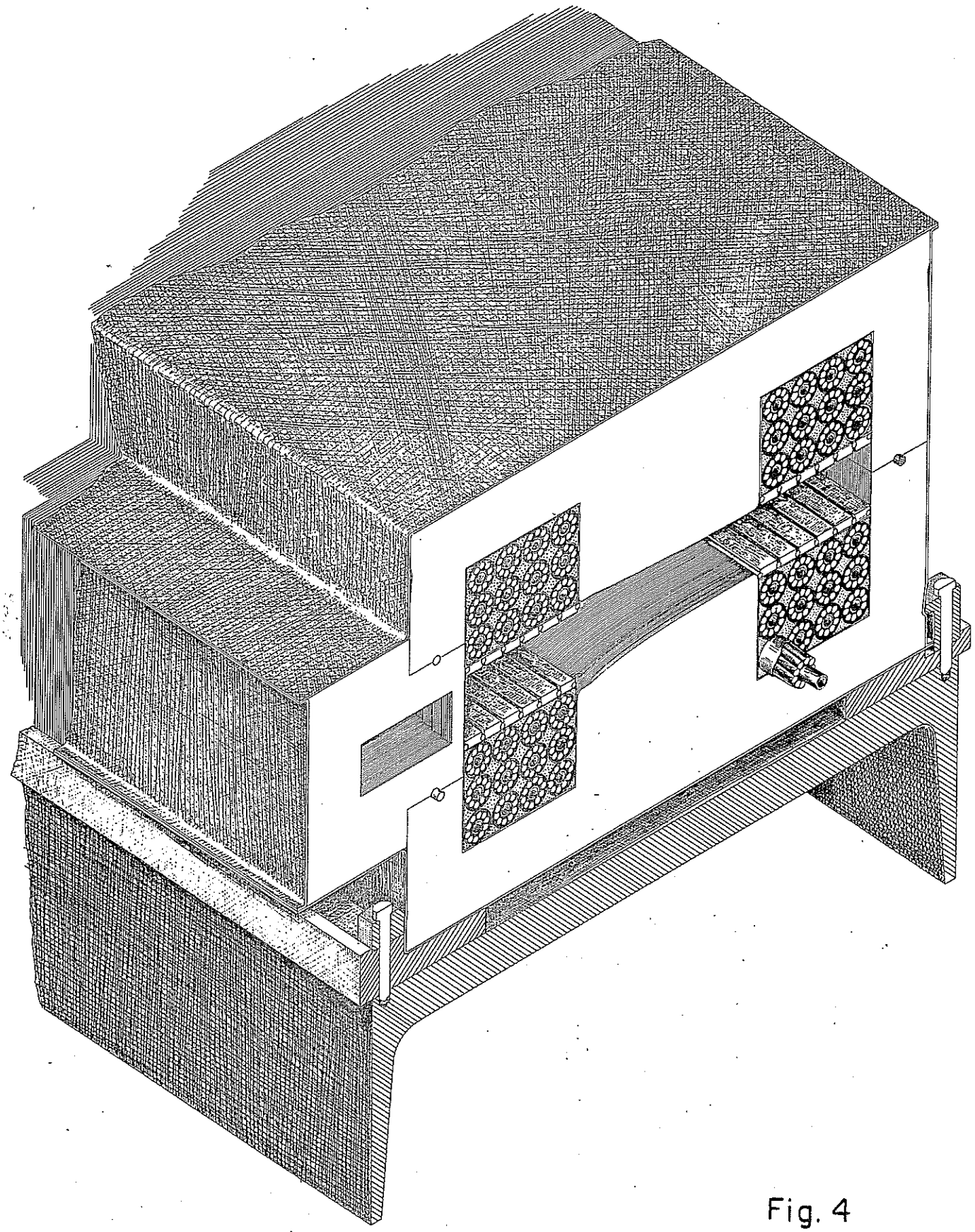

Fig. 4

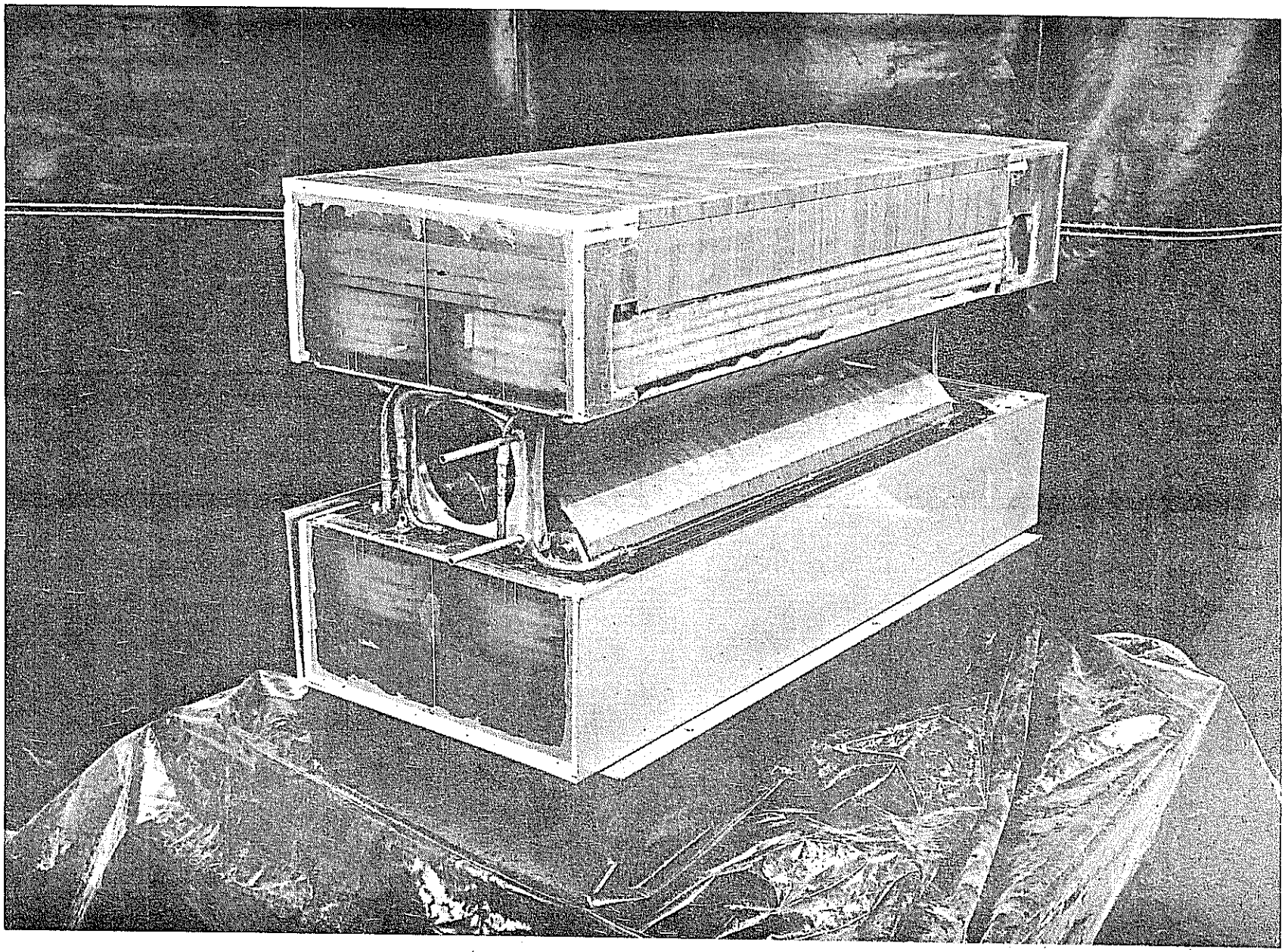

Fig. 5a

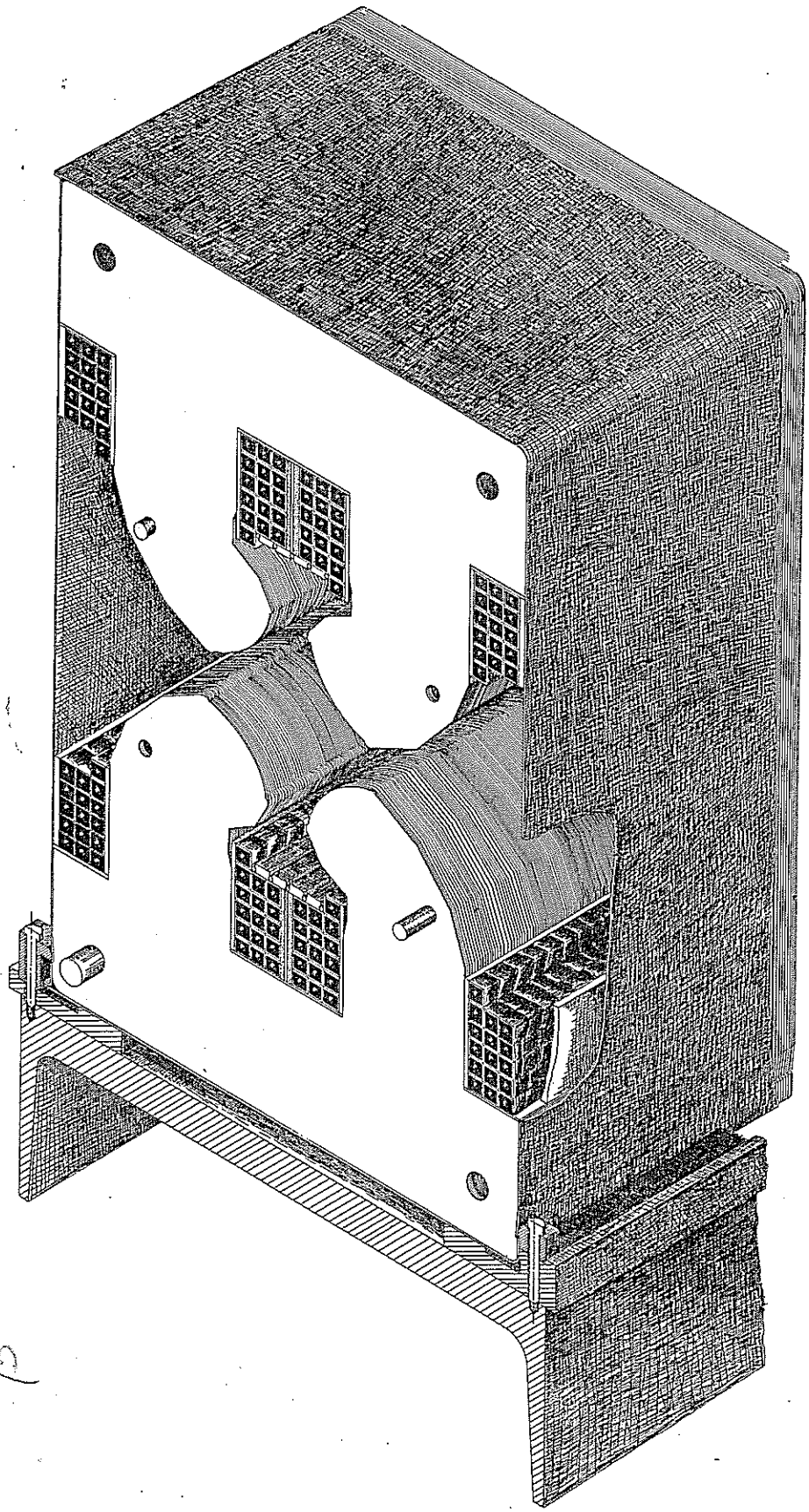

Fig. 5b

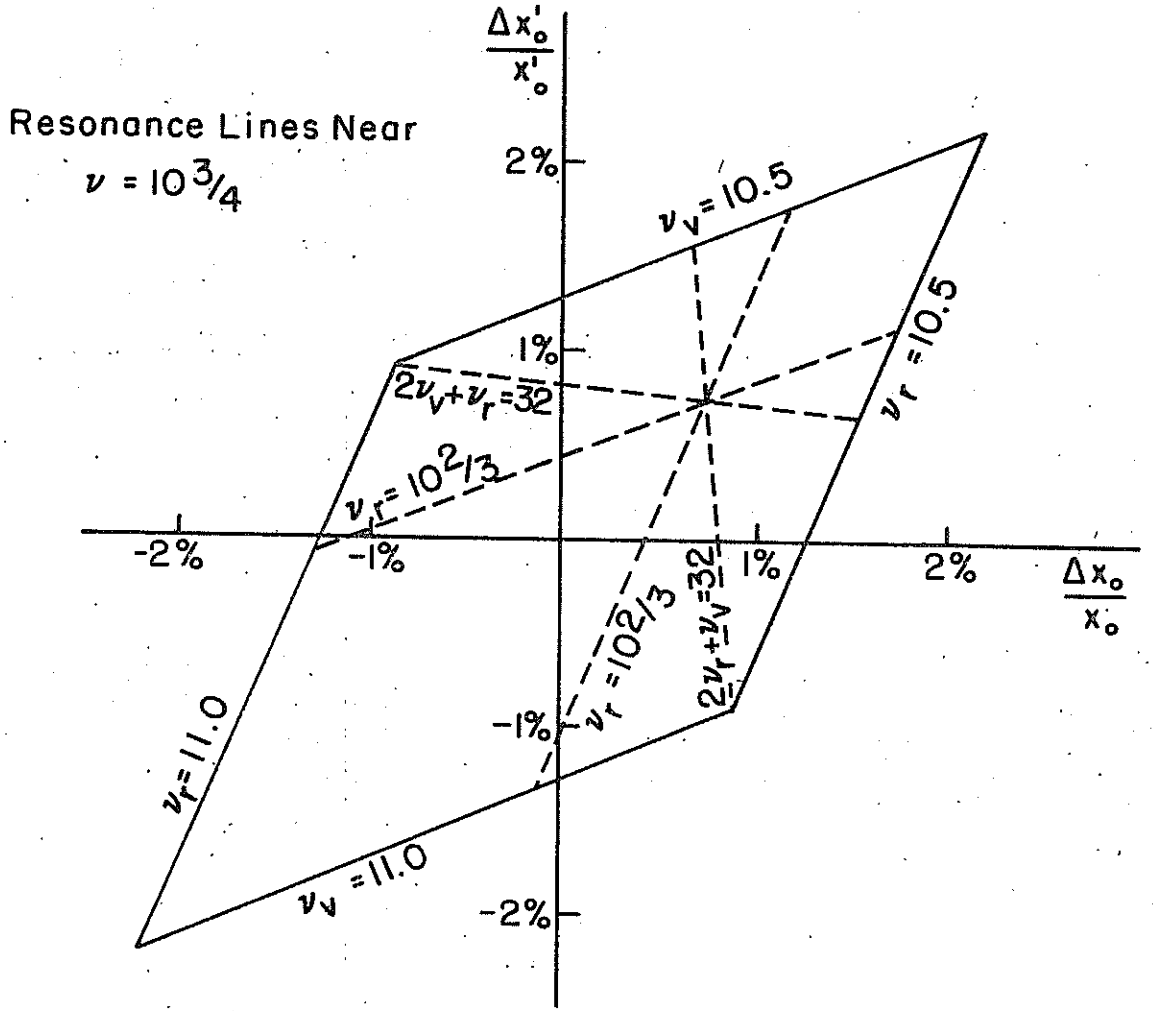
Resonance Lines Near
$\nu = 10\,3/4$
$\frac{\Delta x'_o}{x'_o}$
2%
1%
-1%
-2%
-2%
-1%
1%
2%
$\frac{\Delta x_o}{x_o}$
$\nu_v = 10.5$
$\nu_r = 10.5$
$2\nu_v + \nu_r = 32$
$\nu_r = 10\,2/3$
$\nu_r = 10\,2/3$
$2\nu_r + \nu_v = 32$
$\nu_r = 11.0$
$\nu_v = 11.0$

Fig. 6

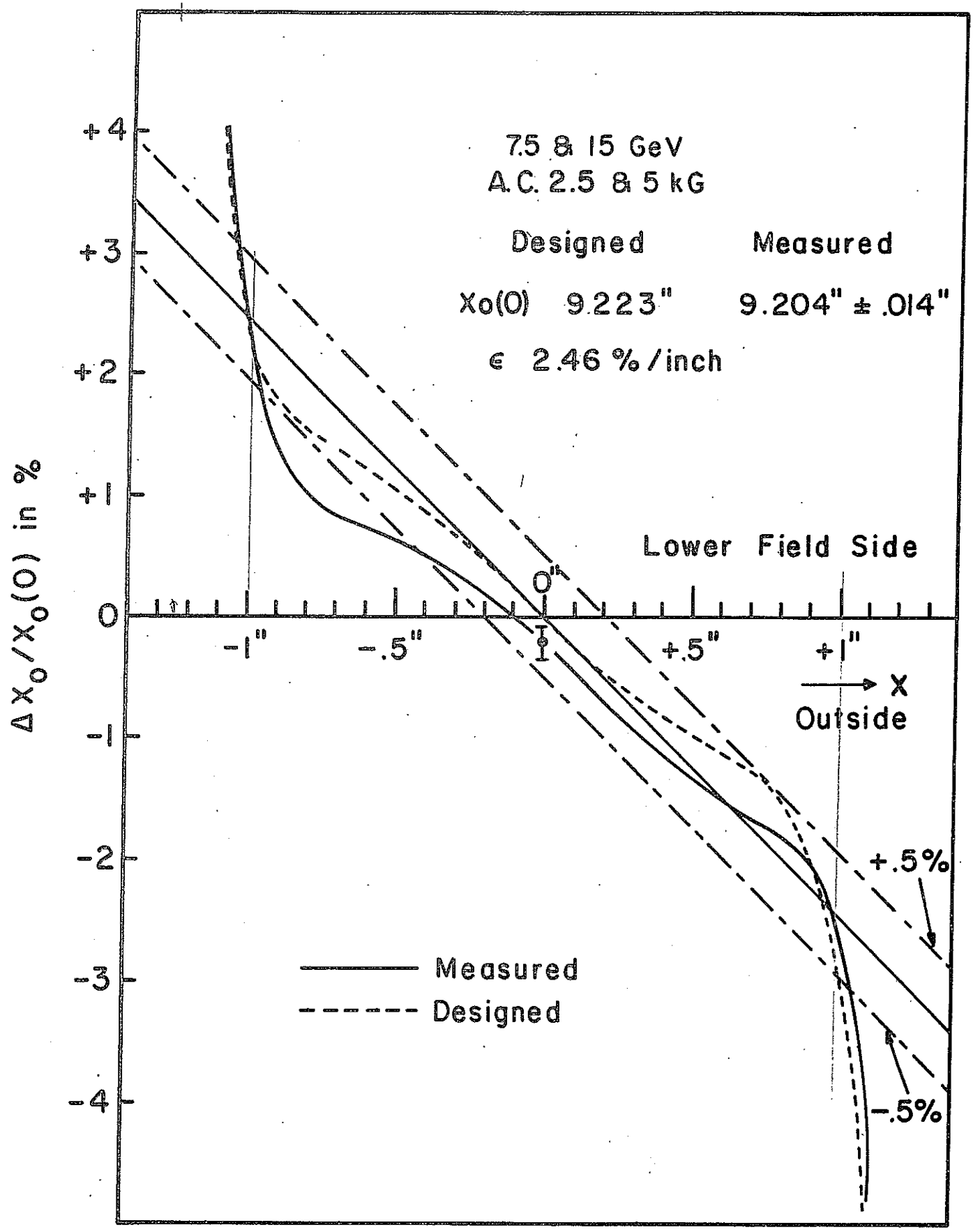

Fig. 7a. $X_0(X)$ Distribution of Wide Gap Magnet

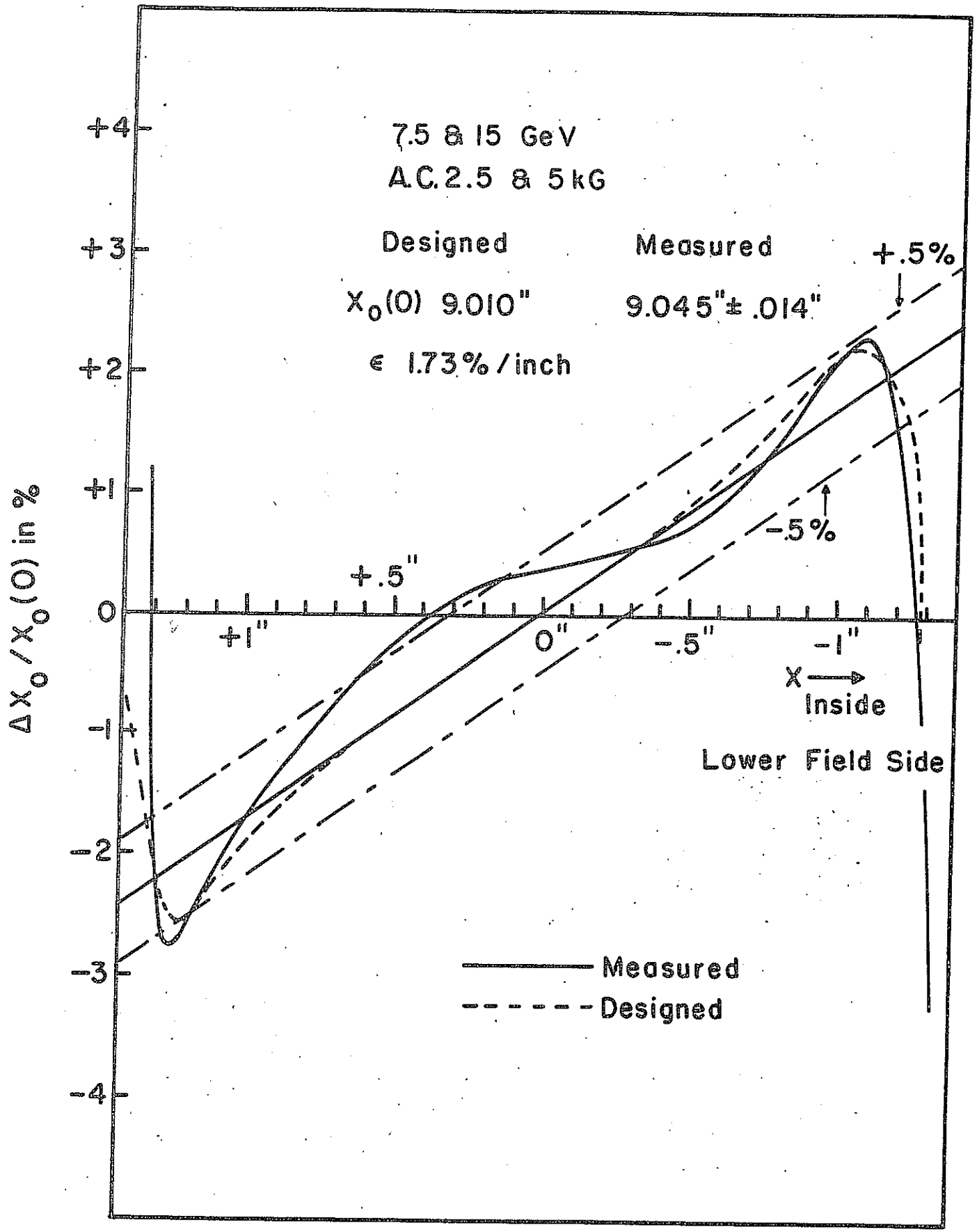

Fig. 7b. X (X) Distribution of Narrow Gap Magnet

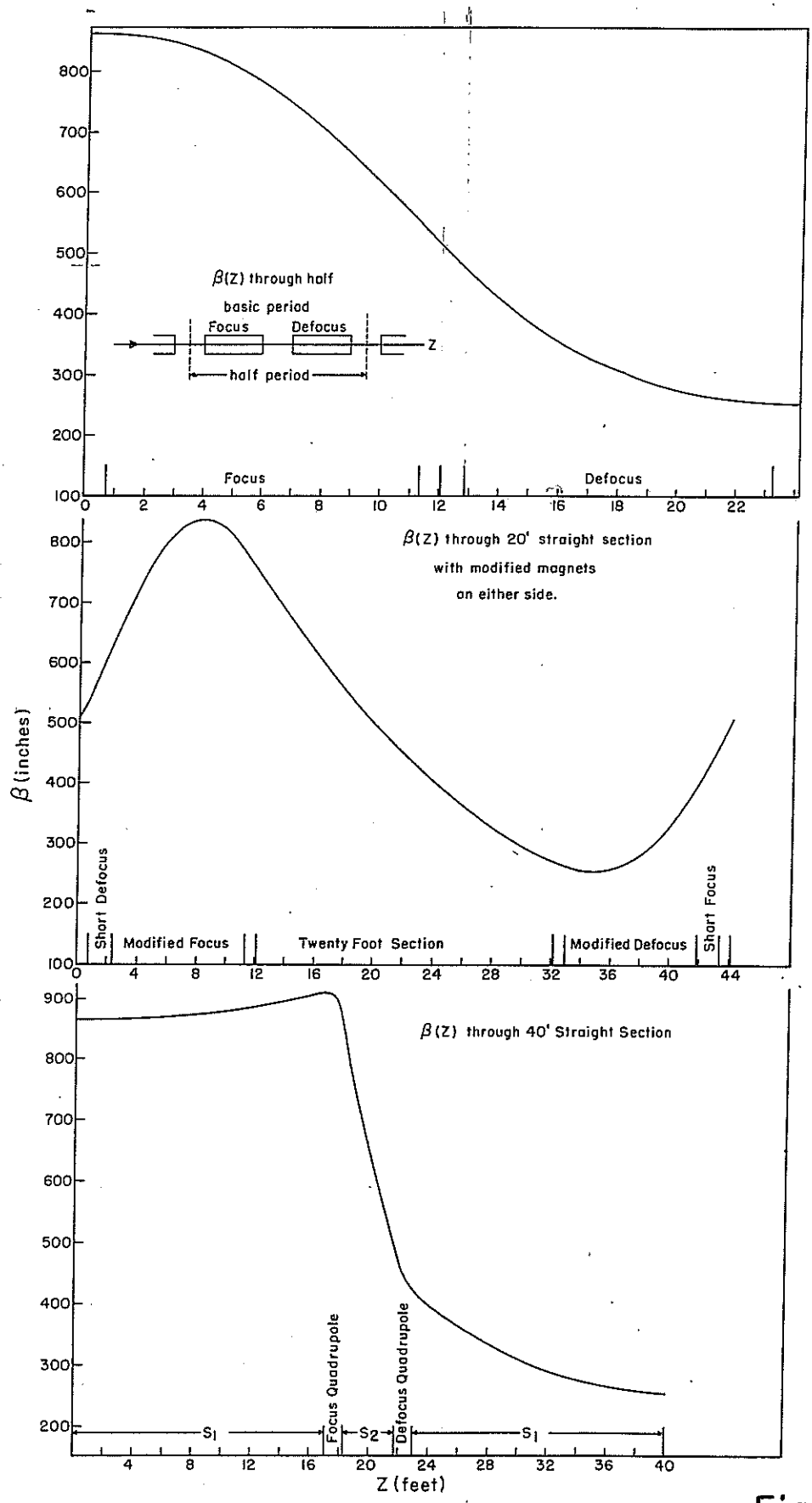
β(Z) through half
basic period
Focus
Defocus
Z
half period
Focus
Defocus
β(Z) through 20' straight section
with modified magnets
on either side.
β (inches)
Short Defocus
Modified Focus
Twenty Foot Section
Modified Defocus
Short Focus
β(Z) through 40' Straight Section
Focus Quadrupole
Defocus Quadrupole
S1
S2
S1
Z (feet)

Fig. 8a

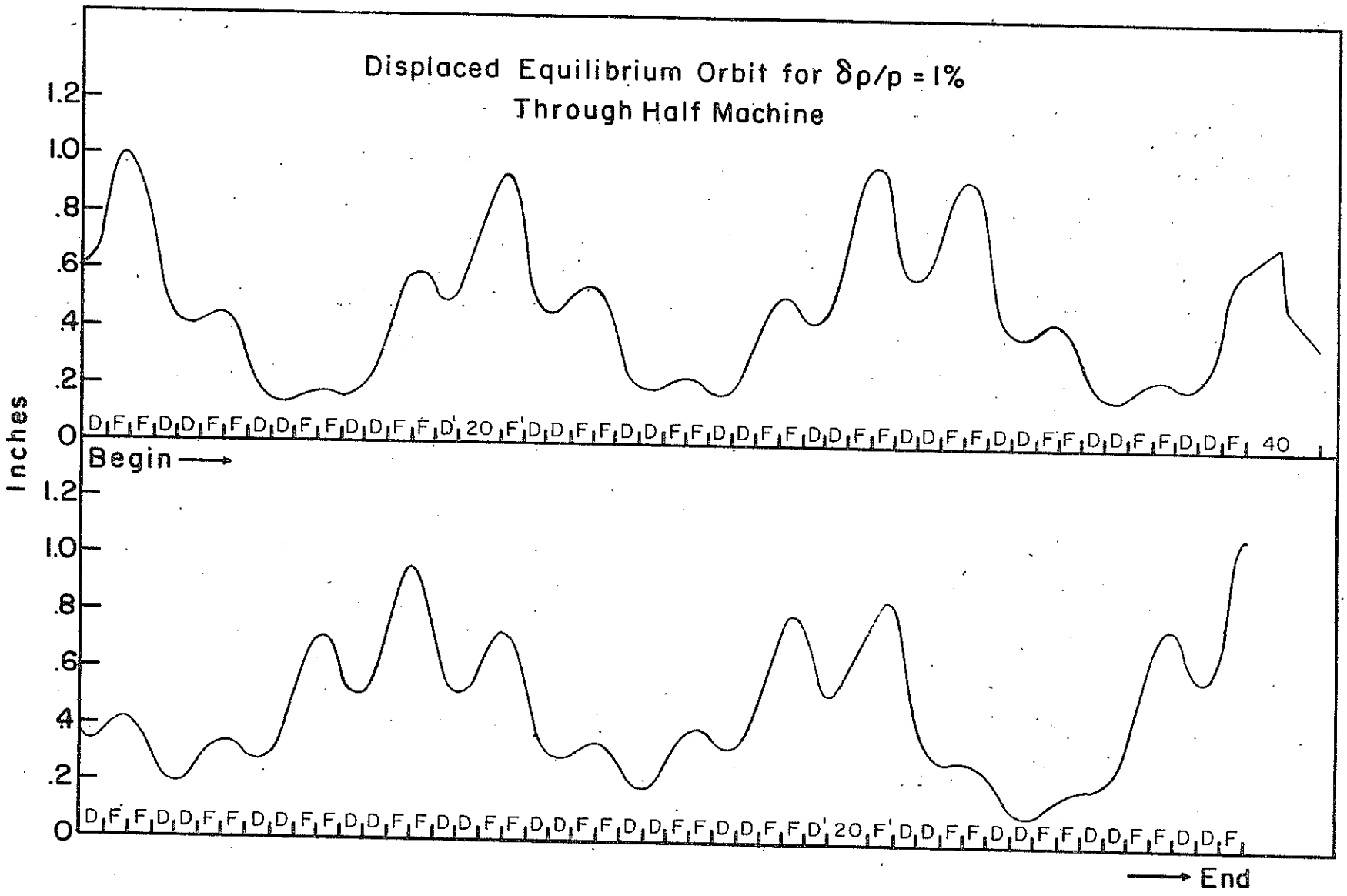
Displaced Equilibrium Orbit for δp/p = 1%
Through Half Machine
Inches
1.2
1.0
.8
.6
.4
.2
0
D F F D D F F D D F F D D F F D' 20 F' D D F F D D F F D D F F D D F F D D F F D D F F D D F F D D F F D D F F D D F 40
Begin
End

Fig. 8b

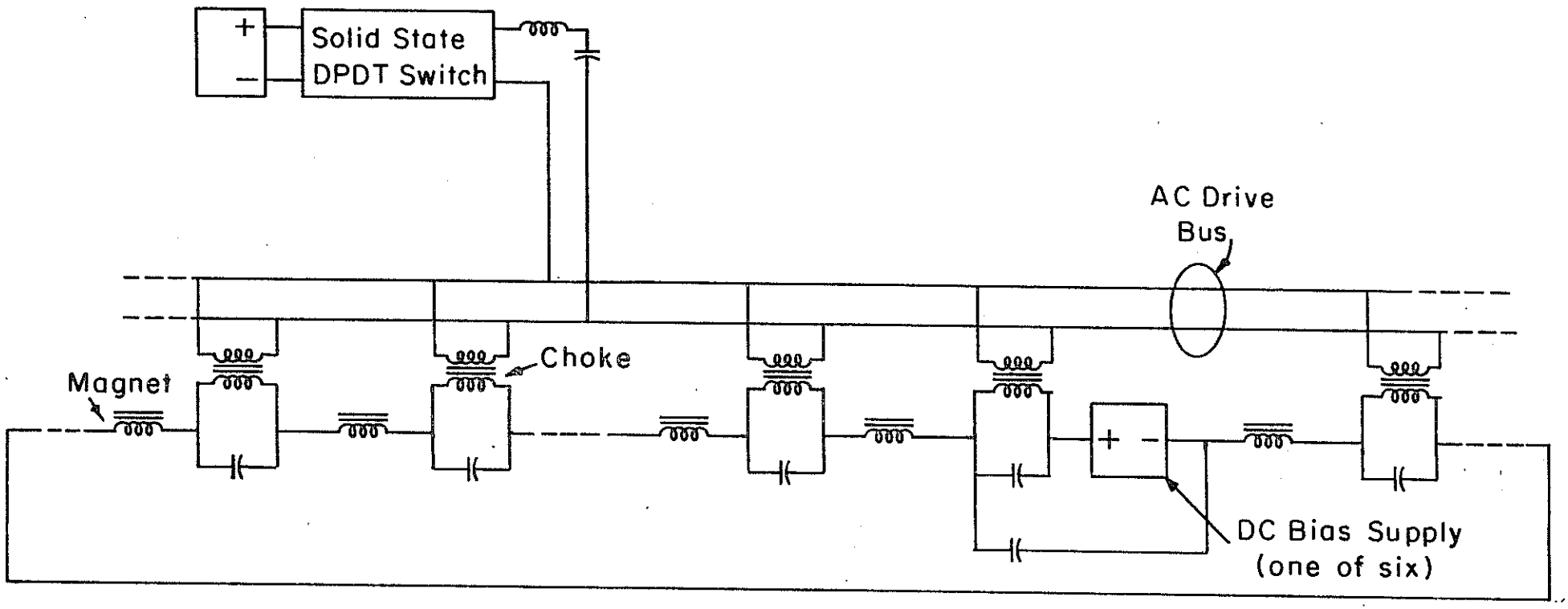
+
−
Solid State
DPDT Switch
AC Drive
Bus
Choke
Magnet
+ −
DC Bias Supply
(one of six)

Fig. 9

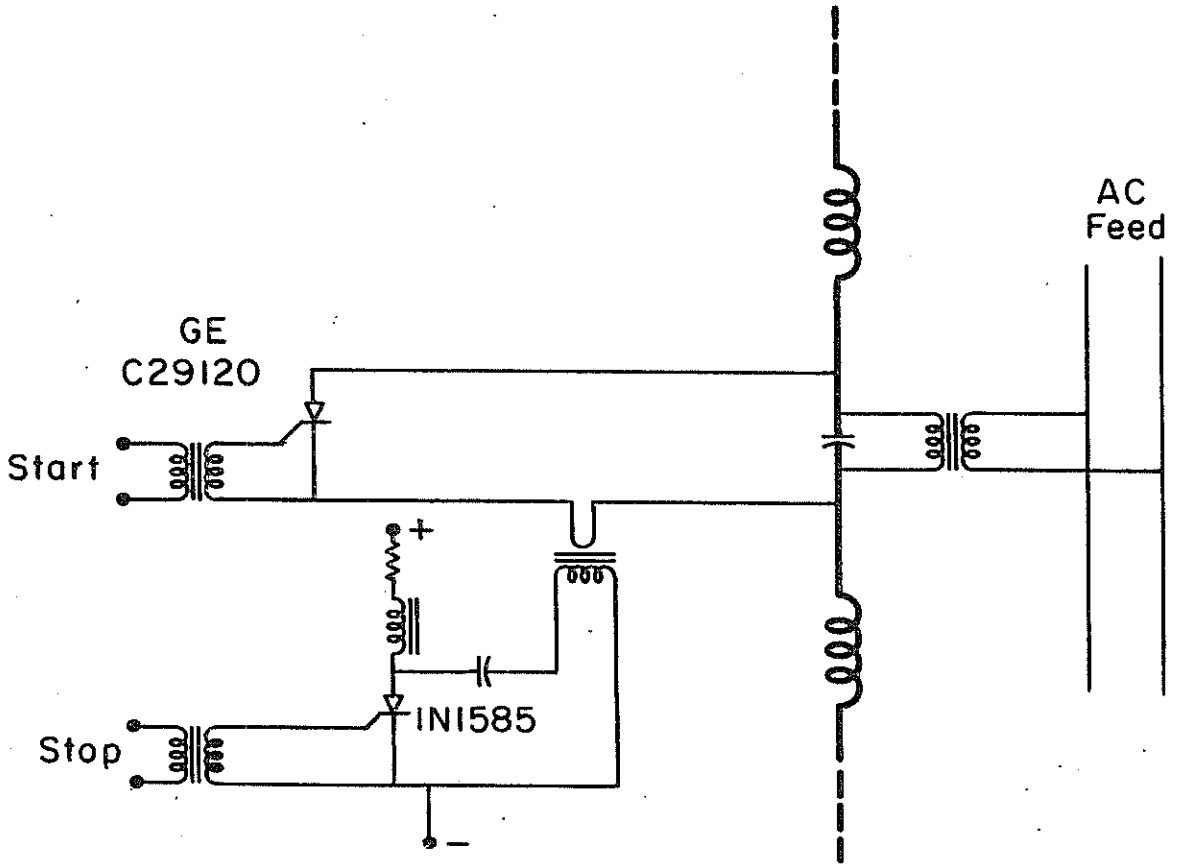

Fig. 10

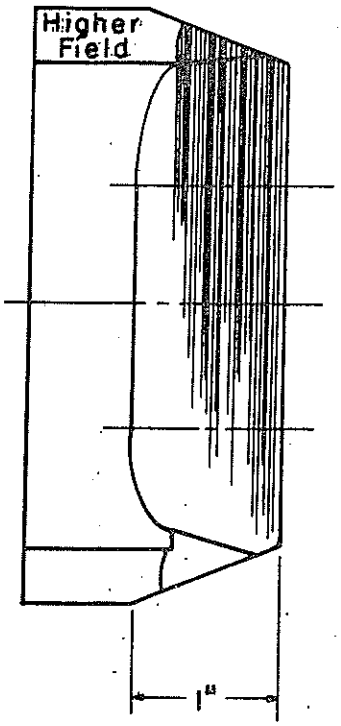

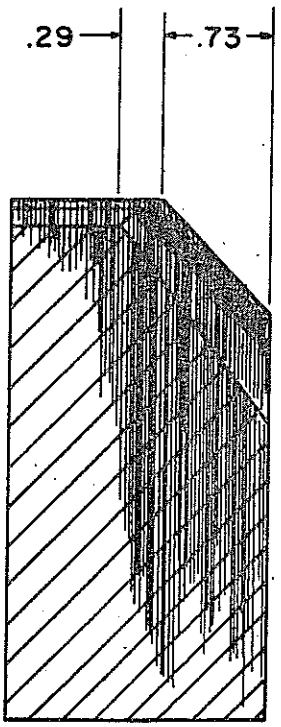

Section A—A

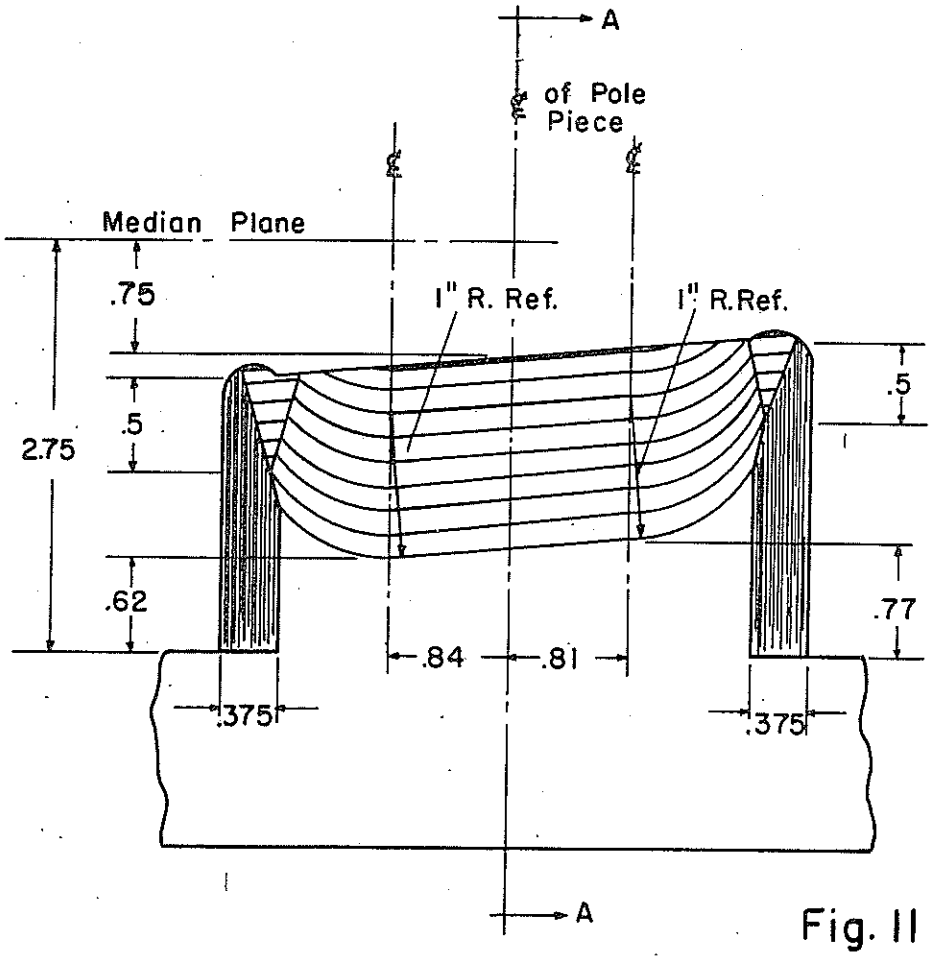

Fig. 11

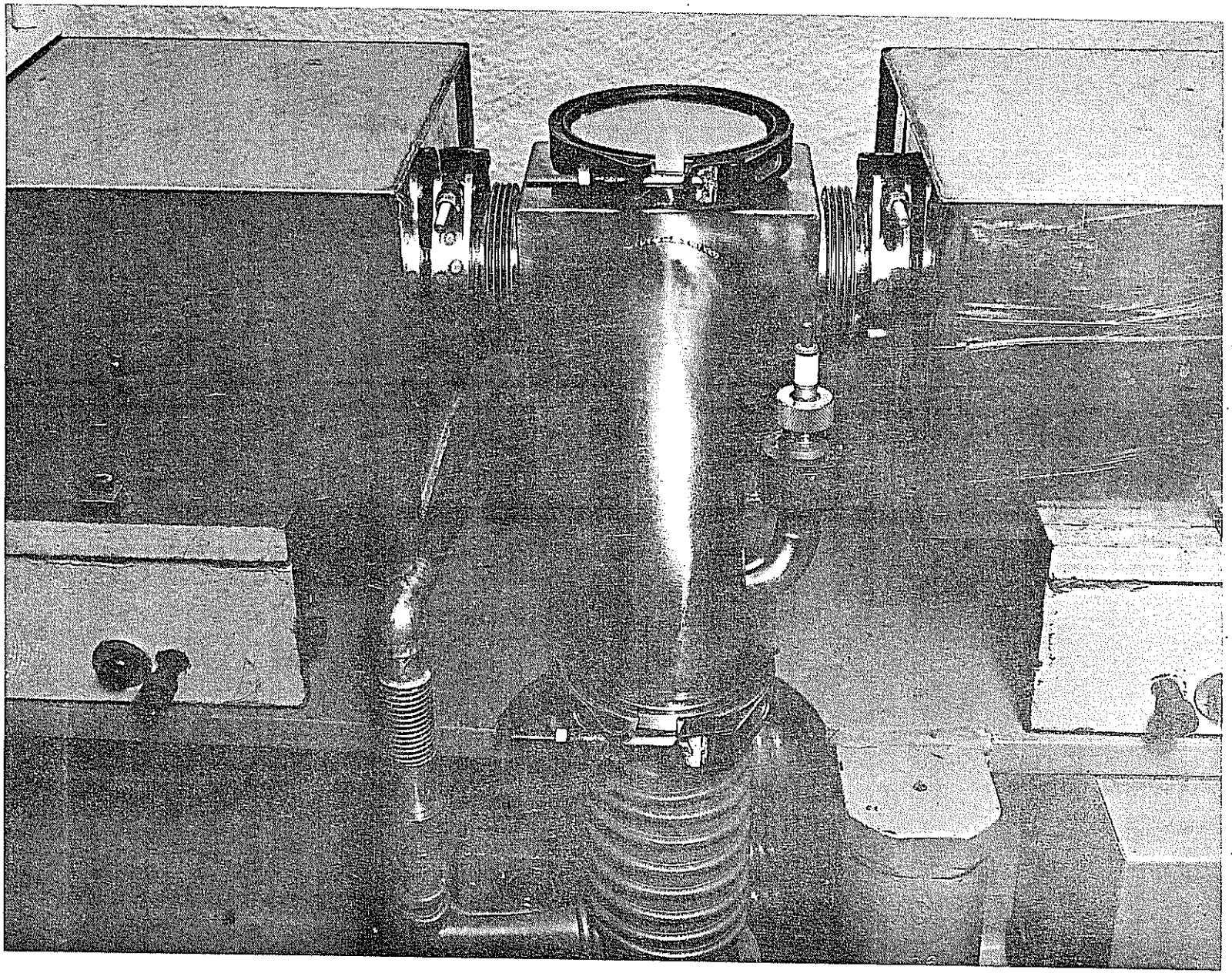

Fig. 12

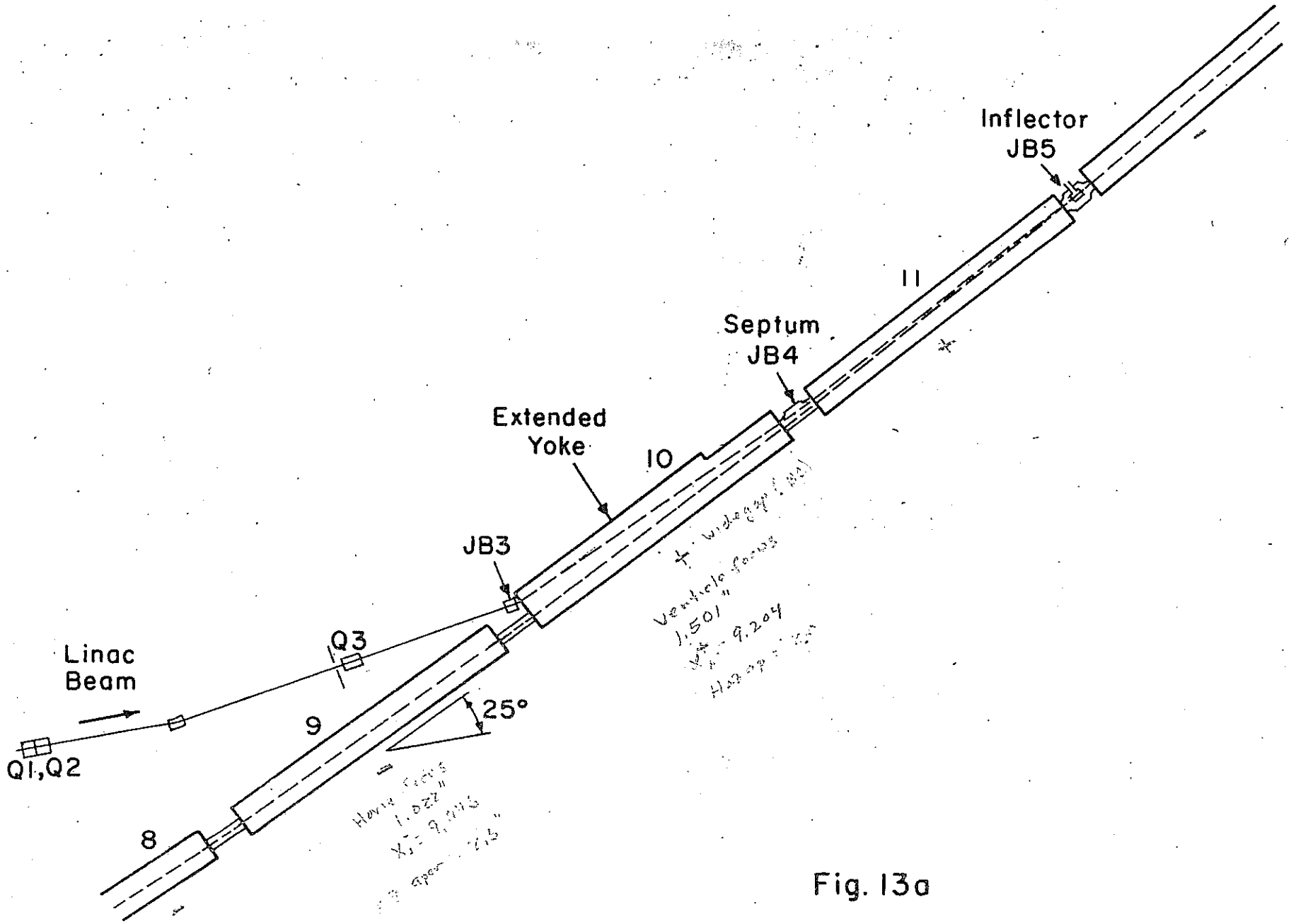
Inflector
JB5
11
Septum
JB4
Extended
Yoke
10
JB3
Linac
Beam
Q3
9
25°
Q1,Q2
8

Fig. 13a

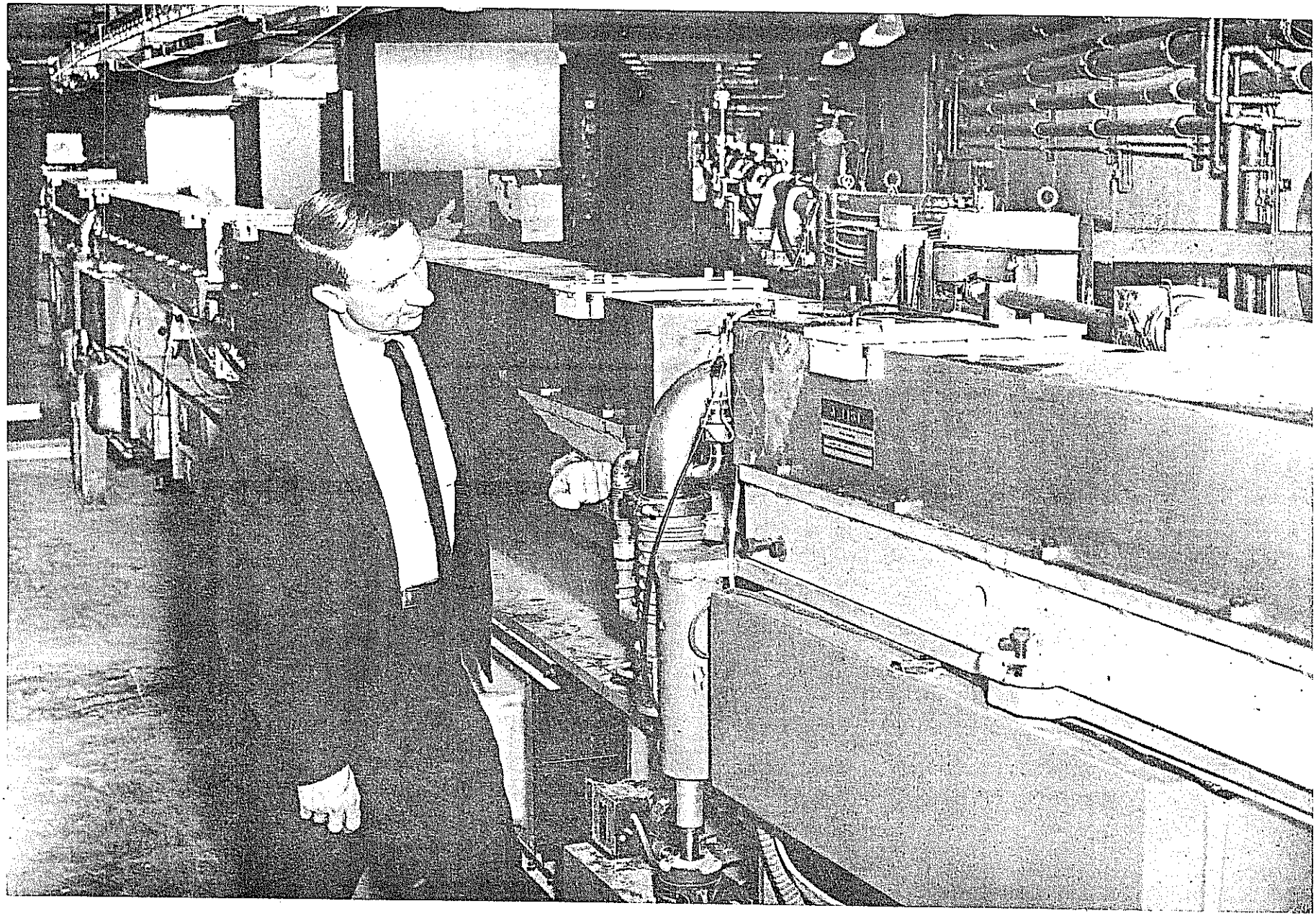

Fig. 13b

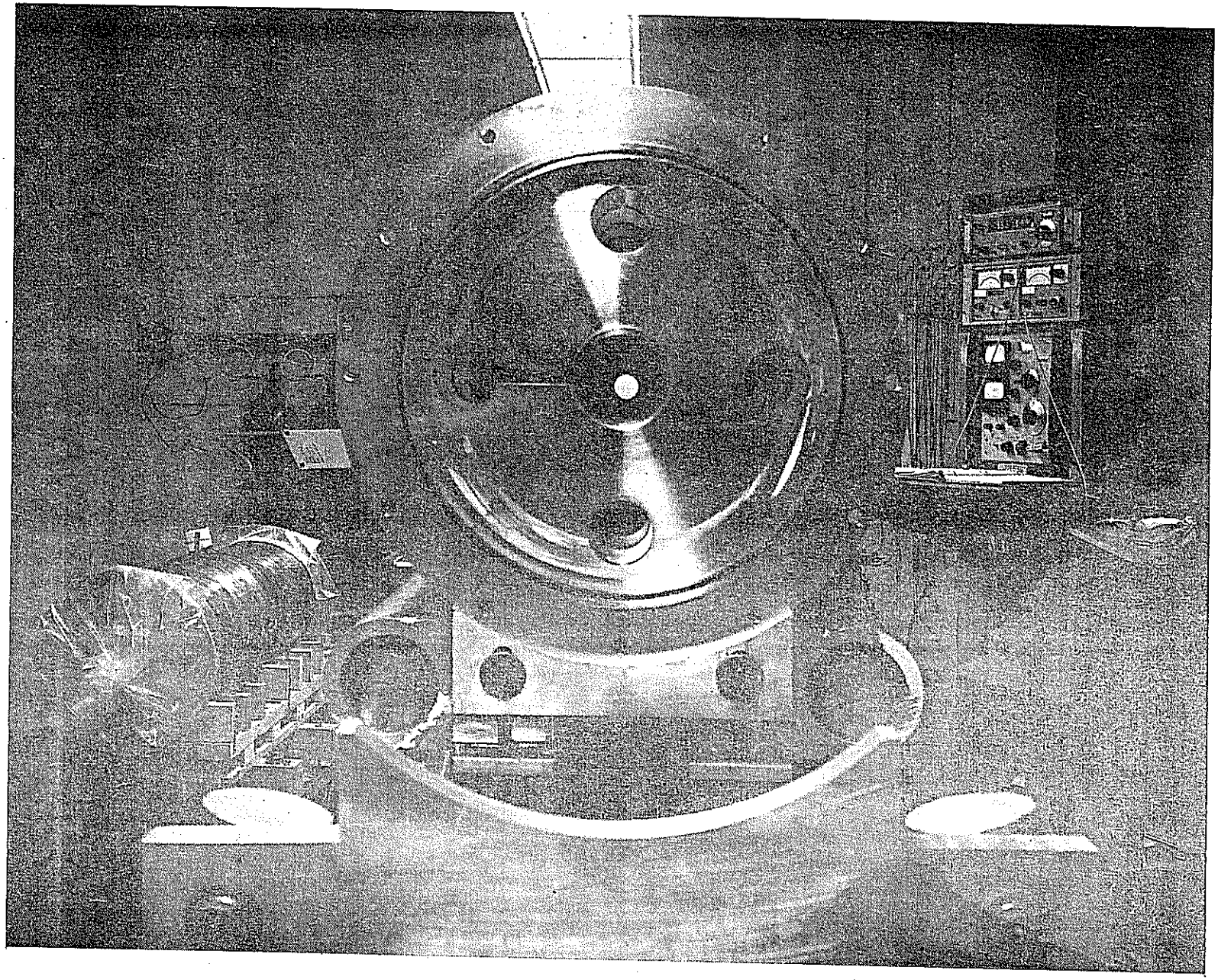

Fig. 14a

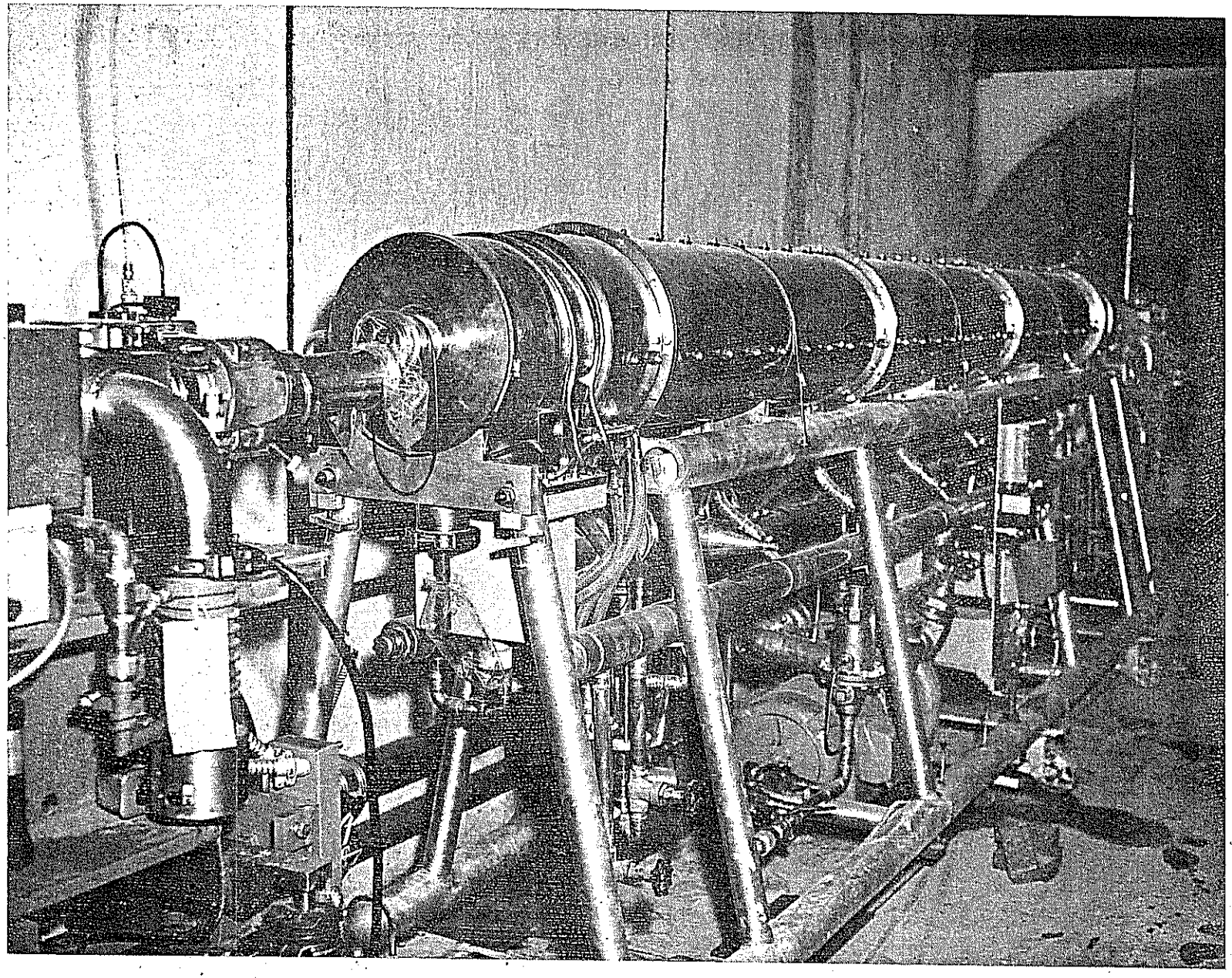

Fig. 14b

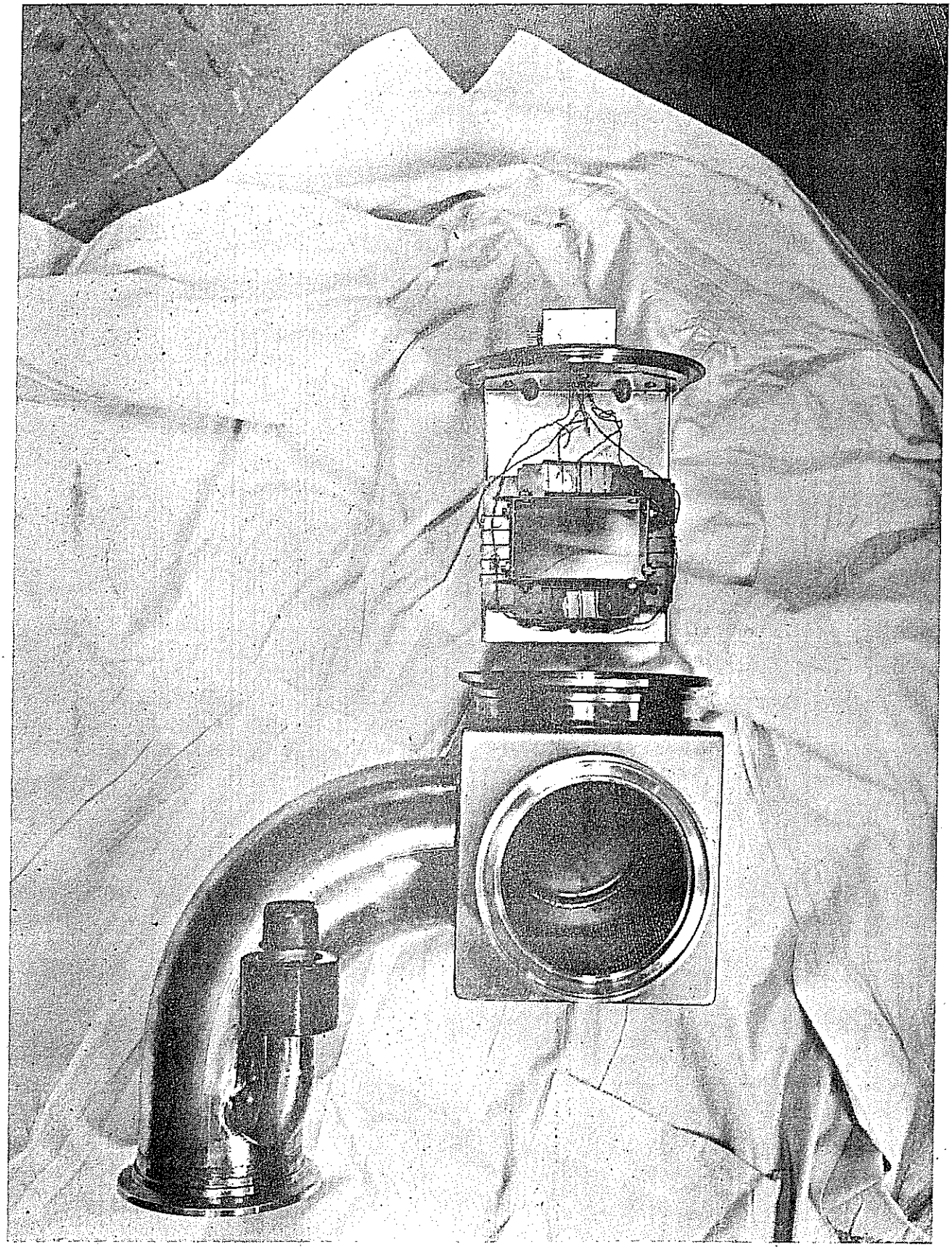

Fig.15

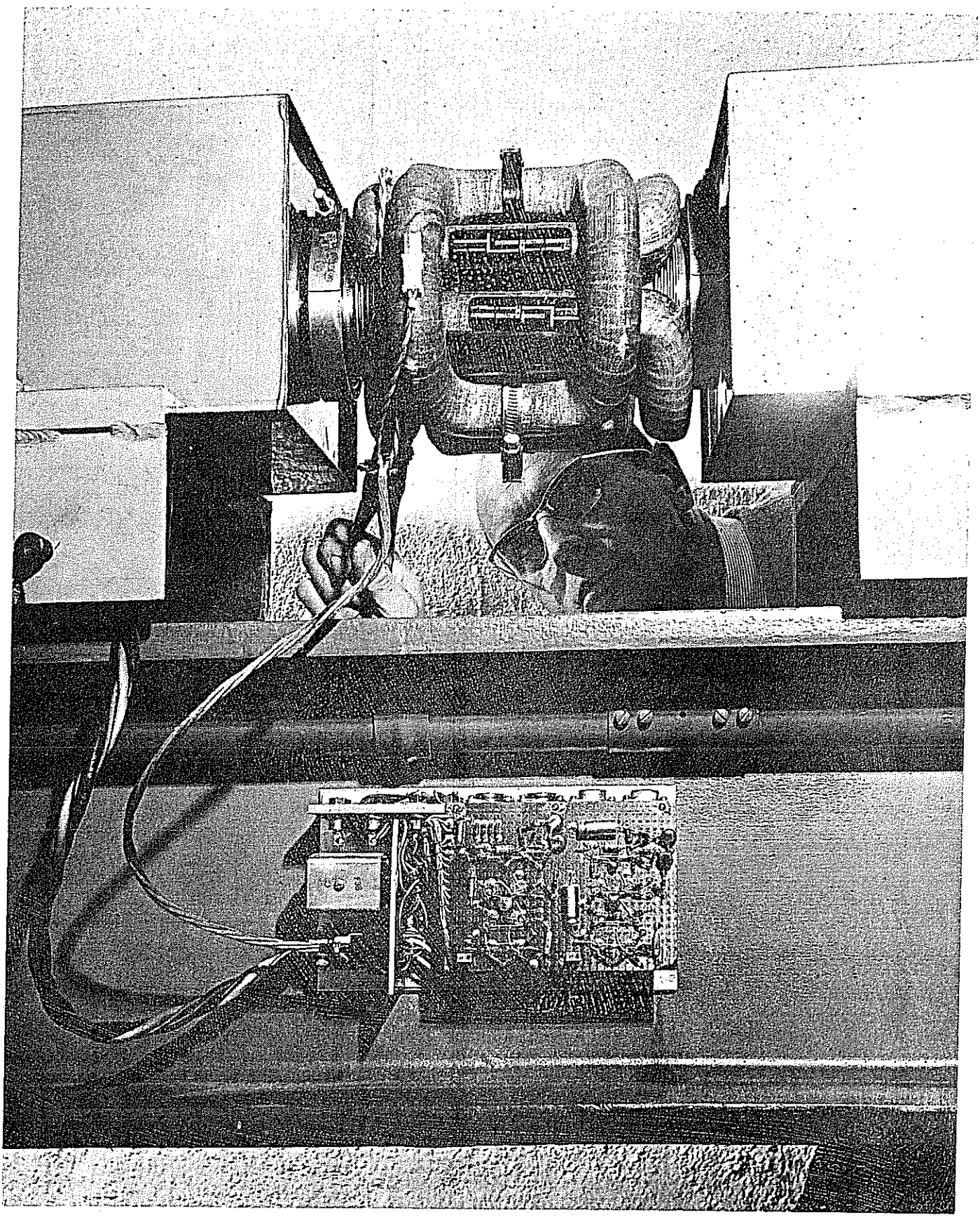

Fig. 16

Fig.17 From left are shown D. Edwards, R. Bower, E. von Borstel, K. Loveless, D. Rust, C. Kellers, J. DeWire, R. Littauer, W. Woodward, R. Matyas, R. Wilson.

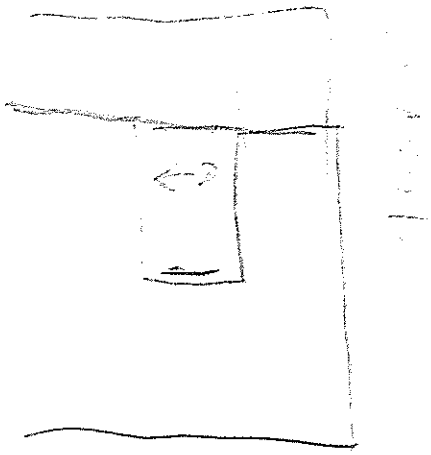

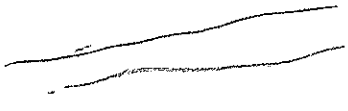

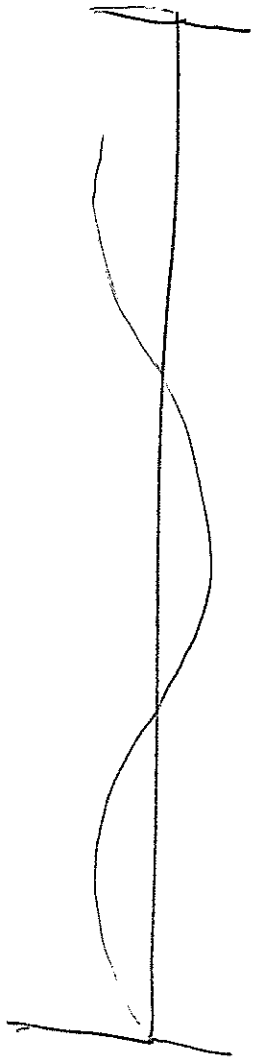

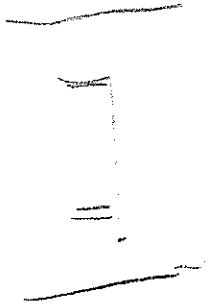

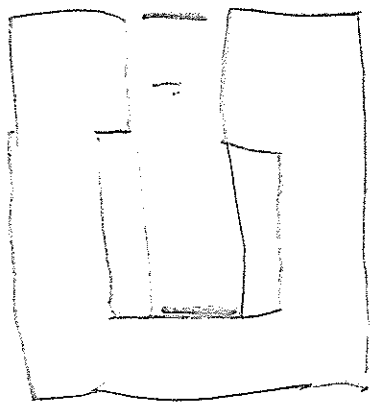

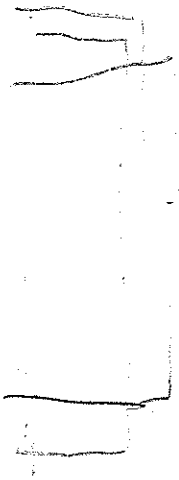

M Tigner

CORNELL UNIVERSITY
LABORATORY OF NUCLEAR STUDIES
ITHACA, NEW YORK

CS-34
K. Berkelman
July 13, 1967

INJECTION BEAM TRANSPORT AND INFLECTOR FOR THE CORNELL 10 GEV SYNCHROTRON

I. OPTICAL DESIGN

A. Introduction

A Varian S-band electron linac having the following properties was chosen as the injector for the Cornell 10 GeV electron synchrotron.

Maximum energy, at zero current	226 MeV
Beam current at 150 MeV	100 mA, pulse
Energy spread	1%
Pulse length	2.32μsec
Maximum repetition rate	60 pps
Emittance (horizontal or vertical)	1.6 mrad-mm

Some of the parameters of the synchrotron ring which are relevant to the problem of injection are:

Magnet pole width	10 cm
Gap height	2.6 cm, 3.9 cm
Horizontal acceptance, at $\Delta p/p=0$	10 mrad-cm
Vertical acceptance	5 mrad-cm
Momentum tolerance	±.89%
Orbit revolution time	2.521μsec
Magnetic field at 150 MeV/c	50 Gauss

For economy of building construction the linac was located inside the synchrotron ring. The linac axis intersects the ring at the ninth magnet (M9) downstream from the L0 long straight section at an angle of about 26°. Figure 1 shows the layout of the injection system. The linac beam is bent through 25.48° by an achromatic beam transport system of two bending magnets JB2 and JB3 and a quadrupole JQ3. Momentum selection is made by slits at JQ3. The second bending magnet is close to the short straight section between ring magnets M9 and M10. M10 has its inside return yoke extended so that the linac beam can pass inside. At the next straight section the injected beam is bent again by a septum magnet placed as close as possible to the nominal synchrotron orbit. Finally in the straight section between M11 and M12 the injected beam intersects the synchrotron orbit and is inflected into the right direction by a pulsed coil.

B. Transport System

The sector magnet plus quadrupole plus sector magnet beam transport system is the simplest solution to the following requirements: (1) Bend the linac beam by about 25° so that it is nearly parallel to the synchrotron orbit, (2) focus the beam on a slit with enough dispersion to allow a 1% momentum selection, and (3) deliver the analyzed beam at the exit of the system almost parallel and with very little dispersion. Figure 2 shows some representative particle trajectories. The first magnet JB2, a uniform-field sector magnet of angle $\theta = 12.74°$ and radius of curvature R=58.6cm, brings an initially parallel linac beam to a horizontal focus at a distance downstream $L = R/\sin\theta = 263$ cm with a momentum dispersion $p_o (\partial x/\partial p) = R = 5.9$ mm per percent momentum deviation. The momentum limiting slit is placed at this focus (actually a little upstream) and the movable jaws are normally set for about 1% full width. A horizontally focusing quadrupole JQ3 immediately downstream of the focus reverses the slopes (relative to the center line) of the off-momentum trajectories that pass through the slit, so that all trajectories in the second half of the system are symmetric about the focus. That is, the particles emerging from the second bending

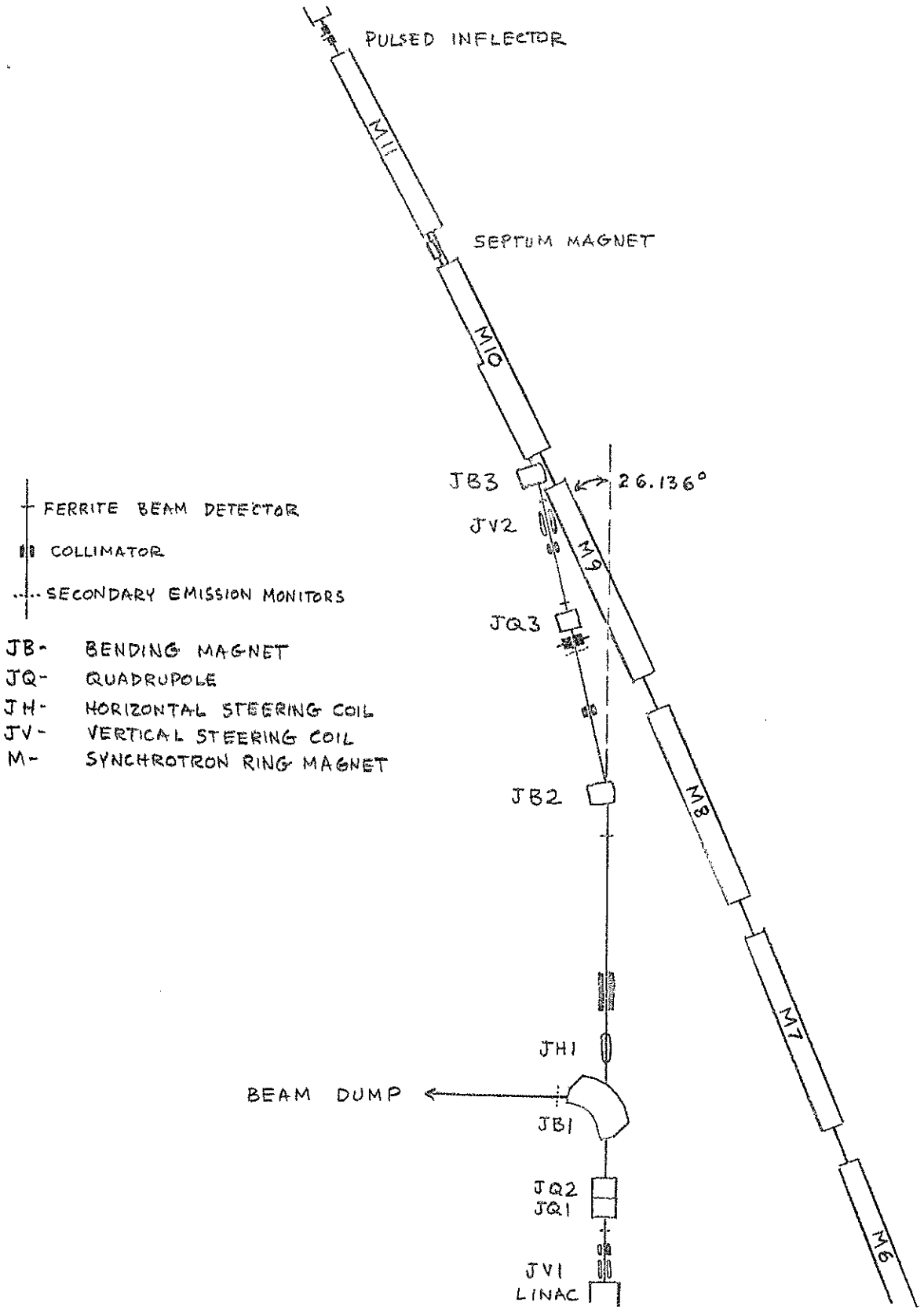

Fig. 1 Schematic diagram of the injection transport system, not to scale.

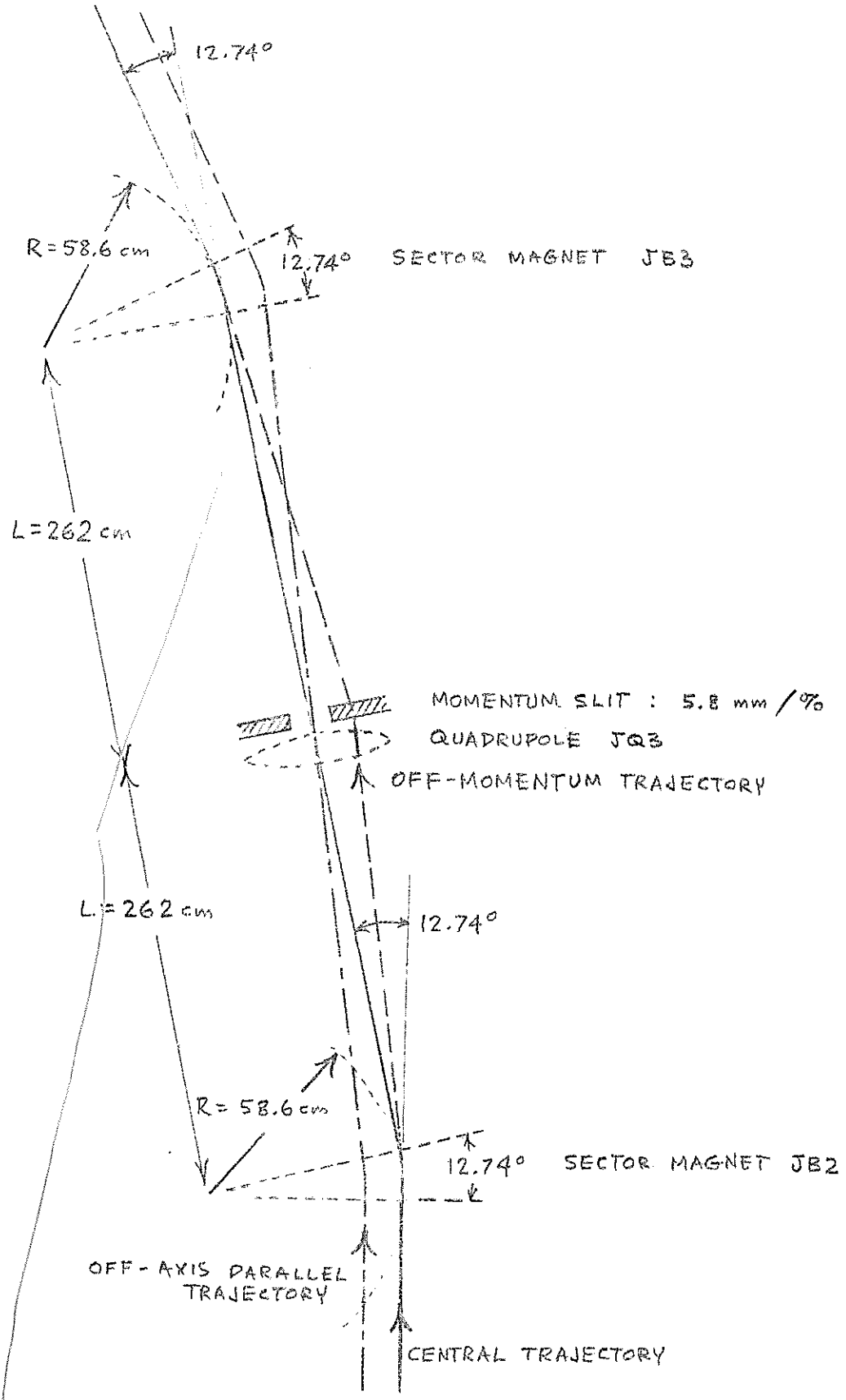

Fig. 2 Diagram to illustrate the beam optics of the achromatic bending and momentum analysis.

magnet JB3 located a distance L downstream from the focus form a parallel beam again with no momentum dispersion. To achieve this the focal length of JQ3 is L/2 and JB3 is identical to JB2. The overall first-order horizontal transfer matrix (displacements, slopes and fractional momentum deviations) from JB2 to JB3 is:

$$\begin{pmatrix} -1 & 0 & 0 \\ 0 & -1 & 0 \\ 0 & 0 & 1 \end{pmatrix} .$$

That is, the exit beam cross section is identical to that of the entering beam, except that the extreme momenta have been removed, the central trajectory has been deflected by 25.48°, and the displacements and slopes are inverted (left to right and vice versa - - of no consequence, assuming a symmetric beam).

At the linac exit is a quadrupole doublet, JQ1 and JQ2, to keep the linac beam parallel in the horizontal plane and to counteract the vertically diverging effect of JQ3. Horizontal and vertical steering coils (see Fig. 1) are placed here and there throughout the system to provide for empirical steering corrections. Upstream of each major magnet there is a 9.6 mm diameter water-cooled copper collimator to protect the magnet coil insulation from deterioration by stray radiation and to define the beam direction well enough to make the momentum analysis meaningful. Downstream from each collimator the beam passes through a ferrite core with a secondary winding to monitor the beam current pulse.

An auxiliary analyzing magnet JB1, called the dump magnet, allows one to divert the linac beam by an angle of 86.7° through a vacuum tank into a shielded cave for linac tunup and energy analysis without injecting into the synchrotron. A movable collimator, called the shutter, immediately downstream serves to protect personnel in the synchrotron tunnel from accidental irradiation while the dump is in use. When the linac beam is being injected into the synchrotron, the dump magnet field is turned off and the shutter is opened.

C. Septum and Inflector

In general, a multiturn inflection system has the advantage of permitting beam injection over a longer duration and thus getting more particles into the synchrotron. One pays for this by not being able to put all of the particles into stable synchrotron orbits. In our case multiturn injection loses its advantage because the linac beam pulse duration does not exceed the orbit period. Consequently a single-turn (in the pulse-length sense) center-line pulsed inflector is the obvious choice.

The second sector magnet JB3 fits into the 25 cm straight section between ring magnets M9 and M10 so that the incoming linac beam just misses the yoke of M9. The yoke of M10 is extended (see Fig. 3) in the beam plane to allow the injected beam to enter the synchrotron vacuum. At the center of the M9-M10 straight section the injected beam is 14.0cm from the nominal synchrotron orbit. If the pulsed inflector were placed at the next straight section, it would have to deflect the injected beam through an angle of about 1.5° in order to put it on the central orbit. Since a fast pulsed magnet for 150 MeV/c particles with the required geometry (angle, length and operture) is not easy to construct, we have chosen to minimize the problem by putting a DC septum magnet as close as possible to the synchrotron central orbit in the M10-M11 straight section so that in the following straight section where the injected beam finally intersects the nominal synchrotron orbit, the required inflection angle is only .7° (12.2 mrad).

The choice of bending angles for the sector magnet, septum magnet, and pulsed inflector, and the choice of clearance between the injected and circulating beams at the septum were determined by comparing trajectories (computed by W. Evanco) through the synchrotron field (including fringing) for various assumptions of inflection angle. An inflection angle of .7°, implying a septum deflection of 1.28° (22.5 mrad) and a separation of 4.9 cm at the septum, was chosen as a reasonable compromise between low inflector field and large septum clearance.

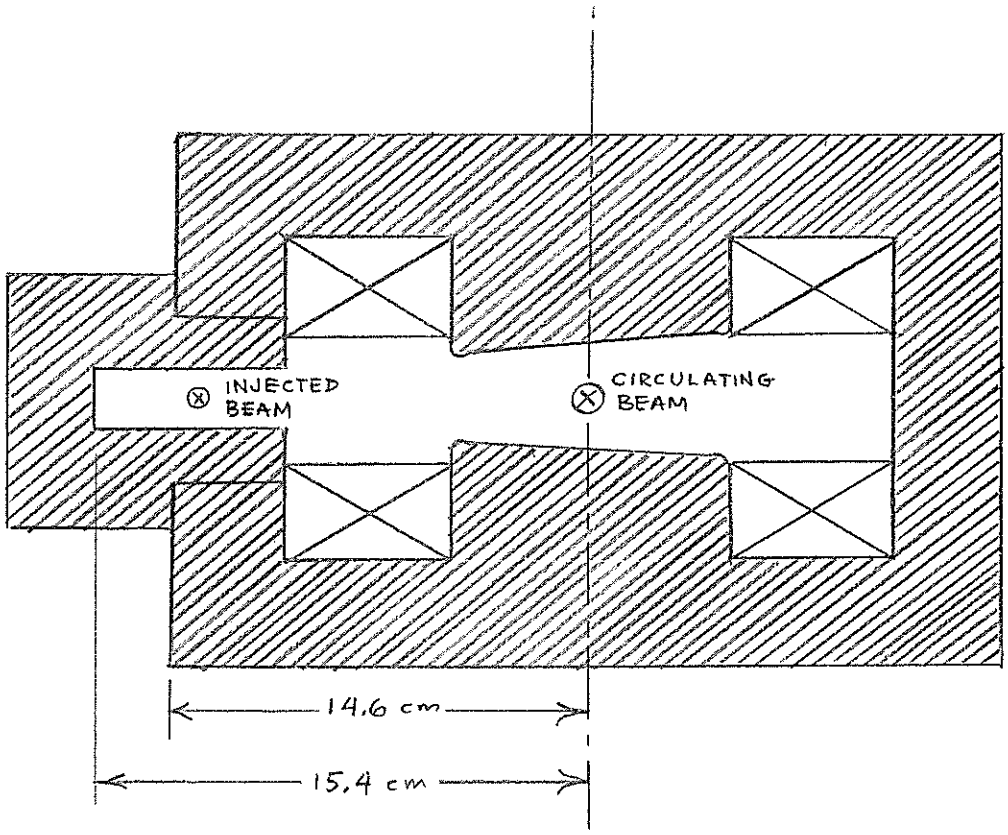

Fig. 3 End view of the upstream face of synchrotron magnet M10, showing the modification of the yoke to accommodate the injected beam.

The horizontal and vertical acceptance ellipses for stable synchrotron orbits starting at the inflector straight section (Fig. 4a,b) were propagated backward through the inflector and the M11 field along the injectron trajectory to the septum straight section (Fig. 4c,d), and then through the septum magnet and the M10 fringe field to the sector magnet straight section (Fig. 4e,f). The phase voume corresponding to trajectories which lead to stable synchrotron orbits is very much larger than the phase volume (emittance) of the linac beam delivered to the synchrotron, so that precise matching is not necessary. This means that the injection efficiency should not be very sensitive to error or uncertainty in the details of the magnetic field plots or to misalignment, higher-order focusing and defocusing effects, or space charge. Empirical optimization of the beam monitor signals using the various steering and focusing elements in the system can compensate for almost any defect in the beam optics.

II BEAM TRANSPORT MAGNETS

Bending Magnets

These are two identical uniform-field C magnets. The poles are cut so that a trajectory of radius 58.6 cm intersects the entrance and exit pole edges at right angles and the angle of deflection is 12.74°. There is a shield plate just outside the gap so that the fringing field of JB3 (.2% of the gap field 13 cm away from the beam line) will not perturb the circulating synchrotron beam. The first magnet JB2 is known as the Analyzing Magnet; the second JB3 is called the Trimmed Magnet. They are powered in series by one supply; the second magnet has an extra smaller supply, the "trim", which can add to the main current. The magnets and supplies were designed and manufactured to Cornell specifications by ARCO, Walnut Creek, California. Some of the important parameters are listed below:

Bend angle	12.74°
Bend radius	58.6 cm

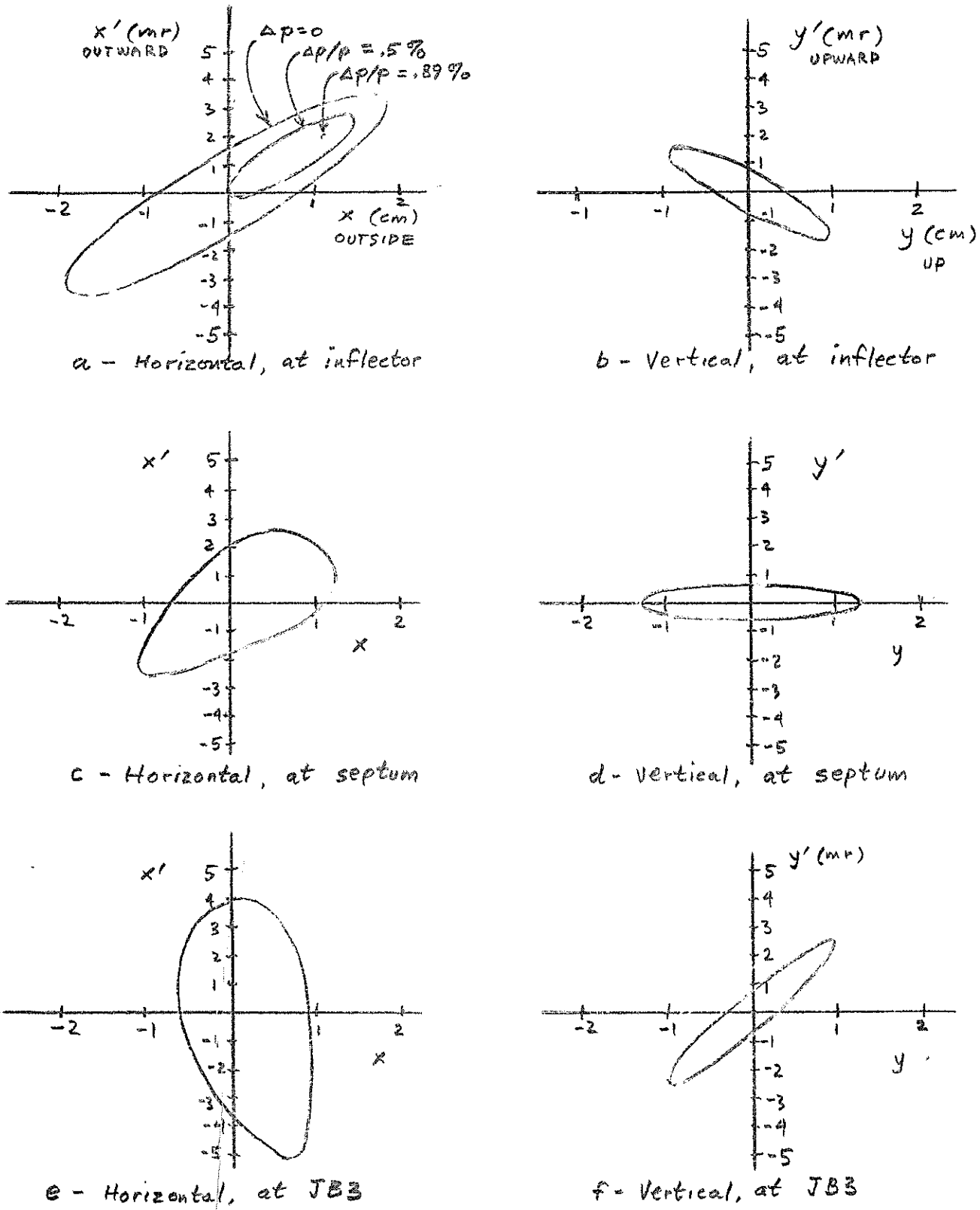

Fig. 4 Synchrotron acceptance ellipses. A particle displaced from the nominal central trajectory by displacements x and y and slopes x' and y' whose values lie within the closed curves will be captured in a stable orbit. These curves were computed by W. Evanco by tracing trojectories through the design synchrotron fields.

Arc length		12.4 cm
Gap height		2.22 cm
Cooling	water: approx. 3 gpm @ 25 psig	
Interlocks	water flow, temperature	
Maximum current		32 A
Resistance (both coils of one magnet)		1.25 Ω
Maximum field		11.8 kG

For the required bending angle the relation between magnet current, magnet field, and particle momentum is plotted in Figure 5.

Power Supplies:

Maximum output current	30 A (series), 4 A (trim)
Maximum output voltage	150v " 75v "
Current regulation	.1% (each)
Current programing constant	12.3 Ω/A, 130 Ω/A
Remote programing resistor	0-500Ω, 2 1/2 w (each)
Metering shunt	50mV @ 30 A (each)
Input	208v, 3φ, 5kW (total)

Sources of more Information:

Specifications for Cornell Injection Magnets and Supplies SPEC:KB-1.

Proposal for an Injection Magnet Assembly AR-1008, ARCO.

Test Results and Power Supply Instructions, ARCO.

ARCO drawings: Magnets-BH-2734, BH-7114
Supplies-BG-0084A, BG-0074C, BG-0133, BF-9303, BF-9313, BG-9524, BG-9534, BH-2264, BH-2253.

Quadrupole Magnets

The quadrupoles JB1, JB2, and JB3 are identical, except that the first two are joined together to make a doublet with a common yoke and an effective separation distance of 25.4 cm. They were manufactured

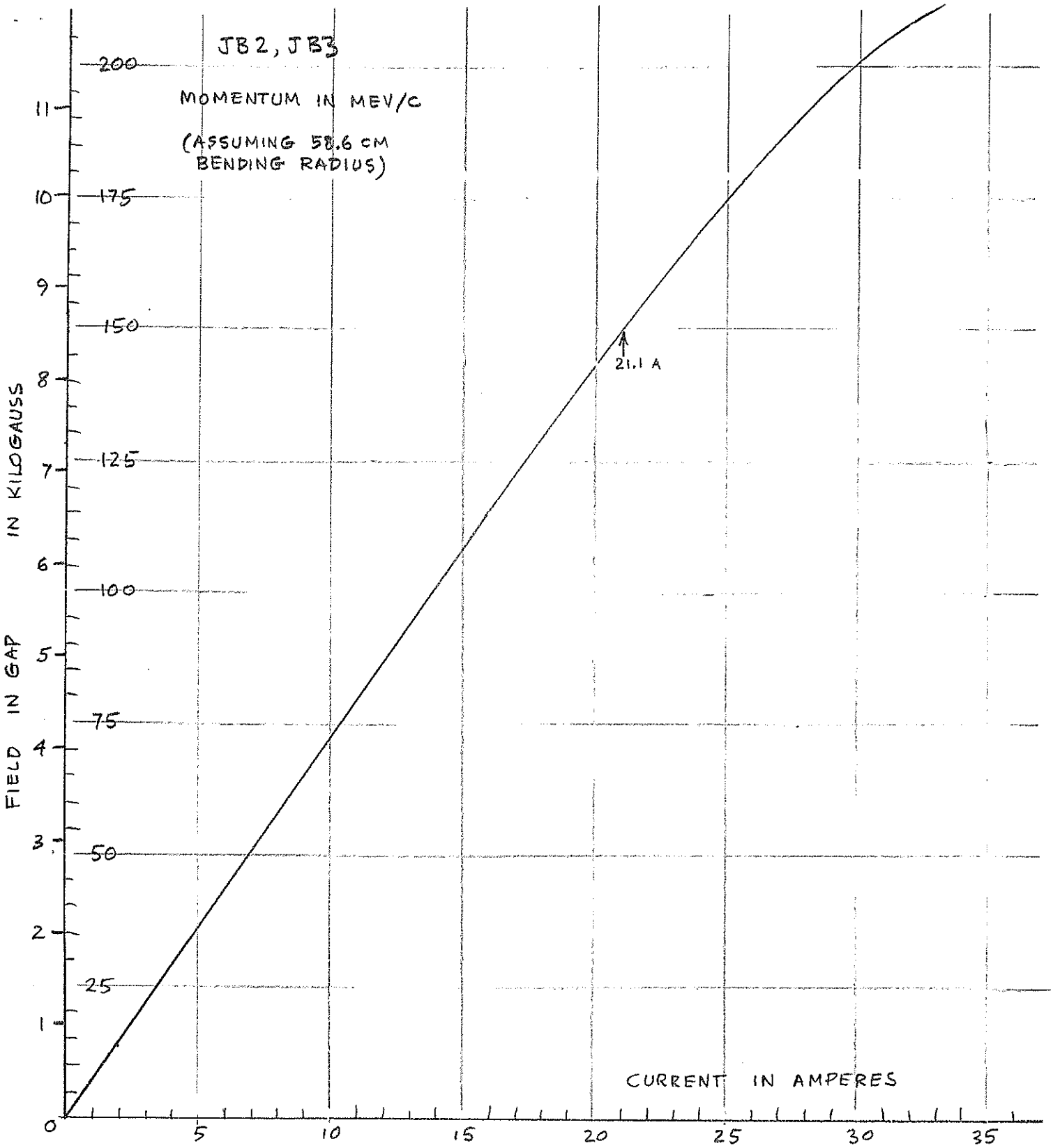

Fig. 5 Nominal calibration curve for the momentum analysis magnets of the beam transport system, obtained from field measurements made by the manufacturer, ARCO.

by Spectromagnetic Division, Hayward, California (catalog numbers 1006 and 1050).

Inscribed diameter	5.08 cm
Effective length	12.7 cm
Cooling	convection
JQ3 current at 150 MeV (nominal)	3.66 A
Maximum current	12A
Resistance (all coils of one quad)	1.1Ω
Maximum gradient	1.0 kG/cm
Minimum focal length at 150 Mev/c	40 cm

Each quadrupole is powered by a Harrison Lab #6427A supply with the following specifications:

Maximum output current	15 A
Maximum output voltage	18 v
Current regulation	1%
Current programing constant	1 5 Ω/A
Remote programing resistor	0-200Ω, 2 1/2 w
Metering shunt	50 mV @ 15A
Input	120v AC, 450 w

Sources of more information:

Specifications for Cornell Injection Magnets and Supplies SPEC:KB-1.

Spectromagnetic Magnetic Quadrupole Lenses: Spectromagnetic advertising bulletin.

Spectromagnetic drawings A35887-1A, A35886-1A

Operating and Service Manual Model 6427A DC Power Supply, Harrison Laboratories.

C. Dump Magnet

The dump magnet JB1, a uniform-field edge-focusing C magnet, was adapted from one of the quadrant magnets of the Cornell storage ring project by widening the gap and drilling a hole through the yoke for the undeflected linac beam. It was manufactured by P.E.M., Oakland, California.

Bend angle	86.7°
Orbit radius	47.8 cm
Gap height	1.59 cm
Cooling	water: 7.5 gpm @ 60 psi
Interlocks	water flow, temperature
Maximum current	800 A
Resistance (both coils)	.056 Ω
Maximum field	15.6 kG

For the nominal bending radius the relation between magnet current, magnetic field, and particle momentum is plotted in Fig. 6.

The magnet is powered by two Sorenson DCR 40-500 A supplies wired in parallel. Each supply has the following specifications.

Maximum output current	500 A
Maximum output voltage	45 v
Current regulation	1%
Current programing constant	.3 Ω/A
Remote programing resistor	0-100Ω, 5 w
Metering shunt (both supplies in parallel)	50 mV @ 800 A
Input	480 v, 3ϕ , 26 kW

Sources of more information:

Zero Gradient Magnet Test Data and Instruction Manual, P.E.M.

Drawings DH 3220, CM 1227 B.

Specifications for 10 GeV Synchrotron 800 Amp. Magnet Supply, SPEC:KB-2.

Instruction Manual for Model DCR 40-500 A, Sorenson.

D. Steering Magnets

Two vertical steering magnets are located at the extreme ends of the transport system, JV1 near the linac exit and JV2 near the synchrotron entrance. A horizontal steering magnet JH1 is located near the

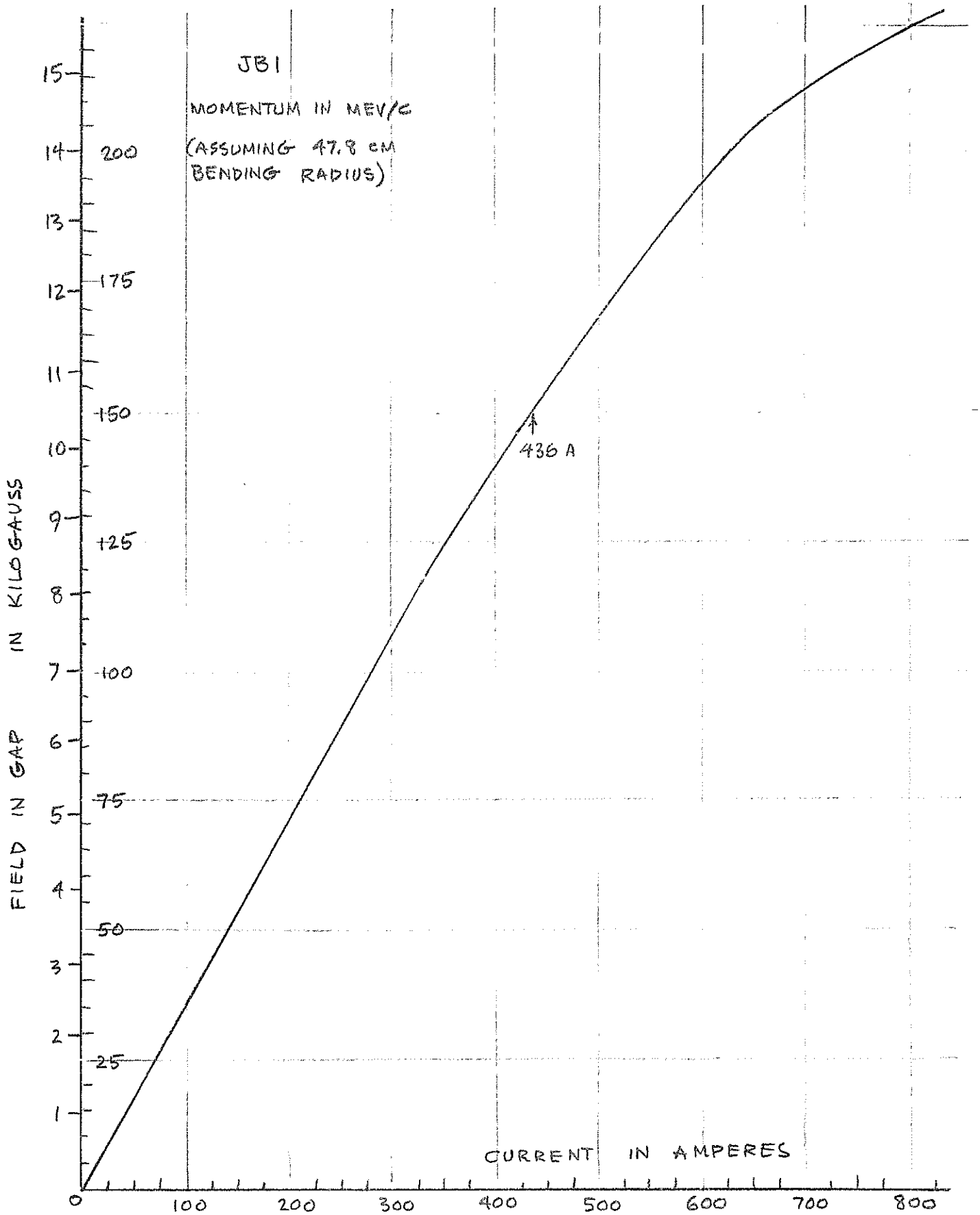

Fig. 6 Nominal calibration curve for the dump magnet, obtained from field measurements made by the manufacturer, P.E.M., corrected for the increase in gap height from 9.53 mm to 15.88 mm. The correction was made by assuming that the current for a given field was increased by 5/3.

dump magnet. These three magnets plus the trim current in JB2 are used to optimize the beam centering. Each steering magnet consists of a pair of coils wrapped close to the 3.8 cm diameter beam pipe, about 28 cm long. Each coil is 120 turns of #18 varnished wire potted in epoxy and wrapped with glass fiber tape.

Maximum current (pair of coils in series)	6 A
Resistance	3.8 Ω
Maximum field	165 Gauss
Maximum bend angle at 150 MeV/c	9 mrad = .5°

Each of the three steering magnets is powered by a Lambda LH 122S DC supply with the following specifcations:

Maximum output current at 30° C	5.7 A
Maximum output voltage	20 v
Current regulation	<1%
Current programing constant	about 20 Ω/A
Remote programing resistor	100Ω, 2 1/2 W
Metering shunt	50 mV @ 5A
Input	120v AC, 300w

For more information see the Lambda instruction manual.

III. BEAM PIPE

A. Vacuum System

The beam pipe is made of stainless steel tubing, 3.8 cm outer diameter, 1.6 mm wall. Sections are flanged together with conoseal flanges, manufactured by Aeroquip Corp., Los Angeles: female flange 55291-150S, male flange 55292-150S, copper gasket 55666-150EC, coupling 50773H150. The layout is given on drawing DH 3249, which has references to detailed drawings of the individual parts. The bending magnets JB1, JB2, JB3 require special vacuum chambers which fit between the poles.

There is a fast-acting pneumatically-controlled metal-gasketed gate valve at the linac exit, and near the synchrotron entrance there is a gate valve of the same type as used in the synchrotron ring. Between these valves the beam pipe is evacuated by two pumps: a 50 ℓ/s Varian vacion pump near the linac end and an oil diffusion pump (as in

the synchrotron ring) near the synchrotron end. Upstream of the diffusion pump is a cold trap which the beam passes through. The trap is cooled by a compressed-air operated mechanical refrigerator (Welch series 3150 cryorefrigerator). Since the pumping speed through the beam pipe is very low, the vacuum at the linac end can be considerably better than the synchrotron vacuum.

The tables which support the beam pipe and the components of the transport system are surveyed into position so that the beam center line is 20.3 cm (8.00") above the top surface of the tables. The alignment of all components is made with respect to a line scribed along the top surface of the tables.

B. Collimators and Slits

Collimators and slits are used at various points along the beam pipe to limit the lateral extent of the beam, in order to define its position, direction, and momentum accurately, and to protect the various components from the deteriorating effects of stray radiation. Their dimensions are tabulated below and their locations are given in Fig. 1:

DESIGNATION	LENGTH	HOLE	DRAWING
Linac exit	10.2 cm	9.5 mm I.D.	CH 3131
Shutter	30.5 cm	9.5 mm I.D.	CH 3221, DH 3300
JB2 exit	10.2 cm	9.5 mm high x 25.4 mm wide	CH 3135
Mom. Slit	10.2 cm	9.5 mm high x 0-19.0mm wide	BH 3188
Synch. entrance	10.2 cm	9.5 mm I.D.	CH 3131

The linac exit, JB2 exit, and synchrotron entrance collimators are fixed in position and brazed to the beam pipe at the ends. The shutter is similar except the beam pipe has bellows in it so that the shutter can be rotated to block the beam line. The momentum slit has two movable jaws mounted in a vacuum box. They connect to drive motors and the cooling water supply through bellows in the sides of the box. All the collimators are made of copper and are water cooled. The jaws of the momentum slits have water channels drilled in them; the others have copper tubing soldered to the outside of the 7.6 cm diameter body of the collimator. Each collimator is surrounded by lead shielding.

C. Beam Detectors

Immediately downstream from each collimator (except JB2 exit), is a ferrite beam monitor. The steel beam pipe is interrupted by a short ceramic pipe section around which is placed an inductive beam current pickup similar to those used in the synchrotron ring: a ferrite core with secondary windings (the beam is the primary). The sensitivity is of the order of 10 mA of beam current per volt of signal.

On the upstream face of each of the jaws of the momentum slit is a set of three secondary emission monitors. Each monitor consists of six 50μ stainless foils alternately connected to about 1kV. The monitors are spaced about 1% apart in momentum, and provide a continuous indication of the intensity and momentum distribution of the part of the linac beam which does not pass through the slits. The sensitivity is of the order of 1mA of beam current per mV of signal.

At the exit of the dump magnet is a similar set of six secondary emission monitors so that the linac beam can be analized in momentum without injecting into the synchrotron. The detectors are spaced by 1.5% in momentum, except that the low momentum detector covers about 4%. The central trajectory to which the magnet calibration applies is the fourth detector.

IV SEPTUM

A. Septum Magnet

Although in principle the septum magnet could be run DC, the current is actually pulsed to simplify the cooling. To prevent eddy currents in the iron it is made of .22 mm silicon steel laminations (see drawing BH3112) punched from the steel salvaged from the flux bars of the old Cornell 300 MeV synchrotron. The magnet is excited by eight turns of #16 wire (1.29 mm diam.). The insulation, which must survive the full intensity of the linac beam for arbitrarily long periods, consists of tubes of AlSiMag ceramic, 1.40 mm I.D. and .14 mm wall. Because the ceramic is very brittle the coil is made up in straight sections and soldered together. Sheets of stainless steel hold the

finished coil in place in the magnet. The magnet is mounted in an oversize version (drawing DH3160) of the standard synchrotron pump box. The edge of the iron is located 2.04 cm (.800") from the line passing through the centers of the vacuum flanges. The magnet parameters are listed below.

Gap height	12.7 mm
Gap width	27.4 mm
Septum coil thickness	2.67mm
Length of laminations	13.43cm
Inductance	25μH
Maximum peak current	165 A
Nominal bending angle	1.28° = 22.5 mrad
Current for 150 MeV/c	90 A
Field - current ratio	about 10 Gauss/A

B. Septum Current Supply

Figure 7 shows a diagram of the current pulsing circuit. At the start of a cycle neither SCR is conducting and point A is at a negative voltage. When an "on" trigger is received, SCR_1 fires discharging C through the septum magnet L_1 . A current oscillation in the L_1C loop starts but is extinguished after half a cycle because the current through SCR_1 cannot reverse. This leaves C oppositely charged. Soon a "recharge" trigger turns on SCR_2 and C begins to discharge through L_2 starting another half cycle of oscillation, which this time leaves point A at a negative voltage. Now the circuit is ready for another "on" trigger.

A careful analysis of the circuit shows that the voltage swing at A and the peak current through the septum magnet L_1 are limited only by the losses in the circuit, mainly in the effective septum magnet resistance R.

$$V_{A\ max} \approx -V_{A\ min} \approx V(4Q-\pi)/\pi, \text{ where } Q = L^{1/2} C^{-1/2} R^{-1}$$

$$I_{pk} \approx 4\ V/\pi R$$

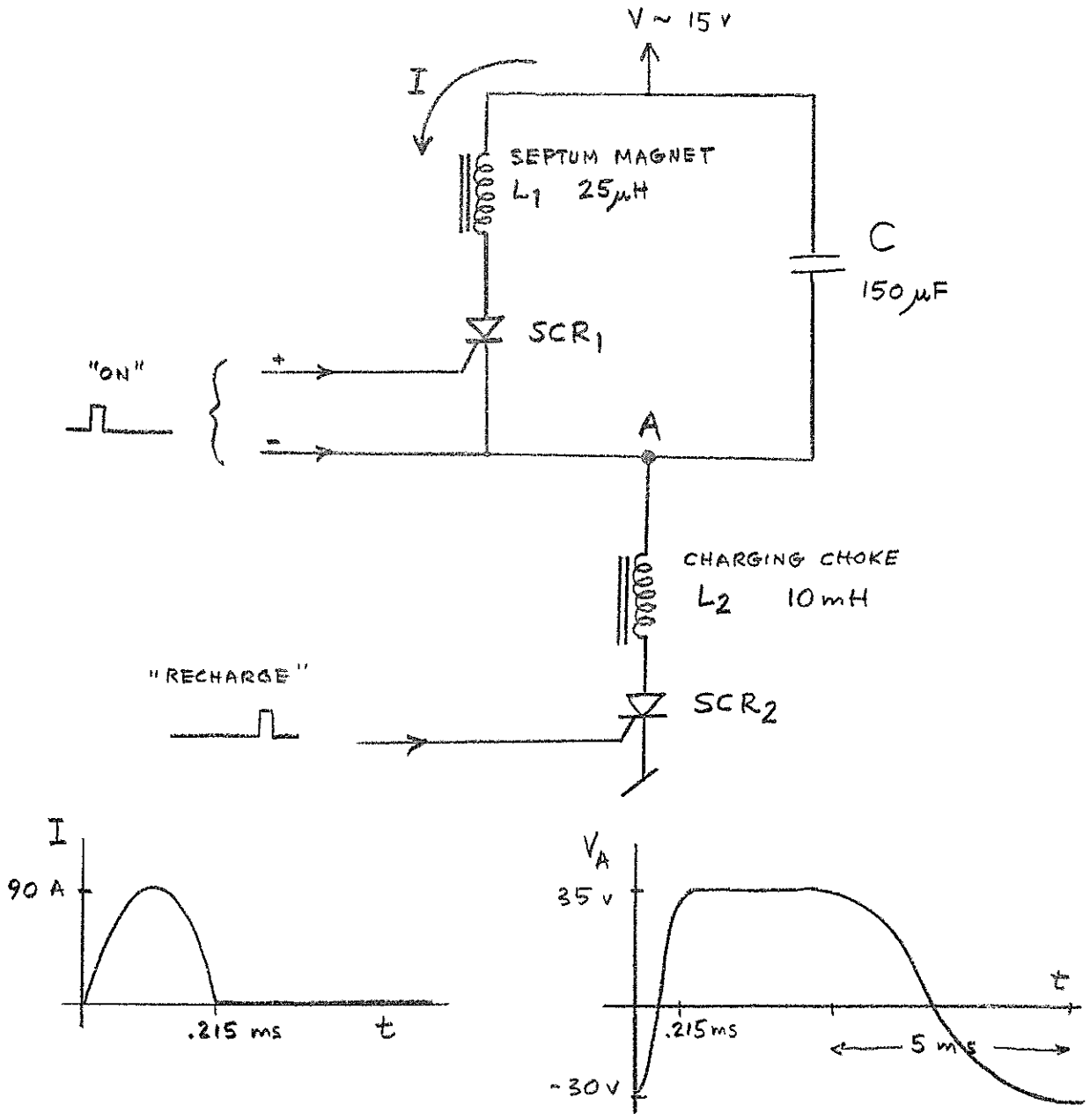

Fig. 7 Simplified schematic diagram of the septum magnet pulsing circuit, showing the important waveforms.

The circuit parameters and waveforms are shown in Fig. 7. For a bend of 1.28° at 150 MeV/c a supply voltage of about V=17v is required. This is provided by a Technipower L-40.0-6.0 voltage regulated supply. The "on" and "recharge" pulses come from the Septum Trigger Circuit, which is triggered by a standard timing pulse.

V INFLECTOR

A. Inflector Coil

The inflector and its pulsing circuit are similar to those used in the early days of operation of the Cornell 2 GeV synchrotron - now replaced by a multiturn inflector system. The injected beam intersects the normal synchrotron orbit at an angle of about 12 mrad and is deflected by a pulsed magnetic field so that it emerges on the central orbit. Since the same electrons pass through the inflector again on their second time around 2.52 μ sec later, the magnetic field must be shut off in a time which is a small fraction of 2.52 μ sec so that they will not be deflected out of the synchrotron. A magnet which can be turned off rapidly must have low inductance, which means that to get a large enough field, the current must be large; and rapid switching of large currents requires high voltage.

The "magnet" is a four-turn coil of #7 wire (drawing DH3334) mounted in a standard 8.9 cm diameter (3 1/2") pipe between synchrotron magnets M11 and M12. The dimensions, 24 cm long by 4.5 cm wide by 3.2 cm high, are determined by the available space in the straight section and the required beam aperture (see Fig. 4). The inductance is 2.5μH. The field and current for a 12 mrad deflection of a 150 MeV/c particle are 230 Gauss and 700 A, respectively.

The coil is supported by ceramic spacers. A retractable secondary emission probe (drawing DH3336) can be inserted into the center of the coil to help in centering the beam before turning on the inflector pulser.

B. Inflector Pulsing Circuit

The current supply for the inflector must provide around 1,000A and turn off in a fraction of a microsecond. The tolerance on the current before and after turnoff, however, is not very severe since we only have to bend the beam by 12 mrad, and since the horizontal aperture of the synchrotron is about ±1 mrad (Fig. 4a), we can allow the top of the pulse to deviate from flatness perhaps by as much as ±5% and we can tolerate a comparable current remaining after turnoff. The pulsing circuit is therefore rather simple (Fig. 8). A lumped-constant delay line of 8 sections (two spare sections are also available) with a characteristic impedence of R_d=12.5Ω and a delay of about 1.2 μsec is charged to double the supply voltage V through a choke and a high-voltage semiconductor diode stack. The other end of the line is connected to the anode of a EGG HY-32 hydrogen thyratron by four RG-217/U 50Ω cables in parallel. When the thyratron (located near the inflector) is pulsed into conduction the line discharges to ground through the inflector L and the terminating resistor R_t, a 8.33Ω , 4.5 kW bank of six resistors in parallel. The discharge current rises in a time of the order of L/R_d to a plateau $I=2V/2R_d$. After a time equal to twice the delay time of the line, the leading edge of the current pulse is reflected and the current falls to zero again approximately symmetrically. The rise and fall times are slightly lengthened because of the high-frequency cutoff of the lumped-constant line. The line alone would limit the rise time to no less than .14 μ sec.

The actual value of the terminating resistance is adjustable in steps and is determined from an empirical optimization of the current pulse shape. The 1-4 μ H inductors in the line (drawing CH3158) are also tuned empirically. The pulse length was chosen to be equal to the synchrotron orbit frequency so that the periodic reflections in the inflector current would perturb the synchrotron orbit only when the empty portion of the beam orbit, corresponding to the turnoff time, passes the inflector. In practice the inflector pulse is flat within ±5% for about 90% of its length, the turnoff time is about .7 μ sec, and except for the harmless reflections, the current after turnoff is less than 10% of the peak current. At the time of this writing

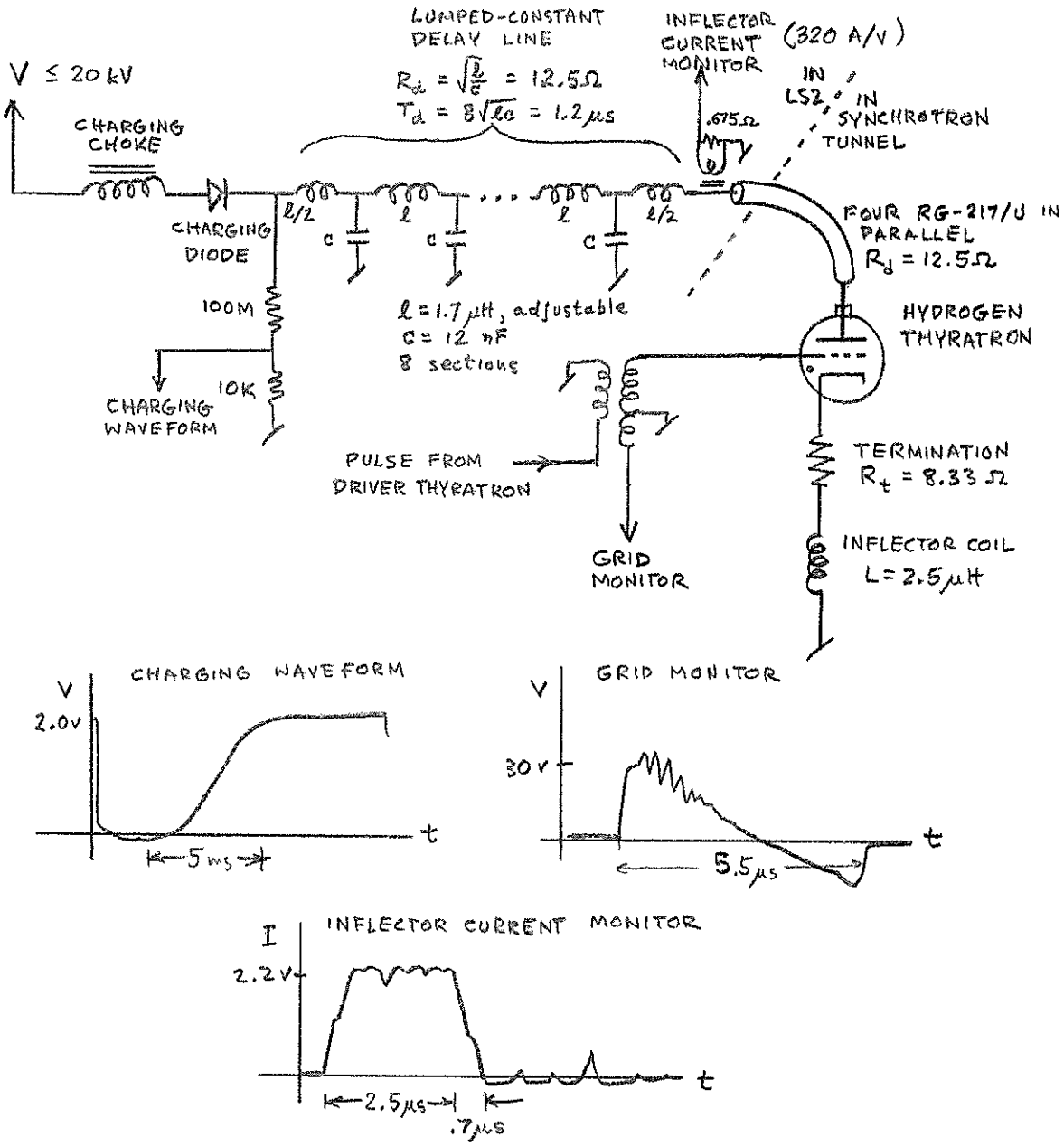

Fig. 8 Simplified schematic diagram of the inflector pulsing circuit, showing the important waveforms. For more details see drawing CH3800.

there is a plan to replace the lumped-constant delay line with a continuous coaxial cable line in order to improve the shape of the current pulse.

The DC charging voltage comes from a 20 kV, 300 mA unregulated supply manufactured by Del Electronics (Model PS 20-300-1, see operating Instruction Manual for details). The three-phase input comes from a 208 v, 3ϕ autotransformer which can be used to vary the inflector current. The AC input is regulated. The current can be monitored by the DC supply voltage or by a signal obtained from a current transformer at the output of the charging line (320 Amps per Volt of signal). The trigger source for the HY-32 thyratron is a 4C35 hydrogen thyratron (called the "driver" and located near the inflector, drawing AM 1258A), which is driven by a vacuum tube pulser. The pulse waveform at the grid of the HY-32 is available for trouble diagnosis.

CORNELL UNIVERSITY
LABORATORY OF NUCLEAR STUDIES
ITHACA, NEW YORK

CS-35
R. Wilson
August 25, 1966

20 Gev from the Cornell 10 Gev Synchrotron?

Robert R. Wilson

The Cornell electron synchrotron has been designed and is being built to give 10 Gev. However, the radius of curvature was made extra large, 100m, in order to minimize RF problems associated with the large amount of radiation by the electrons and this leaves open the ultimate energy of the machine. By the time that we were making the final design it appeared possible to reach 15 Gev, and the magnet was then "beefed up" so as to reach that energy without saturation. Many of the components were designed for 15 Gev where it was convenient and not too expensive and all the components were designed to be consistent with a later expansion to 15 Gev. There has been some technological progress since the design was made, so it is fair to ask now if it is practical to reach 20 Gev.

In raising the energy from 10 to 20 Gev, three technical questions must be answered: can we supply the 160 Mev per turn that will be necessary instead of 10 Mev per turn for 10 Gev; can we double the excitation of the magnet; and can the growth of radial oscillations be prevented? Finally, we must ask about the cost of the increase.

Providing the factor of 16 increase in the RF voltage needed for 20 Gev would seem to present the most serious problem in raising the energy. It can be solved by installing more of the waveguide accelerators and by using more powerful klystrons. Thus, for 10 Gev operation, we expect to place 16 ft. lengths of 714Mc waveguide, which we call "synacs", in each of the four 20 ft. - long straight sections. We can double this by placing four more of these synacs in the two 40 ft. - long straight

sections. The voltage gradient will not be excessive: it will be 0.8MV/ft., which is small compared to the voltage gradient in an L band linac where the gradient is about twice as great. We supply 400 KW peak RF power to energize the present four synacs to give the 10 Mev/turn that is necessary for 10 Gev operation, hence supplying 800 KW to the eight units would make 20 Mev/turn, and to raise this to 160 Mev/turn would then require a peak power of 51 MW. We expect to use a version of the TRADEX Klystron which has a rated peak power of 5 MW at 1200 Mc. Scaling it to our frequency, 714 Mc, should increase the peak power rating to 7 MW, hence if we power each of the 8 synacs with one of these tubes we should be able to supply 56 MW which is slightly more than required.

So much for the peak power. The average power rating of these tubes is 200 kw each, or 1.6 MW for all eight tubes. Running at 60 cycles per second would require about 6 MW average power. Were we to drop to a repetition rate of 10 cycles per second, we would need 1 MW average power which is well within the average power dissipation of the tubes.

To realize the installation of this RF power, our first step would be to have two or three of the TRADEX Klystrons built for our frequency. We would then install two of the synac units in the 30 ft. X 40 ft. underground chamber at the 40 ft. long straight section. At full power these should make 41 MV in the two synacs which, together with the 10 MV from the other stations, should allow us to reach 15 Gev at 10 cycles per second. To reach 20 Gev it would be necessary to install two more synacs in the 40 ft. straight section in the Synchrotron Hall and to replace the four old klystrons installed for 10 Gev by the new klystrons. Tigner has calculated another possibility, namely, installing six synacs with two klystrons per synac which would allow us to reach 18 Gev at 30 cycles per second or 15 Gev at 40 cycles per second.

Installing the additional RF power would have an additional advantage in that it would enable us to get more beam intensity at lower energies. Thus, at 10 Gev, we will be limited by the RF power to beams

of roughly 10^{13} electrons/sec. This corresponds to a current from the linac of about 10 ma. The linac has given a current some thirty times greater, and it is conceivable that we could accelerate such a current by using the extra power installed to reach 20 Gev, assuming that other limitations such as beam blow-up or radiation damage do not interpose insurmountable difficulties.

Now let us turn to the problem of doubling the excitation of the magnet. As I have mentioned, it is already designed to reach 15 Gev except for a few modifications of the primary power supply. Because the return yokes of the magnet are only 1 1/4" thick, saturation becomes noticeable at 15 Gev excitation, where it is 2%. At 20 Gev excitation the saturation has increased to 7.5%, which is not excessive. One way of exciting the magnet to the 20 Gev level is to add identical condensers in parallel with those already installed. This would cause the frequency to drop from 60 cycles to about 40, but the voltage on the condensers and magnet would remain about the same as for 15 Gev operation so that all the present components would be useable. Because of the lower frequency, the chokes will probably saturate, but this can be prevented by inserting identical chokes in series with those already installed. Thus we would have to double the number of chokes and to add about 2/3 the number of condensers that are presently being used. There is adequate room for these additional components in the tunnel right under the presently installed condensers and chokes.

The DC bias on the magnet is now being provided by six separate DC supplies placed at regular intervals around the ring - so as to keep the voltage down. The number of these supplies would simply be doubled. The DC power necessary for 20 Gev operation would be about 2 MW as compared to 0.36 MW for 10 Gev.

The AC power would increase to about 1 MW, to be compared to the 0.4 MW for 10 Gev. At present this power is carried away by water which is heated from about 18°C to 27°C for 10 Gev operation. One way of

dissipating the roughly four times greater power would be simply to double the flow of water and to allow the temperature rise to double.

The orbit dynamics of the magnet may present the most serious problem in attaining 20 Gev electrons. The beam grows in size due to fluctuations of energy caused by the emission of synchrotron radiation. This synchrotron radiation also leads to an antidamping of the betatron oscillations. Calculations by D. A. Edwards[1] show that the r.m.s. radial extent of the beam will be 1 cm at 10 Gev, 5 cm at 15 Gev, and at 20 Gev clearly the beam would be completely blown up. It was for this reason that provision for excitation of the magnet was originally limited to 15 Gev. A new development, however, has been the successful development by K. W. Robinson[2] of a special damping magnet.

Robinson's magnet works by transferring some of the damping of the synchrotron oscillations to the radial betatron oscillations. The synchrotron oscillations damp because the radiation loss by electrons of energy lower than the average is very much less than the loss by electrons of average energy. Since the radiation loss is proportional to $B^2\ell$, by making a large magnetic field B over a short distance ℓ in the straight sections, the radiation loss can be made arbitrarily large compared to that due to the bending magnet. He makes a large negative gradient of $B^2\ell$ with respect to radius, and he alternates B so that both the overall bending and focusing effects are close to zero.

Physically, Robinson's magnet consists of five pairs of poles with alternating fields. The pole separation is 1/2" and the poles are 3 1/2" long in the direction of the beam - the first and last poles are one-half as long as the others. The total length of the magnet is 26". At CEA, the beam is bumped to the position of maximum gradient when the energy has reached 5 Gev. The field in their synchrotron is then 6.3 KG and the field in their DC damping magnet is 13.2 gauss. For our case, with

1 D. A. Edwards CSDS-15, June 15, 1964
2 K. W. Robinson CEAL-TM-155, December 10, 1965

20 Gev, the synchrotron field would be about the same, but the length around our magnet will be greater by a factor of four, hence we would need four AC magnets similar to Robinson's to do the job. In fact, it will probably be more expedient for us to make a larger number of much smaller magnets (perhaps 24) and to distribute them around the orbit in the small straight sections between unit magnets where there is about 6" of clear space. We may also want to make the magnet apertures rather small, as at C.E.A., and to bump the beam into the magnets after the energy has exceeded about 10 Gev.

Were there no damping of the radial betatron oscillations, the beam would grow to an r.m.s. width of several cm. However, it will be much smaller than this because the Robinson magnet provides positive damping.

One might worry also about the intense synchrotron radiation at 20 Gev - some 300 KW for a beam of 10^{13} electrons/sec. The radiation spectrum extends almost uniformly up to an energy of about 180 Kev where it drops off rapidly, but there is still a small amount of radiation at photon energies as high as 1 Mev. The power radiated per unit energy in the constant part of the spectrum per electron varies as E/R and will be only 2/3 of that from our 2 Gev synchrotron in the region where the two spectra overlap, i.e., up to about 22 Kev. Hence for many phenomena, such as those concerned with the emission of secondary electrons, the radiation will not lead to serious problems. The synchrotron radiation will be intercepted by water-cooled copper scrapers that are to be inserted in the vacuum boxes in the spaces between magnets.

Now let us consider the cost of increasing the energy, first to 15 Gev and then to 20 Gev. Most of the components of the magnet are already capable of 15 Gev excitation, i.e., the condensers, chokes, and the D.C. supplies. Only the A.C. power supply need be increased by paralleling additional components. This will cost approximately 50K$. As has been mentioned before, the RF for 15 Gev could be supplied by adding two synac units at a cost of 100K$ which would be powered by two

TRADEX tubes which might cost 300K$ - largely development costs. The DC power supply, 800 KW would come to about 200K$ and various ancillary parts would probably cost another 50K$, making a total of roughly 700K$ to get to 15 Gev.

To reach 20 Gev would require purchasing about 300K$ worth of extra condensers, chokes, and D.C. power supplies. It would cost approximately 50K$ to increase the A.C. power excitation from the 15 Gev level to 20 Gev. The Robinson magnets would cost between 10 and 40K$ depending upon where they are built. Thus to increase the capability of the magnet to be able to reach 20 Gev will cost roughly an additional 400K$. The RF costs are much more difficult to estimate at all reliably. Assuming that six new synacs will have to be installed, we can guess that they will cost about 300K$. The six TRADEX tubes to power these might cost 50K$ apiece to make 300K$. We could use the power supply to be obtained for 15 Gev excitation at a lower duty cycle, i.e., at about 2 pulses per second, in which case we would be able to get some 20 Gev electrons at a cost of about one million dollars in addition to the 700K$ which might be spent to reach 15 Gev excitation. To increase the duty cycle to 10 pulses per second would cost an additional 600K$. Cost estimates being what they are, we should figure on about 2.5M$ as the cost of going from 10 Gev to 20 Gev operation, apart from the experimental equipment and the usual factors that allow for inflation and contingencies.

It appears then that all the questions that have been raised concerning the increase have been answered in the affirmative and furthermore that the cost will not be too excessive. Insofar as this is true, we can assume that the Cornell synchrotron has an eventual capability of accelerating electrons to an energy of 20 Gev - and perhaps even higher.

I have relied heavily on discussions with Maury Tigner about RF problems and Raphael Littauer about magnet problems in reaching these conclusions.

CORNELL UNIVERSITY
Laboratory of Nuclear Studies
Ithaca, New York 14850

CS-36
R. Yamada

January 12, 1968

MAGNETIC FIELD MEASUREMENT II

Introduction

The procedure for the production test of the magnetic field characteristics of magnets for Cornell 10 GeV synchrotron is described and some results are discussed. The production test consists of measurements of the isomagnetic line, the averaged value of Xo, the gap in the back legs, the phase lag measured with a peaking strip, and the remanent field of each magnet.

The high field characteristics of the high gradient magnets are also described.

The magnetic field and field gradient were measured at the injection field of 50 gauss. The measurements were made with biased peaking strips and the results are described.

Production Test

There are 192 magnets for the synchrotron as well as some spare magnets. Each magnet was tested and compared with a standard magnet.

We measured the magnetic characteristics of each magnet, as soon as it is manufactured and baked for obtaining good vacuum. After that it was assembled on the I-beam and installed in the tunnel sequentially. Therefore, we do not have the best possible arrangement of the magnets in the tunnel as far as magnetic field data are concerned.

1). Setup

Every test magnet is compared with the standard magnet (No.1010). They are connected in series and form a resonant circuit with two chokes and two banks of capacitors, tuned to 60 Hz (AC power line frequency). The connection is shown in Fig. 1. As there are two kinds of magnet with different inductance values, we have a switch, which adds trimmer condensers to the two main capacitor banks in case of the narrow gap magnets of a lower inductance value.

A pair of precision-made survey monuments are fixed on every magnet near to both ends. Each monument has a set of four precision pins with a concentric hole in it. The two pins on a magnet, which are near to the ends of the magnet and at the outside of the magnet, are used as the standard points of the magnet when the center line of the magnet is measured. The top surface of the pins are used for leveling the magnet with a precision level.

The standard and the test magnet are set on movable I-beam tables separately, on which the magnets are leveled. These tables have two mill tables on both sides beyond the ends of the magnets. The tables are movable rectangularly to the axis of the magnet, and one of them is movable along the axis as well. A 16 mil diameter phosphorous copper wire is stretched from one of the mill tables to the other through the gap of the magnet and then back to the first one. Thus the wire makes a one-turn coil in the magnet covering the central field as well as the fringing field. The wire is stretched uniformly tight at both ends of the wire on a same mill table with two pulling devices made of wheels and gears. The other mill table, which is movable parallel to the axis of the magnet, is used to stretch the wire much tighter. The spacing of the wire is made constant on both sides of the two magnets by using quartz spacers of the same thickness (around 1" with precision of 0.2 mil.) The four quartz spacers (about 1" x 1" x 1") were cut from a single parallel plate, and are always used at the same orientation. Thus we have one standard one-turn coil in the

standard magnet and another one with equal turn-area in the test magnet.

The position of the geometrical center line of the magnet is determined with a long centering jig and with respect to the position of the standard pins on the survey monuments. The long centering jig is made of a 12' aluminum channel with two aluminum plates under each end of the channel. The flat plates sit on the pins of the survey monuments. A dove pin embeded under one plate fits into the inner hole of one of the standard pins. And a slot under the other plate with its axis parallel to the axis of the magnet, is used to house the other standard pin. At the outside end of a plate, a perpendicular 1" square bar is sticking down. Its both side faces are made parallel to the axis of the magnet, and symmetrical to the center line of the magnet, using a transit, gauge blocks and the special jigs placed on the magnet to determine the center line of the magnet.

A thin parallel plate is placed against the side surface of the perpendicular bar, and the plane can be extended down to the median plane of the magnet. The wire of the one-turn coil is moved toward the surface of the parallel plate until it touches, then the electric loop composed of the wire, the perpendicular bar, a dry battery and a lamp, closes and the lamp goes on. With this method we can determine the position of the wire with an accuracy of a fraction of a mil. With every dimension known, we can determine the position of the wire with respect to the position of the standard pins and then to the center of the magnet.

Error of Setting

The position of the geometrical center of a magnet can be determined with an accuracy of ±10 mils. The various causes and their contributions are as follows:

The pins on the survey monument apparently have a radial accuracy of ±5 mils, due to the mechanical accuracy of the monument itself, and to the procedure of setting the monument on the magnet.

The setting of the wire itself can be done with an over-all accuracy of ±5 mils. They include the possible errors due to the setting of the telescope and the special centering jigs, to the mechanical accuracy of the long centering jig, and to the procedure of reading the position of the wire.

2). Isomagnetic Line Measurement

The isomagnetic line was set at 69 and 131 mils outside the geometrical center of the magnet for the wide gap and the narrow gap magnets respectively, when the profile of the pole piece was calculated and determined assuming 1 mil gap in the back legs.

For the production test the standard isomagnetic line is set at 131 mils outside the geometrical center of the standard magnet (narrow gap). The standard magnet No. 1010 was found to have an average gap of 1.3 mils in the back legs, which is smaller than the average value of other magnets. The isomagnetic line is measured with the above mentioned 1" wide one-turn coils. The center of the coil of the standard magnet is set at the standard isomagnetic line. The center of the other coil of the same width in the test magnet is placed at its geometrical center line with the same device and method. Then the reading of the mill tables is set at zero.

The two magnets are excited in series to 10 GeV in biased operation. The two coils are connected in series to buck each other and their signal is integrated and measured on an oscilloscope, which is triggered by a peaking strip at zero field, as in the measurement of the absolute value of Xo at the center[1]. In this case the setting of the two dividers are set at the same values i.e. 9,000. We move the coil in the test magnet back and forth radially, until the integrated signal becomes zero at the time when the field is at the peak value. From the reading of the mill table, we are able to know where the isomagnetic line of the test magnet is. It is necessary to reduce any temperature change in cooling water for the standard and test magnet.

Shift of the Isomagnetic Line

The typical values of the observed isomagnetic line are 77 and 181 mils outside the geometrical center line for the wide gap and the narrow gap magnet respectively. Therefore the observed values are shifted further outside by 8 and 50 mils than the designed values for the wide gap and the narrow gap magnet respectively. The extimated amounts of shift are -5 and 29 mils for the wide gap and the narrow gap magnet respectively. Their contributions are listed in Table I and are explained in the following.

The back leg gap is not 1 mil as designed, but the typical value of the back leg gap of the production magnets is 2.4 mils for both types of magnets. The standard narrow gap magnet has 1.3 mil back leg gap. This extra gap δ_o=0.3 mil causes the shifting of the isomagnetic line of the wide gap magnet by $(1 + k)X_o\ \delta_o/G$=8 mils, and it is 69 + 8 = 77 mils outside the geometrical center for a wide gap magnet with 1 mil back leg gap. The extra back leg gap widens the main gap and shift the isomagnetic line to the narrow side of the main gap by Δx, which is given by [1)]

$$\Delta x = -(1 + k)X_o \frac{\Delta g}{G}$$

Therefore the typical value of the shifting of the isomagnetic line due to the typical extra 1.4 mil gap is 25 mils inside for the wide gap magnet, and that of the typical 1.1 mil gap is 29 mils outside for the narrow gap magnet.

The typical magnetic length of the narrow gap magnet turned out to be longer by 0.12" than that of the wide gap magnet. The magnetic length is about 127" for both types of magnet. Therefore this deviation causes a 9 mil inside shift of the isomagnetic line for the wide gap magnet.

There was some small systematic deviation in the punching of the laminations. The gap of the lamination for the wide gap magnet is 1 mil less than the design value, and that for the narrow gap magnet is not so bad. This means a 7 mil outward shift for the wide gap magnet.

The calculation of the isomagnetic line was done assuming an infinite value of magnetic permeability. Actually it is $\gtrsim$7,000 at 3.3 kG for ARMCO-6. This finite value of μ reduces the field at the center of the wide gap magnet by 0.2% compared to a value with an infinite μ. The ratio of the air gap length to the magnetic length in iron is different for two types of the magnets. This causes the center field in a narrow gap magnet to be lower by 0.1% than that in a wide gap magnet. Therefore, the isomagnetic line for a wide gap magnet is shifted outside by 11 mils.

The positions of the isomagnetic lines of the production magnets are distributed around the typical values by $\pm$20 and $\pm$30 mils for the wide gap and the narrow gap magnet respectively. The estimation of the variation is also listed in Table I. The principal cause is due to the variation of the back leg gap, which is $\pm$0.6 mils for both types of magnet. Their estimated values are 11 mils and 16 mils for the wide gap and the narrow gap magnet respectively.

The error due to the setting is $\pm$10 mils as described before for the test magnet. But it is much reduced for the standard magnet and may be $\pm$3 mils. The spacing of the parallel wires may have an error of $\pm$0.2 mil and it may cause a variation of $\pm$2 mils. Some magnets are twisted as much as $\pm$15 mils per inch radially at their ends, but the plane of the wire was made parallel to the median plane of the magnet within $\pm$5 mil/inch. Therefore this causes a negligible error. The hard packs are found to have an error in the dimensions of tapering section, which is equivalent to $\pm$40 mils ($\pm$ 0.03%) in the magnetic length. This varies the isomagnetic line by $\pm$3 mils. The agreement between the estimated values and the observed ones are fairly good as is shown in Table I.

Table I Shift of Isomagnetic Line and its Variation

	Wide Gap Magnet		Narrow Gap Magnet	
	Shift (mils)	Variation (mils)	Shift (mils)	Variation (mils)
	(calculated)			
0.3 mil of Std. Mag.	+ 8		0	
Extra Back Leg Gap	-25	±11	29	±16
Magnetic Length	- 9	± 3	0	± 3
Punching Error	+ 7		0	
Finite	+11		0	
Setting Error of Test Mag				
Pins		± 5		± 5
Coil		± 5		± 5
Setting Error of Std. Mag.		± 3		± 3
Width of Wire		± 2		± 2
Total Estimation	- 8	±29	+29	±34
Observed Values	+ 8	±20	+50	±30

3). Averaged Value of Xo

The values of Xo at the geometrical centers of the magnets were designed to be 9.223" and 9.010" for the wide gap and the narrow gap magnet respectively. These values refer to the values well inside the magnet. For the comparison with the values of the production test, we have to take into account also the fringing fields at both ends. Thus the averaged Xo values were calculated to be 9.297" and 9.115" for the wide gap and the narrow gap magnet respectively with 1 mil back leg gap, with the values of the measured magnetic and gradient length[1]. The calcualtion of the averaged Xo value is done in Appendix I.

For the production test we use the same 1" wide one-turn coils,

which cover the fringing field at both ends. We set the centers of two 1" wide coils at the geometrical centers of the standard magnet and the test magnet, and excite the magnet at 10 GeV as in the measurement of the isomagnetic line. The divider for the test magnet is set at a fixed value of 9,000, and that of the standard magnet is adjusted until we get zero signal on the scope. Then the coil is moved radially by +0.500" and -0.500" with the aid of block gauges and dial gauges. At these two points the divider for the standard magnet is adjusted for a zero signal on the scope again. From these three readings of the divider, we can calculate the averaged value of $\overline{X}o=Bo/(\Delta B/\Delta x)$ over the whole magnet. The typical values are 9.324" and 9.145" for the wide gap and the narrow gap magnet respectively.

The possible causes for the variation of Xo are as follows, and listed in Table II. The setting of the survey monument is done with an accuracy of $\pm$5 mils, which is 0.05% of Xo. The variation due to the extra back leg gap is given by $\Delta\overline{X}o=6.1\ (\delta - 18\varepsilon)$ mils for the wide gap magnet and $8.8\ (\delta - 18\varepsilon)$ mils for the narrow gap magnet, where δ is an extra gap in the back leg and ε is the inclination between the top half and the bottom half of the magnet[1]. The typical extra gap of 1.4 mils causes an outside shift of 9 and 12 mils for the wide gap and narrow gap magnet respectively. The observed distributed values of δ and ε are $\pm$0.6 mil and $\pm$0.03 mil/ inch respectively, and they cause $\pm$7 mils and $\pm$ 10 mils in $\overline{X}o$ for the wide gap and the narrow gap magnet respectively. The observed small variation in the shape of the hard packs causes $\pm$0.1" variation in the value of L_G, which is $\pm$ 0.08% ($\pm$ 7 mils) in $\overline{X}o$. Thus the total estimation including the possible errors is about $\pm$30 mils compared to the observed value of $\pm$20 mils.

The main error in the measurement is due to the setting of the coil at the center of the test magnet with respect to the survey pins to measure Bo, which is $\pm$5 mils, and this is $\pm$0.06% of $\overline{X}o$. The error in Δx is $\pm$0.5 mil for 1,000" displacement, and it is

$\pm$0.05% of $\bar{X}o$. We have to take a difference between two five digit numbers to get a value for ΔB, and this cause $\pm$0.02% of $\bar{X}o$. Thus the total possible error is $\pm$0.13%, and corresponds to $\pm$12 mils in $\bar{X}o$.

Table II Shift of Averaged Value of Xo and its Variation

	Wide Gap Magnet		Narrow Gap Magnet	
	Shift (mils)	Variation (mils)	Shift (mils)	Variation (mils)
Extra Back Leg Gap (=1.4 mils)	+ 9		+12	
Variation of Extra Gap		± 7		±10
Setting Error of Pins		± 5		± 5
Setting Error of Coil		± 5		± 5
Error in x		± 5		± 5
Error in B		± 2		± 2
Shape of hard Pack		± 7		± 7
Total Estimation	+ 9	±31	+12	±34
Observed Values	+27	±17	+30	±23

4). Zero Field Measurement with Peaking Strip

The long coils are placed at the geometrical centers of the magnets. A carriage is placed on the two parallel wires of the coil and is moved through the gap of the magnet by an attached fish line. A peaking strip and a Hall probe element are mounted on that carriage. Another peaking strip is placed at a fixed position inside the gap of the standard magnet, which is used to trigger the scope at the zero field.

A test magnet and the standard magnet are excited in series to the excitation level of 7.5 GeV with A. C. current only,

because it is a more severe test at low field than such a test made at the injection field with D. C. bias. First the time of zero magnetic field (which is not exactly zero field time due to the coercive force of the peaking strip and some delay in the cables) is determined on the scope, by placing the peaking strip at the standard position of 1' inside of the standard magnet. Then the peaking strip is transferred into the gap of the test magnet. The signal is continuously monitored through the magnet to see any particular bump, and data are taken at 1' intervals.

The average values of the delay time are -1.5 ± 0.3 μs and 0.8 ± 0.3 μs for the wide gap and the narrow gap magnet respectively. The difference is 2.3 μs. (The value of dB/dt at zero field is 0.8 Gauss/ μs.) This difference is mainly caused by the difference between the typical values of the remanent field of two types of the magnets, which is about 1.6 Gauss. The typical fluctuation inside a magnet is about ± 0.3 μs, which corresponds to the magnetic field variation of ± 0.24 Gauss. In some magnets it goes up to +0.6 μs locally. This fluctuation may be caused by the variation of the remanent field and/or eddy currents. We found some correlation between the variation of the measured dc remanent field and that of the zero crossing time.

5). Remanent Field Measurement

After the foregoing measurements, the magnet is excited up and down several times to the excitation level of 10 GeV with DC current of 400 Amp. The Hall probe element, which is connected to the Bell Gauss-meter with a long cable, is moved through the gap of the magnet on the carriage as the peaking strip. The remanent field on the geometrical center line is monitored continuously and the data is taken at the interval of one foot.

The average remanent field is 2.7 ± 0.4 Gauss and 4.3 ± 0.5 Gauss for the wide gap and the narrow gap magnet. The difference between them is 1.6 Gauss. The magnitude of the remanent field Br is given by $Br = H_c \times (L/G)$, where Hc is the coercive force of the magnet and may be about 2.2 oersted at 10 GeV excitation level, L is the magnetic length in iron, and G is the gap height of the magnet. Then the expected value of the remanent field is 2.8

Gauss and 4.3 Gauss for the wide gap and the narrow gap magnet and gives good ratio between them. The typical variation inside a magnet is $\pm$0.3 Gauss, but goes up +0.5 Gauss locally in some magnets. There is no remanent field bump at the ends of the magnets, as was seen in CEA magnets. The accuracy of the measurement is $\pm$0.2 Gauss.

The difference of the remanent fields between the two types of the magnet can be corrected, if necessary, by the aid of the two turn coil of the narrow gap magnet or by the correction coils in the straight section.

6). Gap in Back Legs

The gap in the back legs is measured by the method reported in the previous report[1]. The reading of Bell Gauss-meter with its element at 3/4" from the gap with a DC current of 154 Amp, gives the direct reading of the gap in mils. The gaps on both sides are measured continuously, data are taken at intervals of 1 foot, and their averaged value is calculated. The averaged gap heights are 2.4 $\pm$0.6 mils, and the accuracy of the measurement is $\pm$0.1 mil. The variation of the gap in a magnet is typically $\pm$ 0.5 mil, but it goes up to +1.5 mils locally in some magnets. This variation corresponds to the arrangement of the clamps, which were used for the assembly of the magnets, but it is not clearly correlated with the variations of the remanent field and the field delay.

In order to eliminate any systematic error, which might occur during the production test period of all magnets, several precautionary procedures were taken periodically. The centering jigs and the whole back leg gap of the standard magnet were checked periodically. The measuring equipments were calibrated and checked every time with the standard devices and the standard points of the standard magnet.

Modified magnets

There are two kinds of modified magnets, which are placed next to the 20' straight sections. About 17" length of the modified magnet is stacked with the normal lamination and the remaining

110" length is stacked with the modified lamination of the opposite stronger gradient. There is a transition hard pack between them of about 3/4" length.

The absolute values of Xo at the center, the radial distribution of Xo(x), and the magnetic and gradient lengths of the modified wide and narrow gap lamination, were measured as in the case of the normal lamination as described in the previous report[1].

The absolute values of Xo at the geometrical center of the modified wide and narrow gap lamination were measured at 7.5 GeV and are shown in Table III. The measured values were corrected for 1 mil back leg gaps, and found to be same as the designed values almost within the experimental error. These values were the same at the excitation level of 15 GeV.

Table III. Absolute Values of Xo at the Geometric Center at 7.5 GeV and 15 GeV

Magnet	Gap Height	Designed Value	Measured Value	Measured Minus Designed
Modified Wide Gap	1,482"	4.854	4.839" ±0.010"	-0.015"
Modified Narrow Gap	1.035"	4.588"	4.592" ±0.010	+0.004"

The radial distributions of Xo(x) of the modified wide and narrow gap magnet were measured at 7.5 GeV and shown in Fig. 2 and Fig. 3 respectively. The agreement of the observed distributions with the designed ones is fairly good.

The hard packs of the modified laminations, which are used at one end of the modified magnets, were made with the same die as in the case of those for normal laminations[1]. The effective magnetic length L'_B and the effective gradient length L'_G of the modified wide and narrow gap magnet are shown in Fig. 4 and Fig. 5 respectively. They are well constant within the usable regions at

the hard packs. Their values with respect to the end of the lamination $\Delta L'_B$ and $\Delta L'_G$ at 7.5 and 15 GeV are listed in Table IV. $\Delta L'_B$ shrinks more with the narrow gap magnet than the wide one.

Table IV. $\Delta L'_B$ and $\Delta L'_G$ of Modified Lamination

Magnet	7.5 GeV		15 GeV	
	$\Delta L'_B$	$\Delta L'_G$	$\Delta L'_B$	$\Delta L'_G$
Modified Wide Gap	+0.376"	-0.253"	+0.357"	-0.247"
Modified Narrow Gap	+0.372"	-0.162"	+0.338"	-0.180"
Estimated Error	±0.010"	±0.020"	±0.010"	±0.020"

The shape of the transition hard pack between the normal and the modified lamination was made to have a smooth magnetic field variation between them. The field at the transition hard pack was measured and is shown in Fig.6 and Fig. 7 for the modified wide gap and the modified narrow gap magnet respectively. The respective gradient lengths on both sides of the transition hard packs were calculated and shown in Fig. 8.

The isomagnetic lines for these modified laminations were calculated with the aid of Fig. 6 and 7. The observed positions of the isomagnetic lines of the modified wide and narrow gap lamination are shown in Table V.

Table V. Isomagnetic Line of Modified Lamination

	Designed Value	Observed Value
Modified Wide Gap	+0.104"	+0.099"±0.010"
Modified Narrow Gap	+0.157"	+0.153"±0.010"

The isomagnetic lines and the averaged gradient values Xo of the modified wide and narrow gap magnet were calculated from the available data and compared with the measured values. They are listed in Table VI.

Table VI. Isomagnetic Line and Xo of Modified Magnets

Magnet	Isomagnetic Line (mil)		$\bar{X}o$	
	Calculated	Observed	Calculated	Observed
Modified Wide Gap (No. 1046)	120	115 ±10	6.159"	6.188" ±0.015"
Modified Narrow Gap (No. 1045)	183	198 ±10	5.867"	5.895" ±0.015"

Low Field Measurement

The magnetic field at injection is 50 Gauss at the center for the injection energy of 150 MeV. The absolute value of Xo at the center and the radial distribution of Xo(x) at 50 Gauss was measured with biased peaking strips[2,3]. A biased peaking strip was placed at a fixed position to trigger a scope, and its bias current was kept constant to give a time signal throughout the measurements.

A probe with two peaking strips as shown in Fig. 9 was made. These two peaking strips have bias coils around them and the radial distance between them is 250 mils. Another pair of bias coils is also used at the same radial positions of the corresponding peaking strips, and connected to buck their bias coils. In order to reduce the mutual coupling between these coils, they are displaced azimuthally from each other. The four coils are connected as shown in Fig. 10, and the signal from the peaking strips are observed on the scope.

The peaking strips are made of 2 mil 74 Mo-Permalloy and their length is 0.6". They are contained in quartz tubes and were annealed in hydrogen gas for 2 hours at 1100°C and cooled down at the rate of 50°C/min. A pick up coil of 260 turns was wound at the center of

the tubes. Two well matched peaking strips with quartz tubes were selected out of ten peaking strips, placed in the ceramic tubes of 100 mil diameter and of 0.75" length, and glued with Epoxy. The bias coils were wound with #32 copper wire (9.5 mil dia.) with a turn number of 68 over 670 mils. The circuit for the precise measurement of the current through the bias coils is shown in Fig. 10. The current was measured with the aid of a potentiometer, which was later substituted by a digital voltometer of seven digits.

The absolute value of Xo at the geometric center was measured with one peaking strip with the full biased operation of 10 GeV. It was placed at the center of the magnet and the signal of the scope was set at one fixed position on the scope. Then it was displaced exactly by ±0.500" radially, and the bias current was adjusted to set the signals at the fixed position. Three readings of the bias current were used to get the absolute value of Xo at the center. The variation of the coercive force of the peaking strip to the change of dB/dt was measured and shown in Fig. 11. This effect and the effect of the pole piece were taken into the calculation of Xo and their corrections are given in Appendix II. The final values of Xo at the center are shown in Table VII. The observed values of Xo at 3.8 kG(10 GeV) on the same magnets are also listed in the table. All the values are not corrected for the back leg gaps.

Table VII Xo(0) at Low Field and High Field

	Wide Gap	Narrow Gap	Modified Wide Gap	Modified Narrow Gap
Xo at 25 G	9.066" ±.036"	8.985" ±.036"	4.803" ±.024"	4.508" ±.024"
Xo at 50 G	9.195" ±.036"	9.042" ±.036"	4.869" ±.024"	4.570" ±.024"
Xo at 3.8 kG	9.207" ±.014"	9.059" ±.014"	4.857" ±.010"	4.604" ±.010"
Deviation of Xo at 50 G	-0.1%	-0.2%	+0.2%	-0.7%

The values of Xo at 25 Gauss are lower than those at high field by one or two percent, but those at the injection field of 50 Gauss are the same with those at high field within a few tenth percents. The error of the measurement is $\pm$ 0.4~0.5%, including the positioning error of the peaking strips ($\pm$ 0.1~0.2%), the error in Δx ($\pm$ 0.05%), the reproducibility of the measurement ($\pm$ 0.1%), and the error in the correction of the coercive force ($\pm$ 0.1%). Therefore, the operation point at the injection seems to be well within the operation diamond without any correction.

The radial distribution of Xo(x) was measured with two peaking strips. Most of the mismatching between two bias coils was corrected by adjusting the fixed variable resistor in Fig. 10 with the reversal of the probe and its connection. The pulses of two peaking strips were added in the opposite polarity from each other. They were set at the same fixed position on the scope by adjusting the main current with 1 kΩ Helipot, and by adjusting the current through the bias coil for the peaking strip at the lower field with a variable resistor. Then the current in two bias coils were measured successively. To cancel out any mismatching between two bias coils, the measurement was done with two orientations of the probe and the averaged values were used to calculate the radial distribution of Xo(x).

The observed variations of Xo(x) at 50 Gauss are shown in Fig. 12 and Fig. 13 for the wide gap and narrow gap magnet respectively. These curves are normalized at the center using the observed absolute value. There is not so much difference between them and those at high field in the general tendency[1].

There are not any field bumps at the end of the magnets at 50 Gauss, as was observed on the CEA magnets.

The magnetic length at 50 Gauss was measured using a peaking strip and shown in Fig. 14 and Fig. 15 for the wide gap and narrow gap magnet respectively. The gradient length is also shown in these figures. They do not differ much from those at high field[1].

Appendix I. Calculation of Averaged Xo Value

Let the magnetic field at $r = 0$ and $\pm a$ well inside the magnet be $Bo(0)$ and $Bo(\pm a)$, and take the r-coordinate so that the magnetic field increases with r.

Then,

$$Xo = \frac{Bo(0)}{(\frac{\Delta B}{\Delta x})_o} \doteq \frac{2aBo(0)}{Bo(+a)-Bo(-a)}.$$

$$(\text{or, } Bo(+a) \doteq Bo(0)(1 + \frac{a}{Xo}))$$

With the long one-turn coil, we are measuring the magnetic field times the magnetic length BoL_B. Then the averaged value Xo over the whole magnet is given by,

$$Xo = \frac{2aBo(0)L_B(0)}{Bo(+a)L_B(+a) - Bo(-a)L_B(-a)};$$

where $2 L_B'(x) \equiv L_B(a) = \int_{-\infty}^{+\infty} B(a,z)dz/Bo(a)$ and "a" is the radial displacement from the magnet center line.

$L_B(\pm a)$ can be expressed as follows:

$$L_B(+a) = L_B(0) \{ 1 + f(+a)\},$$

$$L_B(-a) = L_B(0) \{ 1 + f(-a)\}.$$

In our case L_B is shorter on the higher field, and $f(\pm a)$ is positive. Therefore,

$$Xo \doteq Xo \left[1 - \{f(+a)-f(-a)\} \frac{Xo}{2a} - \frac{1}{2} \{f(+a)+f(-a)\} \right].$$

If $f(+a) = -f(-a)$,

$$\overline{Xo} \doteq Xo \left[1 - f(a)\frac{Xo}{a}\right].$$

In another way,

$$L_G(0) = \frac{\frac{\partial B}{\partial x}ds}{(\frac{\partial B}{\partial x})_o} \doteq \frac{Bo(+a)\ L_B(+a) - Bo(-a)L_B(-a)}{2a(\frac{\Delta B}{\Delta x})_o}.$$

Then,

$$\overline{Xo} \doteq Xo \frac{L_B(0)}{L_G(0)} .$$

Appendix II. Corrections of Peaking Strip Measurement

(A) Effect of Coercive Force of Peaking Strip

The value of the coercive force of the peaking strip is not constant to the change of the rate of the field rise, as is shown in Fig. 11. First the rates of the field rise dB/dt at r = 0" and $\pm$0.5" are calculated by observing the phase angle of the measuring point (e.g. 50 Gauss) on the scope. The corresponding values of the coercive force Hc of the peaking strip are shown on Fig. 11. The delay times Δt of the signal of the peaking strip are calculated from these two values by $\Delta t = H_c/(dB/dt)$. Usually Δt is bigger at lower field side. Therefore, the field value given by the current, which is adjusted to set the signal on the scope at a fixed time, corresponds to an earlier lower field at a place with a smaller value of dB/dt. Therefore, the uncorrected measured value of Xo is smaller than the true value. The differences in Δt between the one at r = 0" and those at r = $\pm$0.5 are calculated, and the corresponding correction $\Delta(\Delta B)$ in the field difference ΔB between the field values at r = $\pm$0.5" is determined. Then the corrected Xo value is given by,

$$Xo = \frac{Bo}{\Delta B - \Delta(\Delta B)} \doteq \frac{Bo}{\Delta B} \left[1 + \frac{\Delta(\Delta B)}{\Delta B}\right] ,$$

where $(Bo/\Delta B)$ is the measured uncorrected value. The correction in our case was about +2.3% at 50 Gauss and +4.6% at 25 Gauss. The amount of the correction might have been reduced by a factor of two or three with the development of a peaking strip with a smaller value of coercive force.

(B) Effect of Pole Piece to Bias Coil

The length of the bias coil of the peaking strip is finite and comparable to the gap height. The field value at the center of the bias coil is lower by a factor F(<1) than that with an infinite length. This factor can be calculated if the bias coil is in free

space. Let the diameter and the length of a coil be 2a and 2b in cm, and its Ampere-turn be an Amp-turn/cm. Then the magnetic field at the center of coil H_{11}, which is parallel to the axis, is given by,

$$H_{11} = \frac{\pi a^2 n}{5} \int_{-b}^{b} \frac{dx}{(x^2+a^2)^{\frac{3}{2}}} = \frac{2\pi n}{5} \frac{b}{\sqrt{b^2 + a^2}} .$$

The field H_{11}^{∞} inside an infinite coil with a same Ampere-turn is given by $2\pi\ n/5$.

Therefore,

$$F = \frac{b}{\sqrt{b^2 + a^2}} \doteq 1 - \frac{1}{2} \left(\frac{a}{b}\right)^2 .$$

This factor is 0.986 for our bias coil.

The factor F increases when the coil is placed near to pole pieces due to its mirror images. Therefore, it is bigger at the higher field and lower at the lower field. And the value of the field measured by the current is lower at the higher field and higher at the lower field. Then the uncorrected measured value of Xo is bigger than a true value.

Assume the pole pieces are flat, and calculate the effect of the first mirror images on both sides. This may be a fairly good approximation, although the pole pieces are curved. Let the gap height be $2x_o$, then

$$H_{11} = \frac{\pi a^2 n}{5} \left\{ \int_{-b}^{b} \frac{dx}{(x^2 + a^2)^{\frac{3}{2}}} + 2 \int_{2x_o-b}^{2x_o+b} \frac{dx}{(x^2+a^2)^{\frac{3}{2}}} + \cdots\cdots \right\}$$

$$\doteq \frac{2\pi n}{5} \left\{ \frac{b}{\sqrt{b^2+a^2}} + \frac{4x_o a^2 b}{(4x_o^2 - b^2)^2} \right\} .$$

The second correction term depends on x_0, and is about 0.2% for $x_0 = 0.5$". With this equation, the variation ΔF of the factor F is calculated at $r = \pm 0.5$" with respect to the value at $r = 0$".

Then the true field values are given by

$B_1 (1 + \Delta F_1)$, $\Delta F_1 > 0$ at high field.

$B_2 (1 - \Delta F_2)$, $\Delta F_2 > 0$ at low field,

where B_1 and B_2 are the values given directly from the value of bias current. Then the corrected value of Xo is given with the measured uncorrected value $X_0^U = (Bo/\Delta B)$,

$$Xo = X_0^U \left[1 - X_0^U \left\{\left(1 + \frac{\Delta r}{X_0^U}\right)\Delta F_1 + \left(1 - \frac{\Delta r}{X_0^U}\right)\Delta F_2\right\}\right].$$

The correction of this effect in our case was about 0.8% for the regular and modified narrow gap magnets and about 0.2% for the regular and modified wide gap magnets.

Acknowledgement

Dr. F.C. Kellers designed and tested the constant current source for the peaking strips, which was indispensable for the field measurement at low field. Director R.R. Wilson, Professor B.D.McDaniel, and Professor R.M. Littauer gave constructive critical advice throughout this work. The cooperation of the personnel for the magnet construction and the machine shop were much appreciated. Dr. R.A. Beth at Brookhaven National Laboratory was kind enough to supply Permalloy wire for the peaking strips.

References

1. R. Yamada and S. Mori, CS-1, April 27, 1966.
2. H. Nysater, Nucl.Inst. and Meth. 4(1959) 44.
3. S. Yamaguchi et al., INS-TH-18 (Tokyo, Japan), Sep. 10, 1957.
   H. Sasaki and T. Yamakawa, INS-TH-44(Tokyo, Japan), July 31, 1962.
   H. Sasaki, Nucl. Instr. and Meth. 14(1961) 252.

Notes Added in Proof:

After the magnets were measured, some were baked out by passing a dc current through the coils for several days. After installation in the tunnel, remanent fields of up to 4 Gauss were observed. It was then discovered that it was not sufficient to excite the magnets with a large ac current to bring all the magnets to similar magnetic states.

If a dc current corresponding to 10 GeV excitation were passed through a magnet, and if this were followed by an ac current corresponding to 20 GeV excitation, then the remanent field could be reduced to only about half that found if only dc were applied. Therefore, a "training" process was used to bring all the magnets to a similar magnetic state. The magnets were excited with successive decreasing dc currents of alternating sign (starting with roughly the current used during the testing and bakeout). Thus, a damped ac excitation of very low frequency was simulated. The dc remanent fields of the magnets were reduced to a few tenths of a Gauss with a scatter of the same order. An additional demagnetization with ac excitation appeared to have some beneficial effect.

Systematic measurements of the instantaneous magnetic field at injection were not made before and after this training process. However, the evidence is compelling; the training process made the early operation of the machine possible.

Some measurements have been made of the variation of the time of zero-crossing of the field immediately prior to injection with a biased excitation corresponding to a few GeV. The narrow gap magnets have zero-crossing times delayed with respect to those of the wide gap magnets. At 4 GeV and an injection slope of 1 MeV/turn the delay is about 4 microseconds and the extreme fluctuations (of magnets of one type) are of the same order. In other terms, the instantaneous remanent field variations may be of the order of 1% of the injection field of 50 Gauss.

FK 11/67

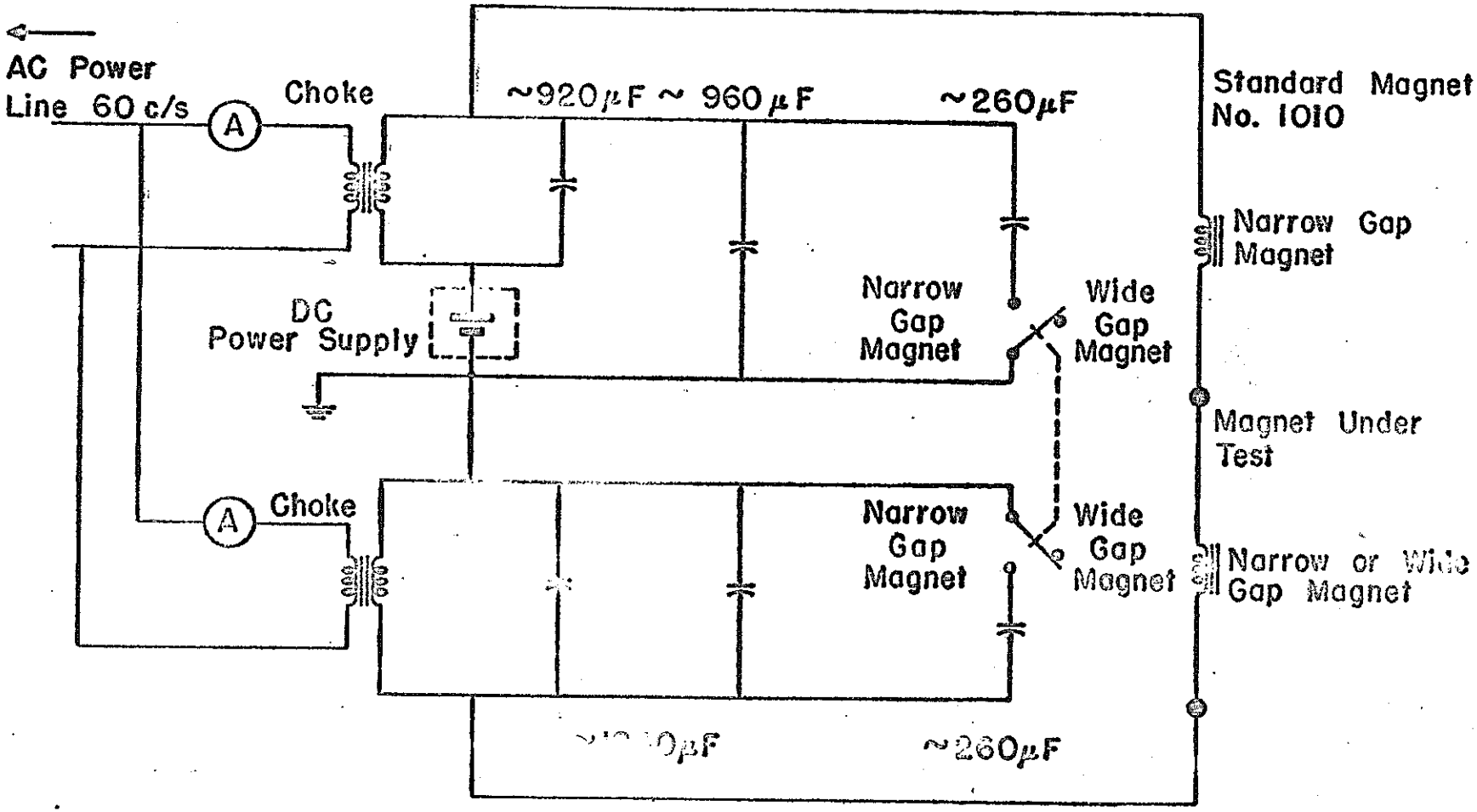

Fig. 1 Connection for Production Test

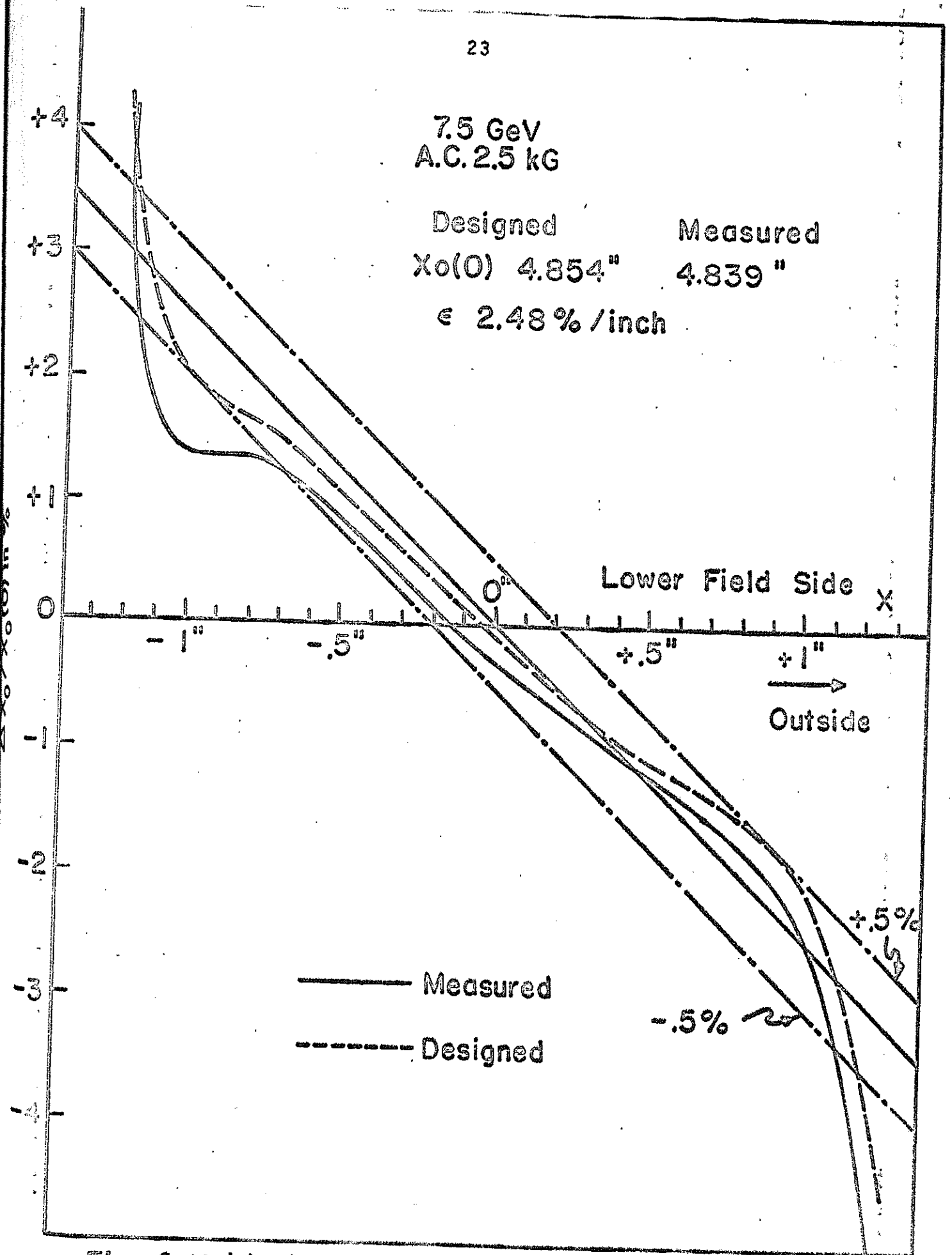

Fig. 2 $X_o(x)$ Distribution of Modified Wide Gap Magnet

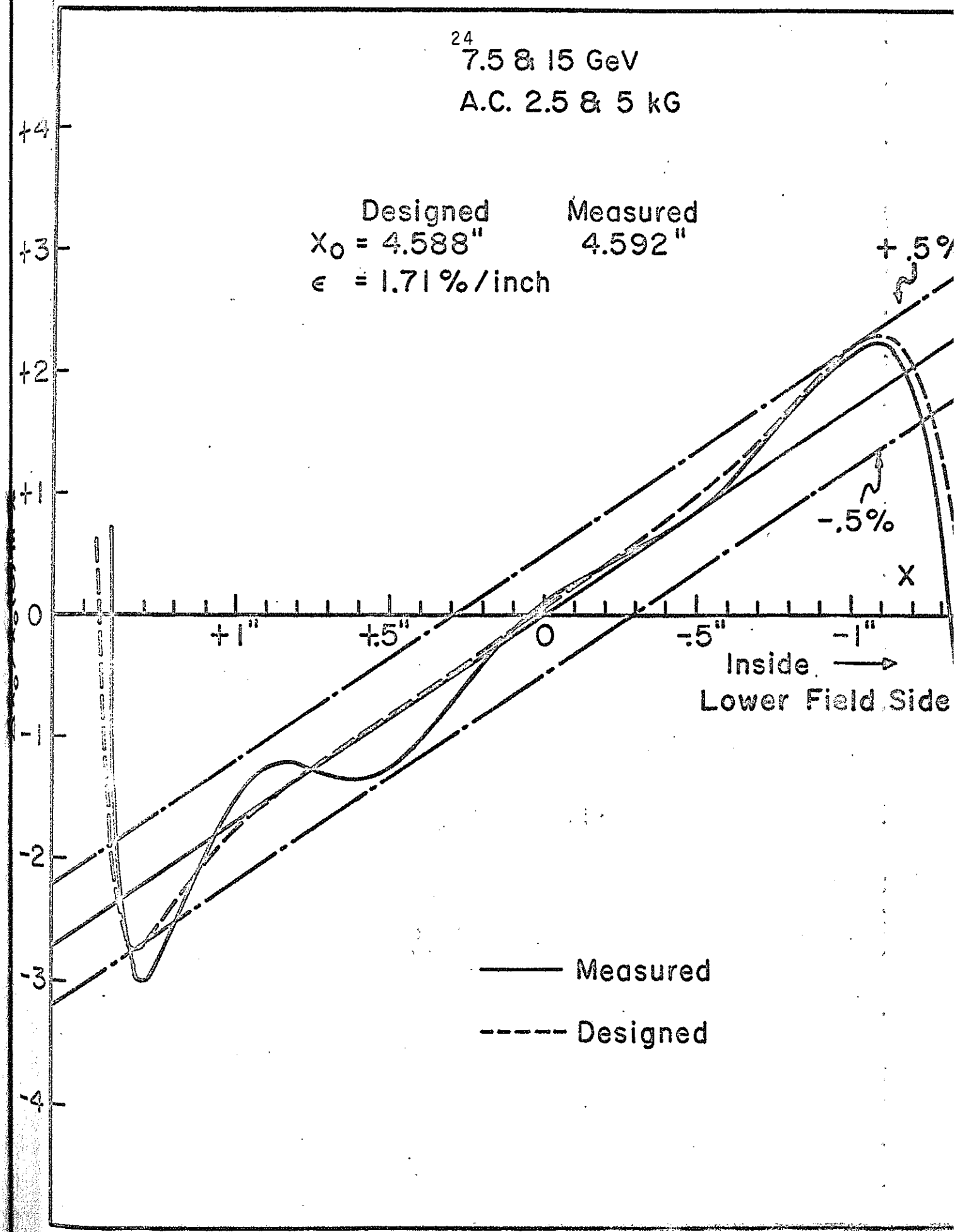

Fig. 3 $X_0(x)$ Distribution of Modified Narrow Gap

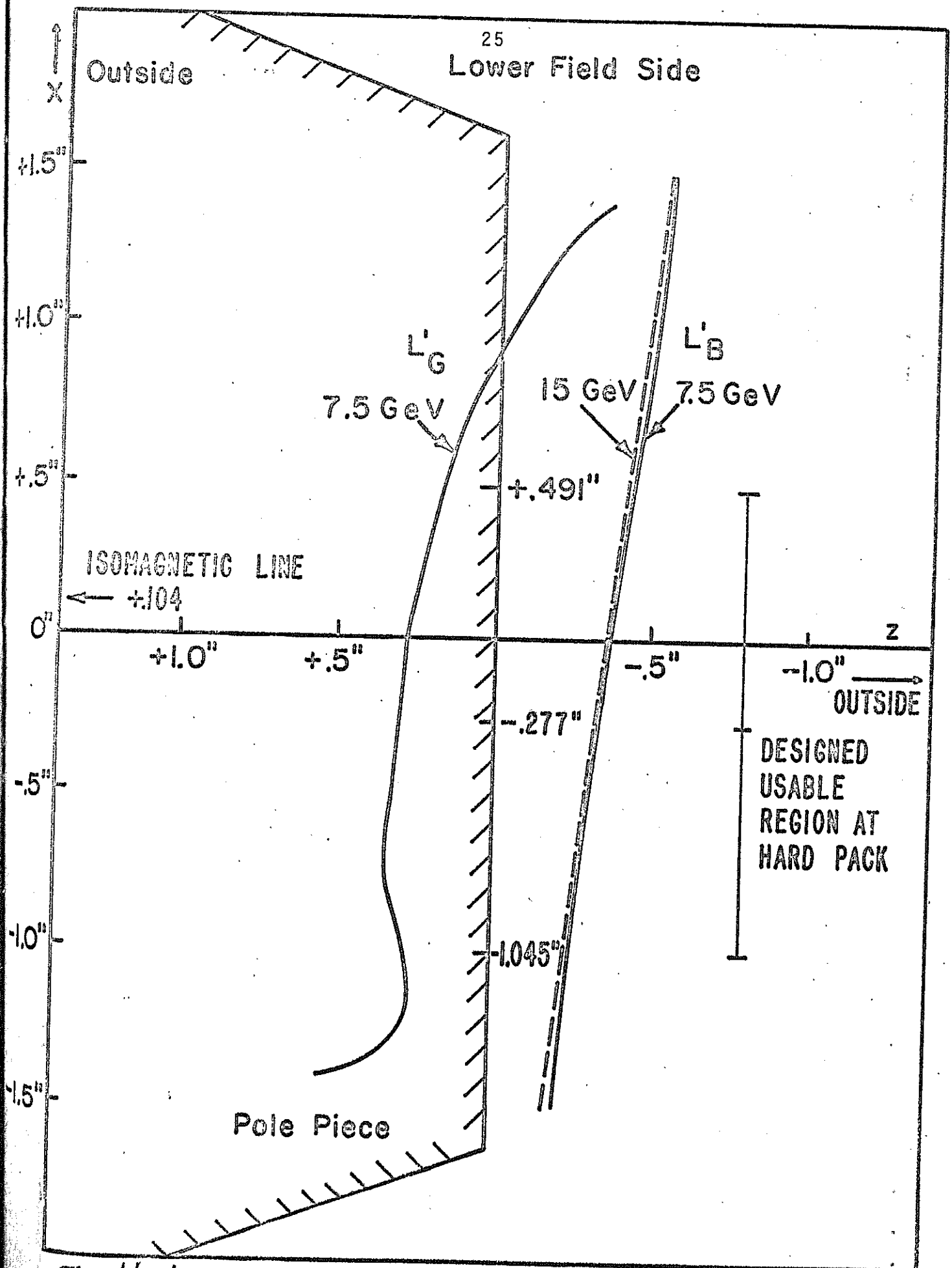

Fig. 4 L'_B and L'_G of Modified Wide Gap Magnet

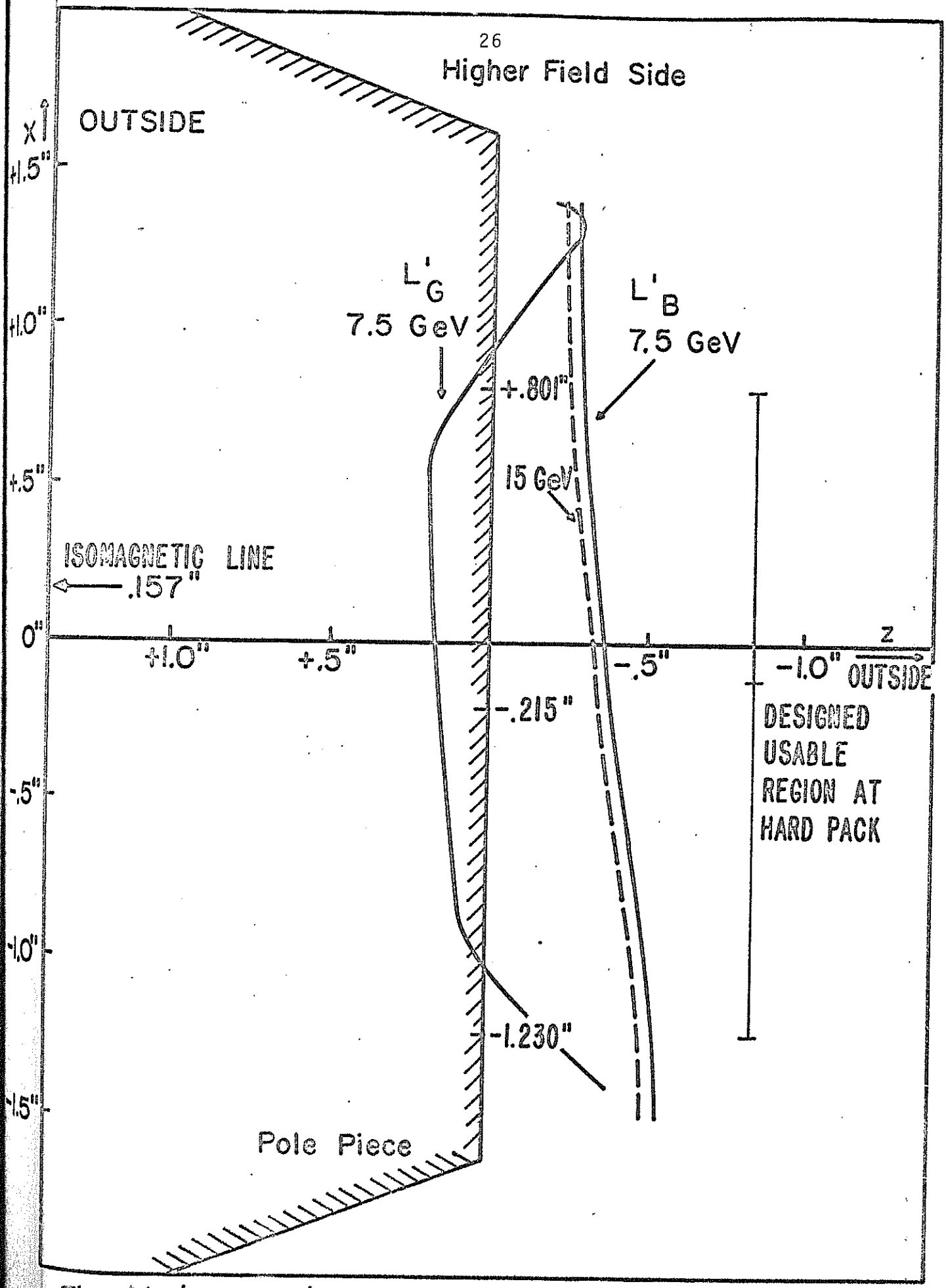

Fig. 5 L'_B and L'_G of Modified Narrow Gap Magnet

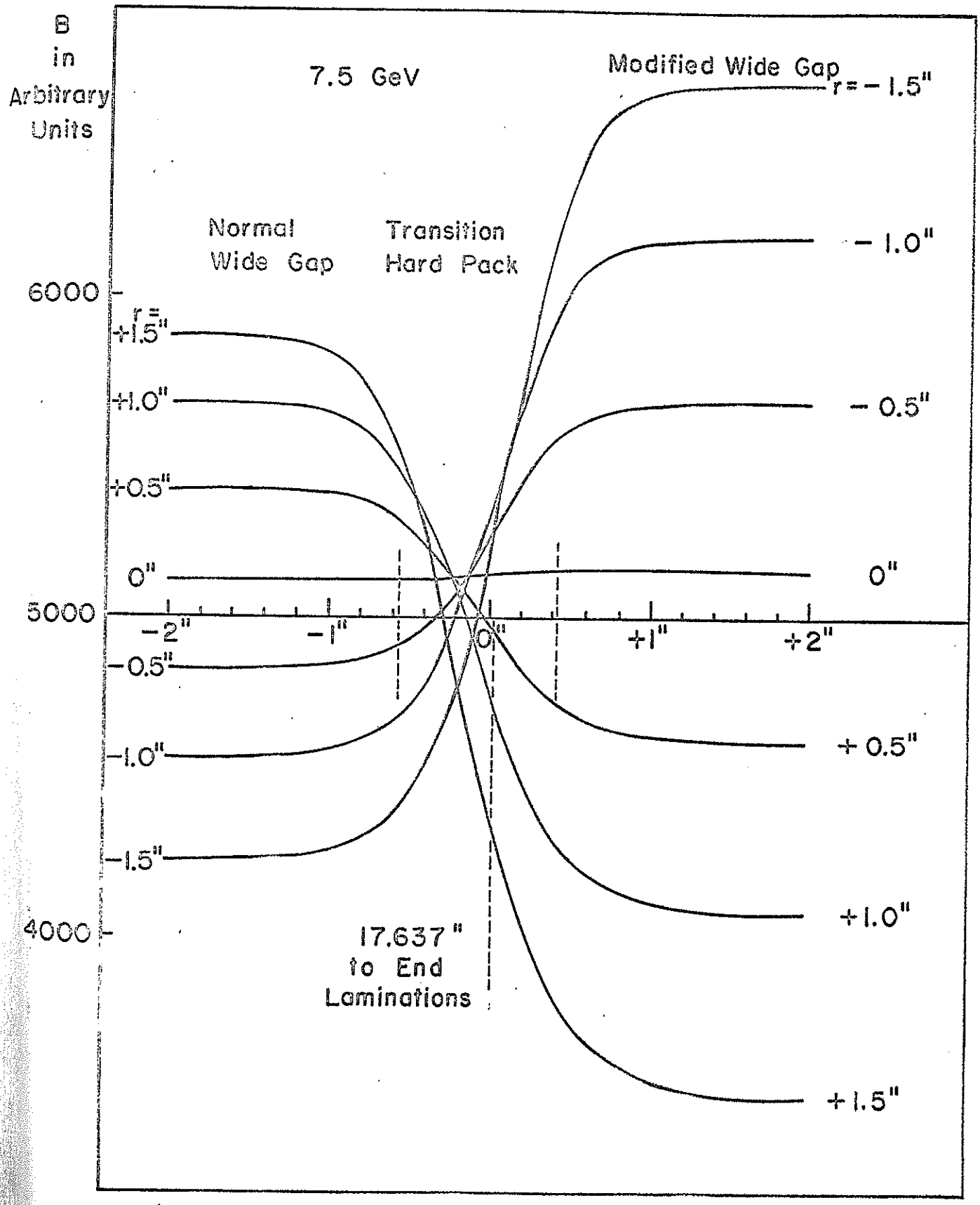

Fig. 6 Magnetic Field at Transition Hard Pack of Modified Wide Gap Magnet

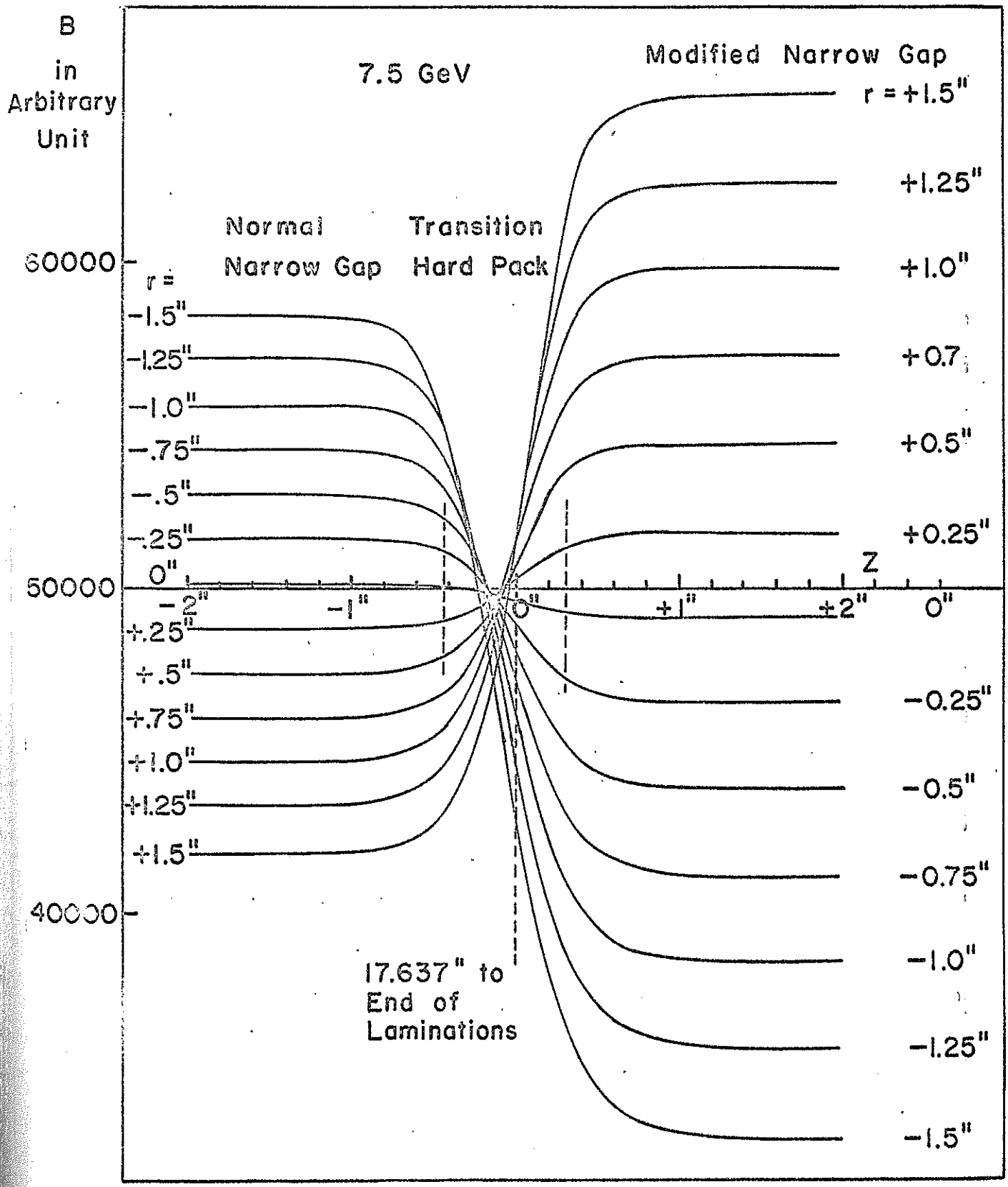

Fig. 7 Magnetic Field at Transition Hard Pack of Modified Narrow Gap Magnet

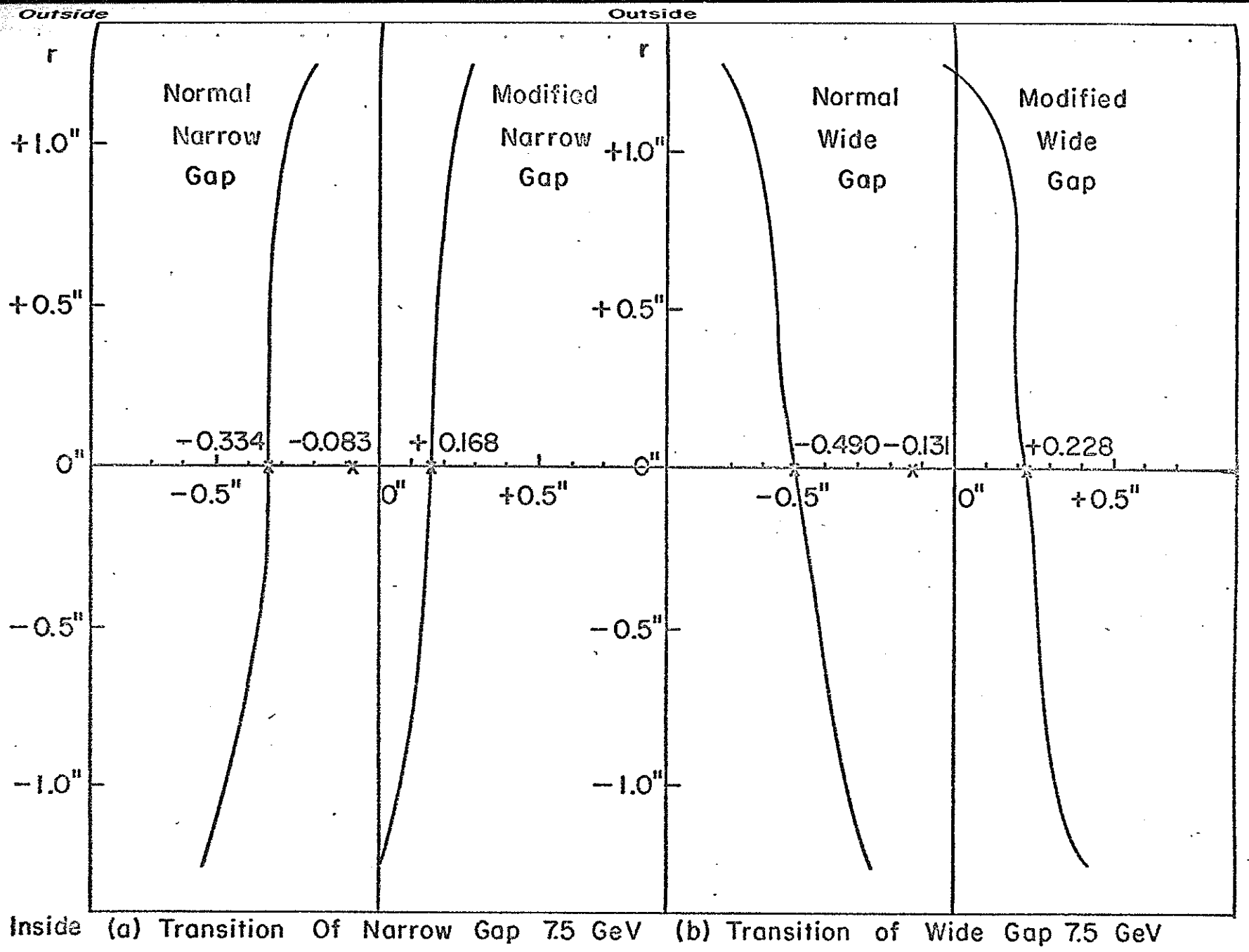

Fig. 8 Gradient Length on Both Sides of Transition Hard Packs.

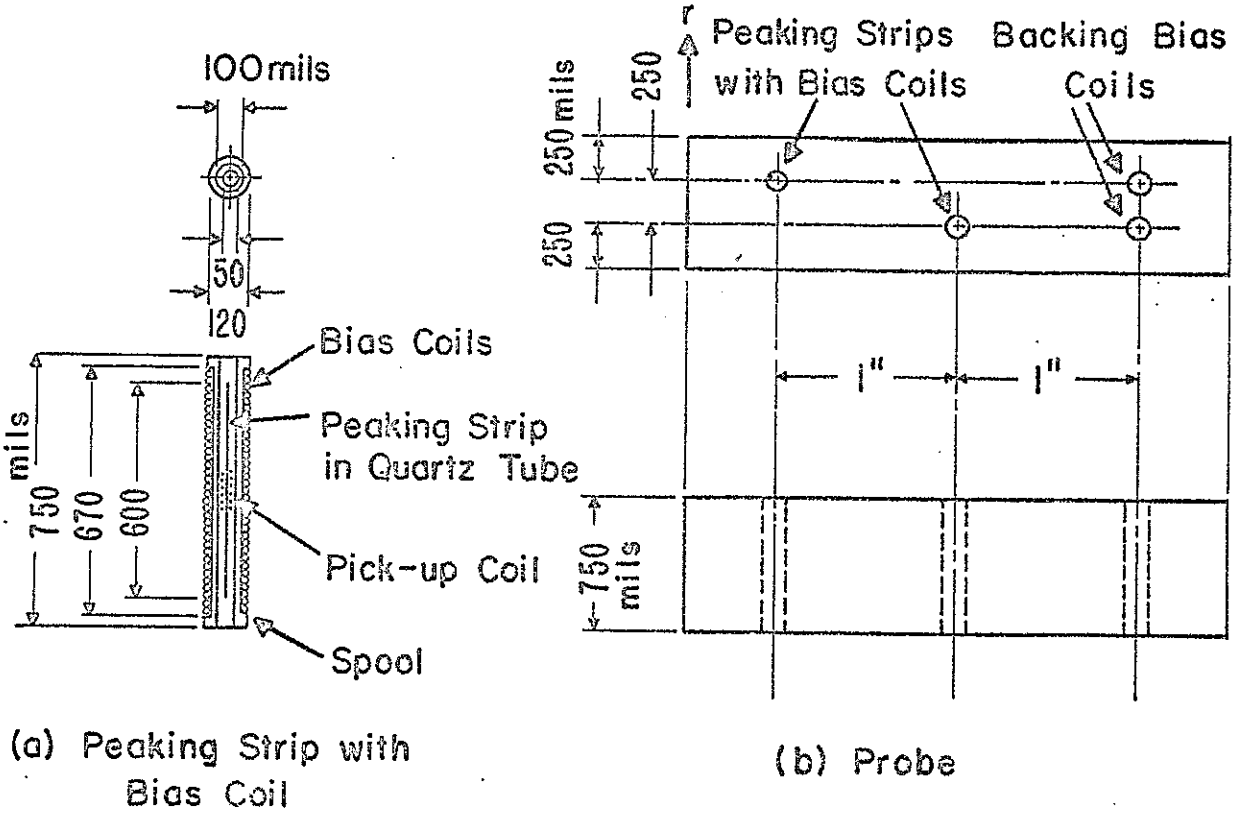

Fig. 9 Peaking Strip and Probe

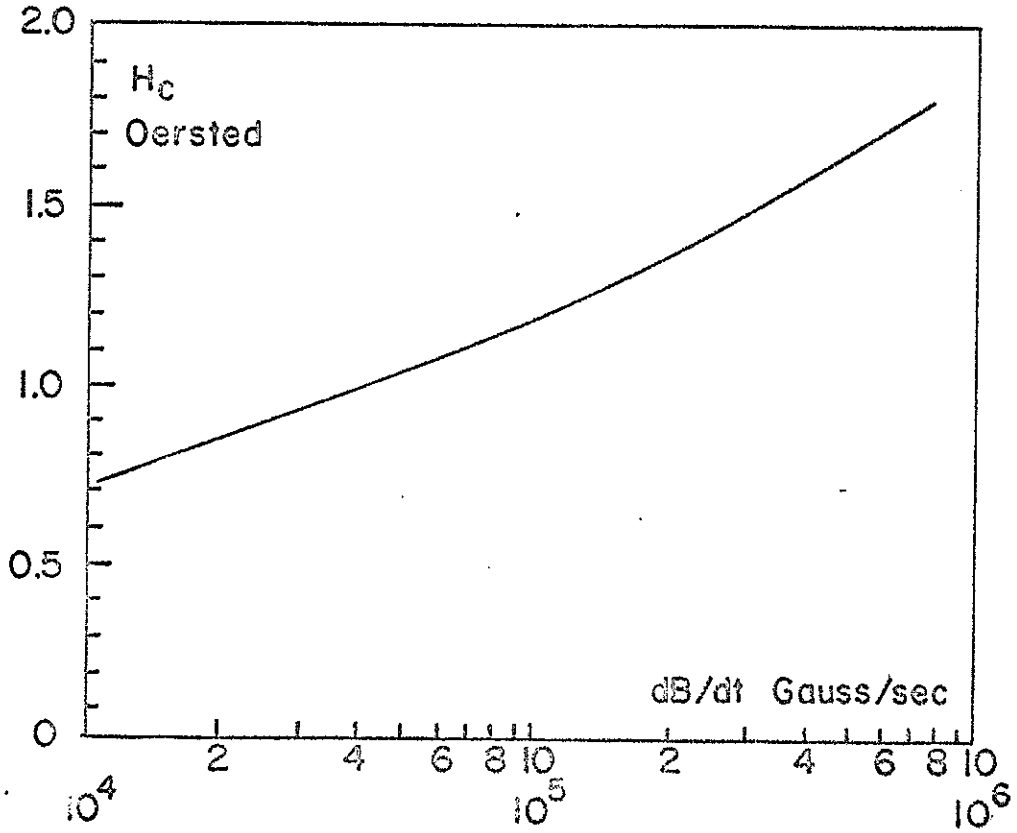

Fig. 11 Coercive Force of Peaking Strip and dB/dt

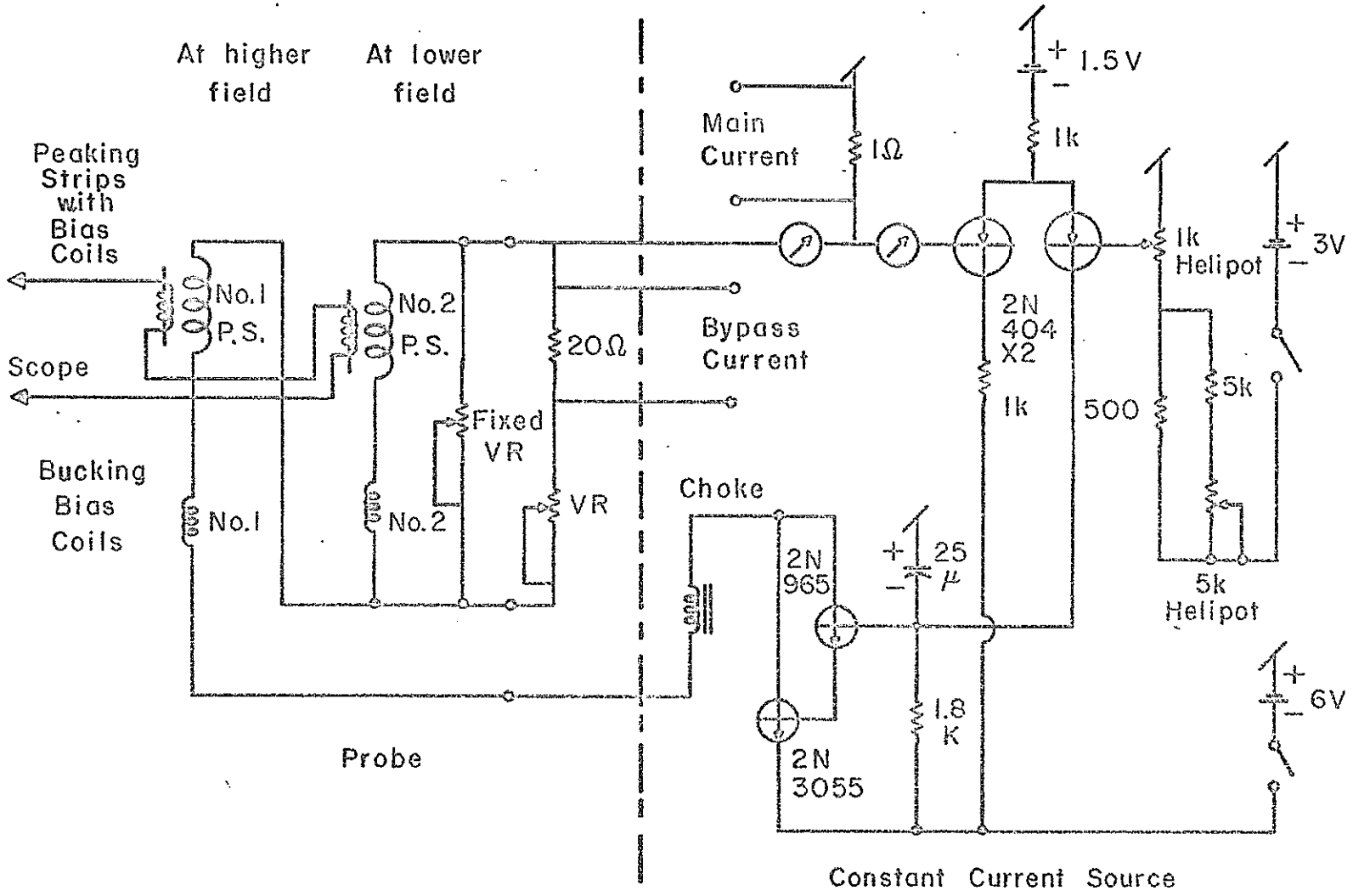

Fig. 10 Circuit for Peaking Strips

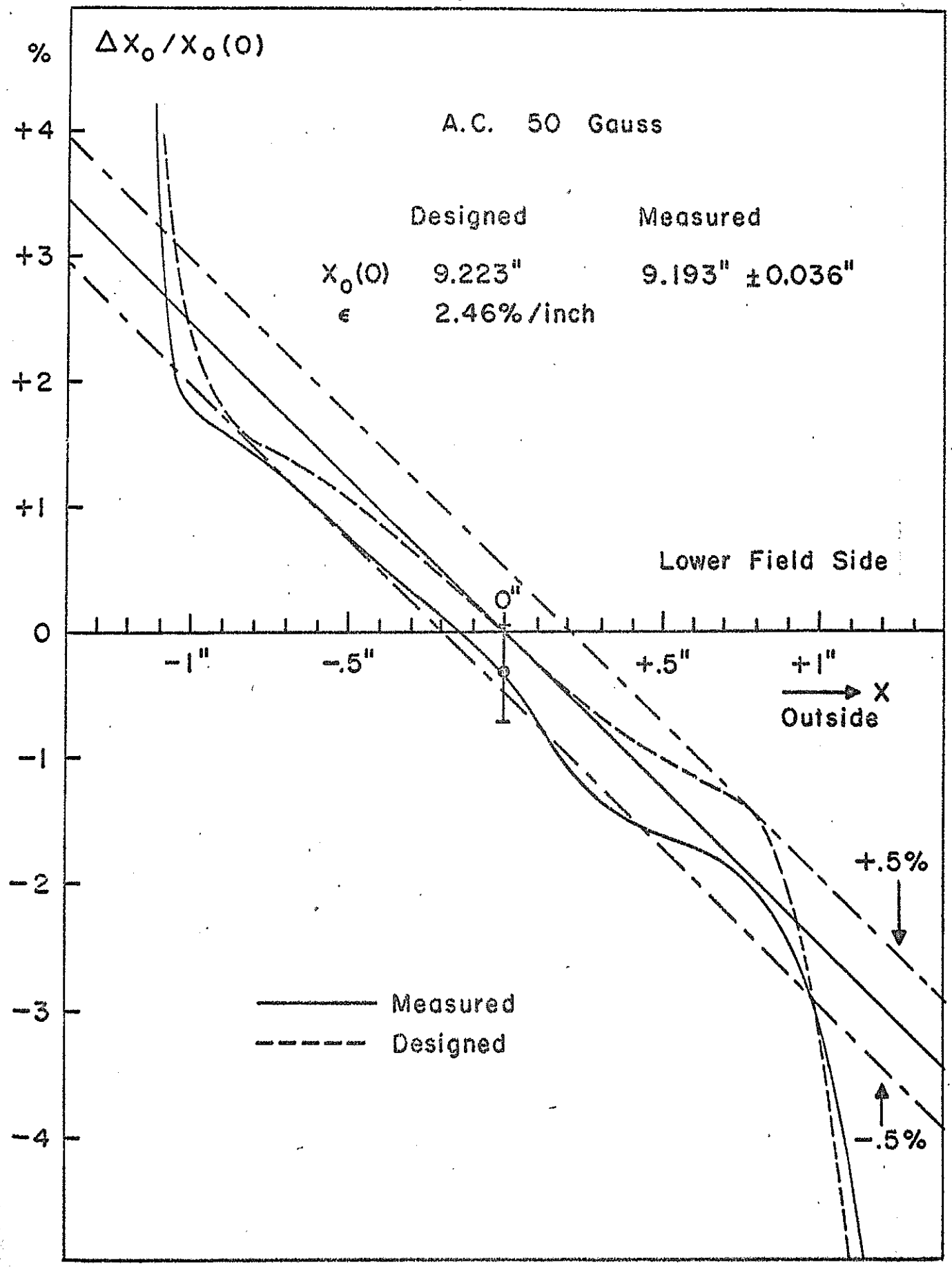

Fig. 12 $X_0(x)$ Distribution of Wide Gap Magnet at 50 Gauss

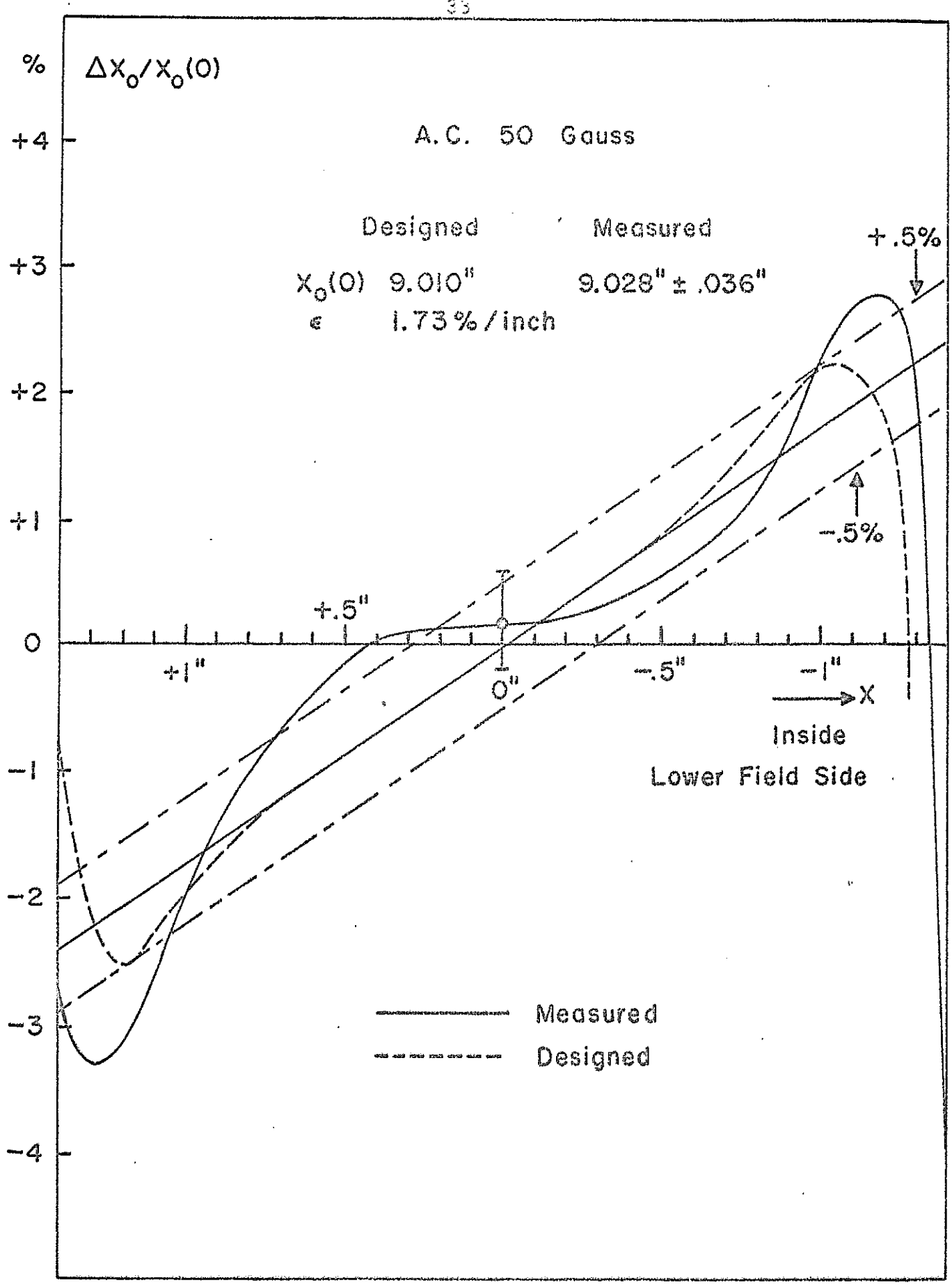

Fig. 13 $X_0(x)$ Disk Section of Narrow Gap Magnet at 50 Gauss

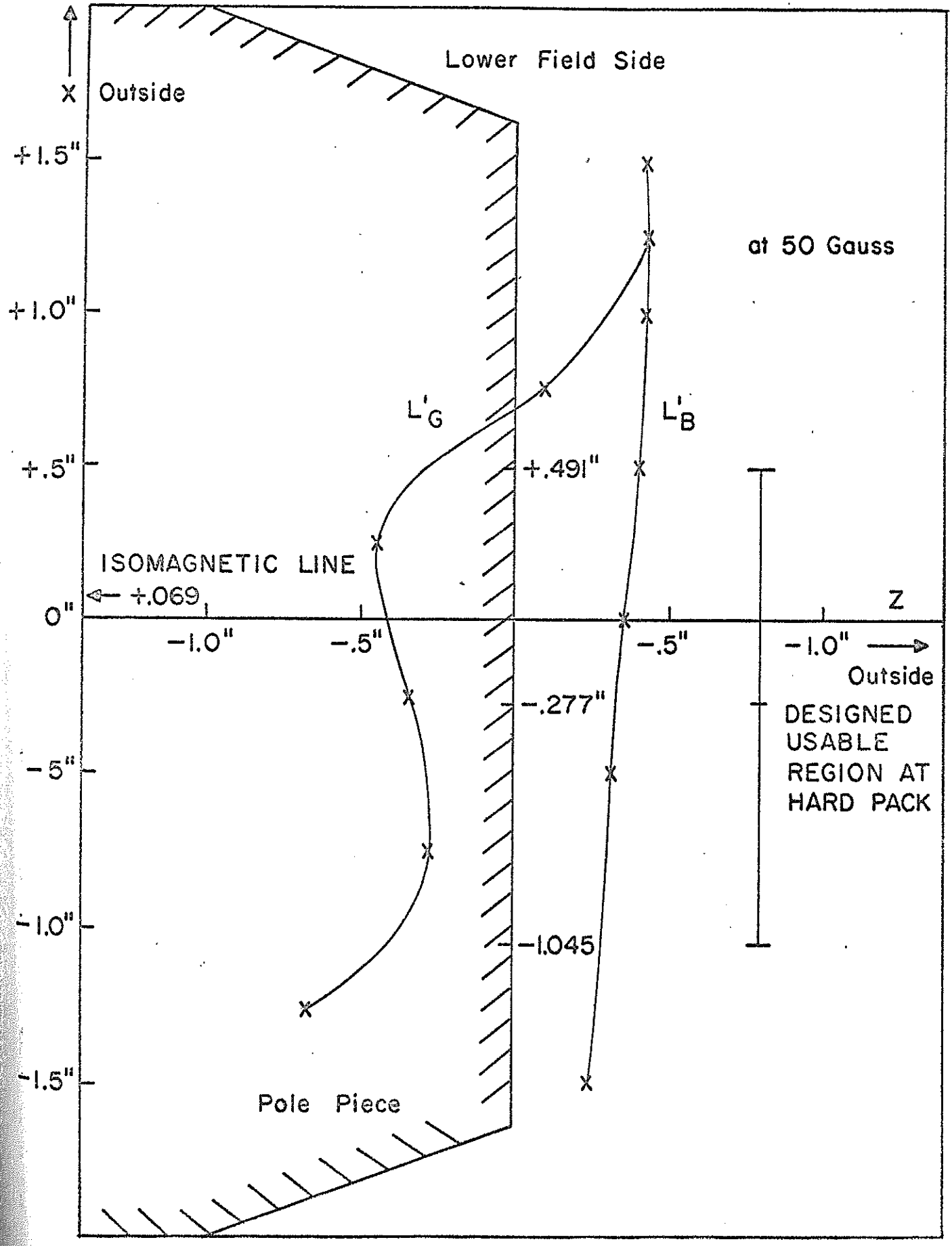

Fig. 14 L'_B and L'_G of Wide Gap Magnet at 50 Gauss

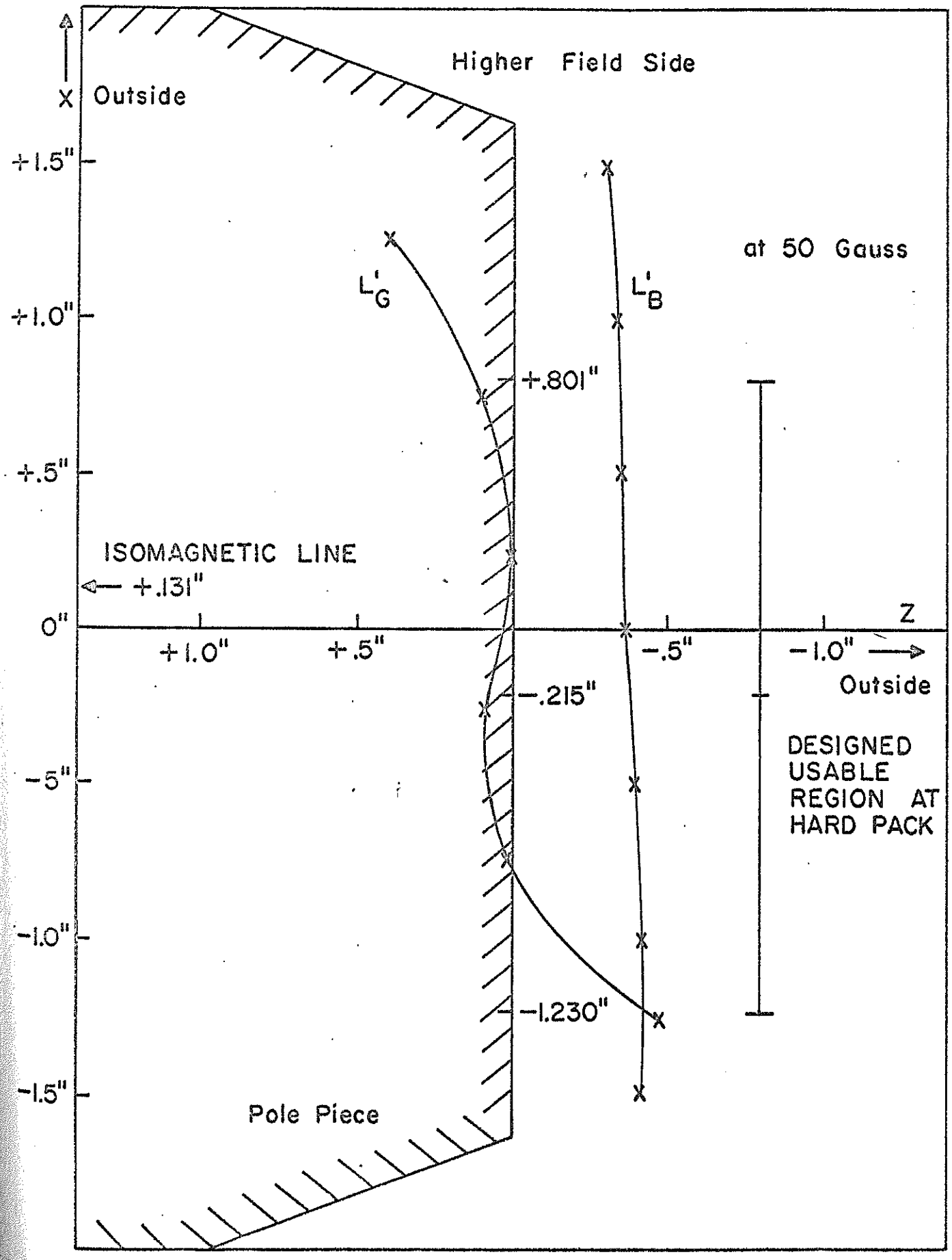

Fig. 15 L'_B and L'_G of Narrow Gap Magnet at 50 Gauss

CORNELL UNIVERSITY
LABORATORY OF NUCLEAR STUDIES
ITHACA, NEW YORK

CS-37
C. F. Kellers
September 5, 1968

MAGNET POWER FOR THE CORNELL ELECTRON SYNCHROTRON

Introduction

The Cornell Electron Synchrotron has an effective radius of curvature of 98.7 meters. It is a fast cycling machine which presently operates at 60 Hz. The magnets are capable of operation to about 20 GeV. The magnets are connected in a White[1] series resonant circuit except that there is no central power distributing transformer. There are 192 magnet and 4 quadrupole modules each with a transformer and resonating capacitors; these components are mounted on the individual magnet support beams. The module transformers are fed through a ring busbar system also housed in the support beam structure. (See Figure 1 for a condensed magnet connection diagram.)

For the AC component of the magnet power, sinusoidal rather than pulse excitation is preferred to reduce the distribution losses in the extended feed system. Also, reduction of the harmonic content in the drive waveform will minimize the excitation of delay line modes of the magnet circuit. Delay line modes (due to various causes) have proven to be a definite, but manageable, problem. The AC magnet power supply operates with about 15% harmonic content in the drive current when the machine is in the sinusoidal mode. Flat-topping is envisaged and will, of course, dramatically increase the harmonic content.

We have taken advantage of technological advances to construct an inverter-type AC supply using only solid-state components, rather than ignitrons. Such a supply is efficient, flexible, quiet, economical, and takes a minimum of space.

For the projected excitation to 15 GeV the AC power requirement is one megawatt of single phase power at 600 VAC and 60 Hz. This is derived from the three phase line in the following steps:

1. Three phase 13.4 kV power transformed to two three phase stars (180° out of phase with one another) with a line to line voltage of 270 Volts.

2. SCR controlled rectification in two rectifiers whose outputs are in series.

3. LC filtering of the outputs of the two rectifiers. Note in Figure 2 that only the center tap of the filter capacitors is grounded.

4. Inversion by solid state DPDT switches[2] (inverters).

5. Filtering of the square wave (voltage) output of the inverters by series resonant circuits. The switches are commutated by the reactive power in the series filters which are tuned somewhat above 60 Hz for this purpose.

Figure 3 is a schematic of one of the inverters (which act as a DPDT switch as shown in Figure 2).

DC magnet power is supplied by six supplies spaced around the ring with only one supply regulated. They are electrically in series with the magnets of the ring.

Inverter Operation

When a diagonal pair of SCRs is triggered, current rises and falls as befits a series resonant load. When the current reverses, the diodes in parallel with the SCRs conduct. The

other SCR pair may then be triggered and a reverse cycle of current through the load begins.

The load conditions under which the current will reverse within the required time (1/120 sec.) are of interest. The steady state condition is simple, the load must be capacitive at 60 Hz. That is to say, the load must be tuned to a frequency greater than 60 Hz.

Even under steady state conditions, the load cannot be adequately represented as a simple series resonant circuit. Figure 4 shows an equivalent circuit sufficient for steady state analysis. Because the current I_{in} from the inverter is reasonably free from harmonic content, it is convenient to consider only the fundament component, V_{in}, of the square-wave voltage applied to the equivalent load.

Figure 4 shows the parallel resonant magnet load as equivalent to a conductance G in parallel with an admittance Ψ. The admittance represents the amount of mistuning of the magnet load. (It is normally about 45° inductive.) The phasor diagram relates V_{in} to the magnet load voltage V_o. In practice, Ψ varies with temperature and line frequency while L_1, C_1, and G do not vary significantly.

To first order, we desire a certain value for V_o and then ask under what conditions (V_{in}, L_1, C_1, etc.) we can obtain this value for V_o.

The load V_{in}/I_{in} seen by the inverter will be capacitive if:

$$\Upsilon \equiv \left(\frac{1}{\omega C_1} - \omega L_1\right)\left(G\right) \text{ is greater than } \tfrac{1}{2}$$

It will commutate only if:

$$Q^* \equiv \left(G^2 \frac{L_1}{C_1}\right)^{\frac{1}{2}} \gtrsim 1$$

If Q* is large, the stored energy in L_1C_1 is expensive. For our operation, $1.2<Q^*<1.6$ is attractive.

Figure 5 is a plot of V_{in}/V_o (times some constant) vs. the phase angle of the magnet load for various values of γ. Normal operation (for $\gamma \doteq 1$) is made by starting with the magnet load nearly in tune (phase angle about 20° inductive). As the resonating capacitors warm up, the tuning becomes more inductive and operation stabilizes somewhere near the minimum in the curve (phase angle about 45° inductive).

It is important to operate near the minimum in the curve where V_o is 90° out of phase with respect to Vscr. This is the region in which the magnet current is independent of the line frequency. (Note that the inverter triggers are generated and timed by signals derived from the power line and that they can be applied to the SCRs only if various conditions, including reverse current in the diodes, are satisfied.) Variations in the line frequency, though small, are difficult to compensate for rapidly. These variations appear as effective changes in the phase angle of the magnet load. Near the minimum, the resultant variations in the magnet voltage (and thus current) are minimized. Power line voltage variations can readily be quickly compensated for in a voltage regulation loop in the rectifiers which preceed the inverters.

We have tried to use a circuit (phase-locked oscillator with high apparent Q) to smooth out the variations in line frequency. However, such a system was not effective because, over a few tens of cycles (the minimum time for effective correction), it was possible for the magnet phase to drift beyond the allowable limits for proper timing of the RF used for acceleration. (The RF being tied to the line phase.)

Analysis of behavior of the currents in the system upon turn-on is difficult, therefore, our "analog computer" was a prototype inverter powering 8 magnets to 10 GeV. We found that the system was stable for $\gamma \gtrsim 0.7$ and for Q*'s between 1.2 and 2.0. At the start of operation the conduction angle of the SCRs oscillates about the steady-state value with a

period of a few tenths of a second. The oscillations damp to the steady state value in about one second. Operation, where possible, below $\Upsilon = 0.5$ shows a much less damped, and occasionally anti-damped, behavior.

If the magnet load is suddenly shorted (crowbarred), the inverter current changes largely in phase and not in magnitude. We could use this happy accident to drain energy from the magnet ring upon detection of a fault.

Figure 6 is a plot of the electrical phase angle Φ through which the diodes (in parallel with the SCRs) conduct. It is plotted vs. the "mistuning" of the magnet ring for various values of the parameter Υ. Note that in the region of normal operation, the conduction phase angle is more or less independent of the "magnet mistuning". This fact has some connection with the ease with which the system may be turned on. One may consider either that upon turn-on the frequency is indefinite or that the magnet load's phase varies as the magnets fill with energy over the first half second of operation.

The magnet ring modules are actually tuned quite carefully to present an impedance to the feed system which is in tune at 10 GeV and slightly capacitive below. The inductive "mistuning" is intentional and is effected by inductors across the feed lines at the output of the supply.

Figure 7 shows the output current of the inverter vs. time for typical operating conditions. The discontinuities each 180° are rounded over a period of about 100μ seconds.

Softening Networks

Figure 8 shows the details of the SCR modules shown in Figure 3. The purposes of the modules are:

1. To limit the initial rate of current rise upon turn-on of the SCR.

2. To keep high frequency spikes from appearing between the terminals of the SCR. Such spikes can cause the device to trigger; the gate-anode capacity provides a mechanism.

3. To limit the rate of rise of the voltage upon turn-off of the diode. When the diagonal pair of SCRs fires, the diode current drops off at a rate limited by: (V_{dc}/L), where L is the sum of the inductors in series with the supply voltage. The turn-off process takes about 100 microseconds. At the end of this period, the SCR voltage rises at a rate limited largely by the softening network. The diode's stored charge is also significant.

Ferrite cores are used to form the inductors. The bus bar to the anode of the SCR passes through the ferrite cores forming an inexpensive and quiet saturable reactance with a frequency response useful to about 500 kHz where the core losses become conveniently large.

Delay Line Modes

The many magnet modules, all in series, have stray capacitances to ground forming a delay line. The period of the delay line around the machine is about 5 milliseconds. Standing voltage waves may be excited by harmonic components in the magnet supply current. The capacitive currents to ground caused by the delay line modes upset the equality of current around the ring. This effect is particularly critical at injection time when the magnet excitation current is instantaneously low; very small quadrature unbalance currents excited by the full drive amplitude then assume importance. The probable excitation of delay line modes and the desire to keep feed-line losses small are important reasons for having chosen a near-sinusoidal excitation system.

We have made provision for damping the delay line modes. This has been done by insulating the cases of the resonating capacitors and then connecting them to ground through a

resistor. In this way, part of the stray capacitance has a low effective Q. Initial tests did not indicate difficulties with the delay line modes. However, it did become obvious that they caused difficulties early in the acceleration cycle when operating at high peak excitation. The beam bump and the DC supplies generate traveling waves of larger magnitude than those produced by the AC excitation.

Control Logic

The control logic for the inverter and start cycle is described in the 3750 series of drawings. Some salient features of the system are:

1. Veto signals. These signals are generated by fault detection circuits. Upon detection of a fault, all SCR triggers are stopped. For example, if the interlock chain is broken for any reason, all further SCR triggers are stopped so that the rectifiers will not be drawing current when the main contactor opens (many tens of milliseconds later).

2. Inverter protection. In order for inverter SCR triggers to be generated, it is necessary that a signal be generated by reverse current flowing in the diodes which parallel the SCRs in the inverter. In this circuit, the generated signal charges a capacitor which provides the supply voltage for a transistor in the final stages of amplification of the SCR trigger rather than as a gate at some earlier point. Of course, to start the system, the signal must be simulated.

3. Additional inverter protection. Also required for continued inverter operation are signals indicating that the SCRs have fired. The presence of this signal insures that, should an SCR fire out of turn such that two SCRs are effectively placed across the DC supply, then such a failure will be detected. Upon detection of such a failure, a crowbar (section entitled Crowbar for Inverter) is activated which can clear the SCRs before damage has occurred.

4. Slow start system. This system assures the correct turn-on sequence. In particular, the rectifiers are not started until after the contactor is closed and the transients in the line voltage have ceased. The inverter is started as the rectifier output voltage slowly rises. The regulation loop is designed so that the turn on is gentle while stabilization is achieved within 30 seconds.

5. Rectifier protection. Serious damage to the filter capacitors is possible if the rectifiers should come on suddenly. The voltage on the filter capacitors could become twice the maximum output voltage of the rectifiers. In order to protect the capacitors, a circuit detects the rate of rise of the rectifier voltage and can shut off the rectifiers before the stored energy in the filter choke is sufficient to damage the filter capacitors. In addition, direct overvoltage protection is provided as well as protection against the rectifier output voltage dropping too rapidly. It has been observed that if the output of the rectifiers decreases too rapidly, it is possible for the inverter SCRs to fire when the conditions are not correct. This occurs most often when the DC magnet power supply drops out and the system is operating in the (normal) slope regulation mode.

Crowbar for Inverter

The inverters are effectively four single-pole single-throw switches sequenced to act as a double-pole, double-throw reversing switch. (See Figure 9.) The load impedance is of the order of one ohm. A limiting choke of about 40 microhenries is in series with the supply. Its purpose is to limit the rate of current rise in the switches (SCRs). Its impedance is of the order of 20 milliohms at 60 Hz. Its impedance must be kept reasonably low so that the stored energy in it will be small compared to the energy absorbed by the load per cycle. Suppose that S_1 should fire accidentally

while S_2 and S_3 were conducting at $t = t_o$. The current in S_1 will rise at a rate of E/L Amps/sec. We could turn off S_1 by closing S_5. S_5 would rob S_1 of current as well as reverse the voltage across S_1 sufficiently to clear the SCR. Clearly, the problem is to then turn off S_5. The solution is to place a capacitor in series with S_5 and to pre-charge the capacitor so that S_5 will starve the inverter of current and will also reverse the direction of current through the faulted leg of the inverter for a sufficient length of time to allow any healthy SCR to clear. (It is not clear if this method will protect S_2 if S_1 should short out completely. During the time of the crowbar, the load current will remain essentially constant. The peak currents in S_5 are about 2500 Amperes which is sufficient to clear S_2 at full load in most cases.)

The inductor, L_f is used to limit the rate of rise of the current in S_5. It is essential that S_5 be triggered in a very vigorous manner to prevent its deterioration. S_5 must also be protected so that if it should fire under normal operating conditions, dI/dt will be limited to a safe (or at least reasonable) value.

At the present time, there is a circuit whereby all eight of the inverter SCRs in the circuit can be fired simultaneously in order that the circuitry detecting faults may be checked.

Note that in Figure 11 the current in L rises and falls sufficiently rapidly to prevent even a fairly small fuse from melting. Also, when I_D stops, the stored energy in the inductors charges up C during which time the voltage across S_1 will rise at a few volts per microsecond until it becomes about 2E+300V.

Fuses

No really adequate solution to the fusing problem exists. The leg fuses shown in Figure 3 present a problem. They are there to prevent major damage should the load short to ground

and also they provide better protection for the SCRs in the event that the SCRs in one leg should be conducting simultaneously. (If all the SCRs fire simultaneously, it is the fuses in the DC^+ lead which protect the SCRs.) However, if the leg fuses fatigue during normal operation (and the others do not) then the stored energy in the load and in the current limiting inductor will cause the fuse voltage to be large which places a voltage stress on the semi-conductor elements in the system.

One can juggle the manufacturer's values of I^2t ratings for the fuses and SCRs under various conditions. The net result is that, except at levels below four or five GeV, the fuses cannot protect the SCRs in the inverter. (They do protect the SCRs in the rectifiers quite well, however.)

It is proposed that we buy SCRs with two parallel semiconductor pellets. These SCRs will be very generously rated for normal operating conditions. In the event of a switching failure, they will also subvert one of the mechanisms of SCR failure; namely, the current in each pellet will rise to no higher than safe levels before the fuses will clear. However, the improvement in the I^2t rating still will not be sufficient at 15 GeV to protect the SCRs should a failure occur which is not cleared by the fuse saver.

Max. allowed I^2t for the present SCRs is about 2×10^5

Max. allowed I^2t for SCRs with parallel pellets is about 3.6×10^5

(Both ratings given with consideration of the actual fault conditions anticipated.)

Fuses could be made which melt and extinguish more quickly than the present ones. However, their arc voltage will be much greater. For the main fuses, this is no disadvantage; for the leg fuses the added arc voltage might put an intolerable stress on the semiconductor elements.

$\frac{(I^2t)\ \text{to clear}}{(I_{\text{rating}})^2} \doteq 0.6$ for present fuses (lower for 10 GeV operation and below)
(Type A50P or A50Z, Chase-Shawmut)

$\frac{(I^2t)\ \text{to clear}}{(I_{\text{rating}})^2} \doteq 0.3$ for fuses contemplated for replacement of present main fuses
(Type A70P, Chase-Shawmut)

Bias Current Regulation

The bias current is controlled by regulating the sum of the voltage outputs of the six DC supplies around the ring with a fast voltage control loop. This is followed by a slow control loop which regulates the current.

There are five unregulated three phase full wave rectifiers (whose outputs are effectively in series) around the magnet ring. The input voltage to the transformer primaries of these supplies can be roughly set. An Inductrol serves to vary this voltage. In addition, there is a phased-back (SCR controlled) supply whose voltage can be varied rapidly. The voltage feed to the unregulated supplies is adjusted (either automatically or manually) such that the voltage of the regulated supply is in the mid-range for the desired current in the magnets. A small rectifier bridge samples the voltage feed to the unregulated supplies. Its output is called the simulacrum voltage. The voltage regulation loop "considers" the sum of some fraction of simulacrum voltage and the regulated supply voltage. The set-point voltage for the voltage loop is provided by both a signal proportional to the current set-point but also an error signal provided by the current regulation loop. The voltage loop has an open loop gain of from 10 to 30 depending on the region of operation. It is not useful to have a very much higher loop gain because the simulacrum voltage is not more accurate than 5% and because the magnet inductance

allows the slower current loop to react before appreciable changes in the magnet current have occurred following a line voltage step. There are also problems associated with the variation of the voltage loop's phase response as the voltage loop's open loop gain varies with operating conditions. If the phase response varies too much it is hard to close the current loop stably.

The current loop measures the shunt voltage and compares this with the current set point. The shunt is placed at the output of the phased-back supply preceeding an LCR filter. At first sight this does not appear to be a favorable point. At very low frequencies the shunt current and the phased-back supply voltage are in phase. At about f = 1/10 Hz the magnet ring's inductance causes a phase lag of the shunt current. At about f = 1 Hz the magnets' inductance resonates with the capacitance of the filter. Above this frequency the shunt current leads the supply voltage. The attenuation caused by the resonance of the magnets' inductance with the filter capacitance with the favorable phase shift in the region of one to ten Hz is utilized. In addition, having the shunt directly at the output of the phased-back supply simplifies the problem of finding a suitable electrical common point for the electronics. (No electrical ground exists in the system.) The system is not without difficulties but the net result is a loop which when closed has useful loop gain at a frequency of about one cycle.

The original design of the current loop had two dominant time constants of about 10 seconds each. The system was stable under all conditions but exhibited unfavorable properties during the periods when the loop was effectively open because the amplifiers were not in their linear regions. Two equal delaying time constants constitutes a virtual delay in the system roughly equal to the time constants themselves. But because of the high loop gain, it is possible for the effective delay to be much longer. Thus, suppose that the

loop is trying vainly to increase the current while the phased-back supply is full-up and the unregulated supplies are putting out insufficient voltage. Now, suppose that the voltage of the unregulated supplies is being increased as rapidly as possible. Suddenly, the current becomes sufficient. However, the delay in the loop cannot allow the phased-back supply to return to a normal voltage for some time. By that time the first amplifier in the loop may be saturated in the opposite direction from the original conditions while the second amplifier may not yet have called for a reduction in the voltage. The net result is that the system may take several time constants to settle down. Presently the system has one dominant time constant of about 100 seconds. Short term regulation is better than 0.05% of 10 GeV excitation.

Slope Regulation

The AC magnet current is regulated by maintaining the slope of the overall magnet ring current at injection time at some desired level. The AC magnet supply consists of voltage regulated DC supplies followed by LC filters and the inverters. The set point of the DC supplies is determined by comparing the observed slope with a desired slope setting. The voltage regulation loop in the DC supplies has an open loop gain of about 30. It may be that this loop should have a higher gain. The problems encountered in stabilizing the slope regulation loop are formidable:

1. The LC filter following the DC supplies has very nasty properties. It cannot be modified to have more gently varying phase and amplitude variations as the LCR filter in the bias current regulation loop has been.

2. The filling time of the magnets is not a clean cut, nor readily measurable, quantity.

3. Without the inclusion of non-linear elements, the open loop gain of the slope control loop would be proportional to peak energy. Such a non-linear circuit is used.

4. The slope loop's open loop gain is approximately proportional to the reciprocal of the slope. Fortunately, at higher slopes, the slope loop response time is less critical. The loop is optimized for slopes corresponding to ½ MeV/turn and is stable as low as ⅕ MeV/turn.

5. Closing of the slope control loop depends upon the existence of a slope reading.

It is impossible to have a slope reading until the AC current in the magnets is approximately equal to the DC current. Providing for a smooth transition from open loop conditions to closed loop operations upon turn-on is a major design problem. A small signal, corresponding to a slope of about 0.1 MeV/turn is provided when there is no real slope signal (to provide smooth turn on).

Originally, the slope control loop had two dominant time constants each of the order of ten seconds. The result of changing to one time constant was similar, but more dramatic, to that encountered with the bias current control loop. Upon turn-on the inverter supply voltage rises until a slope signal is available. At this point, the loop may or may not be open because of saturated amplifiers. Even if the loop closes at this point, the virtual delay (with two time constants) caused the supply to continue to rise for some time. What happened then is that when the control started to "catch", the loop was driven back so far that the AC current is reduced to the point where no slope signal was available. The inverter does not take kindly to rapid variations of the supply voltage and the system often faulted. The solution was to convert to one very long time constant. Upon turn-on, this time constant is discharged and no inverter supply voltage is demanded. By

controlling not only the time constant, but also the maximum rate at which it could be charged, one can control the rate of rise of the supply voltage such that the control loop is always in the linear region so that the moment that a slope signal appears the loop will close (stably) and the effective time constant of the loop will be the dominant time constant divided by the open loop gain.

The slope loop has useful gain at about one Hz. However, many problems still are to be faced. Of these, a better signal representing the slope at injection is the most obvious. Presently, the slope signal is derived by sampling (for 8 microseconds) the voltage on a pick-up coil in the test magnet. This voltage is plagued with "little men" which cause the slope reading to vary from the true value. It is proposed to read, instead, the time between the peaking strip pulses divided by the DC current set-point voltage. A lucky accident allows this quantity to be read easily and also it is fairly accurately proportional to the slope.

Another major difficulty with the AC magnet power control - one which is not unique to it - is that the timing of the inverter and of the rectifiers is determined by zero-crossings of the line voltages. Gross line variations upset these timings considerably. For instance, the inverter timing comes from a power line signal supplying the RF modulation, when the RF crowbars it will very likely trip out the inverter because of a timing error. In addition, there is evidence that the rectifiers for the AC talk to the DC supplies through the lines. Some effort has been made to stop this by placing capacitors to ground on each of the incoming phases to the regulated supply for the DC magnet power. It is known that without these it will not work when other large equipment is working.

SCR Gate Drives

For large SCRs one can consider the gate as extended over a large perimeter. Not all sections of the gate may require the same gate voltage drive. One way to insure that the entire gate is activated at one time is to have the gate drive signal be large in voltage. In addition, the gate, when triggered, activates only a small fractional area of the semiconductor pellet immediately. Activation of the pellet takes about 25 microseconds with a healthy gate drive. Hence, the dI/dt rating of the SCR is partly determined by the rate at which the area is activated and the peak allowed current for the SCR. For the 840 Amp pellets, one would conclude from this mechanism that dI/dt might be of the order of 10,000 Amps/25 microseconds. For these larger SCRs, the manufacturers are very coy about saying directly that higher dI/dt ratings than 50A/μsec are allowed, but they do suggest that they are.

Another turn-on property which must be considered is the instantaneous power per unit area within the junction during the time that the voltage across the SCR drops from the initial large forward voltage to some small voltage (say 10 Volts) during turn-on. If, for example, the voltage takes 4 microseconds to drop (linearly) to a negligible voltage and the dI/dt is 50 Amps per microsecond while the initial forward blocking voltage is 600 Volts, then the maximum instantaneous power would be 60,000 Watts which is about the instantaneous maximum power rating for the entire pellet. (It is interesting to note that at a given initial forward blocking voltage, almost all SCRs have the same dI/dt rating.) Obviously, that section which carries the initial current of the pellet heats very rapidly. It has been observed that the harder one drives the gate, the faster the voltage across the SCR drops. A gate rise time of one microsecond is obviously not conservative.

G.E. is now suggesting that gate rise times of the order of one Ampere in 100 nanoseconds are required. In the light of this statement, the following recommendations are made:

1. Rectifier SCRs. The present transformers are somewhat better constructed than those for the inverters. The rise time of the gate is probably sufficient. However, the 100 nF capacitors in parallel with the gate should be reduced to 20 nF or so. The present drive has a short circuit current of about two amperes and an open circuit voltage of about 10 Volts which is within the original gate ratings. The pulse length must be at least 150 μsec.

2. Inverter SCRs. The present transformers step-down the 24V pulse voltage to 16 Volts. It is not clear what the gate drive specifications on the present (C500X1) SCRs are. The original specifications given to me were the same as for the 470 Ampere SCRs but the specifications for the C501 series are for 16 Volts peak gate drive rather than 10 Volts. The recommended load line for the C501 is for 25V open circuit voltage and about 2 Amps short circuit current. For the present SCRs with the low rate of rise of the current (dI/dt ± 10A/microsec at 10 GeV), it should be sufficient to modify the gate drive by using a 1:1 transformer and changing the feedline to the transformer from shielded-twisted pair to coax. It definitely does appear that the shielded-twisted pair limits the rate of rise of the current considerably. The voltage measured on the transformer primary has a poor rise time while the voltage on the rectifier trigger transformers rises sharply (at the end of a coax of considerably longer length than the shielded-twisted pair). We have shown that, on the bench it is possible to achieve a rise time (into a 7 ohm resistive load) of about one-fourth microsecond/Amp on the secondary of the transformer and with 100 feet of coaxial cable between the transformer and the driving transistor.

One of the gate transformers has been replaced in an inverter. It has 15 turns on each winding. The windings are interleaved. It would be sufficient to have 14 turns or even 12 (the number easily wound on the core in a single layer). The pulse length must be 40 microseconds or longer.

If the C501G1 SCRs are purchased (with parallel pellets) the drive may have to be upgraded to assure that both pellets will fire simultaneously so that both will conduct later in the cycle.

3. Crowbar SCRs. The triggers to the crowbar SCRs are critical because the crowbar will experience a large value of dI/dt upon firing into a fault (dI/dt ≐ 50 A/microsecond) and an even larger value (perhaps twice as high in the event the crowbar should fire without a fault). (The SCRs can handle higher value of dI/dt when operated on an intermittent basis and/or when the pellet is cool.) In addition, a false crowbar firing is done while the voltage across the crowbar SCR is large. Some effort should be made to insure good triggering for the crowbar SCR. It may be necessary to use a SUS or other more complicated circuitry to achieve a fast enough gate drive. We plan to use the 1800V C500's indefinitely for this purpose.

Extension to 15 GeV

There are many problems associated with extension to 15 GeV. Some of them can easily be solved for 14 GeV operation while others, such as fusing, remain intractable. A short list of the important parameters to be considered in such an extension is given below:

1. Different values of L, C, and R will be required in the crowbar.

2. More study of fusing.

3. A study of what will happen to the traveling waves caused by the harmonic content of the DC supplies around the ring when some are run directly off the line and others are fed from the Inductrol.

4. Whether the regulated DC supply is rated for 320 Amps at all output voltages.

5. The power and current required to run the machine (at any particular energy) is significantly higher than anticipated as are the line drops in the incoming power lines.

6. How to handle the mistuning of the magnet ring as the temperature increases in such a way that it will be possible to get to 15 GeV with the AC power supply and the change of phase of the quadrature components of the power supply ripple as the tuning changes.

FOOT NOTES

*Work supported by National Science Foundation

1) M. G. White, F. C. Shoemaker, G. K. O'Neill, A High Intensity Proton Synchrotron, CERN Symposium Bd1, H150, S525 (1956).

2) R. R. Ott, L. A. Schlabach, A Unique Silicon Controlled High-Power Inverter with Sine-Wave Output Voltage. Digest of Technical Papers, 1962 International Solid State Circuits Conference (IRE, AIEE), p. 100. We became aware of this paper after development of our 20kW prototype. They suggest more complicated commutation filters which are desirable when load voltages must be maintained constant while the load impedance varies in phase and magnitude.

3) The SCRs used in the inverter are General Electric C500X1's. They consist of two 840A, 1800V units mounted back to back for use in AC switching. The integral water-cooled heat sink is very attractive. For sinusoidal output from the inverter we are using these SCRs for conduction in one direction only.

4) G.E., SCR Manual, 4th Edition 1967.

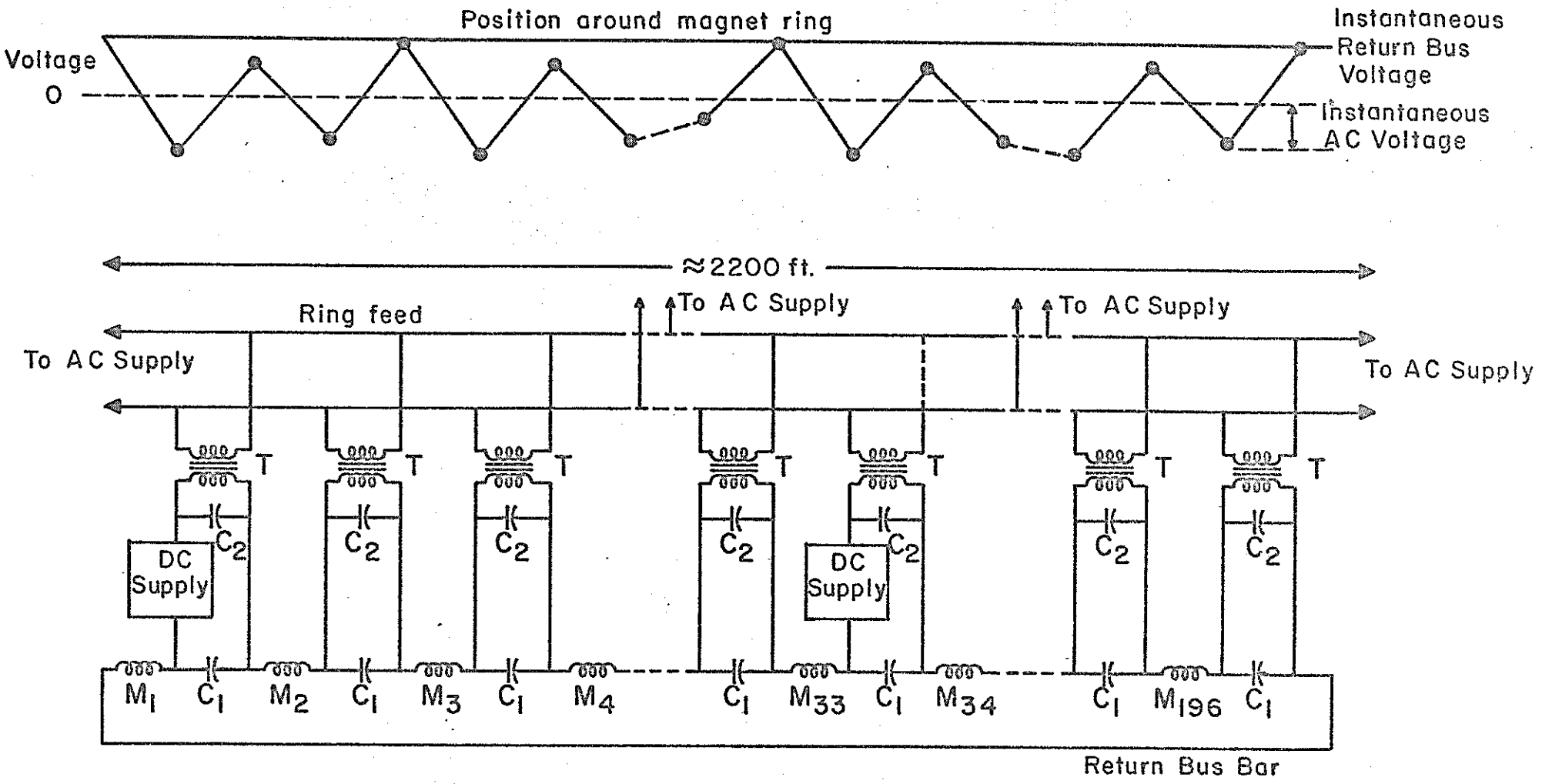

FIGURE 1 SIMPLIFIED DIAGRAM OF MAGNET INTERCONNECTIONS

6 DC SUPPLIES, ONE EVERY 32 OR 33 MAGNETS.

C_1 AND C_2 ARE JOINED AS SINGLE BANKS OF CAPACITORS EXCEPT AT SIX POSITIONS OF DC SUPPLIES, THEY ARE ADJUSTABLE IN 10μfd STEPS

$C_1 \approx C_2 \approx 950$μfds.

FEED FROM AC SUPPLY IS CONNECTED TO "RING" FEED AT THREE POINTS AROUND THE RING.

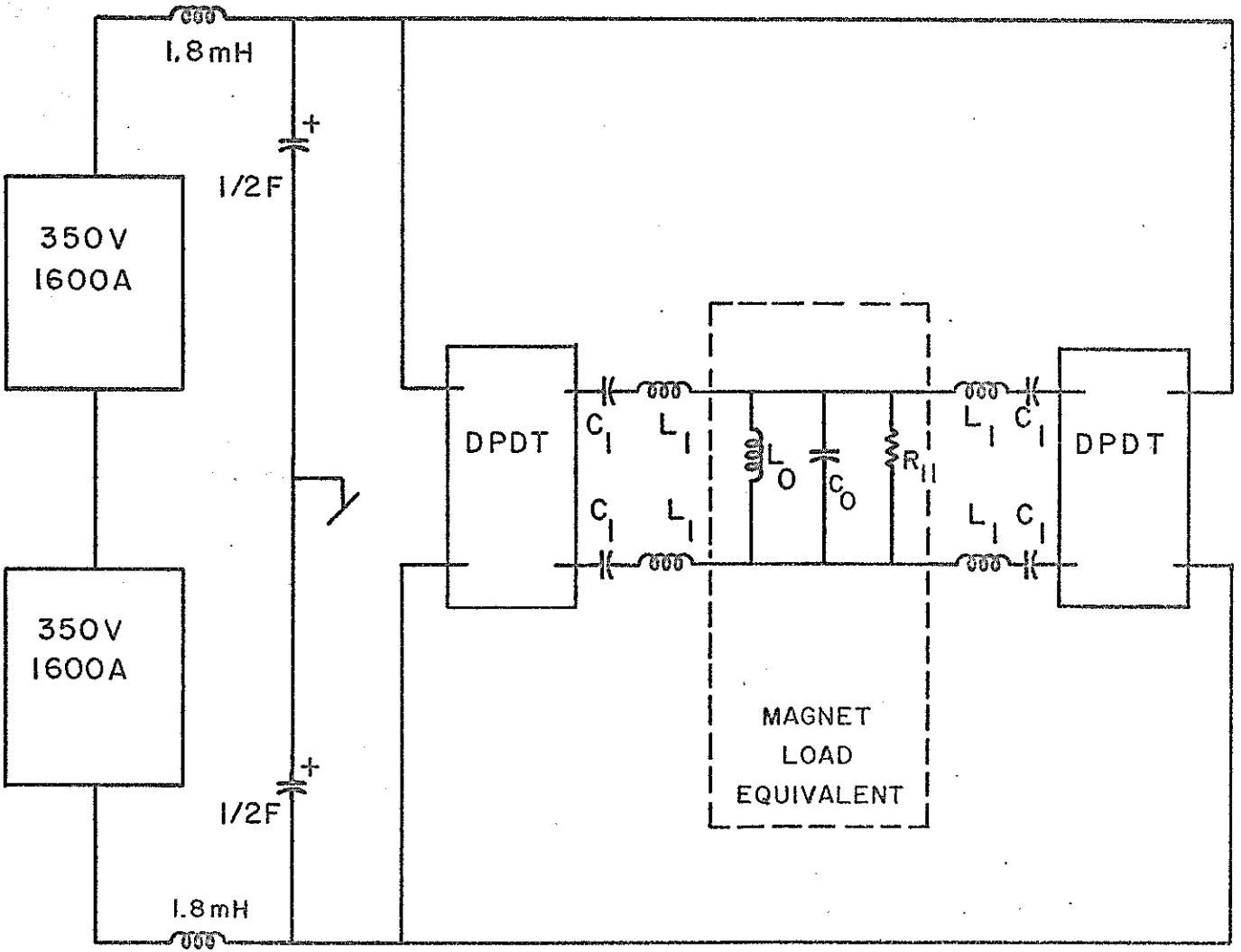

FIGURE 2 INVERTER BLOCK DIAGRAM

$$\omega L_1 \approx 0.5\Omega, \frac{1}{\omega C_1} \approx 0.9\Omega, R_{11} \doteq 0.4\Omega = 60\omega L_0 \doteq 60/\omega C_0, f \doteq 60 Hz$$

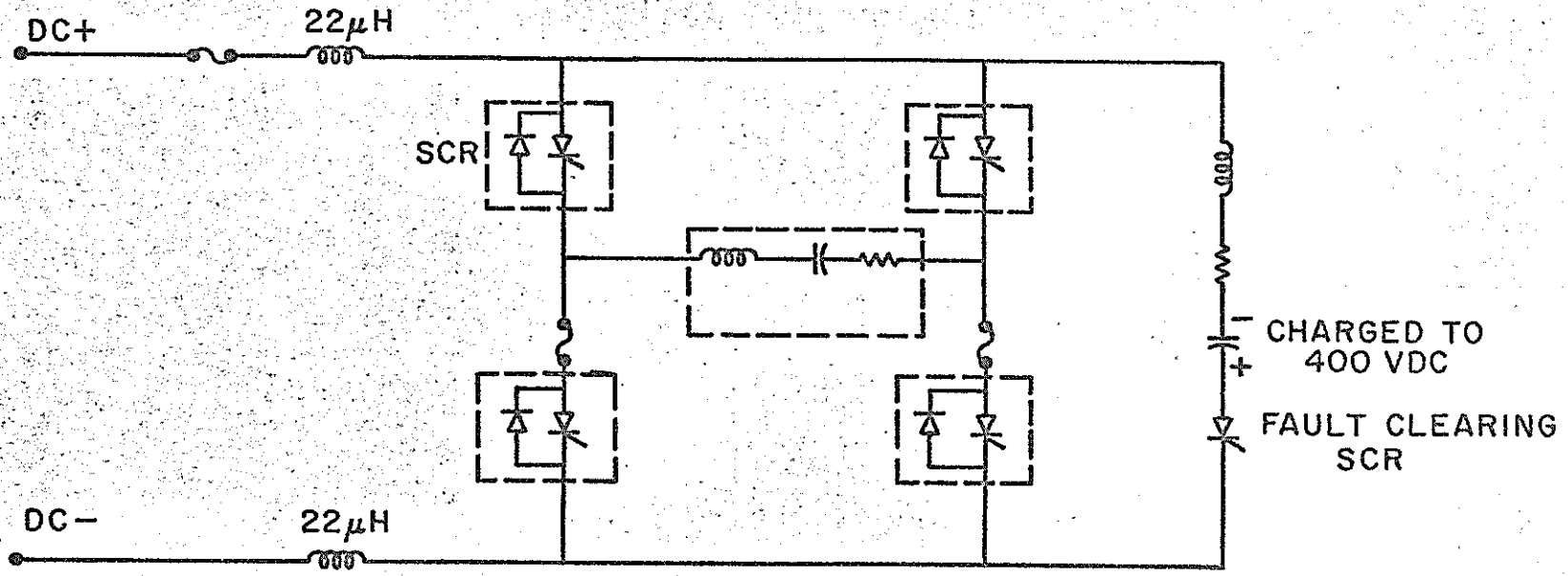

FIGURE 3 INVERTER SCHEMATIC

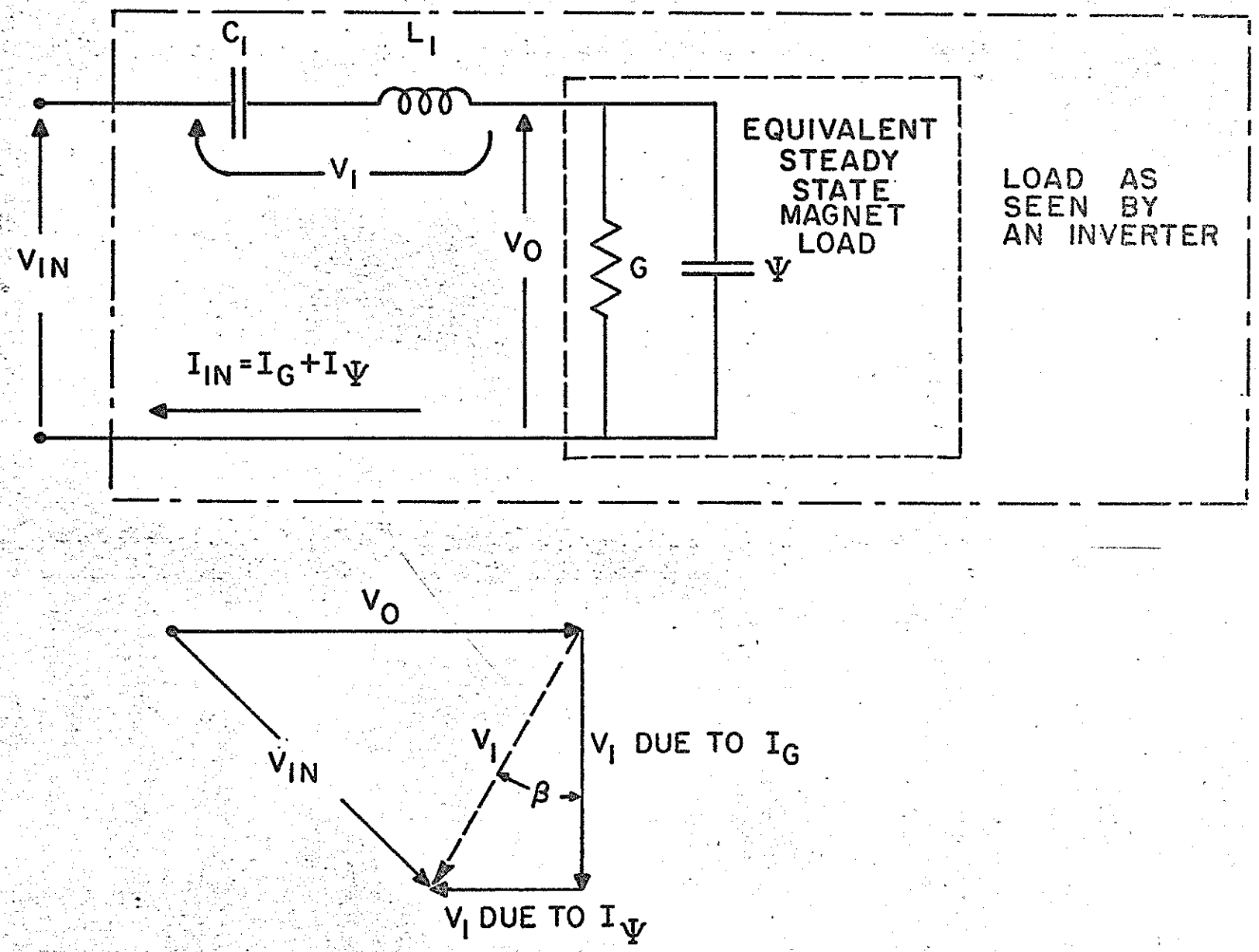

FIGURE 4 EQUIVALENT CIRCUIT FOR STEADY STATE ANALYSIS

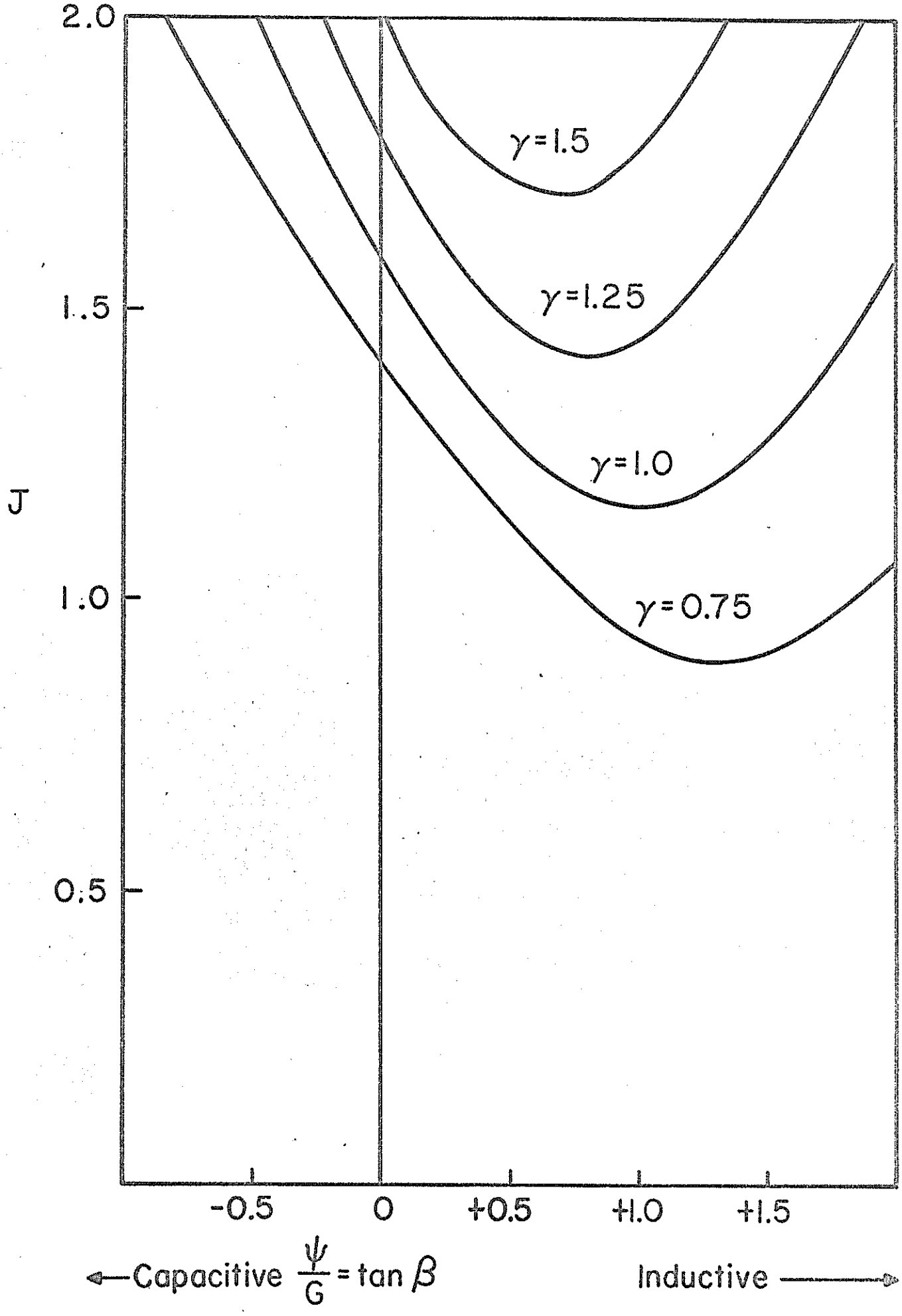

FIGURE 5 RATIO OF INPUT DC VOLTAGE TO AC LOAD VOLTAGE, J, VS, TANGENT OF PHASE ANGLE OF MAGNET LOAD,

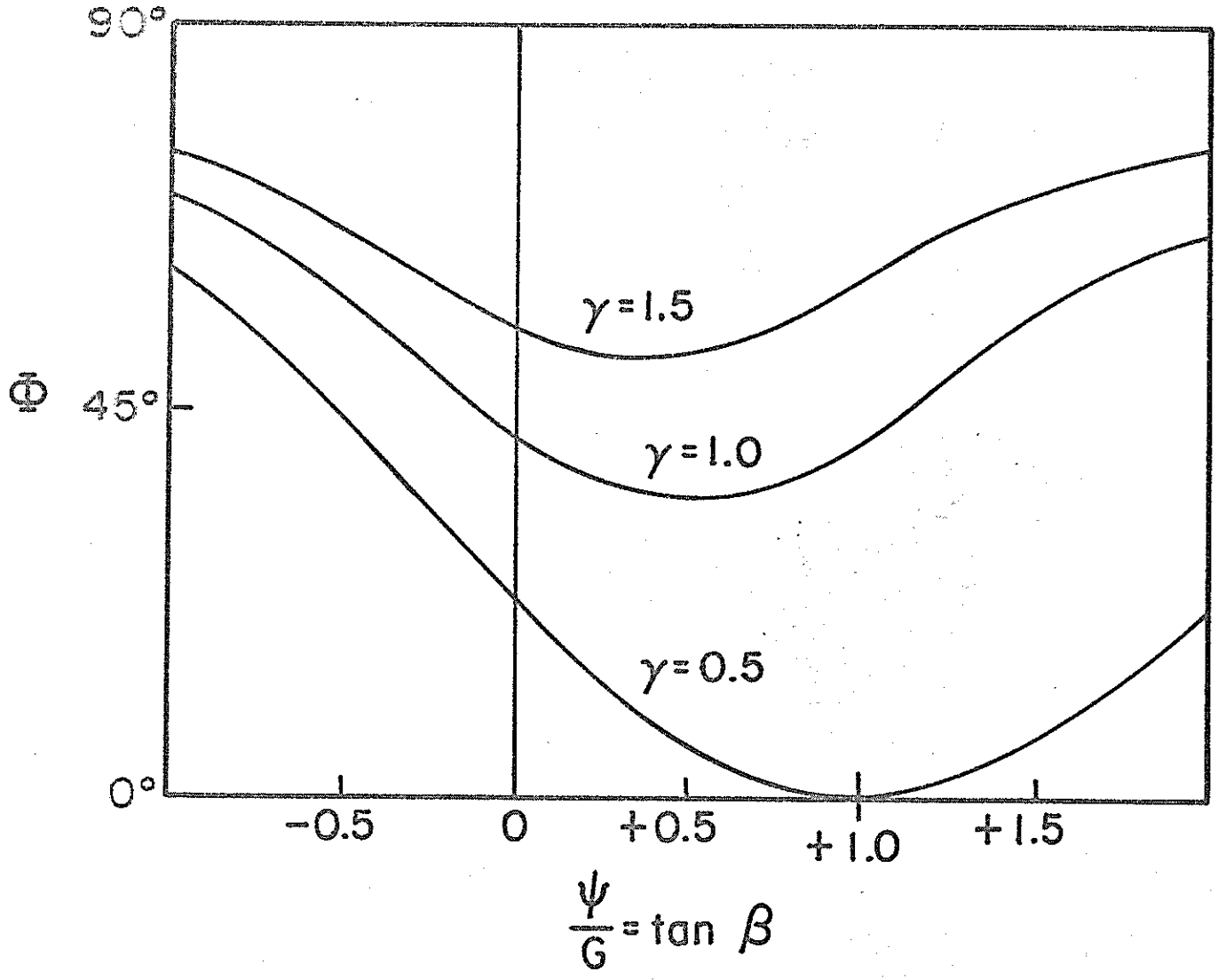

FIGURE 6 CONDUCTION ANGLE OF REVERSE DIODES VS TANGENT OF PHASE ANGLE OF MAGNET LOAD

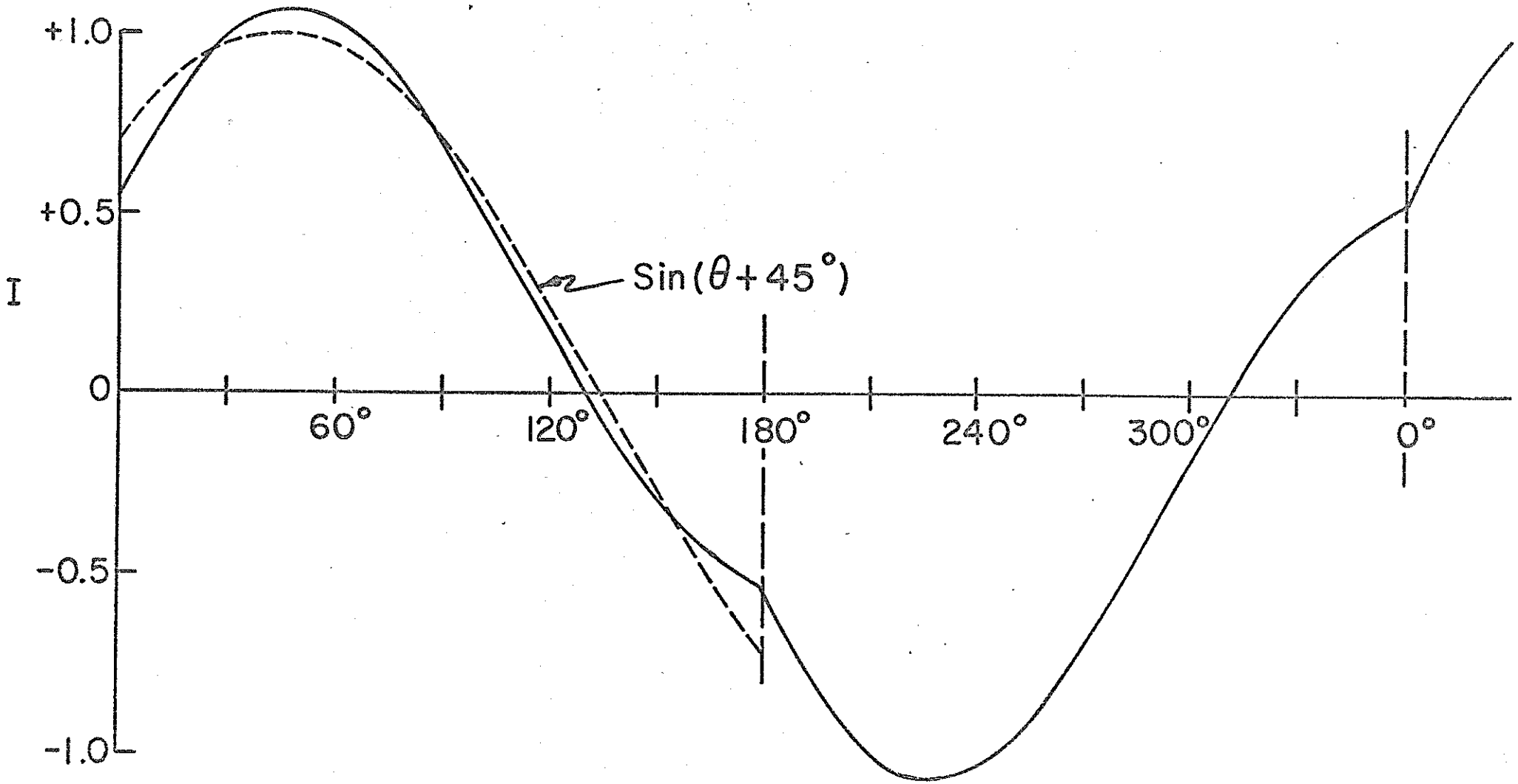

FIGURE 7 INVERTER OUTPUT CURRENT VS TIME

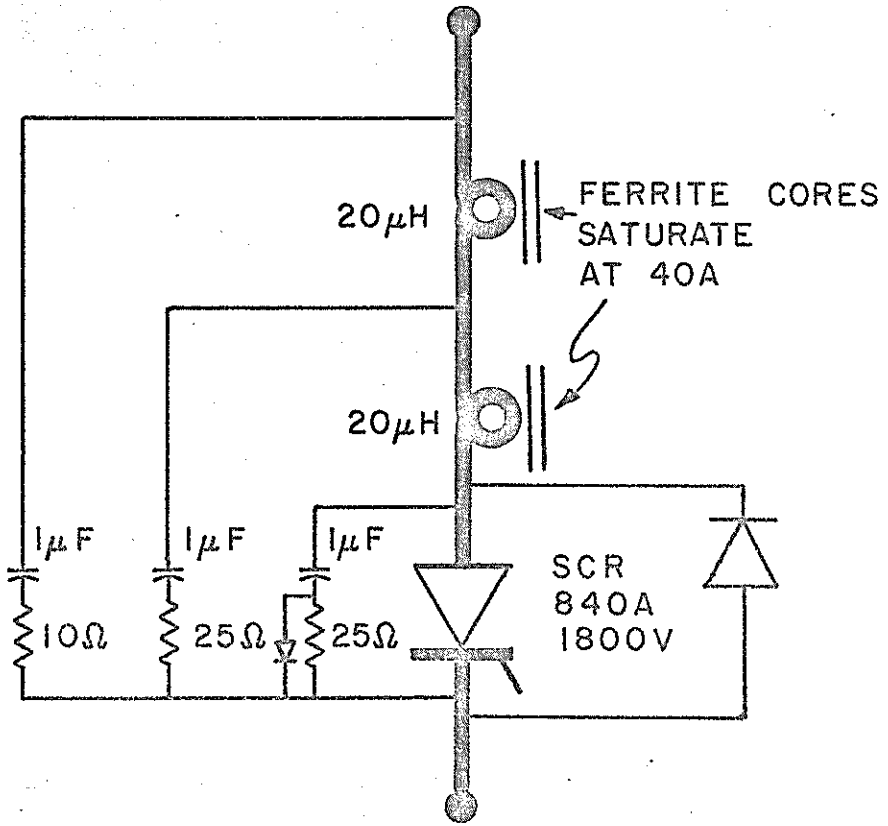

FIGURE 8 SCR MODULE

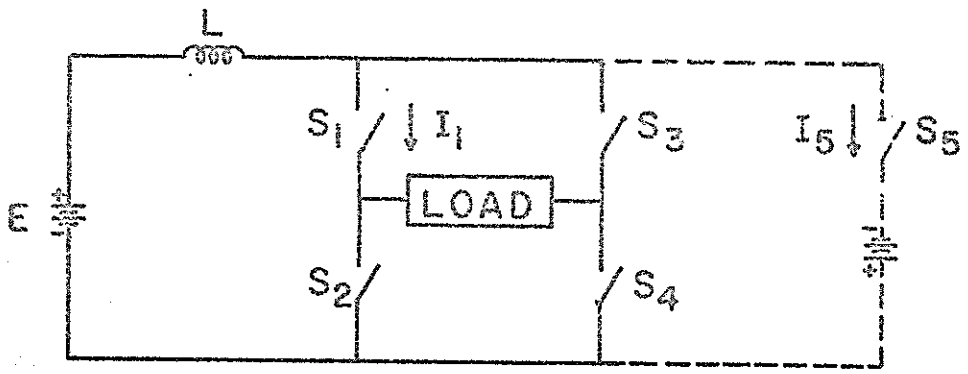

FIGURE 9 SIMPLIFIED INVERTER SCHEMATIC

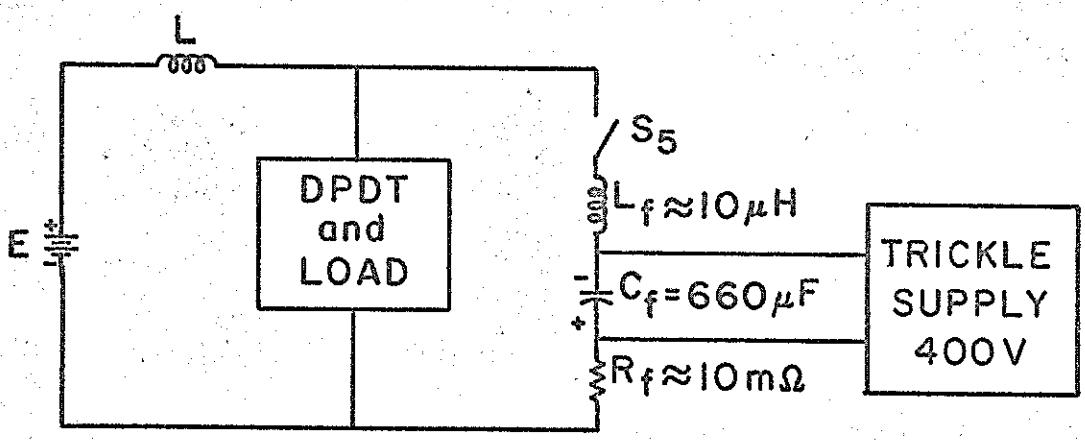

FIGURE 10 CRAWBAR BLOCK DIAGRAM

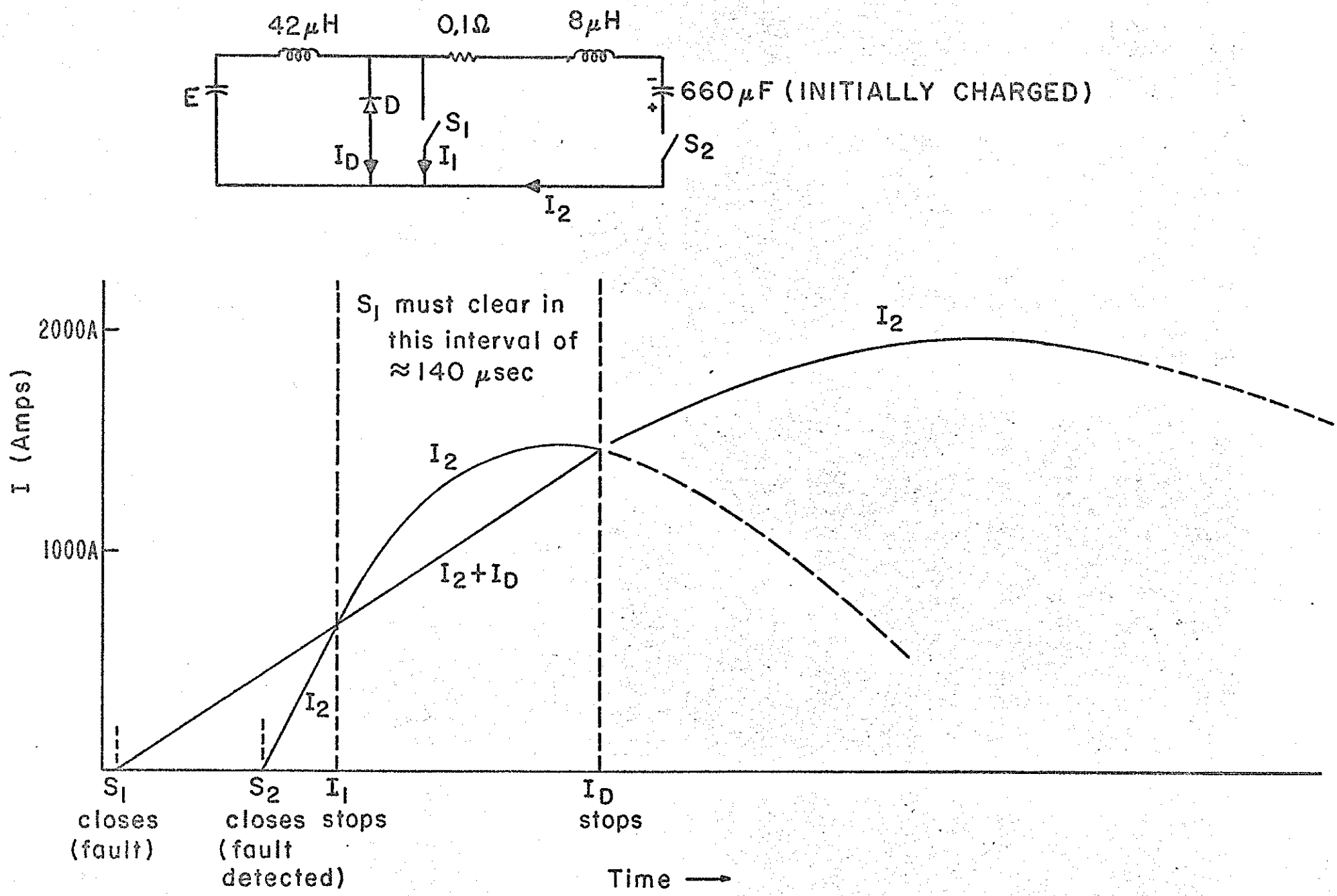

FIGURE 11 INVERTER CURRENTS DURING CROWBAR OPERATION

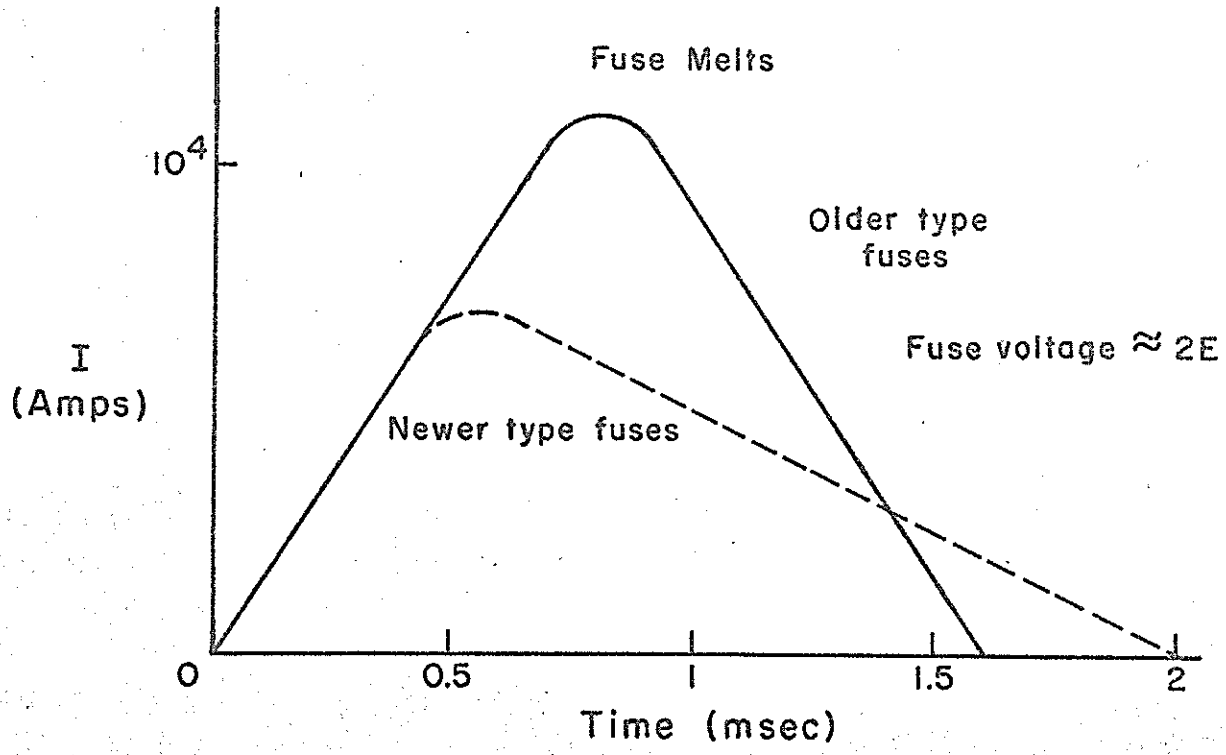

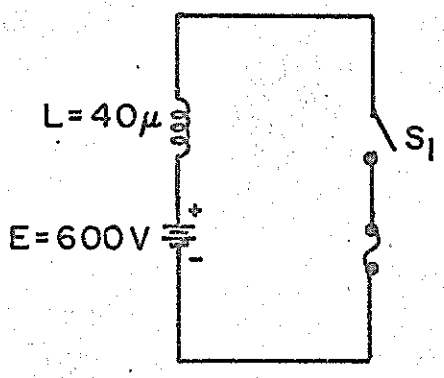

$$\left(\int_0^{\text{cleared}} I^2 dt\right)_{\substack{\text{Older}\\ \text{Type}}} \Big/ (I_{rating})^2 \approx 1$$

$$\left(\int_0^{\text{cleared}} I^2 dt\right)_{\substack{\text{Newer}\\ \text{Type}}} \Big/ (I_{rating})^2 \approx 0.3$$

FIGURE 12 FUSE CURRENT DURING CATASTROPHIC FAILURE (IDEALIZED BUT NOT A BAD APPROXIMATION)

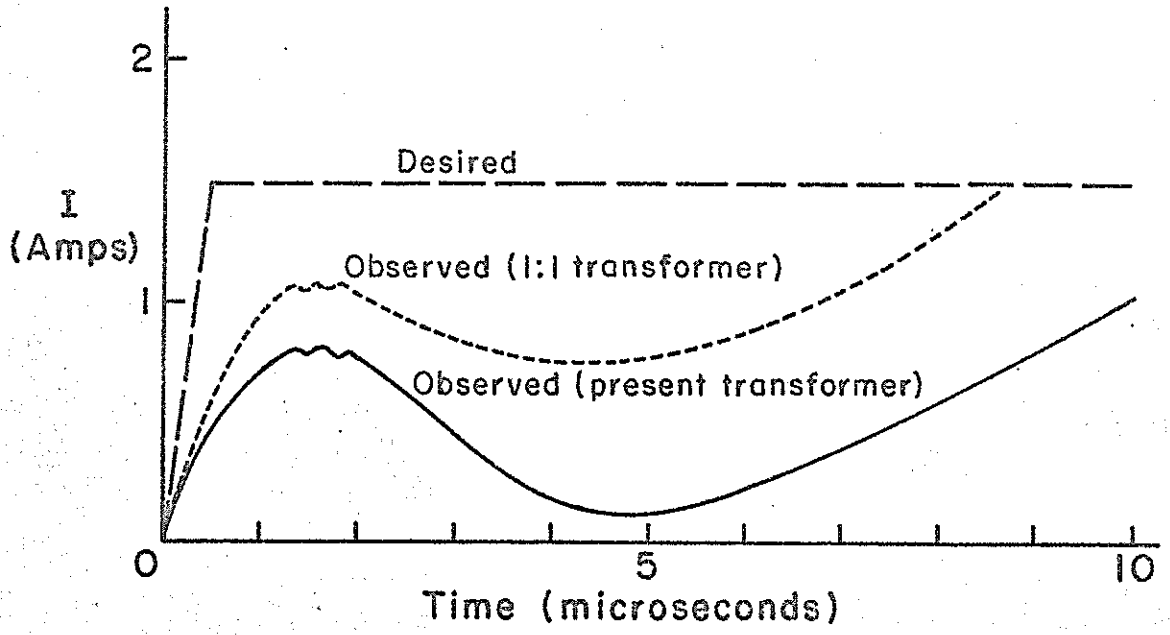

FIGURE 13 SCR GATE DRIVE FOR INVERTERS

CS-38

A 44 CHANNEL DIGITAL VOLTMETER

Laboratory of Nuclear Studies

Cornell University

Wayne Rial

2 January 1968

44 Channel Multiplexing Digital Voltmeter

A multi-channel, multiplexed, digital voltmeter with 4 place accuracy was required for monitoring various DC control voltages throughout the Cornell 10 GeV synchrotron. Since no commercial unit was available that would perform the required functions, we decided to design and construct a custom built DVM to measure the desired parameters.

Basic Philosophy:

A linear, 4000 step staircase is generated by standard D-A techniques using BCD coded 8-4-2-1 binaries and a precision, weighted, resistive-ladder network. The generated staircase-waveform is fed to one input of a differential comparator and the unknown voltage to be measured fed to the other input of the same comparator. When a coincidence in voltage appears between the unknown voltage and the corresponding voltage step of the staircase, the comparator triggers a flip-flop, initiating a readout cycle. During the readout cycle, the number of steps in the staircase to that comparison level is determined, and the number of such staircase steps is subsequently displayed on Nixie readouts. During the readout cycle, the progression of the staircase-waveform ceases and later continues advancing upon completion of the readout cycle. The staircase thus continues advancing until another (higher) unknown voltage coincides with another particular step on the staircase waveform, triggering another differential comparator, initiating a new readout cycle, and displaying that staircase-step number on a different group of

Nixie readouts. Each comparator has a particular bank of Nixie readouts associated with it.

Upon completion of 4000 staircase steps and their appropriate readout cycles, the staircase to waveform is returned to zero, and after a special delay period, commences a new measuring cycle.

The basic scheme thus far appears in Fig. #1.

Physical Description of Instrument:

The 44 channel DVM is completely self-contained except for the unknown voltage input-lines and the remote Nixie-indicator banks. The unit proper contains all the logic, made up of some 50 logic cards, power supplies, three local Nixie banks, and auxiliary switches and controls.

The instrument is divided into sections whose functions are, from top-to-bottom,

top panel - local Nixie readouts
2nd " - blank panel for later additions
3rd " - card file containing 22 input-comparators
4th " - input voltage switches and controls
5th " - card file containing 22 input-comparators
6th " - miscellaneous controls
7th " - card file containing logic, and
" " " logic and Bipco gates
8th " - output switches and remote Bipco connectors
9th " - main power supply

The second through eighth panel sections are mechanically tied together and constructed as a integral unit. These sections should be maintained as a unit to minimize ground loops.

The system employs some 2317 transistors, 2090 diodes, with a total component quantity of about 9000.

There are three Nixie banks of four digits each in the rack (top panel). The left-hand bank displays the reference-voltage step in the staircase waveform which occurs at the 2000th staircase step (exactly in the center of 4000 step staircase) and normally displays the number 2000 during DVM operation. During initial equipment warm-up, the left-hand Nixie bank hunts from 4000 to 0000, settling down to some arbitrary number and thence counting towards the reference-voltage step, eventually arriving at number 2000. Occasionally during normal operation, the reference-voltage Nixies will momentarily jump to numbers 1999 or 2001 while reference-voltage drift is being corrected to correspond to the number 2000.

The central Nixie-bank can display the equivalent input voltage to any voltage-comparator by means of selector switches located on the fourth panel. Thus, the actual input-voltage to any comparator can be monitored locally.

The right-hand bank of Nixies can dispaly locally, the number that any one of the remote Nixie-banks is displaying, by means of selector switches located on the ninth panel. Thus, the measured input-voltage to any comparator can be locally displayed.

The desired readouts (Nixie-banks) are generally located remotely to the main instrument. Provisions have been made for the remote readouts to be placed up to 100 feet (of interconnecting cable) from the instruments. The DVM has been designed so that approximately 12 banks of 3-digit readouts, and 30 banks of 4-digit readouts can be used remotely.

The number of digits per readout can be changed by utilizing different Nixie-driver gates or constructing new gate cards. Thus, it is possible to have all of the 44 Nixie-banks displaying 4 digit accuracy.

The remotely-located Nixies will usually be located on a panel associated with the control which varies the DVM input voltage to be measured. This control may be a manually-operated potentiometer or a motor-driven potentiometer operated by slewing switches or computer control. A remote Nixie-bank may also, of course, indicate the voltage measured across a sampling resistor not associated with a manual control.

Electrical Characteristics of the Instrument:

The input voltages to be measured by this instrument are negative D.C. values with respect to system ground (input reference) with a maximum of -10 V amplitude. The system can follow a rate-of-change of input voltage $(\frac{de}{dt})$ not greater than about 50 volts per second, although such input rates-of-change can not be followed visually on their respective Nixie readouts.

The transistors in the comparator input circuit are protected against overvoltage of the input lines so that accidental application of excessive positive or negative voltage will not incapacitate the instrument.

Instrument Logic:

In the description of the logic, all functions are considered true when the waveform goes to a positive value. The actual circuit waveforms may or may not be true for positive going values. The logic utilized in the instrument uses both positive and negative

logic and care must be exercised when deciphering the logic sequence. The timing-chart shows the true-false relations of the various switching functions, and the respective timing-chart waveforms are not to be construed as the actual logic waveforms.

In studying the logic, reference must be made to the timing chart, block diagram, and the following definitions.

Logic Definitions

$\overline{|Q}$ = leading edge of Q function

$\overline{|\bar{Q}}$ = leading edge of $\bar{Q}$ function

$\overline{Q|}$ = trailing edge of Q function

$\overline{\bar{Q}|}$ = trailing edge of $\bar{Q}$ function

$M \longrightarrow N$ means a transition of M causes N to go true

$M \longrightarrow \bar{N}$ means a transition of M causes N to go false

G = H means G produces H (true)

		Location	
1.	CFF = comparator flip-flop	comparator	card
2.	RFF = readout flip-flop	clock	"
3.	DFF = main delay flip-flop	clock	"
4.	A Gate = A Gate output pulses (UCP)	clock	"
5.	B Gate = B Gate output pulses (DCP)	clock	"
6.	C = clock pulse	clock	"
7.	XFF = special delay flip-flop	clock	"
8.	YFF = special delay flip-flop	clock	"
9.	SFF = strobe flip-flop	strobe	"
10.	PDC = pause delay flip-flop	strobe	"
11.	JAM = jam pulse	strobe	"
12.	UCP = up count pulses	clock	"
13.	DCP = down count pulses	clock	"

14.	LP-30 = Commercial D to A converter	LP-30 card
15.	OA-30 = Commercial operational amplifier	OA-30 "
16.	FZ_1 = first zero flip-flop for 1's digits	Fst& Snd zero card
17.	FZ_{10}= first zero flip-flop for 10's digits	" " " "
18.	FZ_{100}=first zero flip-flop for 100's digits	" " " "
19.	FZ_k = first zero flip-flop for k's digits	" " " "
20.	SZ_1 = second zero flip-flop for 1's digits	" " " "
21.	SZ_{10}= second zero flip-flop for 10's digits	" " " "
22.	SZ_{100}=second zero flip-flop for 100's digits	" " " "
23.	SZ_k = second zero flip-flop for k's digits	" " " "
24.	SZ OR = OR'ed output of second zero flip-flops	down count pulse gates card
25.	PFF = pause flip-flop	up-down counter#4 card
26.	SZD_1= delayed second zero flip-flop for 1's	snd zero delay card
27.	SZD_{10}=delayed second zero flip-flop for 10's	" " " "
28.	SZD_{100}=delayed second zero flip-flop for 100's	" " " "
29.	SZD_k = delayed second zero flip-flop for k's	" " " "
30.	CLC = comparator latch circuit	comparator card
31.	K = 2000th staircase step binary output	up-down counter#4 card
32.	Ref CFF = reference flip-flop	reference comparator card
33.	STR = strobe pulse (ungated)	strobe card
34.	TPC = ten pulse counter output	10 pulse detector
35.	ZFF = special delay flip-flop	10 volt reference card
36.		
37.	C Gate = C Gate	down count pulse gates card
38.	D Gate = D Gate	" " " " "
39.	E Gate = E Gate	" " " " "

40. F Gate = F Gate down count pulse gates card
41. 4KC = 4000 count FF output
42. CFF_R = reference comparator FF

Logic Equations

1. $\overline{\overline{CLC_N}} \rightarrow CFF_N$
2. $\overline{\overline{CFF_N}} \rightarrow RFF, DFF$
3. $\overline{\overline{DFF} \cdot \overline{C}} \rightarrow XFF$
4. $\overline{\overline{XFF}} \rightarrow YFF$
5. $\overline{RFF} \cdot \overline{PDC} \cdot C$ = A Gate pulses (UCP)
6. $RFF \cdot \overline{DFF} \cdot C$ = B Gate pulses (DCP)
7. $\overline{\overline{DFF} \cdot \overline{C}} \rightarrow SFF$
8. $\overline{\overline{YFF}} \rightarrow \overline{DFF}$
9. $\overline{\overline{SZ\ OR} + \overline{4KC}} \rightarrow \overline{RFF}, \overline{XFF}, \overline{CFF}$
10. $\overline{\overline{4KC}} \rightarrow PFF$
11. $\overline{\overline{SZ\ OR}} \rightarrow \overline{PFF}$
12. $\overline{\overline{PFF}} \cdot STR \rightarrow PDC$
13. $\overline{\overline{PFF}} \cdot STR \rightarrow \overline{PDC}$
14. $SFF \cdot STR$ = staircase strobe pulses
15. First "0" from 1's down counter $\rightarrow FZ_1$
16. Second "0" from 1's down counter $\rightarrow \overline{FZ_1}$
17. $\overline{\overline{FZ_1}} \rightarrow SZ_1$
18. $\overline{\overline{SZ_1} \cdot \overline{C}} \rightarrow SZD_1$
19. B Gate $\cdot \overline{SZD_1}$ = C Gate pulses
20. etc. for $\overline{FZ_{10}}$, SZ_{10}, $\overline{SZD_{10}}$, = D Gate pulses

21. Etc. for FZ_{100}, SZ_{100}, SZD_{100}, = E Gate pulses

22. Etc. for FZ_K, SZ_K, SZD_K, = F Gate pulses

23. $\overline{DFF} \rightarrow \overline{FZ_1}$, $\overline{FZ_{10}}$, $\overline{FZ_{100}}$, $\overline{FZ_K}$, $\overline{SZ_1}$, $\overline{SZ_{10}}$, $\overline{SZ_{100}}$, $\overline{SZ_K}$

24. $\overline{SFF} \rightarrow JAM_1$ Reset all Bipcos

25. $\overline{PDC} \rightarrow \overline{CLC_N}$

26. $\overline{K} \rightarrow ZFF$

27. $\overline{K} \cdot \overline{UCP} \rightarrow \overline{ZFF}$

28. $\overline{K} \cdot CFF \cdot \overline{ZFF}$ = pump staircase

29. $CFF_1 \rightarrow$ Bipco $gates_1$

    $CFF_2 \rightarrow$ Bipco $gates_2$

    " " " "

    $CFF_N \rightarrow$ Bipco $gates_N$

30. Bipco-bank current driver pulse = Bipco output pulses:

    $9_{1's} + 9_{10's} + 9_{100's} + 9_{k's}$

31. $\overline{SZ\ OR} \rightarrow SFF$

D to A Conversion

The generation of the 4000 step, linear staircase is accomplished by one of the most basic D-A conversion techniques. This technique involves clocking a chain of binaries, the outputs of which are each connected to a common point through weighted resistors. The weight of each resistor is a function of the weight of each binary in the chain. The current through each resistor is summed at the common-connection point and the sum current is required to flow through an output resistor, the voltage thus generated being a staircase waveform. The precision of the staircase waveform is a function of the accuracy of the levels of the individual binaries, the accuracy of the weighting resistors, and of any reference voltage associated with the conversion process.

In this instrument, the staircase-generating binaries are arranged in four groups. The binaries of the least-significant group and the two next significant groups are connected in the BCD configuration. These BCD groups are termed UP 1's, UP 10's, and UP 100's respectively. Interconnecting these three groups in a chain provides decimal counting to 1000. The binaries of the most significant group contain two series-connected binaries providing counting to 4, the group being designated UP K's. The serial connection of all binary groups, therefore, provides counting of 4000 input pulses.

The actual conversion of the binary-stage outputs to the staircase waveform is accomplished through the use of four commercial D-A converter cards labeled LP-30. The LP-30 cards are

designed to accept BCD inputs to give a staircase output. The LP-30 card associated with the most-significant bit (MSB) group of binaries has been modified to accept only the 2^0 and 2^1 binary outputs. The modified LP-30 card must not be interchanged with any other LP-30.

A precision reference voltage of -10 volts is required for referencing the LP-30 cards. This precision reference voltage is generated through logic and will be discussed later.

One other unit is required here to complete the staircase waveform generation. This is the commercial operational amplifier named OA-30. This amplifier converts the staircase output of the LP-30's to a low-impedance, high-current output needed to drive one input of each of the 44 comparator cards. Its output capability is ± 10 volts at 20 ma. Maximum load permissible is 500 ohms and 500 pf to ground.

See the block diagram for interconnections between UP counters, LP-30's, -10 volt reference amplifier, OA-30, and comparators.

The final generated staircase-waveform is positive going, 10 volts p-p amplitude. Each staircase step is 2.5 mVpp high, the leading edge of which is coincident with a clock pulse transition.

The clock frequency is approx. 25 kc making each step width 40 us., which requires about 160 ms. for generating the complete staircase. In addition to the staircase period are the readout periods making a maximum cycle time of about 200 ms. or 5 conversion and comparison cycles per second.

Sequence of Events I

We shall start considering the sequence of events at an arbitrary step in the staircase waveform and follow through a complete cycle. Reference should be made to the timing chart. Assume that a normal cycle has been in progress and we are starting our study at a staircase step between numbers 1 and 2000.

The top waveform shows 3 staircase steps occurring before a readout cycle is initiated. In the center of each staircase step is a strobe pulse of about 5 to 10 mVpp amplitude and 1 to 5 us width sitting on top of the staircase step. This staircase waveform (positive going) is fed to one input of each differential comparator from the operational amplifier OA-30. Each unknown voltage is fed to the remaining input of each of the 44 comparators and when the differential voltage between a step on the positive staircase and an arbitrary negative unknown input-voltage is slightly more positive than zero volts, the comparator flips producing a positive voltage transition at its output. This positive-going comparator output-transition forces a latch circuit into conduction (called comparator-latch-circuit or CLC) which completely immobilizes the differential comparator for the remainder of the cycle. Refer to comparator card schematic. The triggering-into-conduction of the CLC produces a negative-going transition at its output, setting a flip-flop called comparator flip-flop or CFF.

Each comparator follows the above sequence in turn starting with the comparator whose unknown input-voltage is lowest in

magnitude and continuing to the comparator whose input voltage is greatest in magnitude. The triggering sequence of the comparators is random, dependent upon the unknown input-voltage magnitudes.

If the unknown-voltage inputs to all comparators were connected in parallel, all comparators, all CLC's, and all CFF's would simultaneously flip in turn, providing that each comparator had been calibrated correctly. Therefore, it is possible that more than one Nixie readout-bank will display the same value of equivalent input-voltage.

The outputs of all CFF's are connected in parallel through disconnect diodes and continue through an AND gate (pos. logic) on the strobe-logic card to eventually set the readout flip-flop (RFF) and delay flip-flop (DFF) on the clock-logic card.

The flipping of a differential comparator, and subsequently CLC, CFF, RFF, and DFF begins a readout cycle. The setting of RFF closes A Gate which prevents the transmission of clock pulses and thus further staircase steps from being developed.

The setting of DFF resets all first and second zero flip-flops (FZ_1, FZ_{10}, FZ_{100}, FZ_K, SZ_1, SZ_{10}, SZ_{100}, SZ_K); and DFF plus a half cycle of the clock (C) sets a special delay flip-flop (XFF) and the strobe flip-flop (SFF). The output of XFF sets another special delay flip-flop (YFF). The output of SFF produces a husky positive pulse which resets all the Bipco modules (Nixie-logic drivers), and also jams the count state of all BCD down-counters.

The UP-counters and Down-counters are arranged in groups, i.e., the "units" UP and Down counters are associated on one card, the "tens" UP and Down counters are associated on another card, etc., etc. Thus, upon completion of the JAM operation, the count state of the UP and Down counter for "units" is the same, the count state of the UP and Down counters for "tens" is the same, etc. It is realized that the groups of UP-Down counters, i.e., "units", "tens", etc. do not necessarily contain the same count, as the number stored in each counter is continuously changing from staircase level-to-level. Also, the number stored in each UP counter previous to JAMming is the BCD equivalent of the 1's, 10's, 100's, and K's of the number of steps in the staircase waveform.

Returning to XFF sets YFF, the next negative transition of the anti-clock waveform ($\overline{C}$) resets YFF whose output resets DFF. The combination RFF.$\overline{DFF}$ opens B gate allowing clock pulses to be fed through the previously opened C, D, E, and F gates.

B gate now being opened transmits clock pulse through gates C, D, E, F, to the inputs of Down counters for 1's, 10's, 100's, K's and to the inputs of the previously reset Nixie logic (Bipcos) for displaying the appropriate 1's, 10's, 100's, and K's.

B gate pulses cause each Down counter (which are backwards-counting BCD counters) to start counting backwards from the count state previously JAMmed in during the JAMming operation. As any Down counter changes count-state from count one to count zero, an output pulse is produced which flips the previously reset first-zero flip-flop (FZ_1, FZ_{10}, FZ_{100}, and/or FZ_K). The backwards

counting continues, i.e., 9, 8, 7, 6, etc. until a second one-to-zero transition occurs. Upon detection of this second "zero" FZ_N flips again, whose output flips (sets) the second-zero flip-flop (SZ_1, SZ_{10}, SZ_{100}, SZ_K). The setting of SZ_N thus indicates that two "zeros" have been counted in the backwards (down) counting scheme.

Next the setting of SZ_N plus a clock pulse sets a corresponding second-zero-delay flip-flop (SZD_1, SZD_{10}, SZD_{100}, and SZD_K) whose output closes gates C, D, E, and/or F. The sequence in which these gates close depends upon the count state of the down counters at the time of detecting the second zero. For example, if each down counter had state "2" (equalling number 2222) JAMmed in, gates C, D, E, and F would close simultaneously. If number 1803, gate E (for "0") would close first, then gate C, then F, and finally D.

Closing any of the gates C, D, E, or F, prevents clock pulses from continuing on to the Bipco units and thus discontinues Bipco counting. The last pulse entering a Bipco before closing any of these four gates decides the final count state of the Bipco unit and, therefore, the number displayed on the respective Nixie display tube.

The backward counting of the down counters provides a means of obtaining four independent serial pulse trains, the total of which have counted the number of steps generated in the staircase at the point where a readout cycle was initiated.

The completion of detecting all second zeros, plus a clock pulse, produces a group of clock pulses from the second-zero OR gate (SZ OR). The first transition produced by SZ OR resets XFF, RFF, and any CFF that was previously set.

Each bank of Bipcos has associated with it a gate controlled by a particular CFF which allows or prevents the serial pulses from gates C, D, E, or F from arriving at the Bipco input terminals. Resetting any CFF (from above) then prevents that particular Bipco unit from changing numerals the rest of the machine cycle. The next cycle, when that CFF again sets, the same Bipco bank will display the same numerals, providing that the input voltage to its associated comparator has not changed value.

The next transition of the SZ OR gate sets the strobe flip-flop (SFF). The resetting of XFF, RFF, CFF and setting SFF will allow the staircase to advance again until another readout cycle is initiated through the flipping of another comparator. The process of advancing the staircase, producing readout cycles, advancing the staircase, etc., continues until 3999 staircase steps have been produced. One more clock pulse out of the A gate will return the staircase waveform to 0000.

Sequence of Events II

The transition of the K's UP-counter from 3 to 0 (between staircase levels 3999 to 0000) flips the Pause flip-flop (PFF). PFF and the next strobe pulse sets the pause delay flip-flop (PDC). The transition occurring from the setting of the PDC initiates a special readout cycle and "forces" all comparators that have not previously flipped to flip.

This means that any comparator that had not previously been involved in a readout cycle will now be deliberately flipped and subsequently their associated CFF's. The pulse that forces these comparators to flip is called the "force" pulse and is

generated by $\overline{\text{PDC}}$. Regardless whether any comparators are forced, this special readout cycle is always initiated because $\overline{\text{PDC}}$ also sets RFF.

Following the setting of RFF, a JAM pulse is again produced (as before) JAMming the state of the UP counter into the Down counter. This time PFF is in the set state allowing the number 8000 to be JAMmed into the down counter. Thus, the forcing of any unused comparators (and CFF's) allows all unused Bipco gates to open and the number 8000 will be displayed on all Bipco modules that have not previously displayed. This cycle continues until all second zeros have again been detected and RFF, XFF, and all CFF's have been reset by $\overline{\text{SZ OR}}$.

The next half cycle of the clock generates $\overline{\text{SZ OR}}$ as before, and $\overline{\text{SZ OR}}$ resets PFF and sets SFF (as before). Resetting PFF generates a pulse called latch-reset. This pulse resets all comparator latch circuits (CLC) to the enable condition, "priming" the comparators for the start of another complete measurement cycle.

The resetting of all CLC's, then, is actually the beginning of a new DVM cycle.

The next half cycle of the clock resets PDC whose output again sets RFF, initiating another readout cycle. A strobe pulse is also generated at this time which allows any comparator to flip whose input is 0000 volts, or any comparator will flip whose input is a positive potential (wrong input polarity). All Bipco displays whose corresponding comparator input-voltage is zero or positive will now indicate 0000 because the count-state 0000 is JAMmed in

the down-counter when JAMming occurs in this part of the cycle. This cycle of events proceeds as before, detecting second zeros, closing gates C, D, E, and F, etc., and finally ending the readout cycle.

Upon completion of the above readout cycle, the staircase is again generated, a step-at-a-time until such time as an input voltage to a comparator causes it to flip, initiating a new readout cycle.

The above descriptions of the sequence of events describe the major events in a complete operation cycle of the DVM. Several other sequences of events also occur during each complete cycle which will be described below.

Staircase Reference Voltage

A precision -10 volt reference voltage is required for referencing the LP-30 D-A converter modules. This voltage is required to be stable within about 1 mv DC for many DVM operational cycles, and capable of being adjusted to -10 volts dc $\pm$ 100 mv. A precision reference was designed which would be self-calibrating and which would not require precision components. Refer to schematic #CH3954.

The philosophy of the reference amplifier is this: An operational amplifier with a very low-leakage input stage and a capacitor in the feedback loop is designed to have -10 v DC output when there is zero charge at the input terminal. The leakage rate of the input stage is low enough to allow the feedback capacitor to change its charge very slowly, therefore, changing the output voltage at a very slow rate. Two diode-pumps are

connected to the reference amplifier input terminal, one producing a positive-going voltage step under certain conditions, the other producing a negative going step under other conditions. The inputs to these diode-pump circuits are obtained from logic gates. The logic is so arranged that only one diode-pump can produce an output at a time, never simultaneously. When the logic voltages at the input of these gates indicate that the main 4000 - step staircase is too low in amplitude, one diode pump produces an output which causes the capacitor in the feedback loop to increase its charge towards -10 v (which is the LP-30 D-A converter reference voltage), generating a higher-amplitude main staircase during the next DVM operational cycle. If the logic to the diode-pump gates again indicate that the main staircase is still too low in amplitude, that diode-pump again produces an output which further increases the charge on the feedback capacitor towards -10 v. This process continues until logic indicates that no increase in reference voltage is necessary, at which time there is no input to one of the diode-pumps.

If the 4000-step staircase is too high in amplitude, logic produces an input to the other diode pump causing the feedback capacitor to be reduced in charge, a step-at-a-time until logic indicates to no further decrease in reference voltage is necessary.

The position on the staircase waveform used as a reference for the logic is step number 2000. This is obtained from one of the UP-count flip-flops in UP-Down counter #4 and is used as one of the logic inputs to the diode-pump gates.

A D.C. voltage of -5.000 volts is obtained from a temperature compensated zero diode (see schematic #CH3965). that is the input to one particular comparator (comparator #1). When this comparator is correctly calibrated and with the -5.000 volt input and a correct-amplitude main staircase input, at staircase step #2000 the comparator will flip and consequently its CFF. The CFF output from this particular comparator is another one of the inputs to the diode-pump gates.

Another input to the diode-pump gates is the output of a flip-flop called the Z flip-flop located on the -10 v reference amplifier card. It is set at staircase step #2000 and reset on the next clock pulse (at step #2001).

The diode-pump gates generate the function $\overline{K4}$. CFF . $\overline{Z}$ = pump. K4 is the #2000 staircase step transition of its UP-count flip-flop, and CFF the output of the special comparator flip-flop used for -10 v reference-voltage generation. Figure #2 shows the time relations of these various waveforms.

The input leakage current to the reference amplifier is determined from $I = \frac{C.E.}{T}$

where C = 1 uf

E = 1 mv

T = 60 sec.

$I \approx 16.7$ pA from above calculation. A very low-leakage F.E.T. was selected for the amplifier input whose max I_{gs} = 50pA. Tests on our unit indicate leakages of considerably less than this as determined from the drift rate of the reference amplifier.

Ten Pulse Detection

Another special feature of the DVM is an internal Bipco checking scheme. This scheme provides a means of continuously monitoring all Bipco counting and comparing the actual remote Bipco counting with the logic in the instrument. If a discrepancy is found between the instrument logic counting and the Bipco counting, a "tilt" lamp becomes lit indicating the miscount of some Bipco unit.

Since all the Bipcos in a particular module are reset to the same number simultaneously whenever reset occurs, and the count-pulse inputs to those Bipcos occur in parallel, Bipco counting occurs in parallel. Also, since the total number of serial pulses on any Bipco input line is the desired number plus 10 (because of detecting the first and second zeros described previously), all Bipco counting in that module passes through the number 9 (or any other numeral) simultaneously, if counting in that module is proceeding correctly.

Bipco modules produce a pulse output for each count state that the counting is passing through. See the Bipco spec sheet enclosed. In this Bipco fault detector, the number 9 output pulse from each Bipco in the display module is put into an AND gate (negative logic). See schematic #CH3963-(Ten Pulse Detector). The output of the AND gate is converted to a current pulse which is returned to the DVM rack via a coax cable. This current pulse is the converted back into a voltage pulse for use in the ten-pulse detector circuitry.

An internally generated pulse that occurs at the same time the Bipcos #9 output pulse occurs is derived from a BCD counter (called TPC). The input to this counter is down count pulses (DCP) from the logic B gate. At the count of 10, an output of the BCD counter sets a flip-flop, the output of which closes a gate at the input of TPC, preventing any more DCP's to be counted by TPC.

The 10 output of TPC, any CFF output, and the converted voltage pulse from the 9's Bipco outputs are all used as inputs to an AND gate. This gate is arranged such that no output is produced when Bipco 9's, CFF, and the 10 output of TPC occur simultaneously. If any of these gate inputs do not occur simultaneously, the gate produces an output pulse which sets a special flip-flop which has to be manually reset. The output of this flip-flop eventually drives an indicator lamp which indicates fault.

The output of the 3-input AND gate is the function

$$\text{AND } 9 \cdot \overline{\text{TPC}} \cdot \overline{\text{CFF}} = \text{tilt}$$

The timing relations of the ten pulse detector are shown in Figure #3.

LP-30 D-A Converters

Three of the commercial LP-30 D-A converter cards are used as obtained from the manufacturer. These three cards are the ones associated with the least-significant-bit up counter and the next two most-significant-bit counters (1's, 10's, 100's). The LP-30 associated with the K's up counter (most-significant-bit) has been modified to accommodate a 4-wire 2 bit binary input instead

of the usual 4-wire BCD input from the UP counters. This modification involved re-assigning the weight of the MSB in the K's group of numbers. See Appendix for LP-30 details.

OA-30 Operational Amplifier

One commercial operational amp is used to transform the medium impedance staircase waveform generated by the LP-30's to a low impedance staircase required by one input of each comparator. The OA-30 has been modified to allow the amplification to be adjustable over a small range by means of a potentiometer installed on the amplifier card. One additional resistor has been installed to allow the amplifier gain to be approximately 2.5. See the Appendix for OA-30 details and modifications.

The strobe pulses that sit in the center of each staircase step are also added to the input of the op.amp. See block diagram.

Special Comparators

Comparator #1 is permanently reserved for measuring the internal -5.000 reference potential which when compared with staircase step #2000 will (through logic) produce the -10.000 volt reference previously described required for D-A converter operation.

Comparator #2 is reserved for measuring the voltage appearing at the input of any other comparator, by means of switches described below.

Front Panel Controls

Panel #4 contains a set of two switches labeled "Input Selector" which can select any input voltage to be measured that comes into the DVM rack. There are two special positions on the

left-hand switch labeled "T" and "J". The "T" position allows a locally generated DC voltage that appears at the output of the helipot labeled "test voltage" to be switched to the input of comparator #2, providing a variable voltage for test purposes.

Position "J" allows an external voltage patched-up through the connectors labeled "test jack" to appear as the input to comparator #2. Both test jacks are in parallel so that the external-voltage input may be measured with another instrument for calibration of the DVM.

Positions #01 and #02 on these switches are not used as comparators; 1 and 2 are used for special local functions.

Panel #6 provides a jack labeled "Op. Amp." which make available the staircase waveform at the front panel, and a jack labeled "scope trig." providing a square-wave signal output for triggering an oscilloscope. The righthand side of this panel has a push button labeled "reset" which can reset the flip-flop used to hold the "failure" lamp in the on state. This failure lamp indicates a discrepancy between any Bipco readout and the internal logic as described previously.

Panel #8 has selector switches allowing the actual Bipco drive pulses from any Bipco-gate card to be sent to the right-hand display module labeled "selected output" on panel #1.

From these selectable switches, all inputs and all outputs of the DVM can be checked locally.

On the power supply panel, the red indicator lamp indicates the +200 volt power being ON and the amber lamp indicates main (low-voltage) power supply ON.

SIMPLIFIED BLOCK DIAGRAM

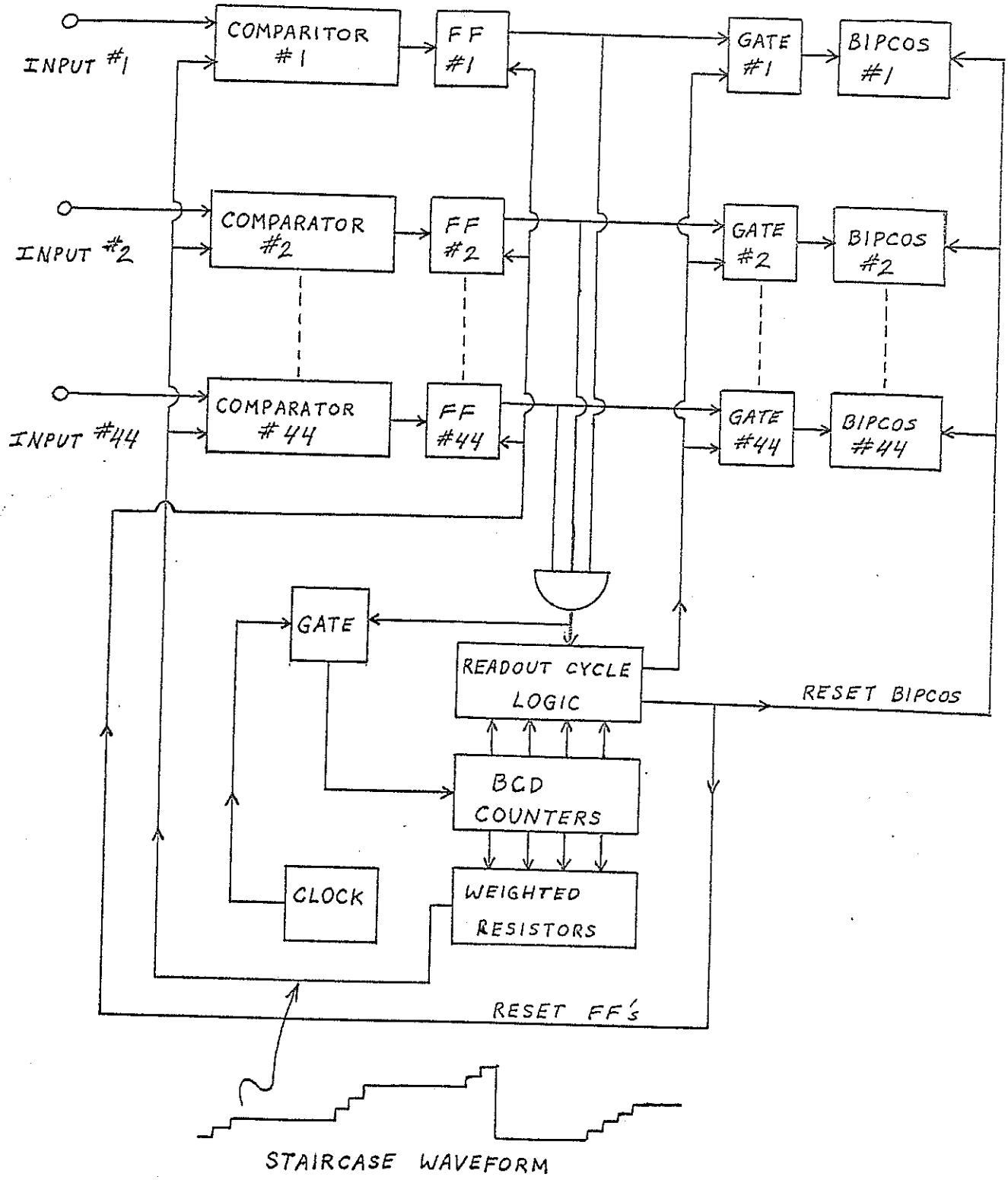

FIGURE #1

REFERENCE AMPLIFIER WAVEFORMS

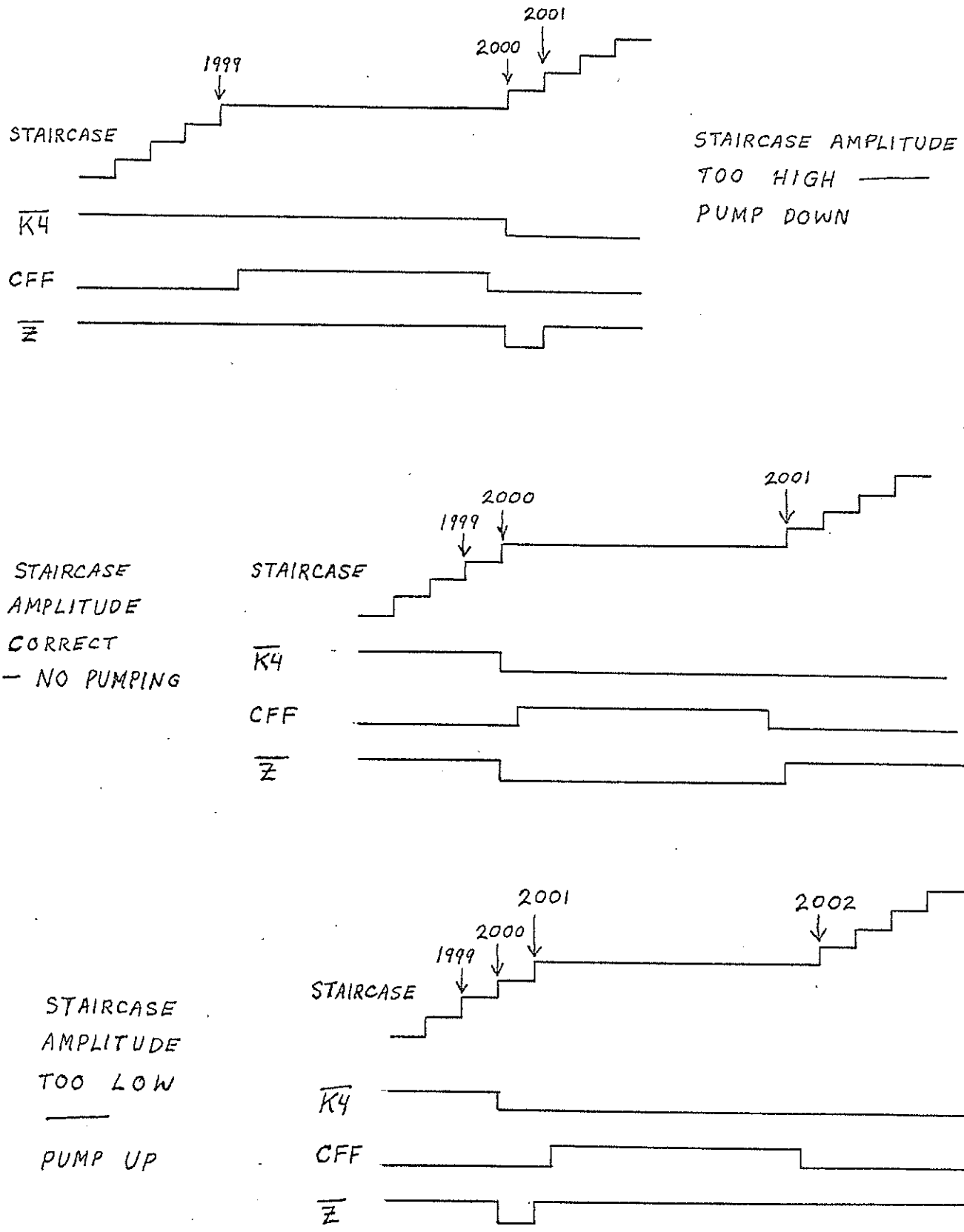

FIGURE #2.

TEN PULSE DETECTOR WAVEFORMS

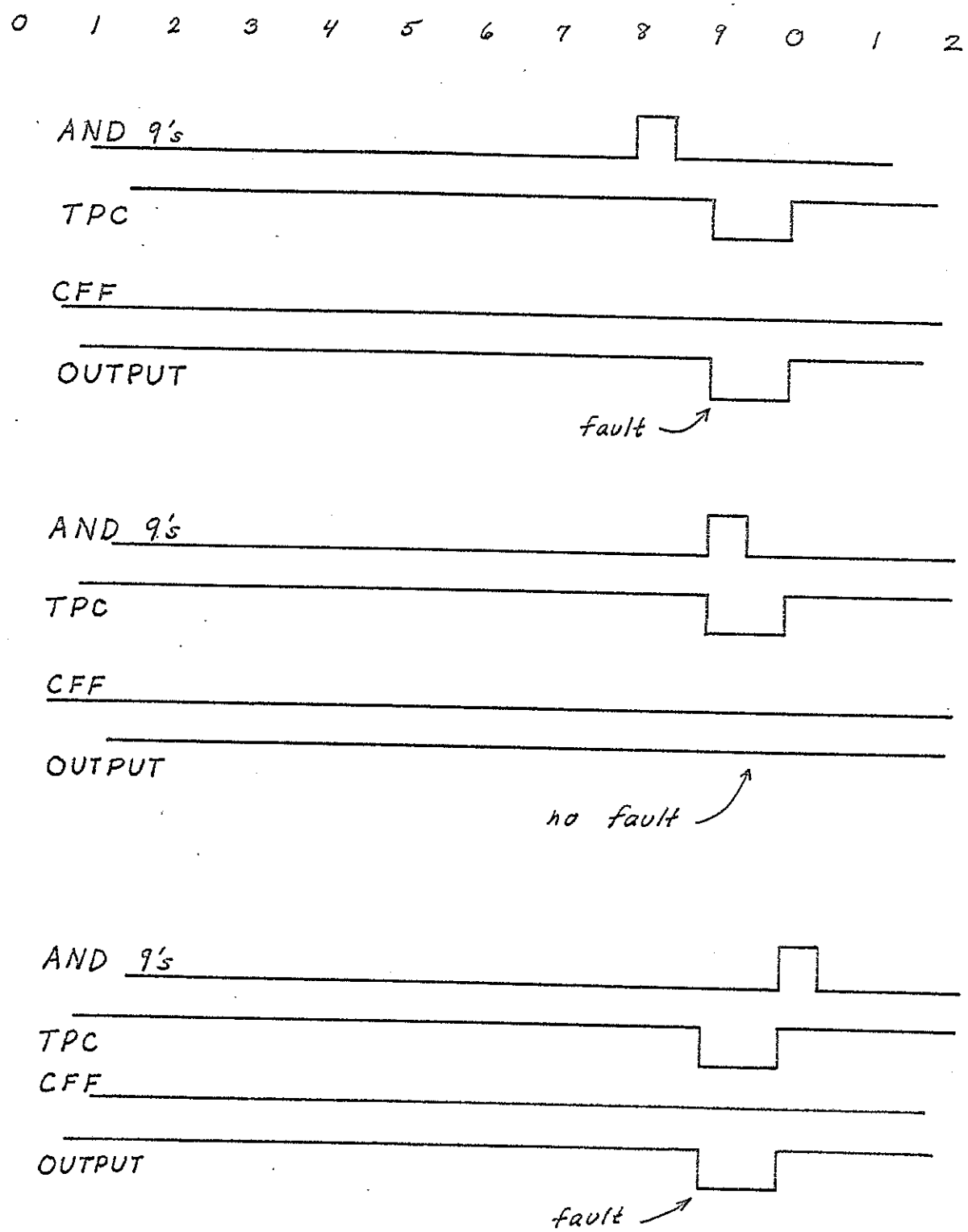

FIGURE #3

7-8-68

Addenda #1

DVM Interface to Computer and Energy-Meter Display

A card-file of electronics auxiliary to the main frame of the DVM proper has been installed immediately above the local readouts (labeled panel #1 in the text). This card-file contains two subsystems of the DVM, one being interfacing circuitry between the DVM and the computer, the other being circuitry to drive incandescent lamps for the energy-meter display permanently assigned to DVM channel #3. See interface block diagram #DH3973.

DVM interfacing to the computer is necessary to provide a means of recording various voltage values as read by the DVM and subsequently using these computer-recorded values in computer programs, allowing analysis of various synchrotron parameters. All parameters measured by the DVM may not be useful in machine analysis, although provisions are made to send the information from any DVM channel (channels #3 through #44 only) to the computer. The input to the computer from the DVM is a 14 bit word containing any voltage level of the 4000 step staircase generated in the DVM. The computer is instructed to read, on command, one selected DVM channel at a time and when a readout cycle is occurring in the DVM for a particular channel, the corresponding BCD staircase values are set into a register, the output of which is transferred into the computer under program control.

Referring to the block diagram for the interface unit, card #1 converts a binary input from the computer to a modified decimal code used for channel selection. Cards #2, 3, and 4 AND this modified decimal code with the DVM's CFF pulses to produce a pulse occurring at the time the computer-selected channel is being read out by the DVM. This special pulse sets a flip-flop whose output strobes a column of flip-flops on card #5, setting these flip-flops to the corresponding staircase voltage which appears at the input of the computer. Before another channel can be read by the computer, a reset pulse must be sent to the interface from the computer to reset the strobe-producing flip-flop.

Card #6 is a current amplifier to provide higher output currents and isolation from the DVM's BCD scaler outputs.

Another function of the interface unit is to generate high currents to drive an incandescent lamp display for the synchrotron energy readout. The cards involved are #7, 8, 9, and 10. The block diagram shows these cards being fed from the DVM BCD current-amplifier, card #6. Cards #7, 8, and 9 convert the DVM's BCD outputs to decimal outputs for the units, tens, and hundreds lamps in the lamp display module. Card #10 provides only a one-thousand output as the lamp display is only required to display a maximum number of 1000 representing 10.00 GEV from the synchrotron. The decimal point in the display is always stationary and is provided by the display itself.

A pulse from the DVM's channel #3 CFF output is used for strobing the storage flip-flops in cards #7 through 10, meaning that only channel #3's (synchrotron energy) output will be delivered to the lamp display module.

Supply voltages for this card cage come from two sources. One source is standard synchrotron-electronics supply-voltages (+15, +6, -6, -15) which must be connected up to the standard-electronics power-supply connector at the rear of the card cage. The other power-supply required is +5 volts for the integrated circuits, supplied from a separate power-supply located at the rear, bottom of the DVM cabinet; (see schematic #AH3970).

The lamp display uses #44 bayonette lamps. Ten lamps are illuminated at synchrotron energies less than 10 GEV and eleven lamps at 10 GEV. The total lamp current is about 2 amps at roughly 5.5 volts and a separate adjustable power supply is used for the display; (see schematic #AH3974).

As a result of installing the GEV readout display and the computer interface electronics, the panels are not as numbered on page 2 of the DVM description.

The order of the panels now is:

Top panel	-	GEV display
2nd "	-	Blank
3rd "	-	Local nixie readouts
4th "	-	Computer interface logic
5th "	-	Odd inputs 23 through 44
6th "	-	Comparators 23 to 44
7th "	-	Even inputs 24 through 44, Odd inputs 1 through 21, Input selector switches
8th "	-	Comparators 1 to 22
9th "	-	Even inputs 2 through 22
10th "	-	Logic
11th "	-	Output switches and remote Bipco connectors
12th "	-	Main power supply
13th "	-	Input signal-cable patch panel

Addenda #2

Measurement and Display of A.C. Line Voltage

A special Bipco module is used for the display of A.C. line voltage. (See schematic CH3972.) This particular readout module must not be interchanged with a standard readout module as shown on CH3968.

A.C. line voltage is measured by transforming the 115 VAC line 1:1, half wave rectifying and filtering the transformer's output and providing precision adjustment of the resulting D.C. voltage. This D.C. output voltage is purposefully selected to be 1.000 volts above the output voltage from a temperature-compensated reference diode. In this case, the reference diode output = +6.214 and the adjustable incoming D.C. set to +7.214 volts. These two D.C. voltages are used as the differential input of an operational amplifier with a gain of -4.000.

The resulting output of the op-amp (negative 4.000 times the differential input) is fed to a 3-digit D.V.M. channel whose output feeds the special Bipco unit mentioned above.

An input voltage of -4.000 volts to the D.V.M. would ordinarily produce a Bipco reading of 1600. The special module has the K's Bipco replaced with a Nixie bulb connected to display "1" only, the K's input connected to the 100's Bipco, 100's input connected to the 10's Bipco, 10's input connected to the 1's Bipco.

The A.C. line-voltage card's calibration (see #BH3423) is adjusted such that 116.0 VAC line voltage reads 1160 on the special module, calibrated by adjusting the 100 ohm pot on the line voltage card.

Measured accuracy is ± .1 volt from 105 VAC to 125 VAC.

Addenda #3

The DVM was originally designed for use with a very low source-impedance input signal. The input impedance of the comparators is 24.0 K, requiring the source impedance to be less than 6 ohms in order to approach the 0.025% accuracy of the instrument. With a finite source-impedance above a few ohms, an error in instrument linearity occurs, the amount of error being a function of the source-impedance and input bias current. A special circuit has been added to each comparator input to compensate for input bias current and, therefore, correct scale non-linearities. See schematic #AH3971.

The input-offset-current (input bias) is zeroed-out by the following method:

1. Short input of comparator of desired channel.
2. Adjust voltage offset pot on that comparator board so that channel output reads 0000.
3. Set up integrator-calibrator box and external resistance decades for 216.000 K ohms in series with integrator-calibrator's internal supplies.
4. Connect commercial DVM to calibrator's output-terminal voltage terminals.
5. Set calibrator voltage to 95.00 volts (DVM should read 3800) and later to 5.00 volts (DVM should read 0200) while calibrating each channel.

6. Adjust 50 K pot in offset circuit for scale of numbers.
7. Adjust 1 K pot in offset circuit for range of numbers.
8. Repeat above steps until commercial DVM and 44 channel DVM agree in voltage.

After input-offset-current compensation (calibration) is completed, the source impedance can be in the megohm range while instrument linearity is maintained within accuracy limits.